

## Development of novel methods and tools to decipher the huntingtin post-translation modifications code

Présentée le 15 décembre 2020

à la Faculté des sciences de la vie  
Laboratoire de neurobiologie moléculaire et neuroprotéomique  
Programme doctoral en biotechnologie et génie biologique

pour l'obtention du grade de Docteur ès Sciences

par

**Anass CHIKI**

Acceptée sur proposition du jury

Prof. H. Altug, présidente du jury  
Prof. H. Lashuel, directeur de thèse  
Prof. C. Becker, rapporteur  
Prof. E. Reits, rapporteur  
Prof. C. Heinis, rapporteur

---

---

## Acknowledgements

First and foremost, I would like to express my sincere appreciation and thanks to my thesis Director Prof. Hilal Lashuel, for giving me the opportunity to join his laboratory and conduct my Ph.D. It is hard for me to find enough words to thank him for all that he has done for me in the last years as a teacher, mentor, supervisor, and friend. First, I thank him for being a great teacher. I will never forget his enthusiasm when he gave us the chemical biology class during my second year of bachelor, that is when I first met him. His passion and devotion to his students made this class memorable. Since then, he had become a mentor and the first person to turn to for advice or guidance during my studies. He gave me the chance to join his laboratory for my master's project and then for a Ph.D. I am grateful for his support, scientific guidance, advice, patience, and sharing of knowledge. His vision, enthusiasm, and motivation have deeply inspired me. He has taught me the methodology to carry out good science and to present complex research data as clearly as possible. It was a great privilege and honor to work under his guidance. I am incredibly grateful for the close supervision he offered me while providing me room to explore my ideas and all the resources to do so. His guidance has not been restricted to the research area, but he also instilled in me professionalism, problem-solving, creativity, integrity, and critical observation. I learned with him multiple soft skills that will shape my future career. He allowed me to collaborate with several research groups around the world and participate in many scientific projects. A big thank you, Hilal, for your trust and support during hard times. I could not have imagined having a better advisor and mentor for my Ph.D.

My gratitude also goes to the members of my thesis defense committee. Prof. Christian Becker, Prof. Eric Reits, Prof. Christian Heinis, and Prof. Hatice Altug for the time and attention they took in evaluating my thesis work.

During my Ph.D., I had a fantastic occasion to collaborate with several research groups and publish amazing science to advance the field together. My heartfelt thanks, especially go to the people who have been implicated in the projects presented Herein: Dr. Andrea Caricasole and his team for a very fruitful collaboration and exciting discussions. Prof. Giovanni Dietler, Francesco Ruggeri and Urszula Cendrowska, whose AFM imaging and analysis have been critical in the completion of the work in chapter II. Prof. Annalisa Pastore and Dr. Domenico Sanfelice for the NMR collaboration and their fast adaptivity during the paper revision. Luciano Abriata, whose knowledge and enthusiasm about NMR brought more inputs to my projects. Prof. Matteo Dal Peraro and Zhidian Zhang for the exciting collaboration and discussion. Their computational work perfectly complemented our experimental work in the third paper presented in this thesis and enabled a better understanding of our data.

These projects could not have been realized without the outstanding contributions from my present and past colleagues: Jonathan Ricci, Ramanath Hegde, Sean Deguire, Annalisa Ansaloni, Zhe-Ming Wang, Ritwik Burai, Sophie Vieweg, and Andreas Reif.

I am very grateful to Jonathan Ricci, who joined the group in the middle of my thesis. However, his contribution was indispensable to finish my thesis, thanks to his hard and meticulous work. Thanks for all the time that you stayed late with me and for your perseverance. Over the years, he became a close friend, and working together was enjoyable.

A special thanks to two of my previous colleagues without whom I could not be the achieved scientist that I am now; they taught me everything I know about biochemistry and biophysics. First, I am grateful to Nadine

---

ait-Bouziad, who taught me how to perform experiments with high quality and meticulousness. She was always available to help with planning and performing experiments, data analysis, and discussions. She is a reliable person on whom I counted. Second, I am filled with gratitude for Ritwik Burai, who taught me most of the chemical methods that I used during my thesis. His guidance and supervision were deterministic to address the challenges in the synthesis at the beginning of my Ph.D. I was always impressed by his innovative spirit. Until now, I still count on his help when I have chemistry-related questions.

I also had the chance to work with two amazing colleagues, namely Driss Boudeffa and Mahmood Haj-Yahya. Their contribution and help during my thesis are too long to fit in here. They are the most reliable people I know. They could drop everything they are doing if I needed help in the lab or outside the lab. They are the first person I turned to when I needed anything. Their friendship made the work in the lab much more enjoyable. They are both like brothers to me. While Mahmood left Switzerland to explore a new career perspective in the pharmaceutical industry, Driss is still in the lab, and I am grateful for all the technical support he provided me but also his dedication to the lab.

I would like to thank also Bruno Fauvet, who hosted me at the beginning of my master's and introduced me to protein expression and purification.

Special thanks to my actual and previous colleagues, who were always open for discussion, sharing exciting ideas, and creating a friendly work environment. I learned a lot from them. Namely: Abid, Bilal, Filip, Loay, Martial, Anne-Laure, Carole, Bohumil, Sonia, John, John W, Nathalie, Céline, Niran, Nathan, Gopi, Johanness, Muhamed, Senthil, Galina, Pedro, Raja, Sergey, and Iman.

I want to thank our former secretaries (Sandrine Favre, Dorothée Demeester) and our current secretary (Marie Rodriguez) for their help with administrative issues.

I am grateful to David Demustas for the interdisciplinary center for electron microscopy (CIME), who taught me how to perform electron microscopy and was always available for EM advice. Thanks also to the proteomic facility team, Marc Moniatte, and Jonathan Paz-Montoya, for their advice related to MALDI analysis.

I am thankful to my mentor Prof. Bruno Correia for his guidance and our friendly discussions.

I want to thank Hilal, Ayah, Galina, and Ramanath for proofreading of the thesis.

Special words of gratitude go to my friends for a great moment spent together, which has been a great source of energy for me. Thanks for offering me advice and supporting me through this entire process: Riad, Tamim, Hamid, Ayah, Maxime, Bilal, Florin, Saleh.

If I am here today, it is thanks to my amazing, wonderful mother, Najia Alaoui, who made many sacrifices to raise me and provide me with all the necessary means to focus on studying despite her limited resources. She was always here despite the Mediterranean Sea between us. Thank you for encouraging me in all of my quests and for inspiring me to follow my dream. Thank you for all your prayer and kind words when it was tough. I hope that I made you proud.

I would like to thank my uncle Abdellah, who believed in my potential when I was young and brought me to Switzerland from Morocco to pursue my studies. I am very grateful to him for this life-changing opportunity and for supporting me financially and morally. He always challenges me, and this was a source of motivation for me during my studies. Until the submission, he kept encouraging me and pushing me to the limits.



---

Spending time with him and my cousins (Rayane and Ismail) was very comforting during the hard days of the Ph.D.

I am grateful to my father and mother in law Montassar and Yassar for encouraging me during all the process of the writing. Thank you for your kindness and for welcoming me into your family as your son.

I will be forever grateful to my brother Ayoub for his noble gesture and saving my life last year. I owe him my life, and without his generous gesture, I could not have been able to finish my Ph.D. thesis. Billions “thank you” are not enough to express my deep appreciation for your sacrifice without a single hesitation.

Last but not least, and above all. I want to express my deepest, warmest, and sincerest gratitude to my beloved wife, Nour Chiki, for her continuous and unconditional love that made this Ph.D. happen. Being in love with her gave sense to my existence and drove me towards outstanding achievements. She is very supportive, helpful, and always finds the correct words to comfort me. She is the smartest person I know, and her help proofreading this thesis was invaluable. Thank you for being my proofreader, my counselor, my recomforting shoulder, my muse, and my best friend. Thank you for bringing joy, fun, and laughs to my life. Thank you for the infinite sacrifices that you made for me in the past and during the writing process. You are my life, and I owe you everything.

---

---

## Abstract

Huntington's disease (HD) is a fatal genetic neurodegenerative disorder caused by a CAG repeat expansion in the Huntingtin gene of more than 36 repeats. This repeat is translated into a polyglutamine (polyQ) stretch within the first exon-encoded region of the Huntingtin protein (Httex1). The aggregation of expanded Huntingtin protein (Htt) in the striatum and cortex has been implicated in neuronal dysfunction and death. Recent studies have shown that mutations that mimic post-translational modifications (PTMs) in the first 17 N-terminal amino acids (Nt17) of the protein dramatically influence the aggregation, subcellular localization and toxicity of Httex1 and full-length Htt proteins. These findings suggest that these modifications may serve as reversible molecular switches for regulating Htt function in health and disease. However, assessing the effect of authentic PTMs and their cross-talk has not been possible due to the lack of knowledge about the enzymes responsible for these modifications. Moreover, the high aggregation propensity of Httex1 with increased polyQ content hampered the development of an efficient method to produce post-translationally modified proteins. By consequence, previous biophysical studies were mostly carried out using tagged Httex1 protein, or model peptides bearing PTM mimetics mutations which do not fully capture the chemical properties of the *bona fide* PTMs.

Therefore, we developed a semisynthetic methodology that permits site-specific modification of the mutant Httex1 (at single or multiple residues). We used this strategy to investigate the effect of acetylation (at K6, K9, or K15) and phosphorylation (at T3), as well as the cross-talk between these modifications on the structure and aggregation of wild-type and mutant Httex1. Our results demonstrated that T3 phosphorylation (pT3) significantly inhibited the aggregation of mutant Httex1 (43Q), whereas only partial inhibition of aggregation was achieved by the phosphomimetic mutation (T3D). Acetylation of single lysine residues, K6, K9, or K15 (Ack6, Ack9, or Ack15), did not affect the aggregation of Httex1. Interestingly, Ack6, but not at Ack9 or K15, reversed the inhibitory effect of pT3. Next, we discovered novel kinases GCK and TBK1 that phosphorylate efficiently and specifically T3 and S13/S16, respectively. We exploited these kinases to produce homogenously phosphorylated recombinant Httex1 at T3 or both S13 and S16. We generated, using this method, suitable for structural and cellular applications. Finally, we combined chemical, semisynthetic and enzymatic methods to produce mutant Httex1 proteins bearing oxidized Methionine at position 8 (oxM8) alone or in combination with other Nt17 PTMs (pT3 or Ack6). We observed that oxM8 delayed the aggregation of mutant Httex1 and decreased the helical content of the Nt17 independently of the presence of other PTMs.

Together, these findings provide novel insight into the role of Nt17 PTMs in regulating the aggregation of Httex1 and suggest that the aggregation and possibly the function (s) of Httex1 are controlled by complex regulatory mechanisms involving cross-talk between different PTMs. The tools presented in this thesis will

---

open new windows of opportunity to decipher the role of Htt PTMs code in the regulation of Htt function in health and disease.

## Keywords

Huntington's Disease, Huntingtin Protein, Huntingtin Exon1, Post-Translational Modifications, Phosphorylation, Cross-Talk, Aggregation, Native Chemical Ligation, Kinases, Protein Structure

## Résumé

La maladie de Huntington (MH) est une maladie génétique neurodégénérative mortelle causée par une expansion répétée des nucléotides CAG dans le gène de la protéine Huntingtine de plus de 36 répétitions. Cette répétition est traduite en une séquence protéique de polyglutamine (polyQ) dans le premier exon codée par la protéine Huntingtine (Httex1). L'agrégation de la protéine Huntingtine (Htt) avec expansion dans le striatum et le cortex est impliquée dans le dysfonctionnement neuronal et la mort cellulaire. Bien que la séquence et les déterminants moléculaires de l'agrégation et de la toxicité de Htt restent méconnus, des études récentes ont montré que des mutations imitant les modifications post-traductionnelles (PTMs) dans les 17 premiers acides aminés du N-terminal (Nt17) de la protéine influencent considérablement l'agrégation, la localisation subcellulaire et la toxicité des protéines Httex1 et Htt de longueur totale. Ces découvertes, combinées au fait que cette courte séquence N-terminale abrite plusieurs résidus qui subissent des PTMs réversibles, suggèrent que ces modifications peuvent servir d'interrupteurs moléculaires réversibles pour réguler la fonction de Htt dans la bonne santé comme dans la maladie. Cependant, l'évaluation de l'effet des PTMs authentiques et de leur interférence n'a pas été possible à cause du manque de connaissances sur les enzymes responsables de ces modifications. De plus, la forte tendance à l'agrégation de Httex1 contenant un long polyQ a entravé le développement d'une méthode efficace pour produire des protéines avec PTMs. Par conséquent, les études biophysiques précédentes étaient principalement menées à l'aide de la protéine Httex1 marquée, ou de peptides modèles portant des mutations qui mimiquent les PTMs, ne capturant malheureusement pas pleinement les propriétés chimiques des PTMs *bona fide*.

Par conséquent, pour permettre l'investigation des PTMs authentiques et étudier le potentiel d'interférence entre différents PTMs de la Nt17, nous avons développé une méthodologie semi-synthétique qui permet la modification spécifique et localisée de la protéine (à un ou plusieurs résidus) et la production, pour la première fois, de plusieurs milligrammes du mutant Httex1 très pure et modifié sans étiquette. Nous avons utilisé cette stratégie pour étudier l'effet de l'acétylation (à K6, K9 ou K15) et de la phosphorylation (à T3), ainsi que l'interférence entre ces modifications sur la structure et l'agrégation de Httex1 de forme sauvage et mutant. Nos résultats ont démontré que la phosphorylation de T3 (pT3) inhibait de façon significative l'agrégation du mutant Httex1 (43Q), alors que seule une inhibition partielle de l'agrégation était obtenue par la mutation phosphomimétique (T3D), démontrant ainsi que cette mutation reproduisait mal l'effet de la phosphorylation *in vitro*. L'acétylation de résidus seuls des lysines K6, K9 ou K15 (AcK6, AcK9 ou AcK15), n'a pas affecté l'agrégation de Httex1. Étonnamment, AcK6, mais pas AcK9 ou K15, a inversé l'effet inhibiteur de pT3. Ensuite, nous avons cherché à filtrer et découvrir les kinases responsables de la phosphorylation de

---

Nt17. Nous avons découvert deux nouvelles kinases GCK et TBK1 qui phosphorylent efficacement et spécifiquement T3 et S13/S16, respectivement. Nous avons utilisé ces kinases, en combinaison avec notre stratégie récemment développée utilisant SUMO comme étiquette, pour solubiliser la Httex1 et produire sa forme recombinante phosphorylée de manière homogène en T3 ou à la fois en S13 et S16. Nous avons généré, en utilisant cette nouvelle méthodologie, une protéine WT (23Q) et mutante (43Q) Httex1, phosphorylée sans étiquette marquée isotopiquement et par fluorescence, qui est adaptée aux applications structurales et cellulaires. Enfin, nous avons combiné des méthodes chimiques, semi-synthétiques et enzymatiques pour produire des protéines Httex1 mutantes portant en position 8 de la méthionine oxydée (oxM8) seule ou en combinaison avec d'autres Nt17 PTMs (pT3 ou AcK6). Nous avons observé que oxM8 retardait l'agrégation du mutant Httex1 et diminuait le contenu hélicoïdal du Nt17 indépendamment de la présence d'autres PTMs.

. Ensemble, ces résultats fournissent un nouvel aperçu du rôle des PTMs du Nt17 dans la régulation de l'agrégation de Httex1 et suggèrent que l'agrégation et éventuellement la (les) fonction(s) de Httex1 sont contrôlées par des mécanismes de régulation complexes impliquant une interférence entre différents PTMs. Les outils présentés dans cette thèse ouvriront de nouvelles portes pour déchiffrer le rôle des PTMs de Htt dans la régulation de sa fonction aussi bien dans la santé que la maladie.

## Mots-clés

Maladie De Huntington, Huntingtine, Huntingtine Exon1, Modifications Post-Traductionnelles, Phosphorylation, Interférence, Agrégation, Ligation Chimique Native, Kinases, Structure De Protéine.

# Content

<b>Acknowledgements.....</b>	<b>iii</b>
<b>Abstract .....</b>	<b>vii</b>
<b>Keywords .....</b>	<b>viii</b>
<b>Résumé.....</b>	<b>ix</b>
<b>Mots-clés .....</b>	<b>x</b>
<b>Content.....</b>	<b>xi</b>
<b>List of Figures .....</b>	<b>xv</b>
<b>List of Tables .....</b>	<b>xvii</b>
<b>List of Schemes .....</b>	<b>xvii</b>
<b>Abbreviations .....</b>	<b>xviii</b>
<b>Chapter I: Introduction.....</b>	<b>23</b>
<b>I.1    Huntington’s disease pathology .....</b>	<b>23</b>
<b>I.1.1    History matters.....</b>	<b>23</b>
<b>I.1.2    Huntington's disease .....</b>	<b>23</b>
<b>I.1.3    Neuropathology and HD hallmarks .....</b>	<b>24</b>
<b>I.1.4    Symptoms .....</b>	<b>25</b>
<b>I.1.5    Treatments .....</b>	<b>26</b>
<b>I.2    Huntingtin protein .....</b>	<b>27</b>
<b>I.2.1    Htt structure .....</b>	<b>27</b>
<b>I.2.2    Physiological functions of Wildtype huntingtin protein .....</b>	<b>29</b>
<b>I.2.3    Effect polyQ tract expansion on physiological Htt functions .....</b>	<b>31</b>
<b>I.2.4    Htt proteolysis and N-terminal fragments .....</b>	<b>32</b>
<b>I.2.5    Httex1 .....</b>	<b>33</b>
<b>I.2.6    Httex1 aggregation models .....</b>	<b>36</b>

I.2.7	Httex1 proteins and peptides models .....	39
I.3	Htt Postranslational-modifications code .....	40
I.3.1	Post-translational modifications.....	40
I.3.2	Huntingtin post-translational modifications .....	43
I.3.3	Previous Protein models to study Nt17 PTMs and their Limitations .....	51
I.3.4	Httex1 semisynthesis.....	52
I.4	Objectives of the thesis.....	54
II.	<b>Chapter II: Mutant exon1 Huntingtin aggregation is regulated by T3 phosphorylation-induced structural changes and crosstalk between T3 phosphorylation and acetylation at K6 .....</b>	<b>55</b>
II.1	Abstract.....	56
II.2	Introduction .....	56
II.3	Results and Discussion .....	56
II.3.1	Semisynthesis of mutant Httex1 .....	56
II.3.2	Threonine 3 (T3) phosphorylation inhibits mutant Httex1 aggregation more effectively than T3D phosphomimetic mutation .....	64
II.3.3	Assessment of the effect of T3 phosphorylation on the structure of Nt17 peptide by NMR .....	69
II.3.4	Acetylation of single lysine residues in Nt17 does not affect the aggregation properties of WT or mutant Httex1.....	71
II.3.5	K6 acetylation reverses the inhibitory effect of pT3 in mutant Httex1.....	74
II.3.6	Conclusion .....	79
II.4	Experimental section .....	80
II.4.1	Materials and Instrumentation.....	80
II.4.2	Solid Phase Peptide Synthesis .....	81
II.4.3	Cloning and expression of His6-Ssp-Htt10-90(A10C)-23Q/43Q and His6-Ssp-Htt18-90(Q18C)-22Q/42Q.....	82
II.4.4	Purification of Htt-A10C-90 23Q/43Q and Htt-Q18C-90 22Q/42Q .....	82
II.4.5	Semisynthesis of Httex1 .....	83
II.4.6	Aggregation Analysis.....	84
II.4.7	Nt17 peptide analysis .....	86
II.5	Acknowledgements.....	87
III.	<b>Chapter III: Site-specific phosphorylation of Huntingtin exon 1 recombinant proteins enabled by the discovery of novel kinases .....</b>	<b>88</b>
III.1	Abstract.....	89
III.2	Introduction .....	89



III.3	Results and Discussion .....	92
III.3.1	Identification and validation of kinases that phosphorylated Nt17 at T3, S13, and S16 .....	92
III.3.2	SUMO-based strategy for the generation of phosphorylated WT and mutant Httex1 .....	96
III.3.3	Generation of fluorescently labeled (ATTO-565 maleimide) phosphorylated WT and mutant Httex1 .....	105
III.3.4	Generation of phosphorylated <sup>13</sup> C- and <sup>15</sup> N-labeled Httex1 suitable for NMR applications .....	109
III.3.5	Structural NMR studies of Httex1-23Q pT3 and Httex1-23Q pS13/pS16.....	113
III.3.6	Real-time monitoring of TBK1 phosphorylation of Httex1 suggests that S13 phosphorylation occurs first and primes phosphorylation at S16. ....	117
III.4	Conclusions .....	123
III.5	Experimental Section .....	125
III.5.1	Materials .....	125
III.5.2	Instruments.....	126
III.5.3	Kinase screening (IKPT service).....	126
III.5.4	Expression of His6-SUMO-Httex1-Qn (n= 23 or 43) .....	126
III.5.5	Expression of His6-SUMO-Httex1-Qn (n= 23 or 43) in minimal isotopic media... ..	127
III.5.6	Immobilized metal affinity chromatography (IMAC) purification .....	127
III.5.7	Quantitative <i>in vitro</i> phosphorylation of SUMO-Httex1-Qn by GCK and TBK1 ....	127
III.5.8	SUMO cleavage and HPLC purification .....	128
III.5.9	Fluorescent labeling with Atto-565-maleimide .....	128
III.5.10	Nuclear magnetic resonance (NMR) spectroscopy .....	128
III.5.11	Coexpression of Httex1-16Q-eGFP and kinases in HEK 293 cells .....	129
III.6	Acknowledgements.....	130
IV.	<b>Chapter IV: Elucidating the role of cross-talk between N-terminal methionine oxidation and neighbouring post-translation modifications in regulating the conformation of Nt17 and Httex1 aggregation using an integrative experimental and molecular simulation approaches.....</b>	<b>131</b>
IV.1	Introduction .....	132
IV.2	Results.....	134
IV.2.1	Production of oxidized mutant Httex1 proteins.....	134
IV.2.2	Oxidation at M8 delays the aggregation of mutant Httex1. ....	140
IV.2.3	Oxidation at M8 decreases the helicity of the Nt17 peptides.....	143
IV.2.4	Atomistic Molecular Dynamics (MD) reveals the consequences of M8 oxidation and its cross-talk with other PTMs on the Nt17 structure.....	147
IV.2.5	NMR structural studies using Httex1-oxM8 .....	148

<b>IV.3</b>	Discussion .....	152
<b>IV.4</b>	Conclusion.....	153
<b>IV.5</b>	Experimental section .....	154
<b>IV.5.1</b>	Materials.....	154
<b>IV.5.2</b>	Expression of His6-SUMO-Httex1-Qn (n= 23 or 43). .....	154
<b>IV.5.3</b>	Production of Httex1-43Q oxM8 and Httex1-43Q oxM8/pT3.....	155
<b>IV.5.4</b>	Semi-synthesis of Httex1-43Q oxM8/Ack6 .....	155
<b>IV.5.5</b>	UPLC-Based sedimentation assay.....	156
<b>IV.5.6</b>	Electron microscopy .....	156
<b>IV.5.7</b>	Circular dichroism.....	156
<b>IV.5.8</b>	Nuclear Magnetic Resonance spectroscopy.....	157
<b>IV.5.9</b>	Molecular Dynamics Simulations .....	158
<b>IV.5.10</b>	Data Analysis .....	158
<b>V.</b>	<b>Conclusion.....</b>	<b>159</b>
<b>V.1</b>	General conclusion .....	159
<b>V.2</b>	Future perspectives .....	161
<b>VI.</b>	<b>Bibliography .....</b>	<b>164</b>
<b>VII.</b>	<b>Curriculum Vitae .....</b>	<b>181</b>

## List of Figures

Figure I-1. Huntington's disease hallmarks. ....	24
Figure I-2. Schematic representation of Htt protein sequence and proteolytic sites. ....	27
Figure I-3. Htt full length structure. ....	29
Figure I-4. Schematic representation of the major physiological function of Htt. ....	30
Figure I-5. Httex1 domains. ....	34
Figure I-6. Httex1 aggregation models. ....	37
Figure I-7. Recombinant Httex1 production model ....	40
Figure I-8. Htt PTMs. ....	44
Figure I-9. Previous Httex1 models <i>in vitro</i> , cells, and Drosophila. ....	50
Figure I-10. Phosphomimetics limitations. ....	52
Figure I-11. Semisynthetic strategies for the production of WT Httex1 pT3 [310]. ....	53
Figure II-1. Purity analysis of the recombinant C-terminal fragments of Httex1 assessed by ESI-MS and RP-UPLC. ....	59
Figure II-2. Analytical characterization of unmodified Httex1-23Q proteins, unmodified, AcK6, AcK9 and AcK15 by RP-UPLC, MALDI-TOF and SDS-PAGE. ....	62
Figure II-3. Analytical characterization of Httex1-43Q proteins AcK6, AcK9 and AcK15 and pT3 by RP-UPLC, MALDI-TOF and SDS-PAGE. ....	63
Figure II-4. Analytical characterization of Httex1-43Q T3D, pT3/AcK6, pT3/AcK9 and pT3/AcK15 by RP-UPLC, MALDI-TOF and SDS-PAGE. ....	64
Figure II-5. Aggregation of mHttex1-pT3 and T3D compared to unmodified mHttex1 at 3 $\mu$ M. ....	65
Figure II-6. TEM length quantification of Httex1-43Q, Httex1-43Q pT3 and Httex1-43Q T3D. ....	66
Figure II-7. TEM analysis of mutant Httex1. ....	66
Figure II-8. Concentration dependence of Httex1-43Q pT3 aggregation. ....	67
Figure II-9. Statistical analysis of AFM images to compare Httex1-43Q unmodified, pT3 and T3D. ....	69
Figure II-10. NMR and Circular dichroism analysis of the Htt1-19 peptides. ....	70
Figure II-11. Aggregation of single lysine acetylated mHttex1 and mHttex1 phosphorylated at T3 and acetylated at-AcK6, AcK9, or AcK15. ....	72
Figure II-12. Characterization of the aggregation of Httex1-23Q Ac6, AcK9 and AcK15 compared to unmodified Httex1-23Q over time by sedimentation (A), TEM (B) and CD (C). ....	73

Figure II-13. TEM analysis of mutant Httex1 (pT3/Ack6-43Q, pT3/Ack9-43Q and pT3/Ack15-42Q Q18A).....	75
Figure II-14. Aggregation characterization of httex1-43Q Ack6 and pT3/Ack6 compared to Httex1-43Q pT3 by AFM.....	76
Figure II-15. <i>In vitro</i> aggregation for Httex1-43Q pT3 and pT3/Ack6.....	77
Figure II-16. NMR analysis of the effects of Acetylation on Htt peptides.....	78
Figure II-17. Circular dichroism analysis of pT3, Ack6 and pT3/Ack6 Ac-Htt2-17 peptides. ....	79
Figure III-1. <i>In vitro</i> T3 kinases validation.....	93
Figure III-2. Coexpression of Httex1-16Q-eGFP in HEK 293 cells with TNIK, HGK or GCK. ....	94
Figure III-3. <i>In vitro</i> phosphorylation of Httex1-43Q by GCK or TBK1.....	96
Figure III-4. SUMO-Httex1-Qn IMAC purification.....	98
Figure III-5. SUMO-based strategy for the <i>in vitro</i> quantitative production of phosphorylated Httex1 23Q and 43Q using TBK1. ....	100
Figure III-6. SUMO-Httex1-Qn phosphorylation by GCK and TBK1.....	103
Figure III-7. Monitoring of the phosphorylation reaction of SUMO-Httex1-23Q .	104
Figure III-8. Generation of phosphorylated and labelled Httex1 proteins.....	106
Figure III-9. Phosphorylation of SUMO-Httex1-Qn P90C. ....	107
Figure III-10. <i>In vitro</i> ATT-565 labelling of phosphorylated proteins. ....	108
Figure III-11. Optimizing the expression of SUMO-Httex1-Qn in minimal media.	110
Figure III-12. Expression, phosphorylation and purification of Httex1-Qn by GCK and TBK1. ....	111
Figure III-13. Phosphorylation and characterization of <sup>13</sup> C/ <sup>15</sup> N phosphorylated Httex1. ....	112
Figure III-14. NMR studies of Httex1-pT3 and pS13/pS16. ....	115
Figure III-15. NMR studies of Httex1-pT3 and pS13/pS16 in function of pH or TFE.	116
Figure III-16. Real-time monitoring of TBK1 phosphorylation of Httex1. ....	119
Figure III-17. <sup>1</sup> H, <sup>13</sup> C plane of a CBCA(CO)NH spectrum collected after 21 hours of reaction between Httex1-23Q and TBK1. ....	120
Figure III-18. Library of tools presented in this paper.....	125
Figure IV-1. Chemical, semisynthesis and enzymatic methods for the generation of mHttex1 with single or multiple PTMs.....	136
Figure IV-2. Purification, oxidation and phosphorylation of mHttex1.....	138
Figure IV-3. Semisynthesis of mHttex1-oxM8/Ack6.....	139

Figure IV-4. <i>De novo</i> aggregation of mutated mHttex1 with different PTMs.....	141
Figure IV-5. Over-time aggregation monitoring by electron microscopy of mHttex1 oxM8 compared to unmodified mHttex1 (at 10 uM). .....	143
Figure IV-6. Far-UV CD spectra of Nt17-WT, and Nt17-oxM8, Nt17-AcK6, Nt17-AcK6/oxM8, Nt17-pT3 and Nt17-pT3/oxM8 at 60 $\mu$ M.....	144
Figure IV-7. CD spectra and helical content for various Nt17 peptides.....	146
Figure IV-8. CD Vs MD helical content of the Nt17 peptides.....	148
Figure IV-9. NMR characterization of Htt exon 1 with M8 oxidized, compared to unmodified Htt exon 1. ....	149
Figure IV-10. Overlay of $^1\text{H}$ , $^{15}\text{N}$ HSQC spectra of wild type exon 1.....	151

## List of Tables

Table I-1. A list of some of the major types of post-translational modifications and the corresponding residues and regulators ( adapted from [240]) .....	41
Table II-1. List of the produced protein showing expected masses and final yields.....	61
Table II-2. List and sequence of the peptides used in the NMR and Circular dichroism analysis.....	71
Table III-1. Expected and observed molecular weights for all the protein generated in this study.....	95
Table III-2. $^1\text{H}$ , $^{15}\text{N}$ , CA, CB assignments for human Httex1 unmodified and pS13pS16 in our working conditions, pH 7, 25 $^\circ\text{C}$ .....	121
Table IV-1. Helical content (%) calculated for the different peptides at 60 $\mu$ M... ..	145

## List of Schemes

Scheme II-1. GST and Intein strategies for the synthesis of Htt(A10C-90)-43Q .....	57
Scheme II-2. Semisynthetic strategies for the generation of Httex1 with PTM's in the Nt17 domain .....	58
Scheme II-3. Semisynthesis of mutant Httex1 optimization.....	60
Scheme III-1. SUMO-based strategy for the generation of phosphorylated Httex1 proteins. ....	97

## Abbreviations

A10C:	Alanine at position 10 is mutated to a cysteine
Ac-K6/K9/K15:	Lysine acetylation at k6, k9, k15
ACN:	Acetonitrile
AFM:	Atomic force microscopy
Akt :	Protein kinase b
ASOs:	Gene antisense oligonucleotides
AUC:	Analytical ultra-centrifugation
BAC:	Bacterial artificial chromosome
BDNF:	Brain-derived neurotrophic factor
BiFC:	Bimolecular complementation cellular assay
C.elegans:	Caenorhabditis elegans
CAG:	Cytosine-adenine-guanine
CBP:	(Creb)-binding protein
CDK5:	Cyclin-dependent kinase 5
CI:	Cytoplasmic inclusions
CK2:	Casein kinase 2
CREB:	Camp-response element (creb)-binding protein
cryo-EM:	Cryogenic electron microscopy
CV:	Column volumes
DUBs:	Deubiquitination enzymes
E.coli:	Escherichia coli
e.g.:	For instance
E1:	Ubiquitin-activating enzyme
E3:	Ubiquitin ligase
EGFP:	Enhanced green fluorescent protein
EM:	Electron microscopy
EPL:	Expressed protein ligation
EPR:	Electron paramagnetic resonance
ER:	Endoplasmic reticulum
FCS:	Fluorescence correlation spectroscopy
FDA:	Food and drug administration
FRET:	Förster resonance energy transfer
GABA:	Gamma-aminobutyric acid
GST :	Glutathione-s-transferase
H <sub>2</sub> O <sub>2</sub> :	Hydrogen peroxide
HAP1:	Huntingtin-associated protein 1
HAP40:	Huntingtin-associated protein 40
HD:	Huntington's disease
HDACs:	Histone deacetylases
HEAT:	Huntingtin, elongation factor 3 (ef3), protein phosphatase 2a (pp2a), and the yeast kinase tor1.

HEPES:	4-(2-hydroxyethyl)-piperazin-1-ethanesulfonsaure
HFIP:	Hexafluoroisopropanol
HIP14:	Huntingtin interacting protein 14
Hsp:	Heat-shock proteins
HTT:	Huntingtin gene
Htt:	Huntingtin protein
Httex1:	Huntingtin exon 1
Httex1-23Q :	Httex1 with 23 glutamine ( referred also as wt httex1)
HYPK :	Huntingtin yeast two-hybrid protein k
IBs:	Inclusion bodies
IKK $\beta$ :	Ikb kinase
INI:	Intranuclear
IPTG:	Isopropyl- $\beta$ -d-thiogalactopyranosid
KATs:	Lysine acetyltransferases
KDACs:	Lysine deacetylases
LB:	Lysogeny broth
LC/MS:	Liquid chromatography–mass spectrometry
M8P:	Methionine at position 8 to proline
MALDI:	Matrix-assisted laser desorption ionization
MALS:	Multi-angle light scattering
MBP:	Maltose-binding-protein
MCI:	Mild cognitive impairment
mHtt:	Huntingtin with expanded polyq-lengths (mutant htt)
mHttex1:	Mutant huntingtin exon1 ( also httex1-43q)
MPAA:	Mercaptophenylacetic acid
MRE:	Molar residual ellipticity
MSN:	Medium spiny neurons
MsrA and B:	Methionine sulfoxide reductases a and b
MWCO:	Molecular weight cut-off
Nbz:	N-acylbenzimidazolinone
NCL:	Native chemical ligation
NES:	Nuclear export signal
NeuroD:	Neuron-specific transcription factor
NF-kB:	Nuclear factor kb
Ni-NTA:	Nickel-nitrilotriacetic acid
NLK:	Nemo-like kinase
NLS:	Nuclear localization signal
NMR:	Nuclear magnetic resonance
NOESY:	Nuclear overhauser enhancement spectroscopy
NRSF:	Neuron-restrictive silencer factor
Nt17:	First 17 n-terminal amino acids
Nt17-Q7:	Nt17 domain linked to 7 glutamines at its c-terminal
NUMA:	Nuclear mitotic apparatus
OD:	Optical density

oxM8:	Oxidation at methionine 8
p53:	Tumor suppressor protein 53
PBS:	Phosphate-buffered saline
PIAS:	Protein inhibitor of activated stat
PIAS1 :	Protein inhibitor of activated stat1
PMSF:	Phenylmethanesulfonyl fluoride
PMSF:	Phenylmethylsulfonfluoride
PolyP:	Poly proline
polyQ:	Poly glutamine tract
PP1:	Protein phosphatase 1
PPII:	Polyproline type ii
PRD:	Proline rich domain
pS13:	Phosphorylated serine 13
pS16:	Phosphorylated serine 16
pT3:	Phosphorylated threonine 3
PTMs:	Post-translational modifications
Q18C:	Glutamine at position 18 is mutated to a cysteine
Q23:	23 glutamines
Q78:	78 glutamines
R6/2 transgenic:	Transgenic mouse expressing human mutant httex1
REST:	Repressor element-1 transcription factor
RNAi:	Rna interference
ROS:	Reactive oxygen species
RP-HPLC:	Reversed-phase high performance liquid chromatography
SDS-PAGE:	Sodium dodecyl sulfate polyacrylamide gel electrophoresis
SEC:	Size-exclusion chromatography
SGK:	The serum- and glucocorticoid- induced protein kinase-1
SH3:	Src homology-3
smFRET:	Single-molecule förster resonance energy transfer
SP1:	Specificity protein-1
SPPS:	Solid-phase peptide synthesis
<i>Ssp</i> :	<i>Synechocystis sp</i>
SUMO:	Small ubiquitin-like modifier
SUMO-K6/K9/K15:	Lysine SUMOylation at K6, K9, K15
T3D:	Mutation of threonine at position 3 to aspartate
TCEP:	Tris-2-carboxyethyl-phosphine
TEV:	Tobacco etch virus
TFA:	Trifluoric acid
TFE:	Trifluoroethanol
ThS:	Thioflavin s
ThT:	Thioflavin t
TrkB:	Tyrosine receptor kinase b
TRX:	Thioredoxin
Ub-K6/K9/K15:	Lysine ubiquitination at K6, K9, K15



## Abbreviations

---

ULK1:	Autophagy activating kinase 1
ULP1:	Ubiquitin-like protein-specific protease 1
UPLC:	Ultra-high performance liquid chromatography
WB:	Western blot
WT Htt:	Huntingtin with unexpanded polyQ-lengths (wildtype htt)
WT:	Wild type
XL-MS:	Cross-linking by mass spectrometry



# I. Chapter I: Introduction

## I.1 Huntington's disease pathology

### I.1.1 History matters

Huntington's disease (HD) has long been known in history as “chorea”, the most prominent and visible symptom of HD [1]. Chorea is characterized by involuntary, disordered, sudden and rapid movements [1, 2]. Etymologically, the term “chorea” originates from the ancient Greek *khoreía*, which is a dance involving quick body movements [3]. The first descriptions of chorea were made in the 16<sup>th</sup> century when people suffering from the symptoms were often considered possessed by devils and were executed [3, 4]. Three centuries later, Georges Huntington gave the first thorough description of HD pathology, which was later named after him [5]. In particular, he accurately determined the hereditary nature of HD and precisely described the different pathological phenotypes of the disease as it is known today [5]. In 1993 fifty-eight researchers from six independent laboratories formed the "Huntington's Disease Collaborative Research Group" with a unique goal to advance the knowledge of HD pathology [6]. Together, they identified the mutation responsible for HD in the gene *IT15*, also called *HTT* [6], that was discovered in 1993 [6] and mapped to chromosome 4 p-arm locus 16.3. This cornerstone achievement ushered in a new era of the molecular biology of HD.

### I.1.2 Huntington's disease

Huntington's disease (HD) is a rare, devastating neurodegenerative disorder with a prevalence of 5–12 per 100,000 in populations of European descent [7-9]. HD is an autosomal dominant fully-penetrant hereditary disease [10] characterized by the poly-expansion of simple repeats in the *HTT* gene [6]. In healthy subjects, the *HTT* gene has a repetition of CAG trinucleotides of variable lengths between 6 to 35 repeats in its first exon (*Httex1*) [8]. *HTT* encodes the huntingtin protein (*Htt*) that, when translated, has an equivalent succession of glutamines (Q) starting from the 18<sup>th</sup> amino acid [11]. It is generally acknowledged that *Htt* with 36 or more polyQ repeats is pathogenic [12, 13], and is referred to as mutant huntingtin (*mHtt*) [11, 14]. Several studies have shown that the length of the CAG repeat is inversely correlated with the age of onset and severity of the disease [13, 15-17]. While the expansion of 40 to 50 repeats is generally associated with HD developing in adulthood, juvenile-onset of HD is linked to an expansion of higher than 60 repeats of CAG [18]. HD syndrome manifests itself through psychiatric and cognitive symptomatology at the early prodromal stages of the disease [19], followed by motor dysfunctions, likely resulting from underlying neurodegeneration leading to brain atrophy [20].

### I.1.3 Neuropathology and HD hallmarks

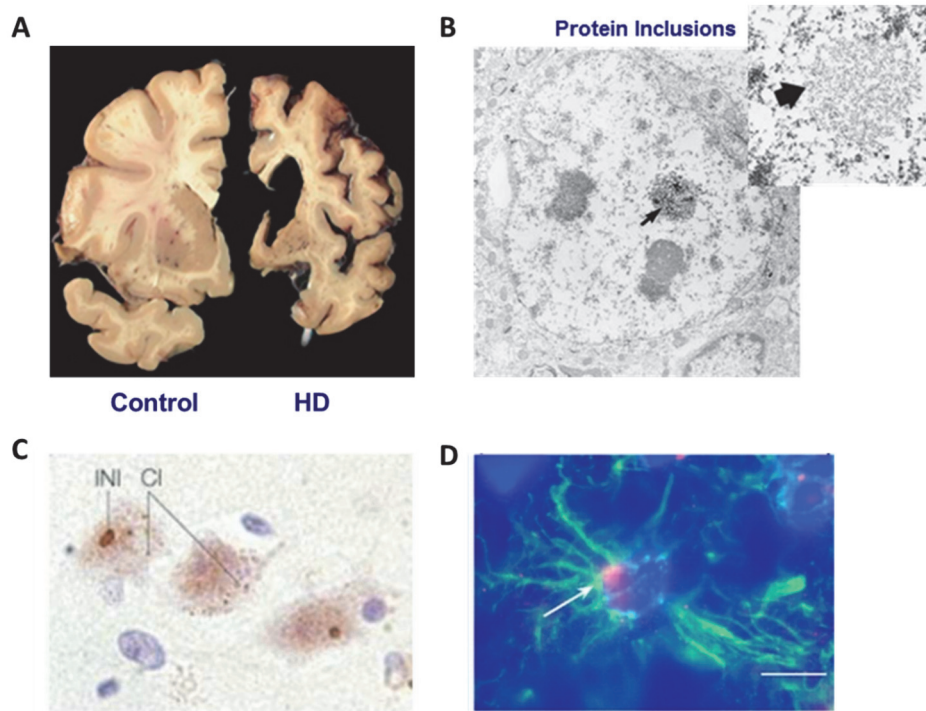


Figure I-1. Huntington's disease hallmarks.

**(A)** comparison between healthy and HD brain showing the loss in brain tissues (courtesy of the Harvard Brain Tissue Resource Center). **(B)** Electron microscopy of inclusion bodies in the HD brain tissues (adapted from [21]). **(C)** intranuclear (INI) and cytoplasmic inclusions (CI) in the motor cortex of an HD patient (adapted from [22]). **(D)** HD brain tissues stained with EM48 (anti-Htt aggregates), indicating the Htt nuclear aggregates (white arrow) (adapted from [23])

Pathological changes associated with HD can be detected at the whole-brain level (Figure I.1-A) and at the cellular level (Figure I.1-D). The brain neuropathology of HD is characterized by degeneration of the neurons located in the caudate nucleus and the putamen in the basal ganglia at the early stages of the disease [24–26], followed by the atrophy of the striatum [27, 28] (Figure I.1). In particular, the first cells to degenerate are gamma-aminobutyric acid (GABA)-ergic medium spiny neurons (MSNs). MSNs project to the external globus pallidus, which plays an essential role in the control of voluntary movements [25, 29, 30]. Analysis of *postmortem* HD brains revealed severe atrophy of the cerebral neocortex (layers III, V, and VI) as the disease progressed. Other brain regions, such as the hippocampus, thalamus, subthalamus, globus pallidus, substantia nigra, and cerebellum, are also affected in HD [31, 32]. Typically, the brain of an HD patient exhibits a loss of 25–30% of its mass in the advanced stages of the disease [33].

The second hallmark of HD is the formation of intracellular nuclear and cytoplasmic proteinaceous inclusions (also called inclusion bodies (IBs) [34]) (Figure I.3-C). IBs are found in neurons and glial cells [35, 36] in several regions of the brain, including the putamen, the caudate nucleus, and the cerebral cortex [21, 22, 37-39]. These inclusions contain mHtt, its N-terminal fragments, as well as other molecular species of mHtt protein [40, 41]. IBs were observed in both mouse models and patient brains [34], and their formation, which was specific to mHtt, occurs before the onset of HD symptoms and neurodegeneration [42].

The pathogenic nature of the IBs and their role in the pathogenesis of HD remain subjects of active investigation and debate. Depending on the cell type and the stage of the pathology progression, the aggregates could be either cytotoxic or confer cytoprotection [43-45]. In fact, IBs were found in all the neuronal cell types, including those which are not vulnerable to neurodegeneration (such as interneurons) [43]. Additionally, it was found that the death of neurons was not correlated with the presence of aggregates [46], while the inhibition of aggregation promoted neuronal death [47]. Finally, other studies showed that the neurons with a higher amount of inclusions were more likely to survive [35, 48-50]. However, even though the aggregates were not directly linked to cell death, they could nevertheless interfere with intracellular organelle dynamics and participate in deforming the endoplasmic membranes, particularly the endoplasmic reticulum (ER), interfering with its activity [51, 52]. Furthermore, aggregates were shown to aggravate the pathology by spreading in the brain through cell-to-cell transmission [53, 54].

## **I.1.4 Symptoms**

### **I.1.4.1 Motor symptoms**

Clinical diagnosis of HD relies on genetic testing or positive family history of the disease, psychological and motor symptoms' evaluation [20]. The timeline of motor symptoms' onset is heavily dependent on the patient's *Htt* CAG repeat number as well as other modifying genetic factors [55] but predominantly occurs between the ages of 35 and 40 [7, 56]. The motor symptoms observed in HD patients include chorea (abrupt brief non-stereotyped movements), dystonia (uncontrollable muscle contractions), akinesia (the inability to perform certain movements) [57], bradykinesia (slowness of movement) [58], impaired gait [59], impaired posture and balance [60], slow or abnormal eye movements [61] and difficulty with speech [62] or swallowing [63]. The progression of motor symptoms may manifest in eating difficulties in the patients, such as dysphagia. This may lead to leading to drastic weight loss [64] and even severe pulmonary infections and death [65].

### **I.1.4.2 Cognitive symptoms**

The cognitive symptoms are challenging to detect at early stages due to the lack of standardized measurement tools. However, according to the MCI scale (for "Mild Cognitive Impairment"), it is estimated

that 40% of pre-symptomatic patients have cognitive impairments [66]. The cognitive abilities of HD patients progressively deteriorate and result in subcortical dementia, characterized by slowness of thought [67], memory, and attention problems [68]. Disorders involving visual cognition such as facial discrimination and visual-spatial perception have also been described in carriers of the non-symptomatic mutation and during the early stages of the disease [69, 70].

#### **I.1.4.3 Psychiatric symptoms**

HD patients show changes in personality that could be detected much earlier than observable motor symptoms. In addition to the motor and cognitive symptoms, patients very often suffer from depression, together with suicidal thoughts [71], making HD the neurodegenerative disease with the highest suicide rate [72]. HD patients are very often anxious, irritated, and apathetic [73]. It is generally thought that behavioral abnormalities (including depression, aggression, disinhibition, anxiety) are associated with the genetic susceptibility of the patients to these conditions, whereas chronic manifestations (apathy, lethargy, repetition, hallucinations, mania) may reflect the progressive neurodegeneration processes [74]. The gravity of the behavioral changes increases as the pathology progresses [74]. These psychiatric problems are often the most difficult to handle for the patients and their families and may require hospitalization [75].

#### **I.1.5 Treatments**

There is currently no cure for HD. The available treatments are predominantly symptomatic for either motor or psychiatric disease manifestations. Drugs such as tetrabenazine (Xenazine) and deutetabenazine (Austedo) [76] are the only medications currently approved by the FDA to treat motor symptoms [77]. These monoamine transport inhibitors allow dopamine depletion in the central nervous system, making it possible to suppress the involuntary jerking and writhing movements associated with HD [78]. Management of psychological and psychiatric symptoms can also be challenging. Drugs such as citalopram (Celexa) and escitalopram (Lexapro) may also be used to treat anxiety, depression, and irritability in HD patients [79]. Some patients also need anti-psychotic [80] and anti-epileptic medicines [81]. In addition to medications, some patients may benefit from psychotherapy and family counseling. A concerted effort of professionals such as physiotherapists, dieticians and speech therapists may be required to preserve the patient's autonomy as long as possible [82]. Although these treatment methods target the symptoms of HD to increase the life quality of HD patients, most of them cause serious side effects.

The researchers in the HD community are focusing their efforts on the discovery of new therapeutics to cure HD and prevent its progression. Recently, novel approaches for targeting HD pathology have emerged and are in clinical trials or at preclinical stages [83]. The main aim of these strategies is the lowering of mHtt. Recent advances in gene therapy, such as Gene Antisense Oligonucleotides (ASOs), RNA interference (RNAi)

and zinc-finger protein and CRISPR-CAS9 system [84] paved the way for the discovery of new HD therapies and allowed the start of clinical trials to explore the potential utility of intrathecal allele-specific and non-allele-specific ASO and miRNA gene therapy [83, 85]. Regardless of all these advances, the HD field is still missing robust molecular tools for the monitoring of the consequences of these therapies during clinical trials.

## 1.2 Huntingtin protein

### 1.2.1 Htt structure

Huntingtin (Htt) is a large intracellular protein comprising 3,144 amino acids (Figure I.2) [6]. Experimental investigations of the structural properties of Htt and their roles in regulating its aggregation and function in health and disease have been limited mainly by the technical complexities brought by the large size and conformational flexibility of the protein. Pure full-length Htt is also notoriously difficult to produce in the quantities sufficient for use in high-resolution biophysical analyses, such as X-ray crystallography or nuclear magnetic resonance (NMR).

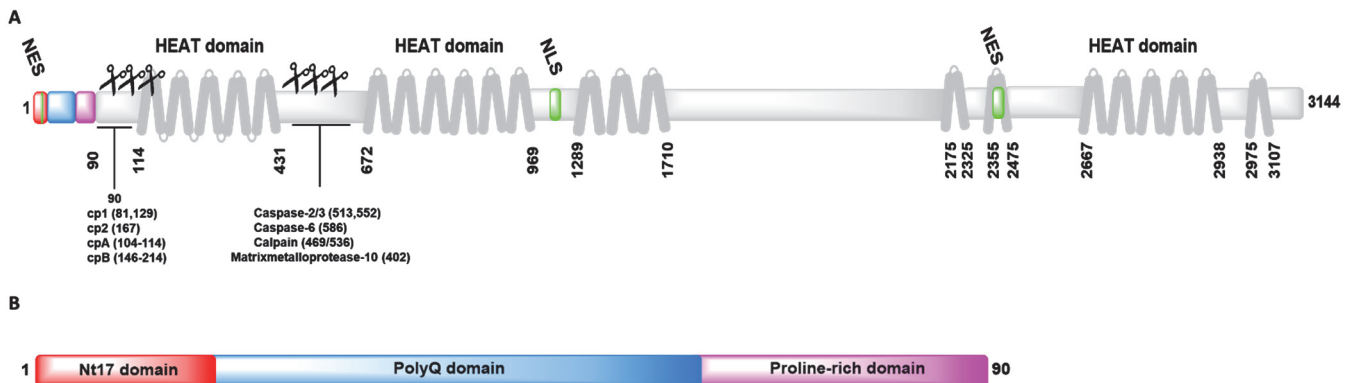


Figure I-2. Schematic representation of Htt protein sequence and proteolytic sites.

Schematic representation of full-length Htt with the Nt17 domain in red, the polyQ domain in blue, and the proline-rich domain in pink. The HEAT repeats are indicated by grey cylinders. Nuclear export signal (NES) sequence and nuclear localization signal (NLS) are highlighted in green. Protease cleavage sites and their responsible enzymes are indicated below the protein scheme. (B) Schematic representation of Httex1 different domains.

Htt is ubiquitously expressed and is localized mainly in the cell cytoplasm, where it is associated with intracellular membranous organelles (endoplasmic reticulum, Golgi, and the mitochondria) [11, 86, 87]. In neurons, Htt is also found in neurites and at the synapses, where it is associated with microtubules, clathrin-coated vesicles, caveolae, and endosomes [88-90]. Htt contains a cytoplasmic retention signal at the N-terminus and a nuclear export signal at the C-terminus (Figure I.2). These sequences enable nuclear translocation of Htt, and modifications of these Htt regions affect its subcellular localization [91-93]

Functional domains of Htt include between 16 and 36 HEAT repeats (Huntingtin, Elongation factor 3, the PR65/A subunit of protein phosphatase 2A and the lipid kinase Tor) ranging from 28 to 36 residues [94], which are distributed throughout the entire sequence of the protein [11, 95, 96]. HEAT repeats are known to regulate protein-protein interactions, intracellular transport, and microtubule dynamics [94, 97, 98]. HEAT repeats form spherical structures – HEAT domains – that assemble into three-dimensional structures called  $\alpha$ -ROD [99].  $\alpha$ -RODs are composed of anti-parallel  $\alpha$ -helix stacks. In Htt amino acids 114–413, 672–969, and 2667–2938 form three  $\alpha$ -ROD domains [99] (Figure I.2-A).

Full-length Htt purified from insect cells exhibited a circular dichroism (CD) spectrum that was consistent with a folded protein with high  $\alpha$ -helical content (Figure I.3-A and 3-B), due to the presence of the HEAT repeats within Htt sequence [100, 101]. Based on the CD, electron microscopy (EM) images and molecular modeling studies, Li et al. proposed a structure that consists of a solenoid [102] (Figure I.3-C and Figure I.3D). Vijayvargia et al. confirmed these findings using three-dimensional reconstruction of negatively-stained full-length Htt using EM analysis supplemented with structural characterization of the protein after cross-linking by mass spectrometry (XL-MS) (Figure I.3-E). These authors proposed a spherical  $\alpha$ -helical solenoid structure of full-length Htt that comprised an internal cavity, which was formed by intramolecular interactions between the different domains of Htt [101] (Figure I.3-E). More recently, a high-resolution cryogenic EM (cryo-EM) structure of full-length Htt in complex with HAP40 (Figure I.3-F) was determined [103]. It was demonstrated that Htt maintained a predominantly  $\alpha$ -helical structure composed of the three main domains. Two larger domains both contained multiple HEAT repeats at the N- and C-terminal and were connected by a smaller bridge domain composed of tandem repeats [103]. Nevertheless, the Htt domain encoded by the first exon of *Htt* (protein product Httex1) that contains the polyQ repeat, which harbors the disease-causing mutation in HD patients, was not resolved as well as the unstructured domain between the HEAT repeats [103].



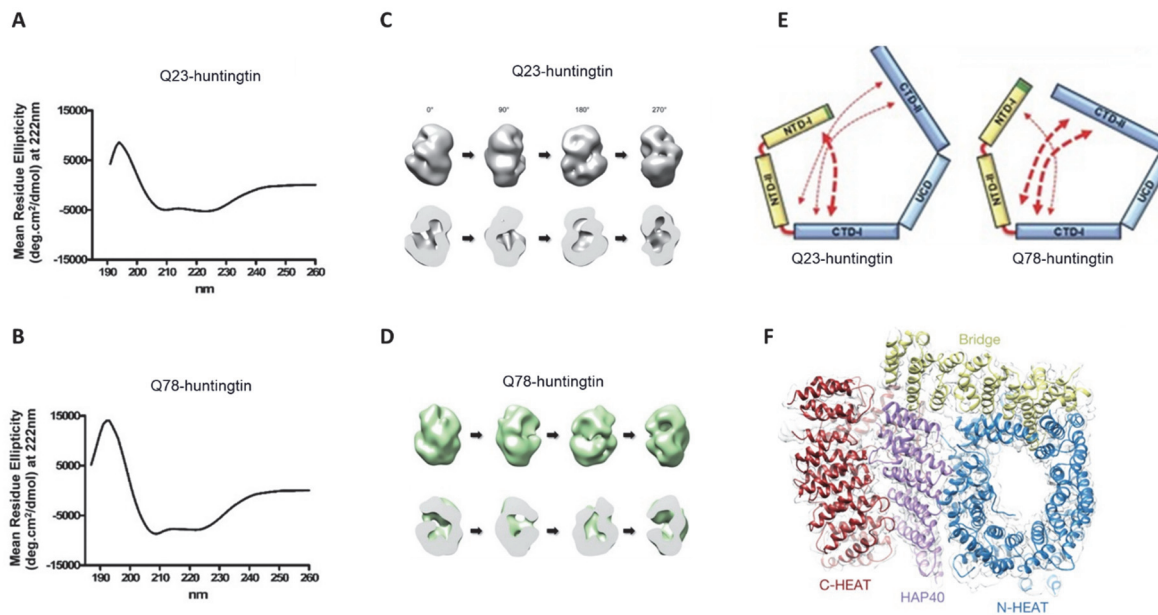


Figure I-3. Htt full length structure.

(A-B). Reported circular dichroism for WT and mutant full-length Htt purified from insect cells (from [101]). (C-D) View of 3D EM map of Q23 and Q78-huntingtin and proposed intramolecular interaction (E) based on XL-MS (from [101]). (F) Resolved structure of Htt full-length in complex with HAP40 based on cry-EM (adapted from [103]).

## I.2.2 Physiological functions of Wildtype huntingtin protein

Htt is considered as a scaffold protein that interacts with other proteins and regulates multiple cellular processes, such as transcription, cell trafficking, endocytosis, survival, and metabolism [96]. Figure I.4 summarizes some of the main physiological functions of Htt protein.

**Vesicle trafficking:** Vesicle transport is one of the multiple functions of WT Htt, where Htt acts as a molecular scaffold that recruits the Dynein/Dynactin complex to regulate both anterograde and retrograde transport of organelles, including autophagosomes [104], endosomes, and lysosomes [105, 106], synaptic precursor vesicles [107], BDNF (brain-derived neurotrophic factor) vesicles [108], and many more. To participate in the molecular motor complex, Htt interacts directly with dynein or indirectly *via* the interaction with Huntingtin-associated protein 1 (HAP1) and p150 dynactin subunit [109-112]. Overexpression of WT Htt improves organelles transport [108], and its deletion in drosophila resulted in malfunctioning of the axonal transport and eye degeneration [113], thus confirming the critical role of normal Htt protein in vesicles transport.

**Cell cycle and development:** Htt protein was also shown to be located at the cell poles of the mitotic spindle and scaffold cell division [114]. During mitosis, Htt facilitates the recruitment of NUMA and LGN to the mitotic spindle poles [114, 115]. Then, WT Htt interacts with Kinesin-1, and assists the transport of the complex

Dynein/dynactin/NUMA/LGN to the cell cortex [115]. This enables the correct orientation of the mitotic spindle during cell division [115].

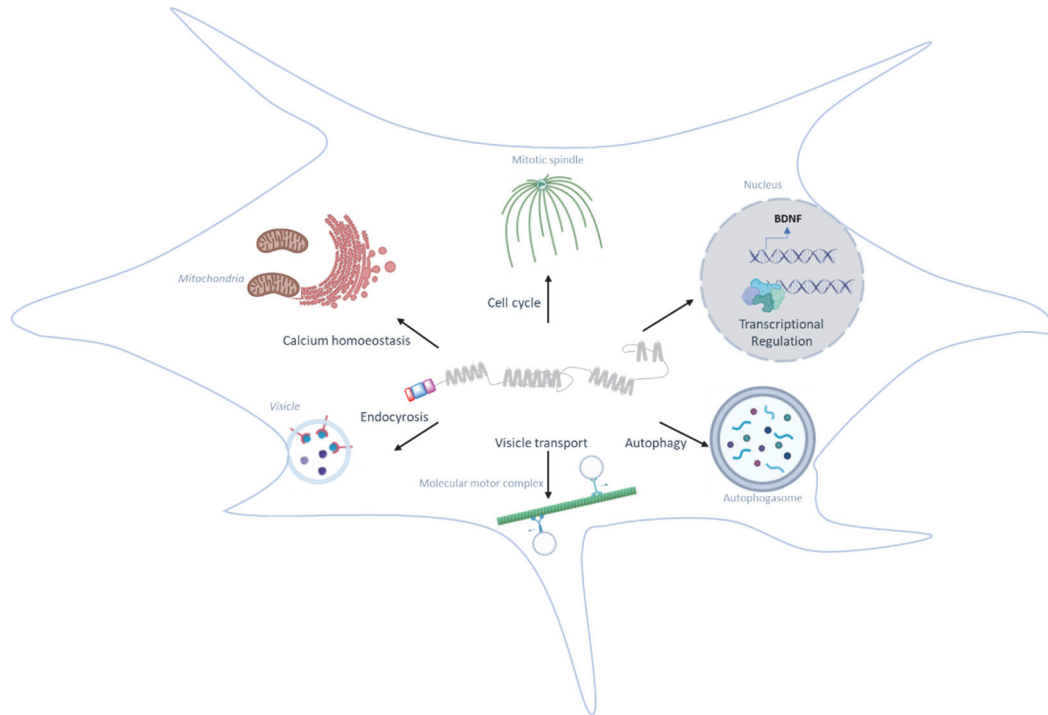


Figure I-4. Schematic representation of the major physiological function of Htt.

The Htt protein has been shown to be essential for the development and neurogenesis [116]. Reducing its levels during embryogenesis causes brain malformation [117], and knockdown of Htt in mice is lethal. These findings demonstrate that Htt is vital for normal embryonic development [116, 118].

*Pro-survival:* Several studies have highlighted the importance of the WT Htt pro-survival properties. It has indeed been found that its depletion makes cells more vulnerable to death [119, 120]. Htt-induced neuroprotection is related to the apoptotic machinery of the cell, where it inhibits the activation of both caspase-3 and -9 [121, 122]. The Htt pro-survival mechanism is also related to the BDNF regulation mechanism [108]. BDNF is an important growth factor that supports the survival of all types of existing neurons, both in the central and peripheral nervous systems [123]. Furthermore, BDNF is considered to be one of the most important factors that stimulate neurogenesis [124]. Htt facilitates the transcription of the BDNF gene and boosts the transport of containing BDNF-containing vesicles to the cortico-striatal synapses [108]. When BDNF is released in the synapses, it activates TrkB receptors, which are essential for survival signaling [106].

*Transcriptional regulation:* Although Htt is cytoplasmic, it is able to translocate to the nucleus and interacts with several transcription factors, such as the neuron-specific transcription factor NeuroD, the cAMP-response element (CREB)-binding protein (CBP) [125], the nuclear factor  $\kappa$ B (NF- $\kappa$ B), the tumor suppressor protein 53 (p53) [94, 126, 127], and the specificity protein-1 (SP1) [128]. Furthermore, it also interacts with transcription activators, repressors, and nuclear receptors [129]. For example, huntingtin inhibits the repressor element-1 transcription factor/neuron-restrictive silencer factor (REST/NRSF) that represses the BDNF transcription [130]. Htt also contributes to chromatin remodeling and, therefore, regulates DNA accessibility [131]. Htt plays important roles in the transcription of multiple proteins; therefore, it mediates important cellular events, such as inflammatory responses, cell division, DNA repair, cellular development, cell survival, cellular stress, and apoptotic cell death [132].

*Autophagy:* Htt has a key role in the regulation of autophagy. Htt promotes the binding of autophagosome component LC3 to the autophagy receptor p62, thus boosting the recruitment to the autophagosome of ubiquitinated proteins, which enables a selective cargo loading of autophagosomes [133] [134]. Moreover, Htt promotes autophagy by binding to ULK1 [133] and can also interact with myosin VI, an actin-based motor protein [135, 136], to mediate the transport of autophagosomes, which is crucial for both their maturation and cargo degradation [135, 136].

### **1.2.3 Effect polyQ tract expansion on physiological Htt functions**

The polyQ expansion was shown to alter Htt protein-protein interactions [137], subcellular localization [138], and structure [101], and as a result, alter many aspects of Htt normal function(s).

When Htt is mutated, its interaction with the molecular motors complex is disturbed [108]. In fact, the expanded polyQ enhanced the interaction between mutant Htt, HAP1, and dynein [108]; as a result, these proteins interact less with microtubules causing axonal transport deficiency [108]. The anterograde transport of BDNF-containing vesicles is also affected by mutant Htt, resulting in neuronal loss [139]. Additionally, the expansion of the polyQ tract alters the binding between TrkB-containing vesicles and the microtubules in striatal neurons and reduces their transport [106].

mHtt can bind and alter the activity of many transcription factors, such as CBP, and increases its degradation. This renders CBP unavailable to bind with CREB, which causes a decreased expression of pro-survival genes [125, 140, 141]. In contrast, mHtt binds less to REST/NRSF, which causes it to accumulate in the nucleus leading to inhibition of BDNF synthesis [142], which has been proposed to contribute to neuronal death in HD [142].

WT Htt was shown to participate as a scaffold for autophagosomes transport [104]. The expression of autophagy-related genes is decreased in HD patients [143]. The transport of autophagosomes was shown to be affected by mHtt [104]. It has been shown that interaction between mHtt, p62, and ubiquitin chains are decreased, resulting in cargo load failure [144]. mHtt also inhibits the fusion between the autophagosomes and the lysosomes, which leads to an accumulation of undesired materials and empty autophagosomes in the cytoplasm [144]. Autophagy dysfunction reduces the clearance of mHtt and, as a result, increases its aggregation and cellular death [145].

#### **1.2.4 Htt proteolysis and N-terminal fragments**

One of the prevailing hypotheses today proposes that fragments of Htt, in particular those bearing the polyQ repeat, rather than the full-length protein, play a central role in the pathogenesis of HD. Several lines of evidence support this hypothesis; 1) N-terminal Htt fragments were found in the *postmortem* brain tissues of HD patients, as well as in animal and cellular models of HD [21, 41, 146-148]; 2) several proteases were shown to cleave Htt protein (Figure 1.2-A), including caspase 2/3 (cleave at residues 513/552), caspase 6 (cleave at residues 586), caspase 3 (cleave at residues 513), and the calpain (cleave at residues 469/536) [149-151]; and 3) mutant Htt appears more prone to proteolysis than Htt with a non-pathogenic number of Qs [152].

It has also proposed that the generation of Htt C-terminal fragments alters the activity of dynamin-1, which interferes with the dynamics of the endoplasmic reticulum and autophagy [153, 154] and causes cytotoxicity. Together, these observations suggest that either proteolytic enzymes' activity is increased under pathological conditions in HD, or that the Htt polyQ expansion causes structural changes that increase the accessibility of the mHtt cleavage sites resulting in the generation of N-terminal fragments *in vivo*, or both. It is plausible that the polyQ domain becomes more exposed in the fragments compared to the full-length protein, which could explain the increased aggregation propensity of mutant Htt fragments compared to the full-length protein. Htt fragments were also found to translocate into the nucleus and form toxic nuclear inclusions [41, 155, 156]. Some studies have suggested that the sizes of the N-terminal Htt fragments were inversely correlated with their toxicity and aggregation, with the shorter fragments appearing more toxic and prone to aggregation than longer fragments [92, 147]. Consequently, the shorter truncated Htt proteins and fragments were widely adopted as model proteins to study Htt aggregation and pathology formation in various cellular and animal models of HD.

Expression of N-terminal Htt fragments in mouse models recapitulated many key features of HD, including behavioral abnormalities, presence of protein aggregates in cells, and progressive neurodegeneration [146,

156-158]. In particular, the expression of the exon1 fragment of mutant Htt (mHttex1) was sufficient to induce HD-like pathology in mice [146]. The N-terminal fragment of Htt 1-586 with 82Q induced severe HD-like neuropathology in an HD mouse model [159]. N-terminal fragments were also shown to cause transcriptional dysregulation [160] and induce neuronal dysfunctions [161]. These observations motivated studies aimed at assessing the therapeutic potential of targeting aberrant Htt cleavage. Preventing the cleavage of Htt by caspase 6 at position 586 in a transgenic YAC128 mouse model ameliorated the HD-like symptoms [162], whereas preventing caspase-2/3 cleavage [162] did not result in HD-like phenotype amelioration. The deletion of the calpain cleavage site decreased Htt-mediated toxicity in cellular HD models [163], consistent with the observed decreased activity of calpain proteases in HD patients' brain tissues and animal models of HD [164]. Not all of the proteases involved in the cleavage and processing of Htt have been identified. For example, enzymes or combinations thereof responsible for cleavage resulting in the generation of Httex1 fragments 81–129, 146–214, and 104–114 remain unknown. Aspartyl proteases were shown to cleave Htt and generate two N-terminal fragments [41]. The first fragment was generated as a result of cleavage between the residues 146 and 214 and named cpB; the second was produced by cleavage between residues 104 and 114 and named pcA [41] (Figure I.2-A). Other N-terminal cleavage sites between residues 81 and 129 (cp-1) and cleavage at arginine 167 (cp-2) [165, 166] have reported, but the enzymes responsible for these proteolytic cleavages were unknown. Together, these observations support the hypothesis that the Htt aggregation and cytotoxicity observed in HD are predominantly mediated by Htt N-terminal fragments rather than by the full-length Htt.

### I.2.5 Httex1

Among the N-terminal fragments mentioned in the previous section, Httex1 was demonstrated to play critical roles in HD pathology formation and HD pathogenesis. The R6/2 transgenic mouse model expressing human mutant Httex1 has been extensively utilized by the HD research community to investigate many aspects of the relationship between Htt aggregation, toxicity, and neurodegenerations. This model exhibits an early-onset progression HD-like phenotype and recapitulates most of the HD pathophysiology [146]. Several animal and cellular models expressing mutant Httex1 showed more severe pathology than models expressing full-length mHtt [167, 168]. A recent study using the HD mouse model demonstrated that Httex1 was continuously generated and responsible for protein aggregate formation in the striatum [169]. mHttex1 contains the HD-extended mutation in the polyQ tract, and it forms amyloid-like fibrils in a polyQ-dependent manner in vitro [170, 171]. Additionally, mHttex1 has been shown to be sufficient to form aggregates and inclusions in various cellular models of HD, as well as in primary neurons [155], and induce higher toxicity in a polyQ-dependent manner [155, 172]. In a *Drosophila* model, mHttex1 was the most toxic out of the N-terminal fragments (Htt 1–586, 1–552, 1–536, 1–513, 1–469, and caused protein aggregation and

cytotoxicity) [173]. The Httex1 fragment can be generated by proteolysis or by aberrant splicing of Htt [148, 174]. This incompletely spliced Htt transcript was found in the HD mouse model [174] and HD patient postmortem brains [148]. Due to the large size of the full-length Htt, most of the structural and aggregation studies addressing the Htt protein in vitro [175-178] are based on using Httex1 proteins. Httex1 is composed of three domains (Figure I.2-B and Figure 5): the disease-causing polyQ tract, the Nt17 domain, and the proline-rich domain.

### I.2.5.1 The PolyQ domain

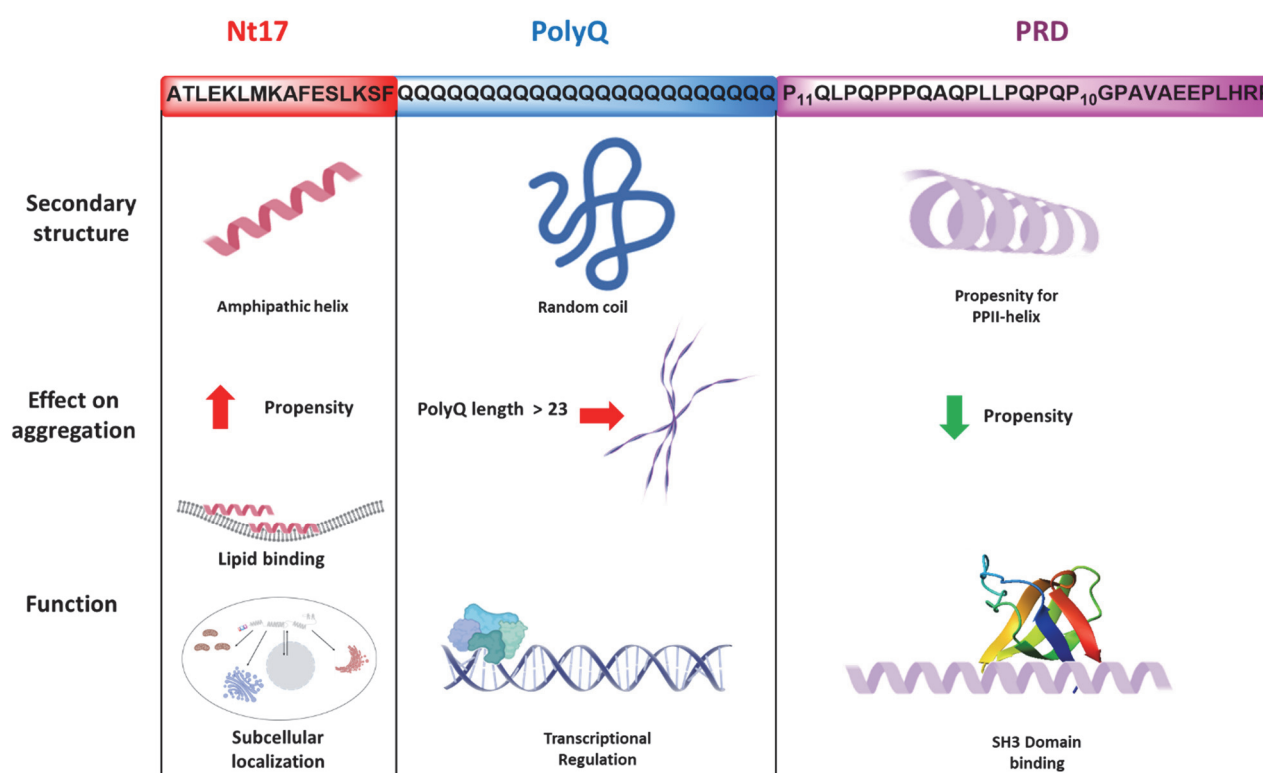


Figure I-5. Httex1 domains.

Schematic presentation of Httex1 sequence and its different domains: Nt17, PolyQ and the Proline-rich domain. The structure, effect on aggregation and major functions are shown for each domain

The polyQ tract is implicated in multiple simple repeat expansion neurodegenerative diseases (Paulson 2018), and specifically in HD pathology within the scope of this thesis. While the research community focused on the roles of the expanded polyQ on the Htt aggregation and cytotoxicity, very little is known about how it implicates Htt physiological functions. The polyQ tracts are present in more than 60 proteins [179] with the evolutionary preservation of the longer polyQ stretches [11]. The polyQ tract was shown to modulate transcription factor activity (Figure I.5) [180]. Furthermore, it was demonstrated that glutamine-rich domains were enriched within regulatory proteins, including transcription factors [181]. The glutamine-rich domains in the CREB protein transcription factor interacted with TAFII130/135 to recruit the RNA polymerase II and

activated transcription activity [182]. Also, it was demonstrated that polyQ tracts stabilize protein-protein interactions [183]. The polyQ repeats were believed to undergo structural changes from disordered form to the  $\alpha$ -helix and mediate protein-protein interaction by interacting with other coiled-coil-containing proteins [183]. The polyQ domain was also shown to regulate autophagy [184].

Several studies have shown that the polyQ repeats can adopt different conformations, including disordered (Figure 1.5) and  $\alpha$ -helical conformations. It was found that the monomeric polyQ domain was mainly disordered [185-187]. It was also shown to adopt  $\alpha$ -helical structures [188, 189] as well as  $\beta$ -sheets that are contingent on the length of the polyQ tract for its forming propensity [190, 191]. The conformational properties of the polyQ domain are significantly influenced by its flanking sequences. For example, a recent study by Urbanek et al. [192] demonstrated, using specific isotope-labeling of each Q, that the polyQ structure was influenced by the Nt17 domain, which exhibited a high propensity to form  $\alpha$ -helix, and this helicity was propagated to the N-terminal Qs in the polyQ tract [192, 193].

### 1.2.5.2 Nt17 domain

Several CD, solution NMR and atomistic simulation studies later proposed that the Nt17 domain was a predominately random coil with a high propensity to form transient helical structure [176, 194-196]. It also has the propensity to form  $\alpha$ -helical structure in the presence of lipids, fluorinated alcohols (e.g., TFE) or protein binding partners [197-200]. Other simulation studies suggested that Nt17 existed in a transient interchange between a two-helix bundle and linear single-helix states [195]. One crystallography of Httex1 fused to MBP showed that the Nt17 existed predominantly as a helix [175]. The sequence and  $\alpha$ -the helical propensity of Nt17 regulate its interactions with lipids [201-204] and intracellular membranous organelles such as mitochondria, endoplasmic reticulum (ER) or Golgi [201, 205, 206].

In addition, Nt17 has been proposed to play key roles in the initiation of Htt aggregation by promoting the formation of helix bundles induced by the interaction between hydrophobic faces of adjacent amphipathic Nt17 helices [207]. Consistent with this hypothesis, the removal of Nt17 significantly slows the kinetics of mutant Httex1 aggregation [176]. Interestingly, an animal model based on BAC transgenic mice expressing full-length mHtt lacking the N17 domain (BACHD- $\Delta$ N17) showed a dramatic increase in the pathology of mutant Htt in the nucleus [208]. Phosphorylation of one or multiple serine/threonine residues within Nt17 delayed the aggregation of the protein. Furthermore, mimicking phosphorylation at S13 and S16 was shown to prevent Htt aggregation and reversed HD-like phenotype in the same model [209].

Mutations or modifications that disturbed the Nt17 structure has also been shown to alter Htt's subcellular localization [201, 210], lipid binding [211], protein-protein interaction [212], It was found that Nt17 could act

as a cytoplasmic retention signal and contained a NES consisting of four hydrophobic amino acids (L4, 7, 14 and F11) [213]. The substitution of a methionine at position 8 to proline (M8P) disrupted the Nt17  $\alpha$ -helical structure and increased Httex1 nuclear translocation and cytotoxicity [206]. The Nt17 domain also played an important role in modulating mHtt interactions with the binding partners [176, 198].

These findings highlight the drastic impacts of small sequence changes on the aggregation propensity and toxicity of this large protein.

### **I.2.5.3 Proline-rich domain**

The proline-rich domain (PRD) flanking the polyQ tract at the C-terminus (Figure I.5) is composed of two polyproline repeats of 11 and 10 proline residues and is located within a mixed polyQ/P repeat. PolyP repeats co-evolved in parallel with the polyQ tract, and their sizes were found to increase with increasing polyQ length [11, 192]. PRD was shown to interact with proteins containing WW domains and SH3 domains (72–75). Structural studies of the PRD have suggested that it contains polyproline type II (PPII) helical structures [175, 214] that can induce PPII-like structure within the polyQ domain. This structural arrangement of polyQ could compete with the formation of the beta-sheet structures and reduce the mutant Httex1 aggregation propensity [215, 216]. These findings, which were derived from computational studies, were verified experimentally by the *in vitro* aggregations studies showing that PRD reduced the aggregation rate of Httex1-like peptides [176, 188]. In a yeast HD model expressing mutant N-terminal Htt, the removal of the PRD increased mHtt aggregation and toxicity [217].

### **I.2.6 Httex1 aggregation models**

Initial models of Httex1 were polyQ tract centric and proposed a dominant role of the polyQ domain in the initiation and progression of mutant Htt aggregation. Htt aggregation was described as a nucleation-dependent polymerization initiated by a non-favorable energetic conformation of the polyQ tract (Figure I.6-C). Subsequent studies showed that the lag phase was terminated by the formation of the first nucleus, such as oligomers and protofibrils, followed the continuous addition of monomers that induced a rapid formation of  $\beta$ -sheet amyloid fibrils (Figure I.6-C) [218, 219]. However, as described above, polyQ is not the only determinant of mutant Htt aggregation and pathology formation. The Nt17 domain was shown to increase the aggregation of Htt, whereas the PRD increases mutant Htt solubility and slows its aggregation.



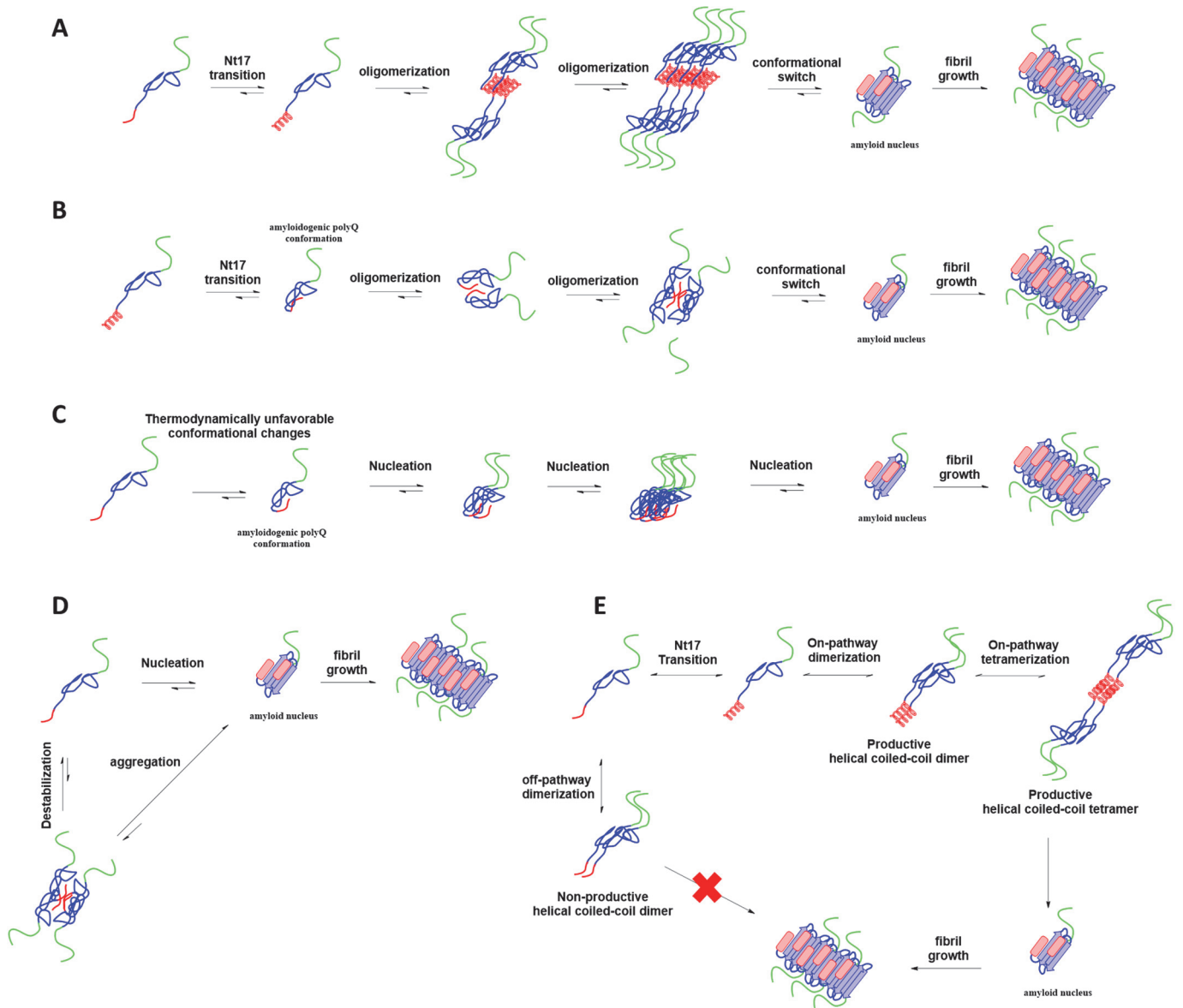


Figure I-6. Httex1 aggregation models.

(A) Nt-17 mediated aggregation model [177, 196, 220-222]. (B) Tadpole-like aggregation model [223] (C) polyQ-mediated aggregation model [218, 219, 224]. (D) Crick et al. proposed model [225]. (E) Coiled-coil tetramer oligomerization model [192]

To date, studies aimed at understanding the mechanisms of Htt aggregation *in vitro* were performed using Httex1/Httex1-like peptides or Httex1 fused to solubilizing proteins, such as GST tag. These studies led to different models that speculated on the effects and roles of the different domains of the mechanisms of Httex1 aggregation. One of the well-established and extensively studied models proposed that the Nt17 domain of monomeric Httex1 exists in an equilibrium between random coil and  $\alpha$ -helical structure, which drives its reversible assembly into tetrameric, octameric, or higher oligomeric forms of Httex1 (Figure I.6-A)

[220]. The oligomers then undergo structural rearrangement and transition to amyloid structure, driven by the high concentration of the polyQ domain at the periphery of the protein. This lead to the formation of an amyloid core that was initiated by the transition of the polyQ repeat domain from disordered conformations to  $\beta$ -sheet-rich structures that grow into amyloid fibrils by monomer addition [226] (Figure I.6-A). On the other hand, Crick et al. proposed a different model based on *in vitro* and computational studies where they speculated that both the Nt17 and the C-terminal fragments of Httex1 were involved in mutant Httex1 aggregation, where the Nt17 domain increases the formation of the fibril and stabilizes non-fibrillar intermediates during the aggregation process, while the PRD decreases the aggregation driving forces (Figure I.6-D) [177].

More recent studies have suggested a revised version of the Nt17- or polyQ-mediated aggregation models. The Lagen group [222] proposed that Nt17 forms an  $\alpha$ -helix that is stabilized through self-oligomerization. Once formed, the oligomers bring the polyQ domains closer, which drives a conformational transformation of these oligomers into  $\alpha$ -helix/ $\beta$ -sheet-rich intermediates, that eventually grow to form fibrils. The same group proposed an aggregation model of Httex1 in the presence of lipid membranes, where the helical conformation of Nt17 drives its association with lipids, which increases the local protein concentration and the encounters between polyQ domains, resulting in the initiation of a conformational switch and fibrils formation [222]. Similarly, recent studies from the Clore group [227, 228] have used relaxation-based NMR studies to demonstrate that the early oligomerization of a peptide model of Httex1 (Nt17-Q7) consisted of two pathways. These included the productive pathway, where the model peptide formed a coiled-coil dimer and self-assembled into an “on-pathway” tetramer (Figure I.6-E), which facilitates further aggregation of mHttex1 into fibrils. In the second – a non-productive pathway – Nt17-Q7 formed “off-pathway” partially-helical dimers that did not undergo further oligomerization (Figure I.6-E) [229]. Another Htt aggregation model, called “nucleated fibril branching”, has also been proposed [224], where the aggregation of mHttex1 occurs through two nucleation mechanisms. During the first nucleation step, a thermodynamically unfavorable conformation of mHttex1 initiated the fibril elongation in a templated polymerization manner. This was followed by a rapid second branched nucleation that consisted of the fibril growth on the surface of the fibrils in the form of branching [224]. Recent work from our laboratory, combining single-molecule FRET (smFRET) and atomistic simulations, showed that Httex1 adopts *tadpole-like* structures, where the Nt17 and the poly-Q domains interact through fuzzy contacts and form a globular head, while the PRD sticks out (tail) [223, 230]. The surface area of the globular head increases with increasing polyQ length. This model suggests that Httex1 tadpole-like structures are more compacted at higher polyQ length and initiate the formation of small oligomers, such as bristled spheres [223], which are converted to beta-sheet-rich amyloid, and finally, to mature fibrils *via* monomer addition (Figure I.6-B) [223, 230].

Despite much interest and research efforts, there continues to be a lack of consensus on the model of the Htt aggregation. Novel approaches and biochemical tools are needed for in-depth investigations of the Htt protein structure and function.

### 1.2.7 Httex1 proteins and peptides models

Several drawbacks exist in the majority of the prior studies using recombinant Htt to study its aggregation. For example, all of the structural and aggregation studies presented above were mainly performed using Httex1-like synthetic peptides consisting of a combination of the polyQ domain and Nt17 [176, 220], with only some studies including part of the polyP domains [177, 196, 231]. Solid-phase peptide synthesis (SPPS) of Httex1 containing the extended polyQ domain is difficult because amino acid deletions and incomplete couplings can occur during the synthesis, resulting in non-pure crude peptides and low yields after purification [232]. Additionally, non-native two lysine residues were commonly added at the C-terminus to increase the solubility of Httex1-like peptides [196, 233, 234], although subsequent studies showed that such non-native sequences alter the aggregation properties of mutant Httex1 [200]. Despite these limitations, these model peptides enabled valuable insight into the Httex1 aggregation mechanisms. However, several studies have shown that the aggregation propensity, structure, and toxicity of Htt were significantly affected by the flanking domains (Nt17, PRD). Thus, underscoring the importance of developing experimental systems using native Httex1 sequences.

Initial efforts to enable investigating the structural and aggregation properties of mutant Httex1 relied on the generation of fusion proteins, where mutant Httex1 is fused to proteins, such as glutathione-S-transferase (GST), maltose-binding-protein (MBP), or thioredoxin (TRX) [170, 219, 235-237]. Additional amino acids were usually inserted between the fusion protein and the Httex1 to enable the enzymatic cleavage by TEV, Factor Xa, or trypsin, and in some cases, an additional tag was also added to facilitate protein purification [212]. The use of fusion proteins has several limitations. First, the enzymatic cleavage is not traceless and often leaves additional amino acids within the Httex1 sequence. Second, non-specific cleavage can occur within the Httex1 sequence and generate a heterogeneous protein sample that is not suitable for biophysical studies. Third, the fusion protein is still linked to Httex1 and only cleaved off *in vitro* before aggregation initiation reaction [224]. Finally, the presence of a large fusion protein during the aggregation reaction can affect its aggregation kinetics. Together, these limitations stress the importance of using untagged and native Httex1 protein to study Httex1 structure and aggregation mechanisms. This, combined with the use of a single native construct, should improve experimental reproducibility and allow for comparing data between research laboratories.

To address these limitations, our group recently reported a strategy for the generation of tag-free native Httex1 by fusion of the *Synechocystis sp.* (*Ssp*) DnaB intein to Httex1 N-terminus [178] (Figure I.7-A). The cleavage of the fusion tag was traceless. However, pre-mature intein cleavage during the expression was observed. In addition, the extended incubation time for the intein splicing was not suitable for the production of mutant Httex1 [178]. To improve our strategy, we replaced the intein with a SUMO tag at the Httex1 N-terminus [238] (Figure I.7-B). The SUMO tag enhanced expression and solubility of Httex1. Also, the cleavage of the SUMO tag by the ubiquitin-like protein-specific protease 1 (ULP1) was found to be rapid and efficient [238]. These improvements allowed us to develop an efficient new system for the production and study of the Httex1 structural properties on a large scale.

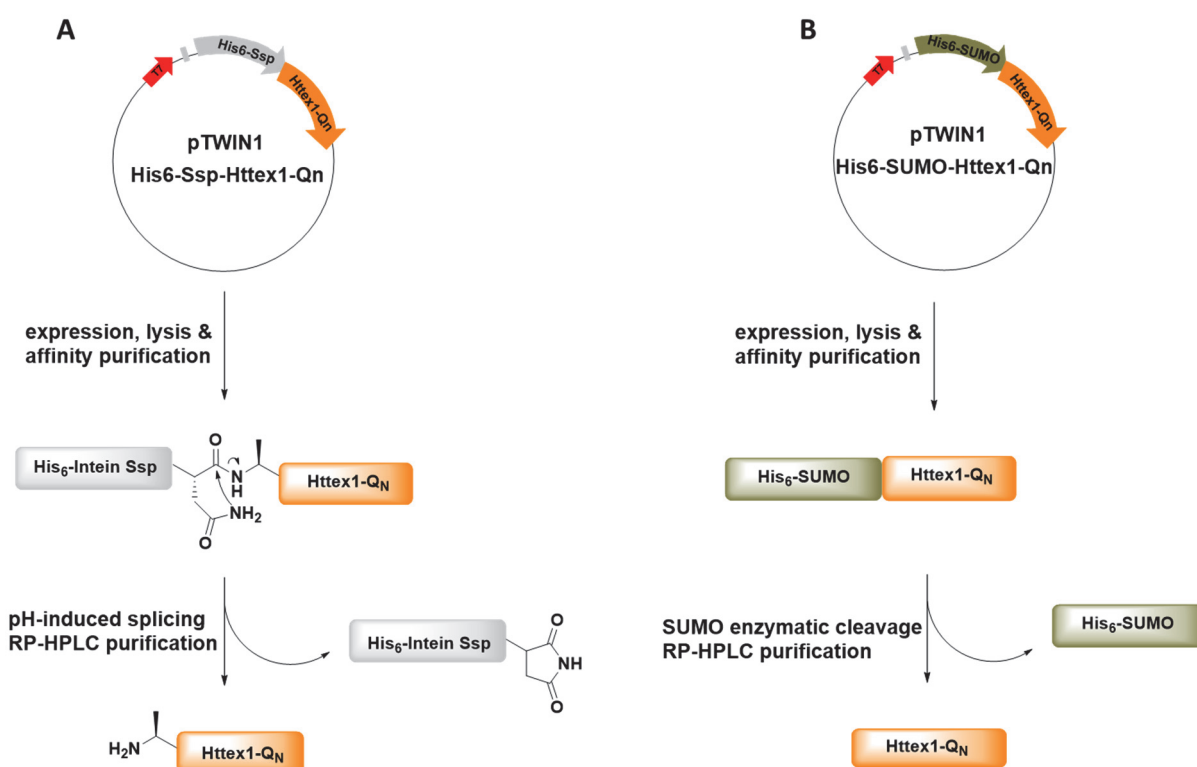


Figure I-7. Recombinant Httex1 production model

(A) Intein-based strategy [178] and (B) SUMO-based strategy [238] for the generation of native untagged Httex1.

### I.3 Htt Postranslational-modifications code

#### I.3.1 Post-translational modifications

Post-translational modifications (PTMs) are generated by both enzymatic and non-enzymatic mediated addition of chemical modifications (e.g., phosphorylation, acetylation, oxidation acetylation, or S-

nitrosylation), sugar groups (e.g., glycation), or proteins (e.g., Ubiquitin and SUMO-1/2) to the side chain of specific amino-acids (Table 1) [239, 240]. Depending on the modification, PTMs may or may not be reversible [239]. Such modifications change the local chemical and physical properties of the targeted amino-acid and alter the protein charge, hydrophobicity, conformation, and life cycle [241]. As a result, PTMs influence the protein's structure [242], interactions with other proteins, biochemical activity, and subcellular localization [243]. PTMs also represent molecular switches that regulate multiple cellular mechanisms and signaling pathways in health and disease and enable cells to respond and adapt to both external and internal changes [244]. Below, I present a brief summary of some of the key PTMs that have been shown to occur on Htt and will be discussed in this thesis.

Table I-1. A list of some of the major types of post-translational modifications and the corresponding residues and regulators (adapted from [240])

Post-translational modification	Targeted residues	Involved proteins and enzymes
Phosphorylation	Tyrosine, serine, threonine	Kinases, phosphatases
Glycosylation N-linked	Asparagine	Glycosyltransferases, deglycosylases
Glycosylation O-linked	Serine/threonine	Glycosyltransferases, deglycosylases
Acetylation	Lysine	Acetyltransferases, deacetylases
Methylation	Lysine, arginine	Methyltransferases, demethylases
Ubiquitination	Lysine	Ubiquitin-activating enzymes, ubiquitin-conjugating enzymes, ubiquitin ligases, deubiquitinases
Sumoylation	Lysine	Ubiquitin-activating enzymes, ubiquitin-conjugating enzymes, ubiquitin ligases, deubiquitinases
Palmitoylation	Cysteine	DHHC protein acyltransferases, acyl-protein thioesterases
S-Nitrosylation	Cysteine, methionine	-
Glycation	Lysine	-
Oxidation/reduction	Methionine	Peroxidases, oxidases, glutathione, thioredoxin

**Phosphorylation:** Phosphorylation is a common and widely studied protein modification. This reversible modification involves the addition of a phosphate group to either serine, threonine, tyrosine, or histidine residues [245]. The enzymes that regulate the addition and removal of the phosphate group are known as kinases and phosphatases, respectively [246]. Phosphorylation has been shown to regulate cell cycle, [247], nuclear transport [248], proteolysis [249], cell signaling [250], protein-protein interaction [251], autophagy [252], apoptosis [253], and several other cellular functions. Phosphorylation contributes to the control of everything from cell division to cell death, and some studies have even hinted that phosphorylation plays more global significant roles, such as maintaining the complete cellular homeostasis [254].

**Acetylation:** Another important PTM is acetylation, which consists of the introduction of an acetyl functional group into the N-terminus of proteins or lysine side chain. Lysine is regulated by lysine acetyltransferases (KATs) and lysine deacetylases (KDACs) (also known as histone deacetylases (HDACs)) [255]. The acetylation reaction removes the positive charge of the lysine side chain, thus modifying the functional state of the proteins implicated in cellular mechanisms, such as cellular localization [256] protein-protein interaction [257], gene expression [258], cell metabolism [259], cell division [260], and intracellular pH [261]. Several studies have shown that acetylation is a key component of a combinatorial PTM code that involves cross-talk

between acetylation and other PTMs, such as phosphorylation [262], ubiquitination, and methylation [263], and regulates many aspects of protein functions (e.g., many molecular chaperones [264, 265], cytoskeletal proteins [266], and transcription factors [267, 268]), and cellular pathways in health and disease.

**Ubiquitination:** Another commonly studied PTM is ubiquitination, which involves the addition of ubiquitin, an 8.6-kDa protein, to lysine residues of proteins [269]. Ubiquitination and deubiquitination are regulated by a large family of enzymes: ubiquitin-activating enzyme (E1), ubiquitin-conjugating enzyme (Ubc or E2), ubiquitin ligase (E3), and deubiquitination enzymes (DUBs; also known as isopeptidases) [270]. The initial addition of a single ubiquitin is followed by the formation of a polyubiquitin chain [271]. The resulting polyubiquitinated proteins can then be recognized by the 26S proteasome, which leads to their degradation [271]. Ubiquitination can also play non-proteolytic roles by recruiting proteins ubiquitin-binding domains [272] and, as a result, regulate mechanisms such as DNA damage responses [273], cell signaling [272], subnuclear trafficking [274].

**SUMOylation:** SUMOylation is a reversible PTM similar to ubiquitination, in which a small ubiquitin-like modifier (SUMO) is covalently conjugated to the lysine side chains *via* a cascade of enzymes [275]. Like all other PTMs, SUMOylation can be reversed by the removal of SUMO by SUMO-specific isopeptidases [276]. SUMOylation is a PTM implicated in many cellular events, such as protein stability [277], nuclear and cytosolic transport [278], and transcriptional regulation [279]. Although the three PTMs highlighted above target the same residues (lysine residues), they exert different effects on the physical, conformational, and cellular properties of the target proteins. These observations suggest that the competition between these PTMs represents an additional mechanism by which PTMs regulate protein functions in health and disease.

**Methionine Oxidation:** The exposure of proteins to a variety of free radicals and reactive oxygen species (ROS) often induces oxidative modifications at specific amino acids within proteins. Methionine is the major amino acid targeted by ROS. Oxidized methionine is more polar and rigid than methionine and, thus, can cause protein structural and functional changes [280, 281]. Moreover, similarly to other PTMs, methionine oxidation is reversible and can be reduced by methionine sulfoxide reductases A and B (MsrA and MsrB) [280]. Therefore, the redox reaction of methionine could act as a regulatory mediator for cellular processes [281].

### 1.3.2 Huntingtin post-translational modifications

Thanks to advances in mass spectroscopy methods for the detection and quantification of PTMs, multiple Htt PTMs have been identified in samples from cellular/mouse models of HD and *postmortem* HD patients tissues [100, 282-289] (Figure I.8-A). Interestingly, Htt PTMs were mostly found in clusters within domains that are unstructured rather than within the expected  $\alpha$ -helically structured HEAT repeats [288]. However, only a few PTMs have been thoroughly investigated (Figure I.8-B). This is due to the lack of knowledge about the enzymes responsible for their regulations, as well as the lack of methods and tools that enable the site-specific introduction of PTMs and reproducing the complexity of PTM profile of the protein as it exists *in vivo*. In this section, I will provide an overview of the various PTMs that have been identified in Htt and what we know about their role in regulating the physiological and pathological conditions, with an emphasis on PTMs that occur within the Nt17 domain.

#### 1.3.2.1 Post-translational modifications outside the Nt17 domain.

##### 1.3.2.1.1 Phosphorylation

Outside the Nt17 domain, the primary modification that is well described and studied in the context of HD is phosphorylation (Figure I.8-B). More specifically, the phosphorylation of serine 421 (pS421). In fact, pS421 was detected in mouse and human brains under physiological conditions, with higher concentrations in the cerebellum and cortex compared to the striatum [290]. It was shown that phosphorylation at S421 is less efficient in the case of mHtt in a YAC mouse model [290]. At least two kinases, Akt and SGK, have been reported to phosphorylate Htt at S421 and that this modification has a neuroprotective role against mHtt toxicity in cellular and mouse models of HD [291-294]. Akt-mediated phosphorylation of mutant Htt at S421 reduces the formation of nuclear inclusion and decreases Htt-induced toxicity in cultured striatal neurons [291] and a mouse model of HD [294]. Coexpression of full-length Htt with Akt kinase led to a significant reduction in Htt levels in N2A cells [295]. Phosphorylation at S421 also prevents Htt proteolysis by caspases, therefore highly reducing HD pathogenesis [295, 296]. For example, mimicking phosphorylation at S421 (S421D) attenuated Htt cleavage caspase-6 [295]. Similarly, phosphorylation at S434 or the introduction of phosphomimetic mutation at S536 (S536D) reduced the caspase-mediated cleavage of Htt at residue 513 and decreased mutant Htt toxicity in cell culture [287, 297]. These observations suggest that phosphorylation at this residue regulates many aspects of Htt proteolysis and clearance.

Moreover, the defect in vesicle transport caused by expanded polyQ was restored by phosphorylation at S421 [292, 298], especially the transport of BDNF-containing vesicles through cortico-striatal projection neurons that are critical for striatal neurons' survival [108, 139].

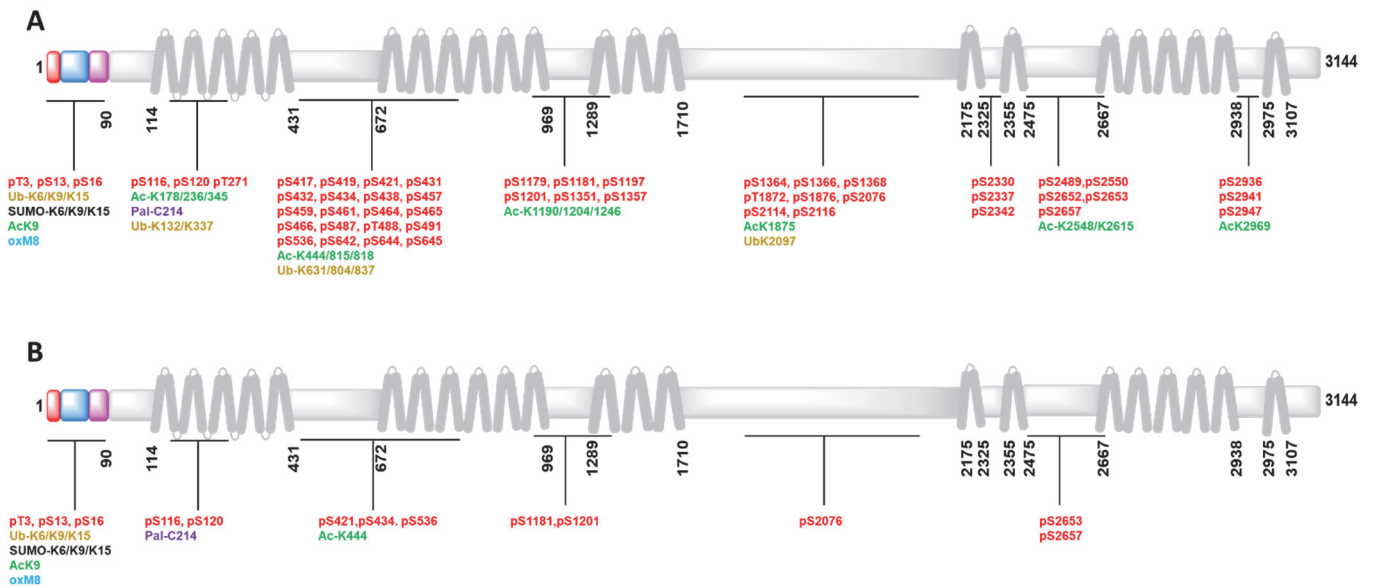


Figure I-8. Htt PTMs.

(A) Schematic representation of Htt full length with the identified PTMs sites in cell culture, HD mouse model, and HD patients brain tissues [100, 282-288]. (B) list of the PTMs described in relation to HD (phosphorylation in red, ubiquitination in yellow, SUMOylation in black, acetylation in green, and oxidation in blue).

Several other Htt serine residues, such as 434 [297], 1181, and 1201 [299] (Figure I.8-B), were also shown to be phosphorylated by cyclin-dependent kinase 5 (CDK5). Phosphorylation at S1181 and S1201 is protective against mHtt induced cellular toxicity [299] and regulates the microtubule-dependent transport of organelles, thus increasing both retrograde and anterograde intracellular transport [299].

pS116 and pS120 were also identified by mass spectroscopy in HEK 293FT cells [285]. Using phosphomimetic (S to D) and phosphoresistant (S to A) mutations of multiple potential phosphorylation sites [285], the authors reported that S116 (S116A) was the mutation with the most significant decrease of toxicity in a cellular model of HD [285], suggesting that the phosphorylation at 116 increases mutant Htt toxicity. Furthermore, Nemo-like kinase (NLK) was demonstrated to phosphorylates Htt at S120 [300] and promote its clearance *via* the proteasome pathway [300]. It has been reported that NLK levels are decreased in *postmortem* HD brains and animal models and that its overexpression in the striatum decreased mHtt aggregation in an HD mouse model [300].

### I.3.2.1.2 Acetylation

Acetylation at K444 has been identified in Htt and was shown to facilitate mHtt clearance *via* autophagy [286]. CBP (CREB-binding protein) binds and acetylates Htt at K444, and as this modification is reversible, deacetylase 1 (HDAC1) is responsible for its deacetylation [286].



K444 is in close proximity to the caspase-6 site at residue 586, which can reduce the activity of CBP acetylase and, as a result, decrease K444 acetylation [301]. However, when increased, this acetylation can promote mHtt trafficking, targeting it to autophagosomes, which leads to neuroprotection [286]. Finally, overexpression of the acetylation-resistant mutation (K444R) in cells and mouse models of HD caused toxicity and aggregation, concluding that K444 acetylation has a protective role against mHtt [286].

### I.3.2.1.3 Palmitoylation

Palmitoylation consists of the addition of fatty acids, such as palmitic acid to cysteine. This PTM is crucial for the transport of various membrane proteins, as well as the functional modulation of their signaling pathways [302, 303]. WT Htt is palmitoylated at C214 [304], a modification that is essential for Htt trafficking by Huntingtin interacting protein 14 (HIP14) [304]. However, when the polyQ tract is expanded, the interaction between Htt and HIP14 is reduced, thus decreasing the levels of C214 palmitoylation [304]. Furthermore, overexpression of mHtt resulted in a decrease of C214 palmitoylation and an increase of neuronal toxicity [305]. Similarly, mutating the C214 to block its palmitoylation led to an increase of mutated Htt aggregation, acceleration of inclusion formation, and cell death [304].

### I.3.2.2 Nt17 PTMs

The first 17 N-terminal amino acids (MATLEKLMKAFESLKSF), hereafter referred to as Nt17, are highly conserved throughout the evolution of mammals [201, 206], implying a major function for these residues or the Nt17 domain. Despite the small number of residues, several types of PTMs have been shown to occur at multiple residues within the Nt17 domain, including T3, K6, K9, K15, M8, S13, and S16. Increasing evidence from *in vitro* studies and cellular and animal models of HD suggest that PTMs in this region play important roles in the regulation of many aspects of Httex1 structure [201], oligomerization [234], fibril formation [211, 234, 306], membrane binding [211, 306], and subcellular localization [282].

#### I.3.2.2.1 T3 phosphorylation (pT3)

Threonine 3 (T3) phosphorylation is, with N-terminal acetylation, the most frequently detected PTM by mass spectroscopy in WT Htt protein purified from mammalian cells or Httex1 from ST14A and HeLa cells [100, 307]. The levels of pT3-Htt have been reported to be the lowest in the striatum of wild-type mice [307]. Furthermore, the levels of pT3 are decreased with increasing polyQ-repeat length in Httex1 expressed in ST14A [307]. Recently, a highly sensitive method to detect pT3 was developed and used to demonstrate that the levels of pT3 were decreased in *postmortem* HD tissues and preclinical models [308]. At the beginning of this project, the kinases responsible for T3 phosphorylation were unknown. Therefore, studies aimed at elucidating its roles in Htt aggregation and toxicity in cells or *in vivo* were primarily based on the use of mutations to mimic (e.g., threonine to aspartate, T3D) or block phosphorylation (threonine to alanine, T3A)

at this residue [307, 309]. The T3D mutation was shown to increase the aggregation of mutant Httex1 in ST14A cells, as well as in a transgenic *Drosophila* model [307]. Surprisingly, the same mutation led to reduced neurodegeneration and lethality in the same *drosophila* model [307]. To explain these contradictory observations, the authors proposed that T3D induces structural changes and prevents Httex1 from binding to cell membranes, causing its accumulation in the cytoplasm, which renders the protein more prone to aggregation. An alternative hypothesis proposed by the authors is that different cellular mechanisms independent from those involved in mutant Httex1 induced toxicity are responsible for the neuroprotective effect observed for T3D in the *drosophila* model [307].

Increasing interest and research on pT3 modification has increasingly pointed to its potential neuroprotective effects. Our group was the first to develop new methods that enabled site-specific phosphorylation of Httex1 at T3, thus paving the way for investigating the effect of *bona fide* phosphorylation on Htt structure and aggregation properties [310]. However, these methods enabled the production of wild type, but not mutant Httex1, because of the high propensity of this protein to aggregate presented serious challenges during the synthesis, purification, and handling of the mutant protein [310]. Despite these limitations, *in vitro* aggregation studies of Httex1-23Q have shown that phosphorylation at T3 inhibits the aggregation of Httex1 [310].

Using a bimolecular complementation cellular assay (BiFC) expressing WT, T3D, or T3A mutant HttEx1, Branco-Santos showed that mutant T3D Httex1 oligomerized but did not form inclusion in mammalian cells [309]. These observations differ from what was observed in *Drosophila*, where overexpression of T3D showed few inclusions compared to S13D or S16D (see below)[309]. Interestingly, the downregulation of PP1 prevented Httex1-97Q aggregation in the presence of serine-phosphoresistant mutations (S13A or S16A), suggesting that PP1 is responsible for pT3 regulation [309]. Flies with Protein phosphatase 1 (PP1) knockdown exhibited a substantial decrease in Httex1-97Q aggregation in *drosophila*.

#### 1.3.2.2.2 S13/S16 phosphorylation (pS13/pS16)

A mouse model expressing full-length Htt with 97Q bearing phosphomimetic mutations at S13 and S16 (S13D/S16D) in Nt17 showed a significant reduction in the number Htt inclusion and HD-like behavioral phenotypes. This is one of the most remarkable findings related to Htt PTMs and highlights how only two modifications within a large protein (347 KDa) could have such a powerful effect on inhibiting mHtt aggregation and protecting against mHtt pathology. Moreover, *in vitro* studies of synthetic mutant Httex1-like fragments have shown that S13D and S16D substitutions (single or double phosphomimetic) reduced the aggregation kinetics and formed fibrils that are different in terms of length, thickness, and morphology compared to WT [209]. Using similar Httex1-like peptides, Mishra et al. [234] confirmed these findings and

performed more in-depth biophysical characterization of Httex1-like S13D/S16D and compared its aggregation to mutant Httex1-like peptides with *bona fide* phosphorylation (pS13/pS16) [234]. Both phosphomimetic substitution and *bona fide* phosphorylation inhibited the aggregation of mutant Httex1-like peptides with pS13/pS16, exhibiting more inhibition [234]. Circular dichroism (CD) and Förster resonance energy transfer (FRET) studies of Httex1-like peptide (HttNTQ37P10K2) have shown that the S13D/S16D double mutation does not influence the overall monomeric structure [234]. The authors hypothesized that S13/S16 phosphorylation inhibits aggregation by reducing the peptide's ability to make the  $\alpha$ -helix-rich tetramers and oligomers, which are necessary for amyloid nucleation [234].

The S13 and S16 residues on Httex1 were reported to be phosphorylated IKK $\beta$  (I $\kappa$ B kinase). In particular, S13 is observed to be a first phosphorylated by IKK, which later primes S16 phosphorylation [282]. Interestingly IKK $\beta$ -mediated phosphorylation was less efficient on mHtt compared to WT Htt [282]. Furthermore, phosphorylation or phosphomimetic mutations at the S13/S16 residue of Httex1 enhanced its degradation by both lysosomal and proteasomal pathways and increased nuclear localization [282]. Expression of phosphomimetic mHttex1 (S13D/S16D) in striatal-cortical rat slice cultures demonstrate reduced toxicity compared to the expression of Httex1. A recent study has shown that in the R6/1 mouse model of HD, IKK $\beta$  is responsible for S13 phosphorylation; furthermore, the IKK $\beta$  knockout in R6/1 mice reduces Htt S13 phosphorylation and enhances HD-like pathology [311]. S13/S16 phosphorylation was also shown to be reduced by Casein kinase 2 (CK2) inhibitors, which led to an increase in the death of *STHdh* cells [312]. N6-furfuryladenine, a molecule known to be released during oxidative DNA damage, was shown to induce the phosphorylation of S13 and S16 *via* CK2, leading to the decrease of nuclear inclusions of mHtt in various models, including the YAC128 HD mouse model [313]. Another molecule, ganglioside GM1, enhanced the phosphorylation of S13/S16 [314] and reduced Htt toxicity, restoring normal motor behavior in YAC128 HD transgenic mice [314]. Httex1 expression based bimolecular complementation assay (BiFC) demonstrated that single S13D and S16D mutations reduced the formation of inclusions bodies in mammalian cells; however, on the contrary, showed a significant increase of aggregates in *Drosophila* [309].

At the structural level, pS13/pS16 reduced a FRET signal between Nt17 and polyP domains relative to WT, indicating a possible change in Htt conformation induced by these mutations [315]. Atwal *et al.* performed a CD-based study and found that the Nt17 synthetic peptide phosphorylated at S13 exhibit a 50% reduction of the  $\alpha$ -helical structure relative to the WT peptide, whereas a double phosphorylated peptide completely disrupted the  $\alpha$ -helical structure [312]. Taken together, these previous studies point to the beneficial effect of pS13/pS16 in reducing the aggregation and toxicity, reversing the HD-like pathology. However, the use of

phosphomimetic mutations showed discrepancies in observations between the cellular and the *Drosophila* model of HD (Figure I.9).

#### I.3.2.2.3 Acetylation (Ac-K6/K9/K15)

After translation, the first methionine in the Htt sequence is removed, and the alanine at position 2 is acetylated by the N-terminal acetyltransferase A and the chaperone-like HYPK protein complex. It was observed that the reduction of NAA10 (NatA subunit) or HYPK lead to the aggregation of huntingtin [316]. Further studies are required to elucidate its role in the Htt function.

The Nt17 domain also contains three potential lysine residues that can be acetylated (K6, K9, and K15); however, only K9 was detected in ST14A cells by mass spectroscopy and was exclusively found when S13 is phosphorylated by IKK overexpression [282]. Moreover, it was found that Hsc70 overexpression increases K9 acetylation and S13 phosphorylation, which leads to the hypothesis that Hsc70 increases the clearance by both proteasomes and lysosomes of WT Htt *via* both S13 phosphorylation and K9 acetylation [282]. Recently, chemical-induced acetylation of all the lysine residues in a Httex1-like peptide model [211] blocked the generation of aggregated fibrils and additionally inhibited lipids binding [211]. However, the structural and functional consequences of single lysine acetylation in the Nt17 are still to be discovered.

#### I.3.2.2.4 Ubiquitination/SUMOylation (Ub- or SUMO-K6/K9/K15)

Nt17 lysines are shown to undergo SUMOylation or ubiquitination, and they both compete for similar residues [284]. A previous study has demonstrated that ubiquitination at K6, K9, and K15 reduces HD-like pathology in a *Drosophila* model of HD and decreases the levels of Htt *via* the proteasomal pathways [284]. Ubiquitination at the K6 and K9 sites was characterized in the Q175 HD mouse model by LC/MS [317] and was observed in both the soluble and insoluble fraction; significant upregulation of K6 and K9 ubiquitination was observed in the insoluble fraction of mHtt [317].

A recent study confirmed these findings using the BACHD rat model. K9 and K6 were specifically ubiquitinated in the striatal and cortical brain regions of BACHD rats but not in the WT rats [318]. Expression of mutant Httex1 (fused to enhanced green fluorescent protein [EGFP]) with ubiquitination sites is mutated to block the modification, showing the formation of small aggregates, which are more toxic than the non-mutated form [318]. These observations suggest that ubiquitination at K6 and K9 attenuates the deleterious effects of mutant Httex1 [318].

Similar to ubiquitination, the Nt17 domain was shown to be SUMOylated at K6, K9, and K15 [284]. It was demonstrated that SUMOylation at these sites of Htt stabilizes and inhibits the aggregation of mHttex1 in cellular models but increased the toxicity, producing a HD-like phenotype, in both *Drosophila* and transgenic

HD mouse model [284, 319, 320]. SUMO E3-ligase PIAS1 (protein inhibitor of activated STAT1) was shown to participate in the Nt17 SUMOylation [321]. Reducing PIAS1 levels in the R6/2 mouse model reversed the HD-like pathology and decreased Htt aggregation levels [322]. A recent *in vitro* aggregation study demonstrated that the Nt17 SUMOylated *in vitro* inhibits mutant Httex1 aggregation but induces the formation of large SDS-soluble amorphous aggregates [306]. Furthermore, Nt17 SUMOylation blocked the mHttex1 binding to lipids *in vitro* [306].

#### I.3.2.2.5 Methionine oxidation (oxM8)

M8 oxidation was detected in the R6/2 HD mouse model with increasing levels with mouse age. It was demonstrated that M8 oxidation could act as a ROS sensor and promote Nt17 phosphorylation [323, 324]. Mitomi et al. have proposed that oxidation at M8 occurs only post-aggregation [325], but M8 oxidation of the Httex1-like peptide model was shown to block the aggregation and reduce its binding to lipids [326]. These observations suggest that M8 oxidation of mHtt plays an aggregation inhibitory role. However, the structural and functional consequences for this are yet to be illustrated.

#### I.3.2.2.6 Nt17 PTMs cross-talk

The Htt Nt17 domain has PTM clusters, with each cluster having multiple regulatory roles. This suggests that many modifications act in concert rather than individually. Furthermore, the Htt PTM code possibly involves cross-talk between different PTMs, in particular those that exist in close proximity to each other. The consequences of this cross-talk can be complementary, when one modification primes the addition of another PTM or enables the binding of an enzyme responsible for a different PTM. The cross-talk can also be preventive, for example, when multiple PTMs are competing for the same residue. An addition of a PTM can also induce local structural changes, causing the inaccessibility to another residue.

Figure I-9. Previous Httex1 models *in vitro*, cells, and Drosophila.

Comparison of the different models used to study Httex1 PTMs *in vitro*, in cells, or using Drosophila (respectively from left to right) and their effect on mutant Httex1 aggregation and toxicity.

The cross-talk mechanism becomes evident when ubiquitination and SUMOylation compete for the same residues in Htt. Ubiquitination reduces the levels of Htt protein *via* the proteasomal pathways [327, 328], while SUMOylation induces the accumulation of Htt proteins, preventing its degradation by the proteasome and increasing the capacity of Htt to repress transcription [284]. Furthermore, oxidation at M8 was shown to

increase the level of S13/S16 phosphorylation in mammalian cells [323]. IKK phosphorylation of S13 and S16 was shown to enhance mutant Httex1 acetylation at K9 and increase its clearance, and the absence of S13 phosphorylation reduces mHtt ubiquitination and SUMOylation [282]. Recent work from our group to understand the effect of PTMs on the Nt17 structure showed that pT3 increases the Nt17 alpha-helical content and that the addition of pS13/pS16 to pT3 abolishes its helicity [329]. Taken together, these findings suggest an essential role for Nt17 PTMs cross-talk as a sophisticated code language regulating the communication of Htt with other proteins and cellular mechanisms, thus orchestrating its functions in health and disease. Understanding the Nt17 cross-talk code in Httex1 was limited to cell culture study using PTM mimicking. However, very little is known about the structural consequences of specific PTM combination and its effect on mutant Httex1 biophysical properties and aggregation due to the lack of chemical or enzymatic tools to generate homogeneous and native Httex1 with single or multiple PTMs.

### 1.3.3 Previous Protein models to study Nt17 PTMs and their Limitations

Nt17 phosphorylation was shown to be the molecular switch of Htt aggregation, toxicity, and functions. However, most of the previous biophysical studies to determine the effect of pS13 and/or pS16 on Httex1 structure and aggregation used Httex1-like peptides with phosphomimetic S13D/S16D mutations (Figure I.9 and Figure I.10). This model presents multiple drawbacks: 1) it does not recapitulate all the native Httex1 sequence; and 2) phosphomimetic mutations enable only partial mimicking of phosphorylation and do not reproduce the dynamic nature, the size, and charge state of *bona fide* phosphorylation (Figure I.10). The phosphomimetic mutations were used in the cellular study (Figure I.9) because the kinases responsible for the Nt17 phosphorylation are not known. To track the evolution of the protein in cells, the phosphomimetic Httex1 proteins were fused to large fluorescent proteins, such as GFP or Venus fluorescent protein [282, 307, 309]. However, these fusion proteins are large compared to Httex1 (Figure I.9), which might dramatically affect its structure and aggregation properties [330, 331]. Consequently, it is not surprising to observe discrepancies in the effects of these phosphomimetic mutations when using different cellular and animal models (Figure I.9). For example, S13D and S16D mutations blocked the formation of inclusion bodies in mammalian cells [309] but significantly increased the number of aggregates in *Drosophila* [309]. An HD mouse model expressing full-length Htt with S13D/S16D reversed HD-like pathology [209] (Figure I.9). The T3D mutation was shown to increase the aggregation of mutant Httex1 in ST14A cells, as well as in the transgenic *Drosophila* model [307], but decreased neurodegeneration in *Drosophila*, while mutant Httex1 T3D (with a venus tag), prevents the formation of inclusion bodies in mammalian cells [309]. It was demonstrated that chemical acetylation of the Nt17 domain in Httex1-like peptide decreases its aggregation [211]. However, chemical acetylation can induce heterogeneous addition of the acetyl group.

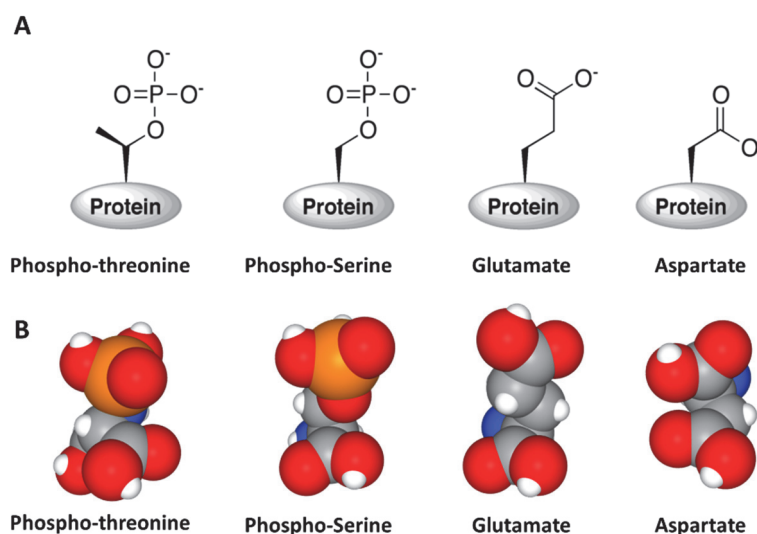


Figure I-10. Phosphomimetics limitations.

Comparison of the structures of phosphorylated amino acids with glutamate and aspartate. (A) Chemical structure of posho-threonine, phosphor-serine, glutamate and aspartate (adapted from [332], and (B) their corresponding space-filling models exported from National Center for Biotechnology Information (<https://pubchem.ncbi.nlm.nih.gov/>).

Moreover, many studies that demonstrated that Htt Nt17 PTMs used the Httex1-like model, which excludes the PRD domain, which is important for Httex1 aggregation [176, 192]. In summary, Httex1 models used *in vitro* and in cells to study Nt17 PTMs had several limitations that can affect the understanding, interpretation, and the reproducibility of the data.

### I.3.4 Httex1 semisynthesis

The increasing interest in the addition of unnatural amino-acids and functional groups into proteins has motivated the development of an impressive method of semisynthesis of protein-based on “native chemical ligation” (NCL) [333]. Protein semisynthesis is based on the combination of recombinant expression with solid-phase peptide synthesis (SPPS) of synthetic peptide fragments containing single or multiple PTMs [334]. Semi-synthesis is accomplished through NCL of the synthetic N-terminal fragment containing an activated thioester [335] and the recombinantly expressed C-terminal protein fragment with an N-terminal cysteine, which enables the introduction of PTMs within the N-terminal fragment by SPSS [334]. The thioester undergoes transthioesterification with the N-terminal cysteine, and then rearrangement *via* an S→N acyl shift results in the formation of a native peptide bond [333] and ligation of the two fragments. This ligation strategy requires a cysteine residue at the ligation site [336]. If a cysteine residue is not available in the protein sequence, a mutation of an amino-acid within the sequence to cysteine is required. Often an alanine



is mutated to cysteine at the desired ligation site, and the resulting cysteine from NCL can subsequently be converted to an alanine residue *via* desulfurization [336].

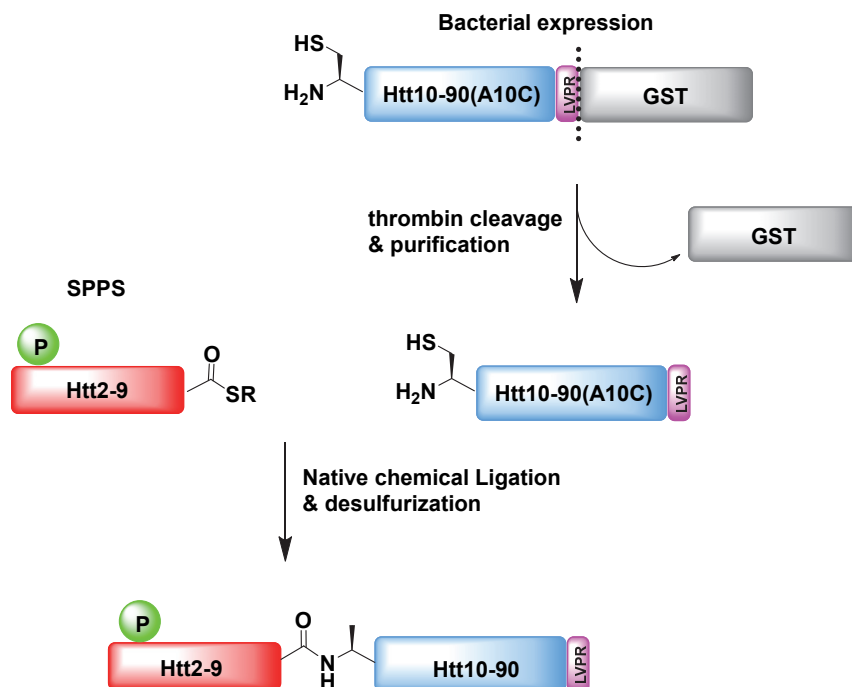


Figure I-11. Semisynthetic strategies for the production of WT Httex1 pT3 [310].

To overcome the drawback related to the use of phosphomimetic mutations and Httex1-like peptides, our group took advantage of the powerful semisynthesis method [310] to produce native Httex1-23Q pT3 (Figure I.11). The ligation site was fixed at Alanine 10. Using SPPS, the N-terminal peptide (2-9-NbZ pT3) was synthesized from positions two to nine, and pT3 and the C-terminal N-acylbenzimidazolinone (NbZ) moiety for thioester formation were introduced during the synthesis. Additionally, the C-terminal containing cysteine (Htt A10C-90 23Q) was fused to GST fusion protein and purified after the GST cleavage by thrombin (Figure I.11). The Htt 2-9NbZ pT3 peptide was ligated with the C-terminal Htt-A10C-90 fragment and, after a desulfurization reaction, the native alanine residue was then recovered (Figure I.11). Unfortunately, when these conditions were applied to achieve the semisynthesis of mutant Httex1 (43Q), the production of the protein was unsuccessful due to the high propensity of aggregation and low solubility of the recombinant mutant C-terminal Htt fragment under standard NCL conditions [310]. Additionally, the produced semisynthetic WT Httex1 proteins contained four additional amino acid residues that resulted from the thrombin cleavage (Figure I.10). Therefore, we sought to develop new tools and methods to produce untagged and native Httex1 with single or multiple PTMs in milligram quantities and determine the effect of these PTMs on mutant Httex1 aggregation and structure.

## I.4 Objectives of the thesis

The objective of this thesis is first to develop new methods and tools to produce untagged and native Httex1 proteins with single or multiple PTMs, and to overcome the limitations of the existing systems: 1) the High aggregation propensity of mutant Httex1 during its production and purification; 2) Previous PTMs studies were carried out using tagged Httex1 protein, or model peptides; 3) The enzymes involved in regulating these PTMs are unknown, thus the researchers relied on PTMs mimetics which do not fully capture the chemical properties of the *bona fide* PTMs. Next, with these proteins in hand, our second objective is to address the knowledge gaps related to the role of the Nt17 PTMs code on Htt structure and aggregation.

More specifically, in chapter II, we report an improved semisynthetic strategy for the production of mutant Httex1. This method enables the production of milligram quantities of homogeneous mutant Httex1 site-specifically modified at single or multiple residues. Using these proteins, for the first time, we investigate the effects of phosphorylation at T3 and acetylation at K6, K9 or K15 on mutant Httex1 aggregation and structure and assess the cross-talk between the two modifications. We report that T3 phosphorylation and acetylation of single lysine residues within the N-terminal 17 amino acids of Httex1 does not modify the aggregation kinetics or structural properties of wild-type or mutant Httex1. In contrast, phosphorylation at T3 inhibits the aggregation of mutant Httex1, whereas the phosphomimetic T3D mutation results in only partial inhibition of mutant Httex1 aggregation. Finally, we observe that K6, but not K9 or K15 acetylation reverses the inhibitory effect of T3 phosphorylation on Httex1 aggregation

In Chapter III, we report the discovery of novel kinases for T3 or S13/S16 phosphorylation and use these enzymes to develop efficient, affordable, and accessible methods that allow the production of milligram quantities of phosphorylated recombinant WT and mutant Httex1 at T3 or both S13 and S16. We report also potential applications of these new methods, such as the preparation of phosphorylated Httex1 that can be fluorescently or isotopically labelled for structural or cellular applications, respectively.

Finally, in Chapter VI, we use chemical, semisynthetic and enzymatic methods to produce mutant Httex1 proteins bearing oxidized M8 alone or in combination with other PTMs (pT3 or AcK6). Then, we combine in this chapter both the experimental characterizations and molecular dynamics simulations. We observe that methionine oxidation at M8 slows down the aggregation of mutant Httex1 and decreases the helicity of the Nt17 domain.

## II. Chapter II: Mutant exon1 Huntingtin aggregation is regulated by T3 phosphorylation-induced structural changes and crosstalk between T3 phosphorylation and acetylation at K6

This research was originally published in *Angewandte Chemie-International Edition* 56(19): 5202-5207.  
[doi.org/10.1002/anie.201611750](https://doi.org/10.1002/anie.201611750)

Anass Chiki<sup>1</sup>, Sean M. DeGuire<sup>1</sup>, Francesco S. Ruggeri<sup>2</sup>, Domenico Sanfelice<sup>3</sup>, Annalisa Ansaloni<sup>1</sup>, Zhe-Ming Wang<sup>1</sup>, Urszula Cendrowska<sup>2</sup>, Ritwik Burai<sup>1</sup>, Sophie Vieweg<sup>1</sup>, Annalisa Pastore<sup>3</sup>, Giovanni Dietler<sup>2</sup>, and Hilal A. Lashuel<sup>1\*</sup>. *Angew. Chem. Int. Ed.* 2017, 56, 5202– 5207

<sup>1</sup>Laboratory of Molecular and Chemical Biology of Neurodegeneration, Brain Mind Institute and <sup>2</sup>The Laboratory of the Physics of Living Matter, Institute of Physics of Biological Systems, Ecole Polytechnique Fédérale de Lausanne (EPFL), CH-1015 Lausanne, Switzerland

<sup>3</sup>MRC National Institute for Medical Research, the Ridgeway, Mill Hill, London NW71AA (UK)

\*To whom correspondence should be addressed: Hilal A. Lashuel, Laboratory of Molecular and Chemical Biology of Neurodegeneration, Brain Mind Institute, Station 19, Ecole Polytechnique Fédérale de Lausanne, CH 1015 Lausanne, Switzerland. Tel: +4121 6939691; Fax: +4121 6931780; Email: [hilal.lashuel@epfl.ch](mailto:hilal.lashuel@epfl.ch)

**Author contributions:** A. Chiki and H.A. Lashuel designed the experiments and wrote the paper. H.A. Lashuel coordinated and supervised the study. A. Chiki conducted and analyzed the experiments. S.M. Deguire performed experiments replications. F.S. Ruggeri and U. Cendrowska performed and wrote the part related to AFM imaging and analysis. G. Dietler supervised the AFM work. D. Sanfelice performed and wrote the NMR part. A. Pastore supervised and wrote the NMR part. A. Ansaloni and Z.M. Wang performed preliminary circular dichroism of the Nt17 peptide. R. Burai helped with optimizing the desulfurization conditions. S. Vieweg developed the intein strategy. H.A. Lashuel acquired the funding for this work

## II.1 Abstract

Herein, we used protein semisynthesis to investigate, for the first time, the effect of lysine acetylation and phosphorylation, as well as the crosstalk between these modifications on the structure and aggregation of mutant huntingtin exon1 (Httex1). Our results demonstrate that phosphorylation at T3 stabilizes the  $\alpha$ -helical conformation of the N-terminal 17 amino acids (Nt17) and significantly inhibits the aggregation of mutant Httex1. Acetylation of single lysine residues, K6, K9 or K15, had no effect on Httex1 aggregation. Interestingly, acetylation at K6, but not at K9 or K15, reversed the inhibitory effect of T3 phosphorylation. Together, our results provide novel insight into the role of Nt17 post-translational modifications in regulating the structure and aggregation of Httex1 and suggest that aggregation and possibly its function(s) are controlled by regulatory mechanisms involving crosstalk between different PTMs.

## II.2 Introduction

Several lines of evidence suggest that the first N-terminal 17 amino acids of the Huntingtin protein (Htt) play important roles in modulating Htt structure, oligomerization, fibrils formation, membrane binding, subcellular localization and interactions with other proteins [337]. This combined with the fact that this short N-terminal sequence harbors several residues that are subjected to diverse post-translational modifications (PTMs), including phosphorylation, acetylation, ubiquitination and sumoylation (Scheme II.1-A), suggests that PTMs may serve as reversible molecular switches for regulating Htt structure, interactome, cellular properties and toxicity [338]. However, the lack of knowledge about the enzymes involved in regulating these modifications has made it difficult to decipher their role in regulating the function(s) of Htt in health and disease.

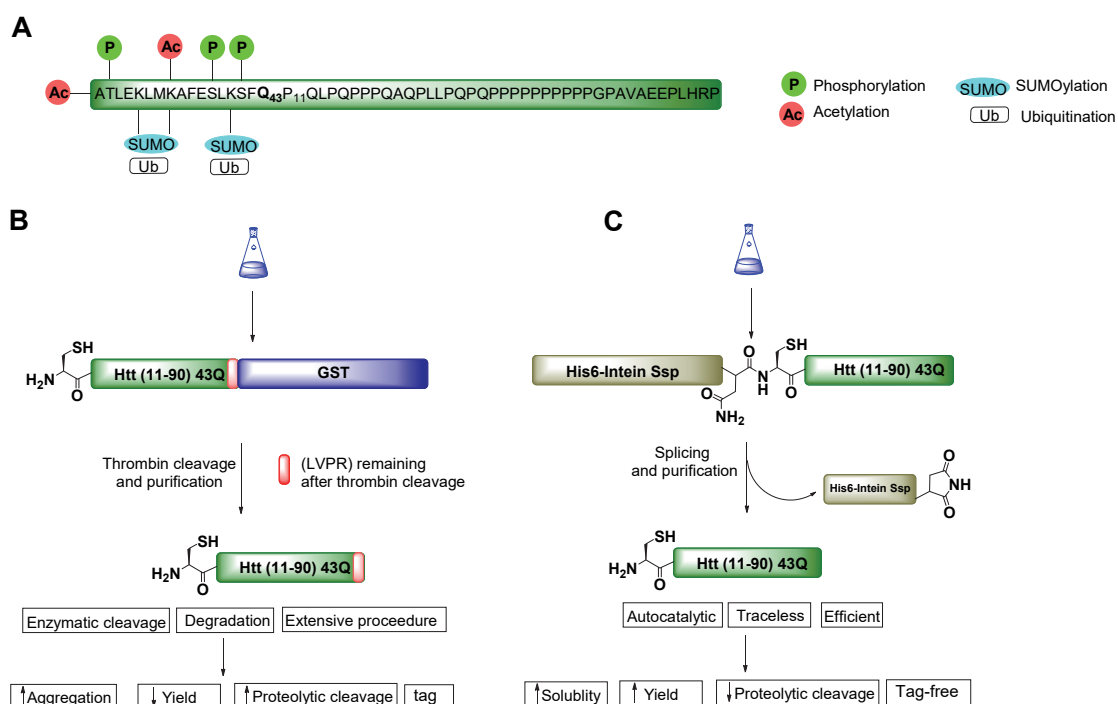
## II.3 Results and Discussion

### II.3.1 Semisynthesis of mutant Httex1

The enzymes responsible for regulating PTMs in the Nt17 region remain unknown. Only one kinase, IKK kinase, has been reported to regulate the phosphorylation of Httex1 at S13 and S16 and the overexpression of IKK $\beta$  enhances T3 phosphorylation.[282, 339] However, *in vitro*, IKK only partially phosphorylates Httex1. Although Singer et al. reported the synthesis of wild-type (WT) and mutant Httex1 using microwave-assisted solid phase peptide synthesis (SPPS) [340], repeated attempts by our group to reproduce the synthesis of mutant Httex1 using their procedures or modified procedures were unsuccessful.

Recently, our group developed a semisynthetic strategy that permits site-specific phosphorylation of wild type Httex1 at T3 containing <23 glutamine residues (Scheme II.1) [310]. This strategy is based on utilizing

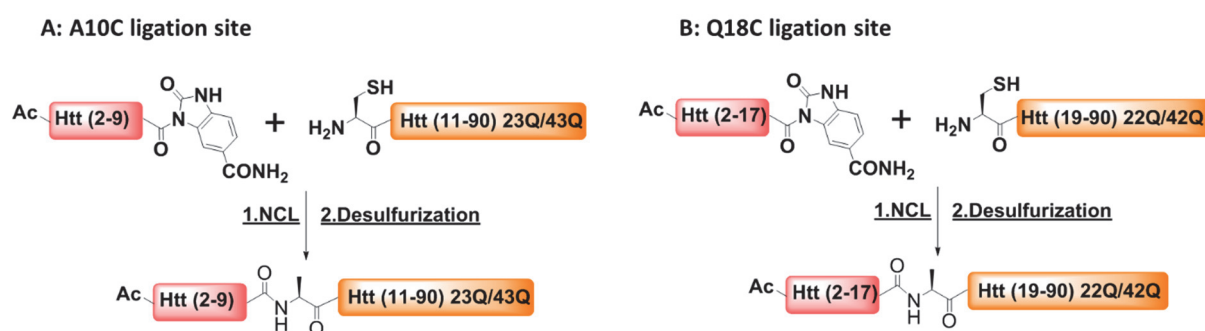
expressed protein ligation (EPL) to ligate  $\alpha$ -thioester peptides formed in situ from Htt Ac-2-9Nbz (1) prepared by Solide Phase Peptide Synthesis (SPPS) and containing the desired PTM to an expressed C-terminal Htt-A10C-90 fragment (2) with the desired polyQ repeat length (Scheme II.2). Our attempts [310] to achieve the semisynthesis of mutant Httex1 using this strategy were unsuccessful due to the poor yields and solubility of the recombinant mutant C-terminal Htt fragment (2) and its high propensity to aggregate under Native Chemical Ligation (NCL) conditions.[310] This protocol also suffered from other limitations. First, the C-terminal fragments (Htt-A10C-90) were produced by proteolytic cleavage of an Htt-A10C-90-GST fusion protein (Scheme II.1-B) [310], resulting in the addition of four non-native amino acids (LVPR). Furthermore, thrombin-mediated cleavage of Htt-A10C-90-GST 42Q was slow, leading to aggregation of the cleaved mutant Htt-A10C-90 42Q fragment. Finally, the denaturing conditions used in native chemical ligation were not sufficient to maintain the solubility of the mutant Htt-A10C-90 42Q resulting in very poor yields for the native chemical ligation reactions and the desired product, mutant Httex1-42Q.



Scheme II-1. GST and Intein strategies for the synthesis of Htt(A10C-90)-43Q

To overcome these limitations, we utilized a new intein-based strategy to produce the recombinant fragment (2) [178]. This was achieved by the expression of Htt-A10C-90 23Q/43Q as an N-terminal Ssp DnaB intein fusion protein, which undergoes rapid, pH-controlled splicing resulting in the generation of Htt-A10C-90 23Q/43Q without any additional amino acids at the C-terminus of the Htt fragment in high yields 5-6 mg/L of

culture (Scheme II.1-C) [178]. To gain access to the full range of PTMs within the Nt17 domain, an alternative ligation strategy was required. To that end, a single glutamine residue (Q18) was transiently mutated to cysteine to produce the fragments Htt-Q18C-90 22Q/42Q using the same intein-based expression and purification strategy (Scheme II.2), resulting in comparable yields (5.5 mg/L, 3.2 mg/L for 22Q and 42Q respectively) and purity (Figure II.1).



Scheme II-2. Semisynthetic strategies for the generation of Httex1 with PTM's in the Nt17 domain

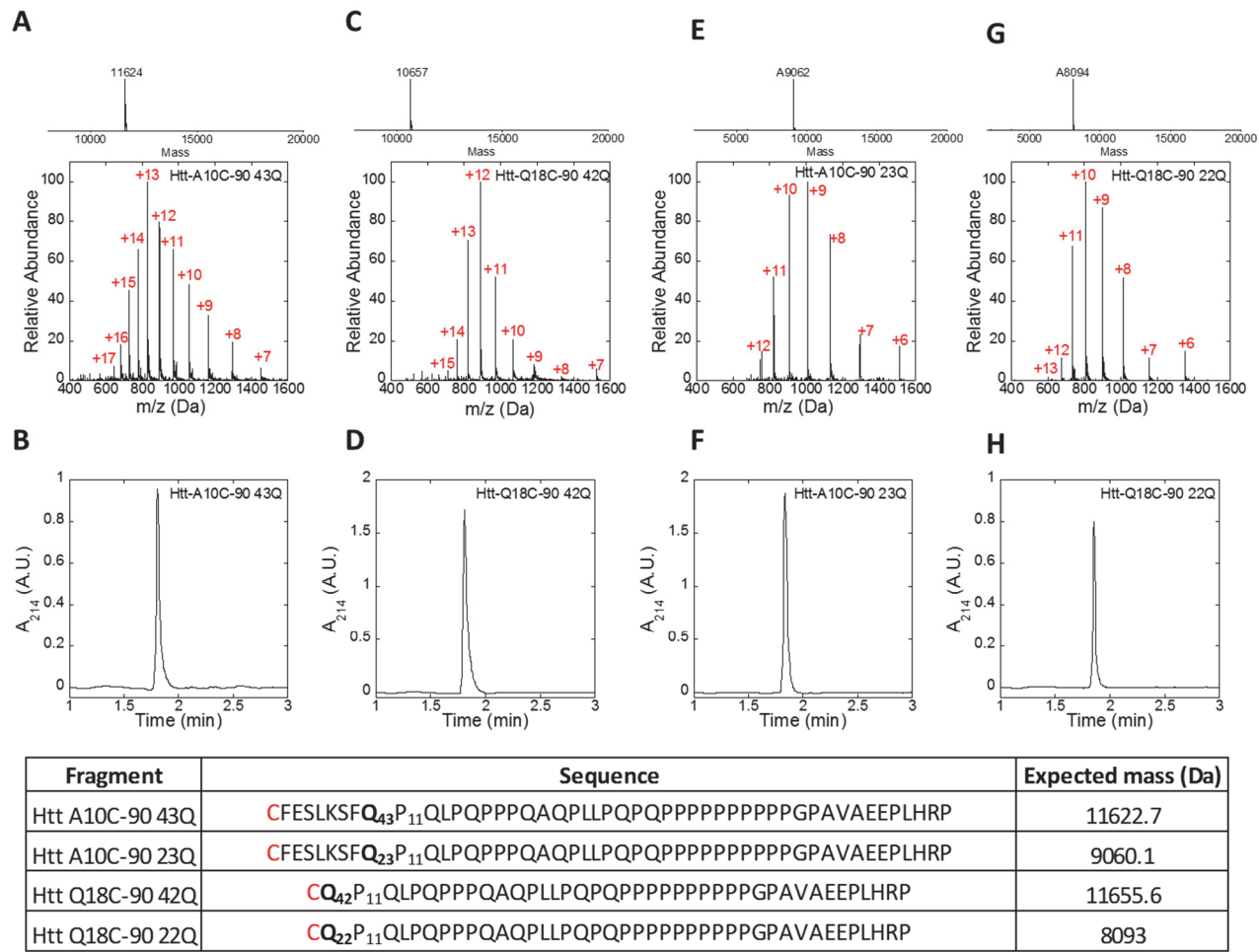
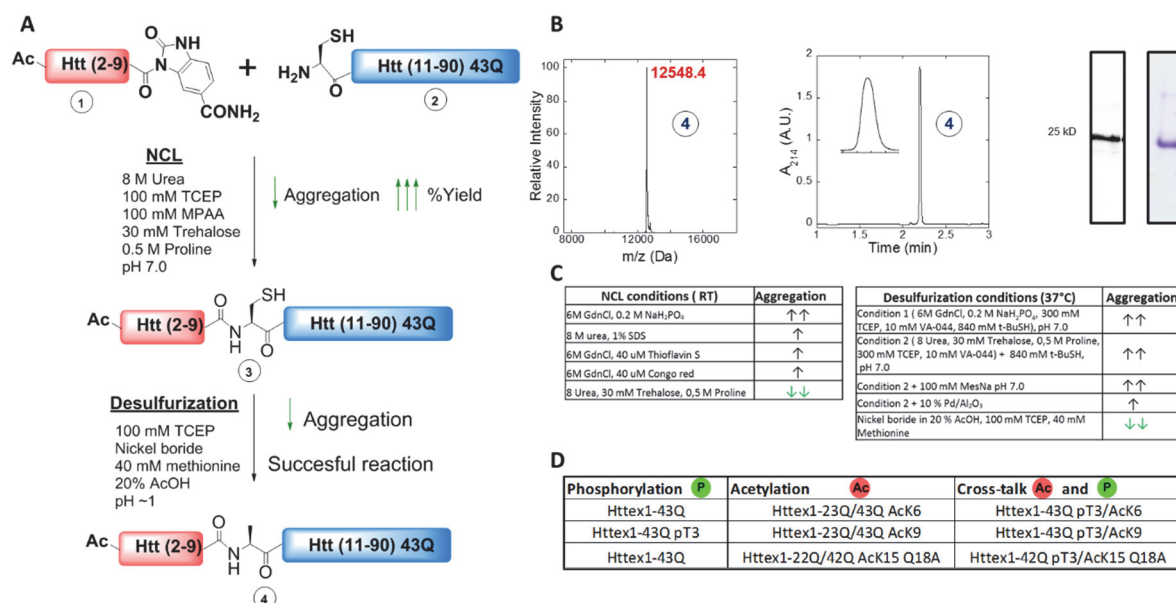


Figure II-1. Purity analysis of the recombinant C-terminal fragments of Httex1 assessed by ESI-MS and RP-UPLC.

Having produced the desired recombinant tag-free C-terminal Htt fragments (2), we focused our efforts on optimizing the conditions for the native chemical ligation (NCL) and generation of unmodified and modified forms of mutant Httex1 (43Q). Initially, we attempted to produce mutant Httex1 under typical denaturing conditions (6M GndCl, pH 7.2) used in NCL and/or in the presence of excess N-terminal peptide Htt Ac-2-9Nbz (1). However, the propensity of (2) and (3) to aggregate under these conditions resulted in poor conversion and low yields. To address these challenges, we screened a range of reaction conditions utilizing



Scheme II-3. Semisynthesis of mutant Httex1 optimization.

Optimized native chemical ligation and desulfurization conditions enabled the production of semisynthetic mutant Httex1. (A) Scheme of the optimized semisynthetic strategy developed for generation of mutant Httex1. As Methionine aminopeptidase cleavage of M1 and subsequent acetylation of A2 were found to be the most abundant protein modifications in Httex1, each peptide was prepared bearing these modifications. (B) MALDI-TOF, RP-UPLC and SDS-PAGE of Httex1-43Q produced with the new methodology (expected mass: 12,549 Da [M + H]<sup>+</sup>). (C) Table summarizing the various conditions tested to arrive at the optimal conditions for solubilization, ligation and desulfurization. (D) table summarizing all Httex1 proteins.

different buffers and small molecules that are known to improve protein solubility and inhibit protein aggregation (Scheme II.3).[341] The best conditions (Scheme II.3) found were those that combined strongly denaturing buffer (8 M urea), a high concentration of L-proline (0.5 M, reported to form a supramolecular assembly that can act as a molecular chaperone),[342, 343] and D-trehalose (30 mM, a known aggregation inhibitor).[344-346] Addition of the N-terminal Htt peptide Ac-2-9Nbz (1) and 4-mercaptophenylacetic acid (MPAA) to a solution of the C-terminal Httex1 fragment Htt-A10C-90 43Q (2) in this ligation buffer provided the desired Httex1-43Q A10C (3) rapidly at room temperature, with no observable aggregation of products or starting materials. HPLC purification provided pure (3).

The desulfurization reaction also proved to be challenging. At the temperature required for radical-mediated desulfurization (37°C) using a variety of denaturing aqueous buffers, we observed significant levels of protein aggregation that prevented complete desulfurization.[347] After screening various conditions, we found that treatment with nickel boride in 20% acetic acid allowed rapid desulfurization while preventing protein aggregation.[348] The addition of methionine (40 mM) to the reaction mixture competitively inhibited the undesired methionine desulfurization to aminobutyric acid [336] and resulted in clean conversion to the



desired product (4), as indicated by a decrease in the molecular weight of the product by 32 Da by MALDI-TOF analysis. Preparative HPLC purification provided Httex1-23Q/43Q and Httex1-22Q/42Q Q18A in milligram quantities (Table II.1) and high purity as determined by MALDI-TOF, RP-UPLC and SDS-PAGE (Scheme II-3). This optimized semisynthetic protocol enabled us to generate milligram quantities of several modified forms of mutant Httex1 containing single or multiple PTMs at high purity (Table II.1, Figure II.2, I.3 and I.4).

Table II-1. List of the produced protein showing expected masses and final yields.

Protein	Expected mass (Da)	Observed mass (Da)	Yield (%)
Httex1-43Q	12549	12548.4	36
Httex1-43Q pT3	12 629	12628.6	26
Httex1-43Q T3D	12 563	12565.2	17
Httex1-43Q AcK6	12590	12590.3	17
Httex1-43Q AcK9	12590	12591.2	20
Httex1-42Q AcK15 Q18A	12533	12532.4	11
Httex1-43Q pT3/AcK6	12 671	12672.2	25
Httex1-43Q pT3/AcK9	12 671	12674.3	21
Httex1-42Q pT3/AcK15 Q18A	12613	12615	25

Protein	Expected mass (Da)	Observed mass (Da)	Yield
Httex1-23Q	9986	9984.8	34
Httex1-23Q AcK6	10028	10030.1	27
Httex1-23Q AcK9	10028	10029.7	20
Httex1-22Q AcK15 Q18A	9970	9970.8	18

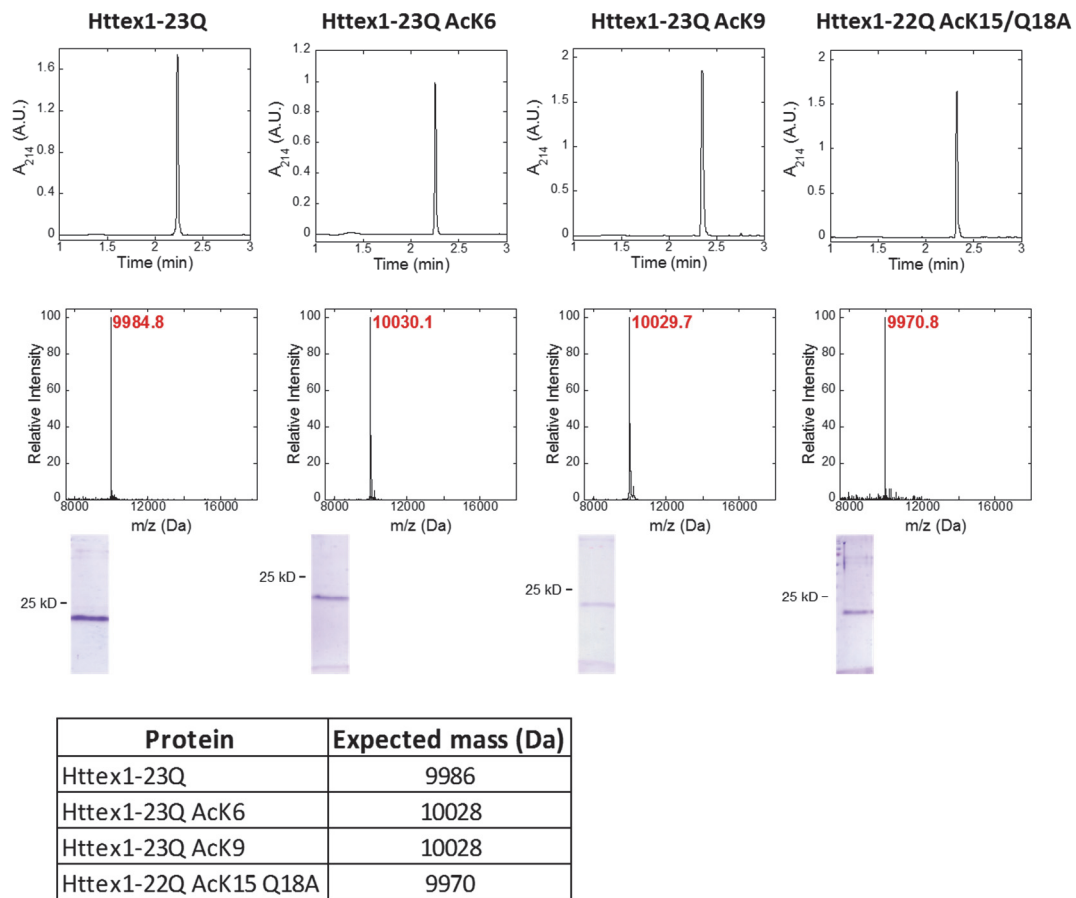


Figure II-2. Analytical characterization of unmodified Httex1-23Q proteins, unmodified, AcK6, AcK9 and AcK15 by RP-UPLC, MALDI-TOF and SDS-PAGE.

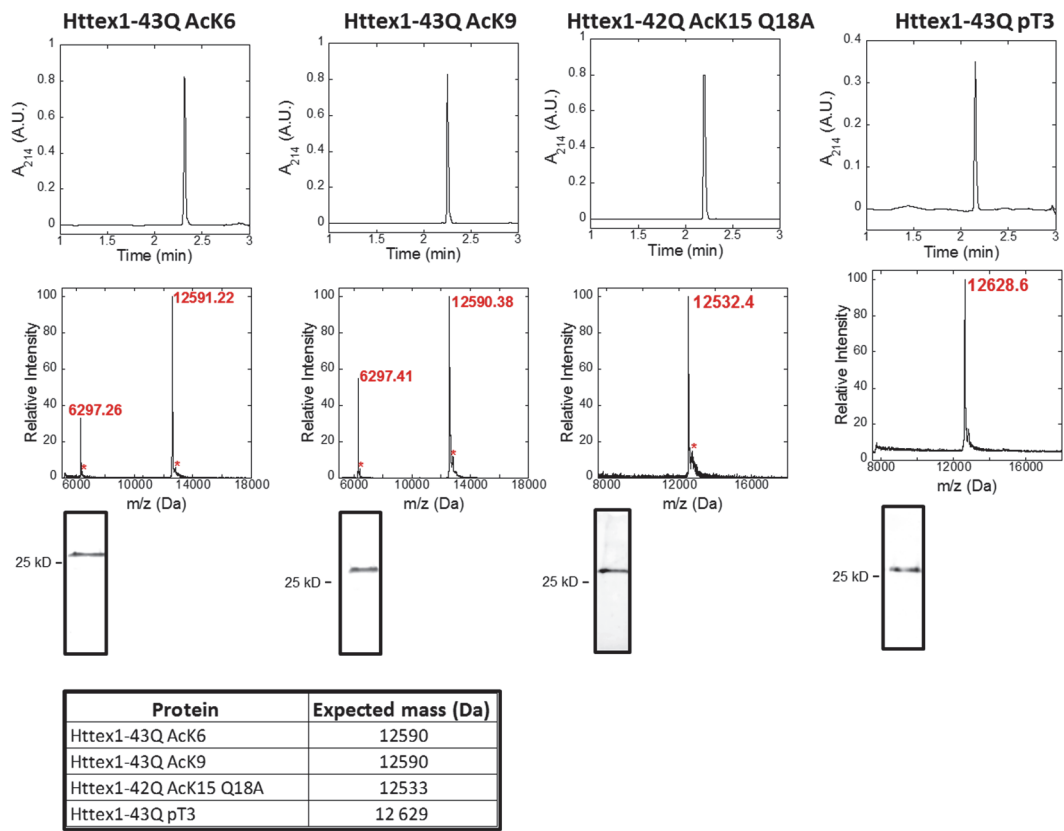


Figure II-3. Analytical characterization of Httex1-43Q proteins AcK6, AcK9 and AcK15 and pT3 by RP-UPLC, MALDI-TOF and SDS-PAGE.

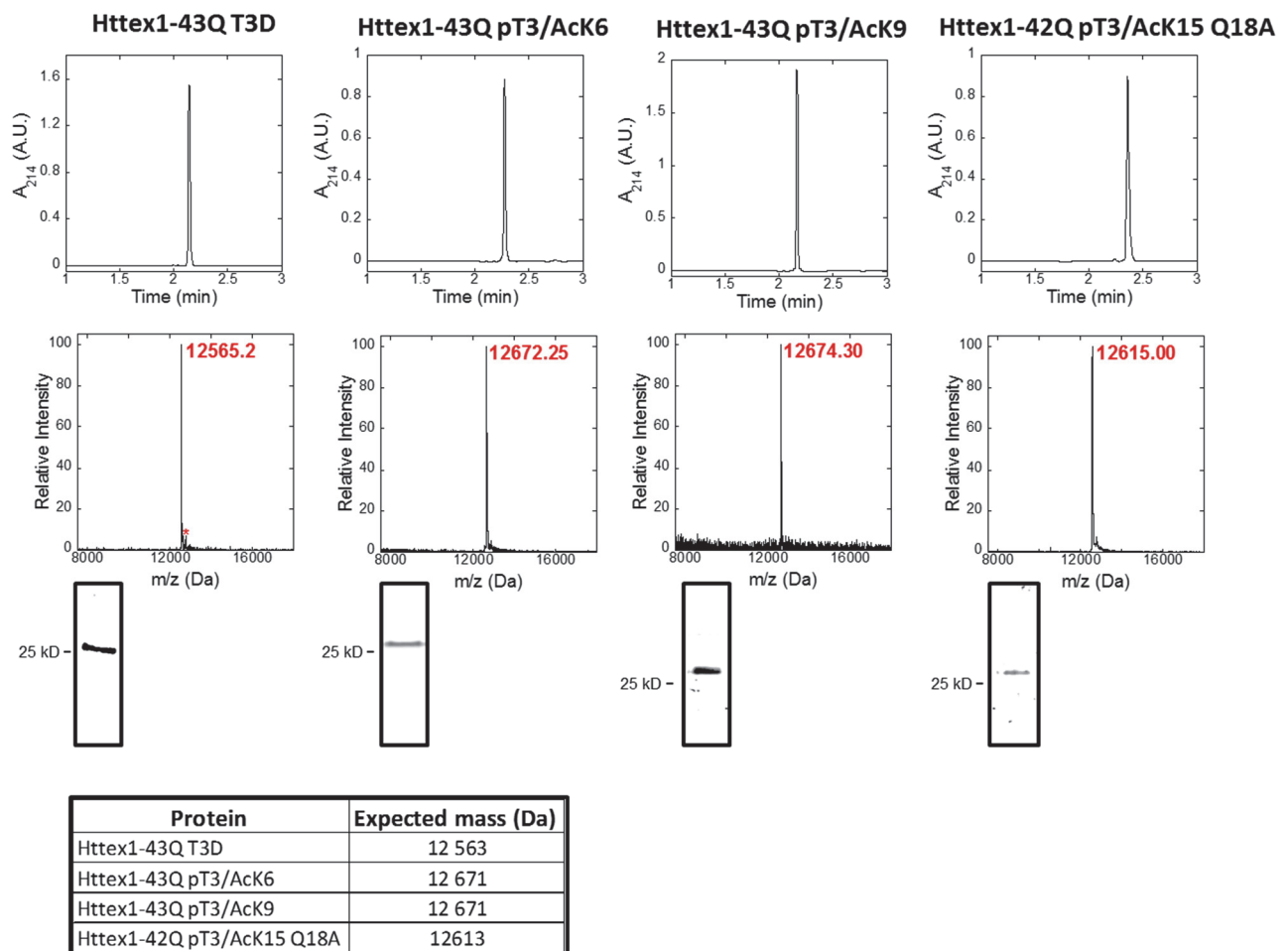


Figure II-4. Analytical characterization of Httex1-43Q T3D, pT3/AcK6, pT3/AcK9 and pT3/AcK15 by RP-UPLC, MALDI-TOF and SDS-PAGE.

### II.3.2 Threonine 3 (T3) phosphorylation inhibits mutant Httex1 aggregation more effectively than T3D phosphomimetic mutation

Threonine 3 (T3) has been identified as one of the most common phosphorylation sites in Htt from ST14A and HeLa cells and was detected at lower levels in the *postmortem* brain regions most affected by HD in a mouse model of HD (CAG140) [307, 339]. Interestingly, the level of T3 phosphorylation was inversely correlated with polyQ repeat length, suggesting that phosphorylation at T3 is decreased in pathological conditions and that restoring the physiological level of T3 phosphorylation might ameliorate HD pathology [307]. Testing this hypothesis has not been possible because the enzymes involved in regulating T3 phosphorylation remain elusive and the extent to which phosphomimetic mutations can reproduce the effect of phosphorylation remains unknown.

To address this knowledge gap, we sought to 1) determine the effect of T3 phosphorylation on mHttex1 aggregation and 2) to determine whether the phosphomimetic mutation (T3D), which is commonly used to assess T3 modification in cellular and animal models of HD, reproduces the effects of authentic T3 phosphorylation on the structure and aggregation of mutant Httex1. To achieve these goals, we prepared pT3 and T3D mHttex1-43Q using the new semisynthetic strategy (Figure II.3 and I.4). Sedimentation analysis of the unmodified mHttex1-43Q showed that ~ 75% of the protein aggregated within 12 h at 37°C and that nearly complete depletion of the soluble protein fraction occurred between 24 and 36 h (Figure II.5-A).

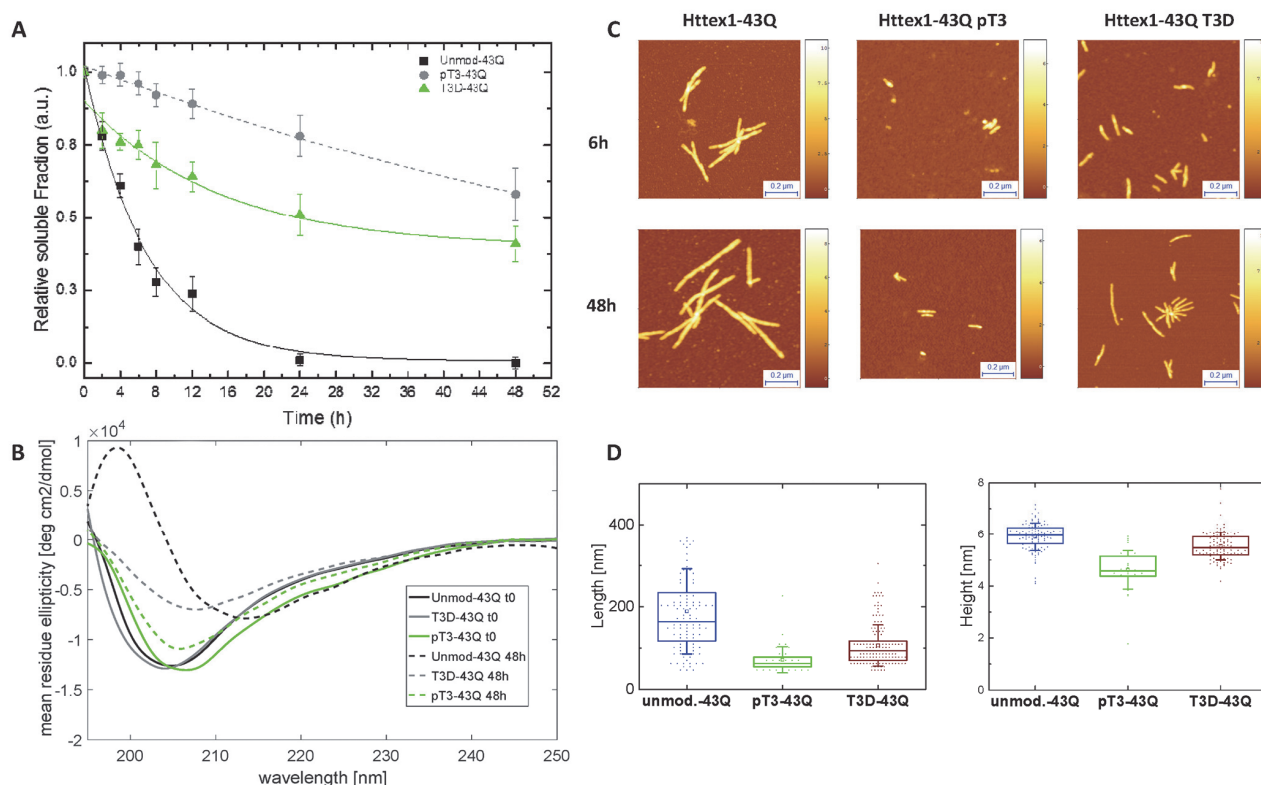


Figure II-5. Aggregation of mHttex1-pT3 and T3D compared to unmodified mHttex1 at 3 μM.

(A) Sedimentation assay (loss of soluble protein) based on RP-UPLC (n=6, fitted with exponential decay). (B) CD analysis of the samples at 0 and 48 h. (C) AFM characterization of unmodified mHttex1 and mHttex1-pT3 and T3D aggregates. The XY scale bars are 200 nm, the Z scales are in nm. (D) Height and length quantification of the aggregates formed by the three proteins at 48 h.

This was accompanied by a shift in the circular dichroism (CD) spectrum that is indicative of a change in secondary structure from a predominantly disordered structure ( $\lambda_{\min}$  205 nm) to a  $\beta$ -sheet-rich structure ( $\lambda_{\min}$  215 nm, Figure II.5-B), consistent with the observation of fibrillar aggregates at 48 h by transmission electron microscopy (TEM) (Figure II.6 and I.7). In contrast, 89% and >60% mHttex1-pT3 remained soluble after 12 and 48 h of incubation respectively (Figure II.5-A). No major change in the secondary structure of Httex1-pT3

was observed by CD even after 48 h (Figure II.5-B). TEM analysis showed mainly oligomers and short fibrillar structures with shorter average lengths than those formed by unmodified mHttex1 (Figure II.6 and I.7).

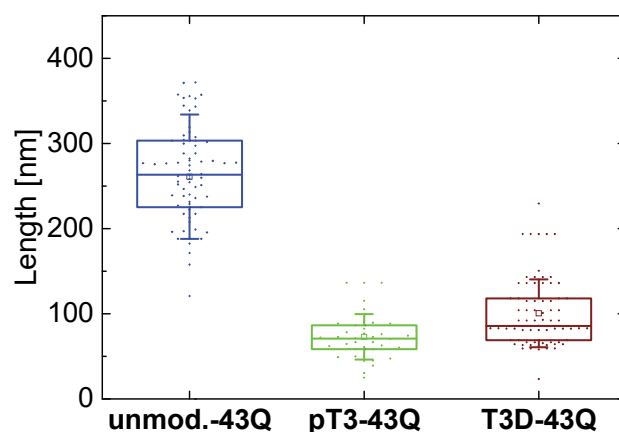


Figure II-6. TEM length quantification of Httex1-43Q, Httex1-43Q pT3 and Httex1-43Q T3D.

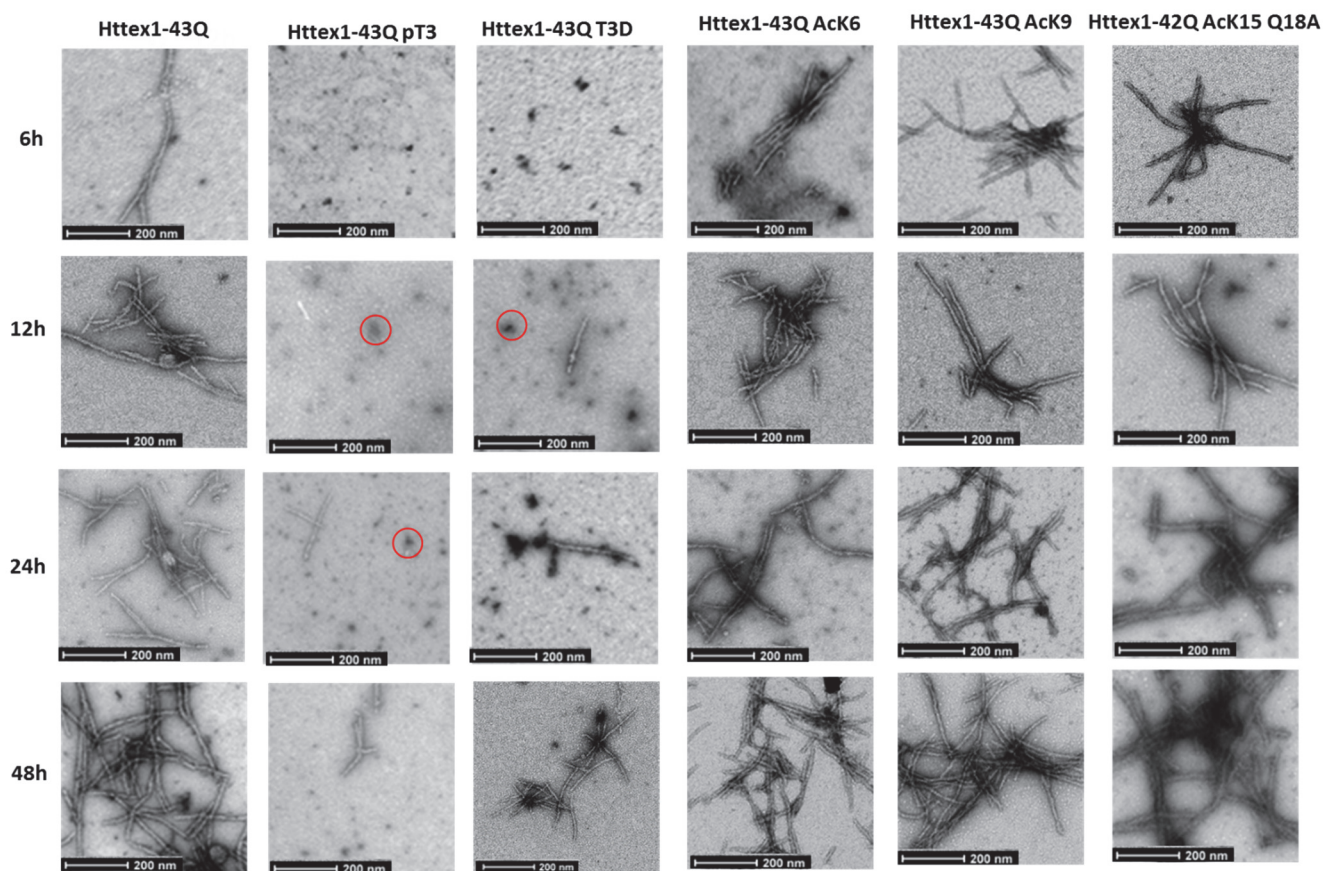


Figure II-7. TEM analysis of mutant Httex1.

TEM analysis of mutant Httex1 (unmodified, AcK6, AcK9, AcK15-42Q Q18A, pT3 and T3D) aggregation monitored overtime. Scale bars = 200 nm.



To further characterize the inhibitory effect of T3 phosphorylation, we assessed Httex1-43Q and Httex1-43Q pT3 aggregation over the concentration range of 5-30  $\mu\text{M}$  using a real time ThS fluorescence assay (Figure II.8). As expected, the aggregation of Httex1-43Q shows a strong concentration dependence, whereas mature fibril formation by Httex1-43Q pT3 was only observed at concentrations of  $\geq 30 \mu\text{M}$ , as evident by the presence of long fibrils that bind ThS and exhibit  $\beta$ -sheet structure. At concentration of  $\leq 20 \mu\text{M}$  short protofibrils and fibrillar structures were observed as the predominant species (Figure II.8 E&F) and significant amount ( $\sim 50\%$ , Figure II.8 C&D) of soluble protein remained in solution even after 14 days of incubation, whereas complete aggregation for Httex1-43Q was observed after 5-40 h over this concentration range. The striking inhibitory effect of phosphorylation at T3 on the aggregation rate and structural transitions to mature fibrils underscores the great impact that PTMs of Nt17 may have on the structure and aggregation of Httex1. Interestingly, the strong  $\beta$ -sheet and aggregation inhibitory effect induced by phosphorylation at T3 were not reproduced by the phosphomimetic mutation (T3D) (Figure II.5). The fibrils formed by mHttex1-T3D were of intermediate size (Figure II.6) compared to those formed by pT3 and unmodified mHttex1 (Figure II.6 and I.7).

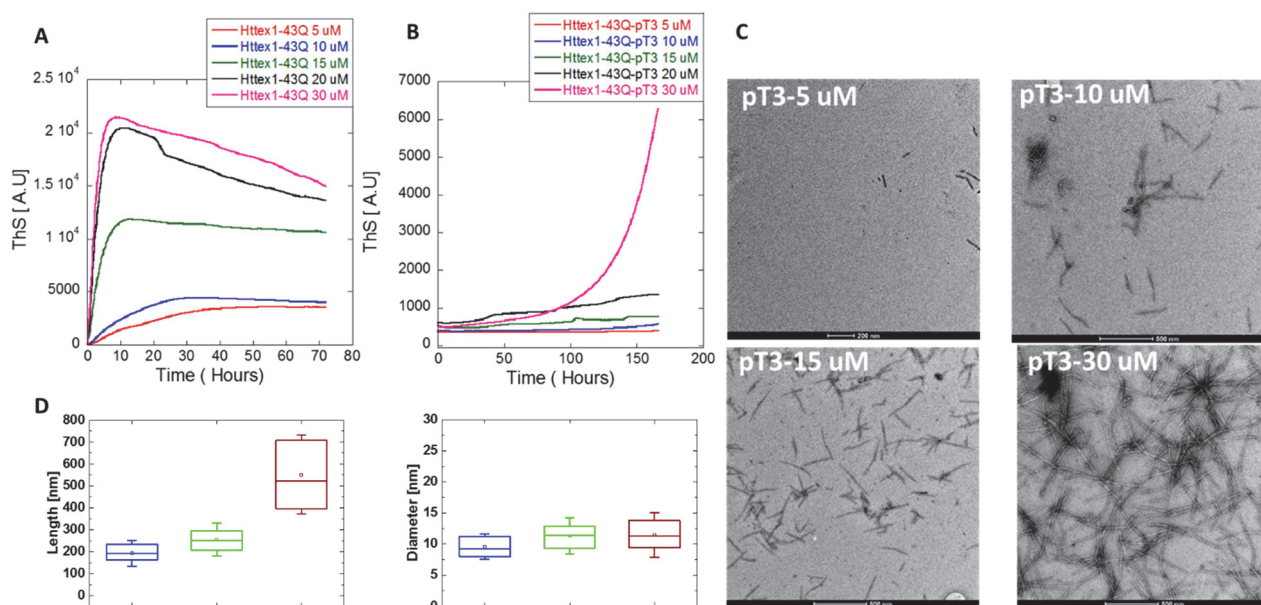


Figure II-8. Concentration dependence of Httex1-43Q pT3 aggregation.

(A-B) continuous aggregation monitored by Thioflavin S binding assay for unmodified Httex1-43Q (A) and Httex1-43Q (B) pT3 at 5 different concentrations (5  $\mu\text{M}$ , 10  $\mu\text{M}$ , 15  $\mu\text{M}$ , 20  $\mu\text{M}$  and 30  $\mu\text{M}$ ). (C) EM analysis of pT3 fibrillization after 7 days of incubation. (D) EM analysis of length and diameter of Httex1-43Q pT3 at different concentration (5  $\mu\text{M}$  did not exhibit enough fibrillar forms for the analysis).

Detailed characterization of the morphology and dimensions of the aggregates formed by pT3 and T3D by high-resolution atomic force microscopy (AFM) was performed. We measured the average height and length of pT3, T3D and unmodified mutant Httex1 aggregates at selected time points (Figure II.9). The maturity of fibril formation is strictly related to the morphology of the fibrils and their cross-sectional dimensions. Typically, mature amyloid fibrils possess a height > 6 nm and exhibit CD spectra that show a prominent signal for  $\beta$ -sheet structures (minimum between 215-222 nm).[310, 349-352] After only six hours of incubation, the unmodified Httex1-43Q contained mature fibrillar species (Figure II.9-A-B) with an average length of  $128 \pm 69$  nm and a height of  $6 \pm 1$  nm (Figure II.9-A-B). At this time point (6h), T3D-Httex1 aggregates were  $5.2 \pm 0.7$  nm in height and were significantly shorter ( $82 \pm 29$  nm). This trend persisted even after longer incubations; the length of the aggregates formed by the unmodified and T3D Httex1-43Q proteins increased only by 20-30 nm and their height remained unchanged (Figure II.9-A-B). Compared to unmodified Httex1-43Q, the Httex1-43Q T3D exhibited shorter fibrils ( $106 \pm 49$  nm) with average heights of  $5.5 \pm 0.5$  nm. In the case of Httex1-43Q pT3, we did not observe a sufficient number of aggregates at 6 hours to perform a valid quantification and no fibrillar structures were observed even after 48h at this concentration ( $3 \mu\text{M}$ ). Instead, mainly protofibrillar-like structures with average lengths and heights of  $71 \pm 30$  nm and  $4.6 \pm 0.5$  nm respectively were observed (Figure II.9-A-B). The correlation of the cross-sectional dimensions (height vs. length) of each aggregate (Figure II.9-C) showed that Httex1-43Q pT3 existed predominantly as a mixture of abundant and predominantly unstructured oligomers (highlighted with red circles in Figure II.7) or protofibrils (height 4-5 nm, length 50-150 nm) and a small population of short nearly mature fibrils (height 5-6 nm, length 50-150 nm), whereas Httex1-43Q T3D formed a mixture of long nearly mature fibrils (height 5-6 nm, length 50-300 nm) and well-defined mature fibrils (height >6 nm, length 50-300 nm) (Figure II.9).



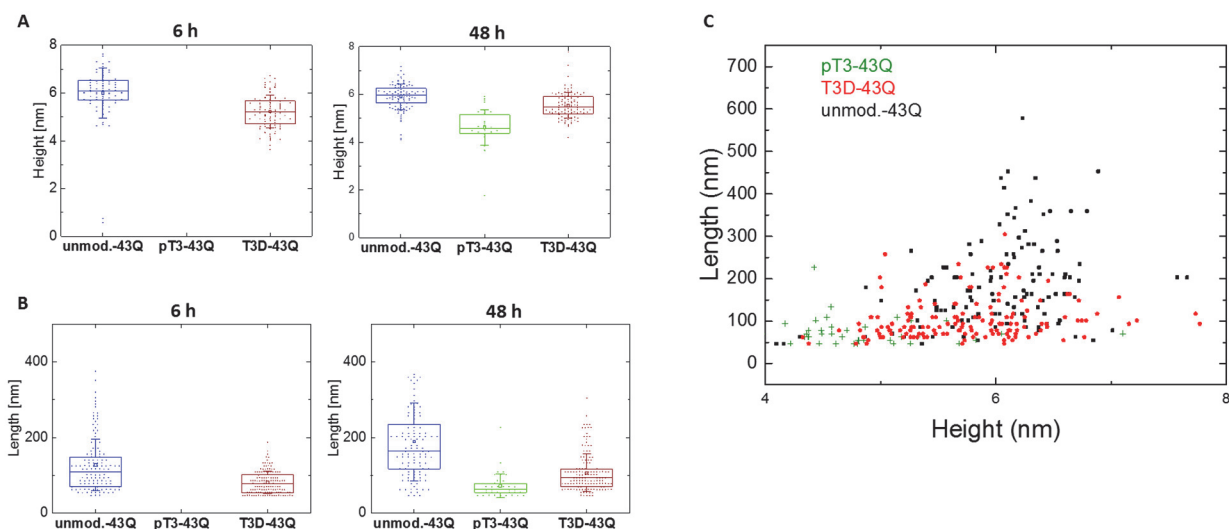


Figure II-9. Statistical analysis of AFM images to compare Httex1-43Q unmodified, pT3 and T3D.

Aggregation characterization of Httex1-43Q pT3 and T3D compared to Httex1-43Q by AFM. Height (A) and length (B) quantification of the aggregates by AFM. (C) Scatter plot – Height vs. Length at 48h.

### II.3.3 Assessment of the effect of T3 phosphorylation on the structure of Nt17 peptide by NMR

To gain insight into the mechanism by which this modification inhibits mutant Httex1 aggregation, we investigated the effects of phosphorylation and phosphomimetics at T3 on the structure of Nt17 peptides. Htt1-19 showed a CD spectrum indicative of a mainly random coil structure mixed with partially  $\alpha$ -helical structures consistent with previous CD and atomistic simulation studies (Figure II.10-A) [198],[312]. In contrast, the CD spectrum of Htt1-19-pT3 showed a double minimum at 208 and 222 nm, indicative of a predominantly  $\alpha$ -helical structure (Figure II.10-A). To the best of our knowledge, this is the most striking stabilization of Nt17 helical conformation without the use of fluorinated solvents (e.g. TFE). The pT3-induced  $\alpha$ -helical structure is pH-sensitive. N-terminal acetylation increases the pT3-induced helicity, but the overall helicity follows the same linear decrease with decreasing pH in the presence or absence of acetylation (Figure II-10-B). The HttAc2-19 T3E and T3D peptides exhibited CD spectra similar to that of the unmodified HttAc2-19 peptide (Figure II10-A), confirming again that these mutations do not reproduce the structural effects of phosphorylation at T3.

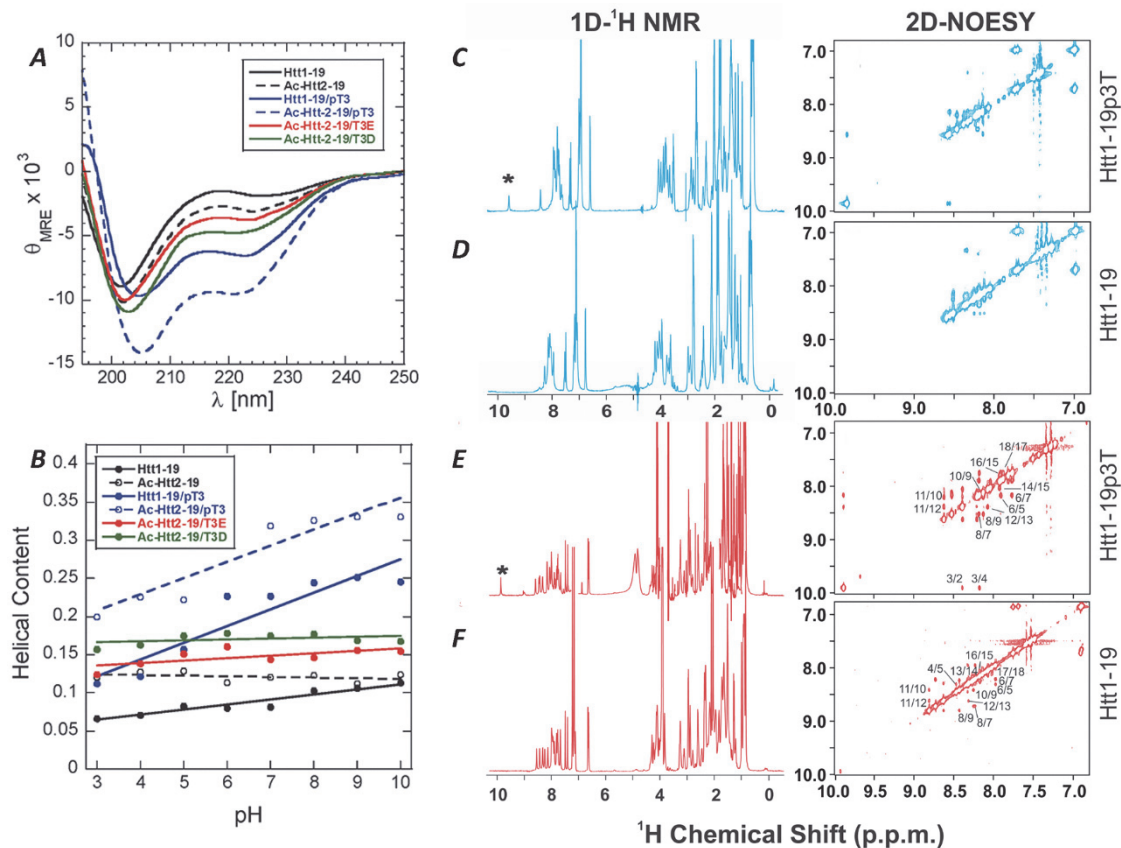


Figure II-10. NMR and Circular dichroism analysis of the Htt1-19 peptides.

(A) Far-UV CD spectra of WT and pT3 Htt1-19 peptides compared to WT, pT3, T3E and T3D HttAc2-19 at pH 7.0. (B) Helical content of each peptide as a function of pH. (C) and (D) 1D WATERGATE and 2D homonuclear NOESY spectra of Htt1-19 phosphorylated in position 3 and non-phosphorylated respectively. (E) and (F) Same as in (C) and (D) in the presence of 33% TFE; also reported is the assignment of the NH-NH chemical shifts typical of alpha helical structure, a star highlights the characteristic signals arising upon phosphorylation of T3.

Next, we conducted nuclear magnetic resonance (NMR) studies of the conformation of Htt1-19 and Htt1-19pT3 (Table II.2) in aqueous buffer and in 2,2,2-Trifluoroethanol (TFE) (33%) and compared their chemical shifts and the NOESY patterns [353]. The spectra of Htt1-19 and Htt1-19pT3 have similar features in aqueous buffer and TFE with similar chemical shifts for residues 6-19. However, the amide proton of T3 appears significantly shifted in Htt1-19 pT3, which is highly shifted downfield at 9.9 ppm (>1.5 ppm) compared to the unmodified peptide (Figure II.10-C-D, left). Phosphorylated peptides do not typically present such a chemical shift variation. Even more notable is the NOE pattern. In buffer (Figure II.10-C-D, right), the spectrum of Htt1-19 has clear features of a nascent helix (HN-HN connectivity) that can be stabilized by fluoroalcohols (TFE) demonstrating a propensity to assume a stable  $\alpha$ -helical conformation. The NOESY spectra of Htt1-19 in TFE (Figure II.10-E) show uninterrupted sequential HN-HN connectivities and other NOE patterns expected for helical structures ( $\text{HN}_i\text{-HN}_{i+1}$ ,  $\text{H}\alpha_i\text{-HN}_{i+4}$  and  $\text{H}\alpha_i\text{-HN}_{i+4}$ ) in the tract 5-19. Residues M1, A2 and T3 are not identifiable indicating a high flexibility of the N-terminus where the helix frays. In the NOESY of Htt1-19pT3,

the resonance of the T3 amide of Htt1-19pT3 forms unmistakable sequential HN-HN connectivities with the previous and following amide groups, indicating that the phosphorylated T3 residue is strongly rigidified compared to the unmodified residue extending  $\alpha$ -helix structure to A2.

Table II-2. List and sequence of the peptides used in the NMR and Circular dichroism analysis.

Peptide	Sequence
Htt1-19	MATLEKLMKAFESLKSFQQ
Ac-Htt2-19	Ac-ATLEKLMKAFESLKSFQQ
Htt1-19/pT3 ( Htt1-19p3T)	MA(pT)LEKLMKAFESLKSFQQ
Ac-Htt1-19/pT3	Ac-A(pT)LEKLMKAFESLKSFQQ
Ac-Htt1-19/T3E	Ac-AELEKLMKAFESLKSFQQ
Ac-Htt1-19/T3D	Ac-ADLEKLMKAFESLKSFQQ
Ac-2-17 WT	Ac-ATLEKLMKAFESLKSF
Ac-2-17 pT3	Ac-A(pT)LEKLMKAFESLKSF
Ac-2-17 AcK6	Ac-ATLE(AcK)LMKAFESLKSF
Ac-2-17 pT3/AcK6	Ac-A(pT)LE(AcK)LMKAFESLKSF

### II.3.4 Acetylation of single lysine residues in Nt17 does not affect the aggregation properties of WT or mutant Httex1

Although acetylation of lysine residues within Nt17 has been proposed to play a role in regulating its association with membranes [211], only K9 was reported to be acetylated in HEK cells [283] and was proposed to play an important role in Htt clearance [282]. Chaibva et al. reported that acetylation of Httex1 retards fibrils formation *in vitro* [211]. However, it is noteworthy that their findings were based on nonselective chemical acetylation of all lysine residues in a model peptide of Httex1 lacking the last 39 C-terminal residues and containing two non-native lysines residues which were also partially acetylated. To investigate the effect of lysine acetylation on Httex1 aggregation, we produced both WT (23Q) and mutant (43Q) Httex1 acetylated at single lysine residues (AcK6, AcK9, and AcK15). Figure II.11 demonstrates that acetylation at single lysine residues does not influence the aggregation of WT or mutant Httex1 (Figure II.11, Figure II.7 and I.12), except for acetylation at K6 that appeared to slightly delay mHttex1 aggregation. In all cases, the loss of soluble protein was accompanied by a shift in the secondary structure from random coil to  $\beta$ -sheet structure (Figure II.11B) and by the formation of fibrillar aggregates of comparable morphology and length (Figure II.11-C, Figure II.7). These findings suggest that lysine acetylation at K6, K9 or K15 alone does not play a critical role in the regulation of Httex1 aggregation *in vitro*.

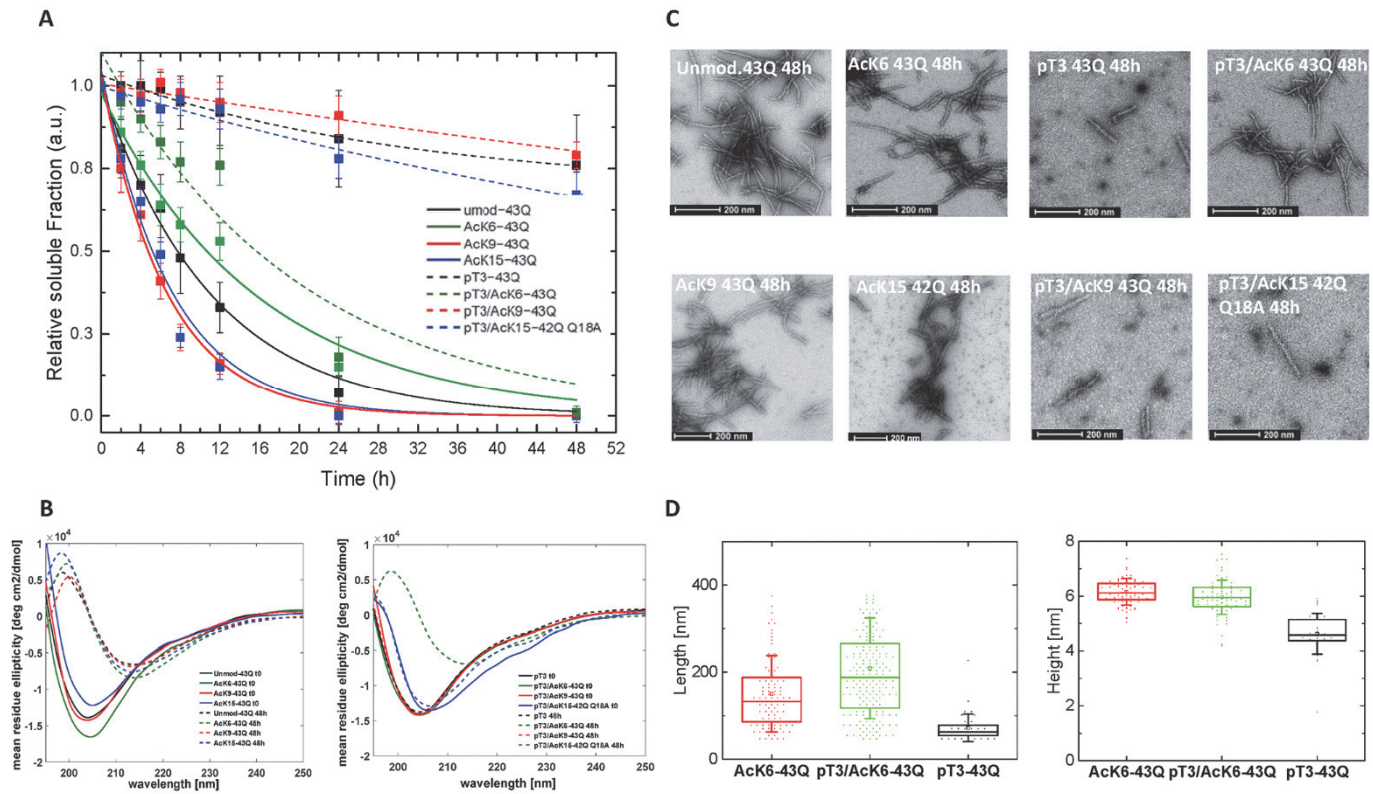


Figure II-11. Aggregation of single lysine acetylated mHttex1 and mHttex1 phosphorylated at T3 and acetylated at-Ack6, Ack9, or Ack15.

(A) Sedimentation assay (loss of soluble protein) based on RP-UPLC (n=6, fitted with exponential decay). (B) CD analysis and (C) TEM micrographs of the proteins after 48h of aggregation. (D) Height and length quantification of the aggregates by AFM at 48h.

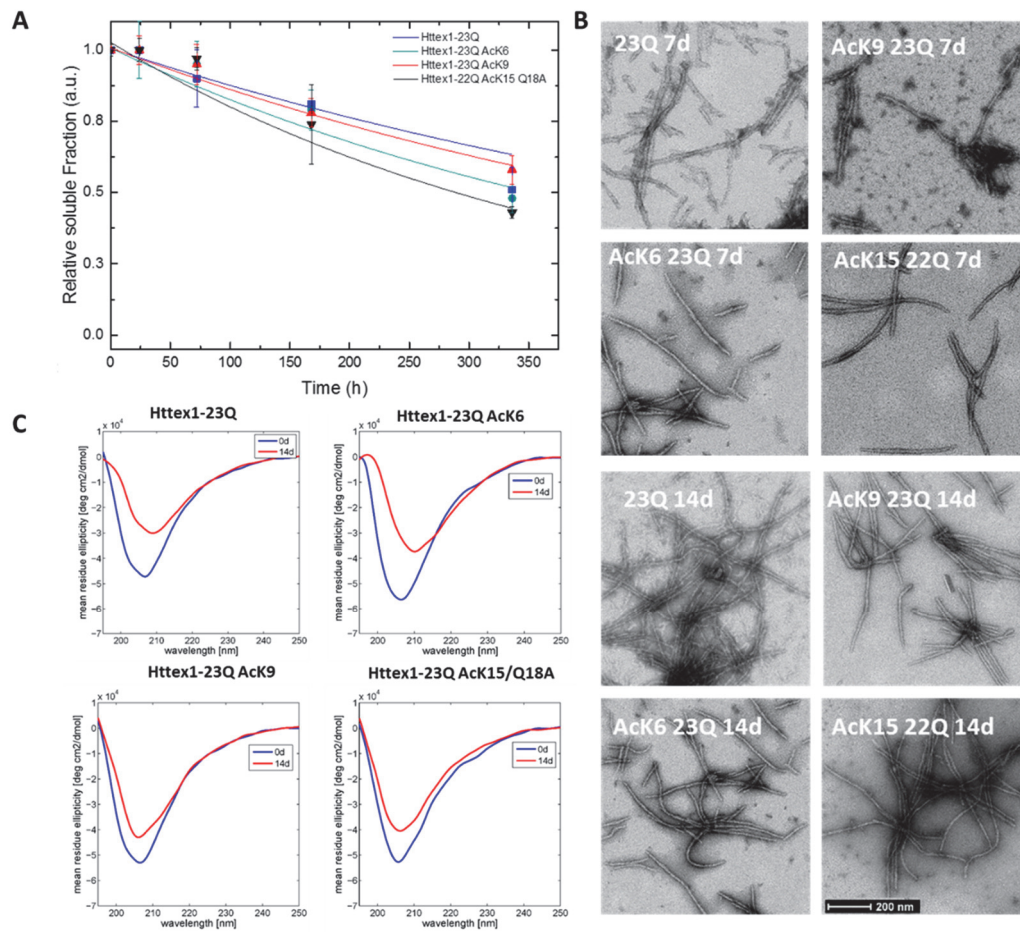


Figure II-12. Characterization of the aggregation of Httex1-23Q Ac6, Ac9 and Ac15 compared to unmodified Httex1-23Q over time by sedimentation (A), TEM (B) and CD (C).

### II.3.5 K6 acetylation reverses the inhibitory effect of pT3 in mutant Httex1.

Given the close proximity of lysine residues K6, K9 and K15 to neighboring phosphorylation sites (T3, S13 and S16), we examined the potential crosstalk between lysine acetylation and phosphorylation within Nt17. We focused initially on phosphorylation at T3 and acetylation at K6 because of the close proximity of the two residues, also due to the role of K6 in stabilizing pT3-induced Nt17 helix formation and the striking inhibitory effect of pT3 on mHttex1 aggregation. Sedimentation analysis showed that mHttex1-pT3/AcK6 exhibited similar aggregation profile as unmodified mHttex1 and mHttex1-AcK6 (Figure II.11-A), whereas mHttex1-pT3/AcK9 and mHttex1-pT3/AcK15 Q18A, exhibited similar aggregation profiles as mHttex1-pT3. These findings indicate that K6, but not K9 or K15 acetylation partially reverses the inhibitory effect of T3 phosphorylation on mutant Httex1 aggregation. Consistent with this hypothesis, only mHttex1-pT3/AcK6 converted to  $\beta$ -sheet-rich fibrillar structures after 48 h of incubation, whereas mutant mHttex1-pT3, mHttex1-pT3/AcK9 or mHttex1-pT3/AcK15 exhibited CD spectra consistent with a predominantly disordered conformation (Figure II.11-B, I.11-C and I.13). At 6 hours, AFM analysis (Figure II.14-A) of the cross-sectional dimensions of Httex1-43Q pT3/AcK6 showed the formation of short not-mature fibril like structures with an average length of  $111 \pm 54$  nm and an average height of  $5.1 \pm 1.4$  nm. In contrast, Httex1-43Q AcK6 formed mature fibrils ( $133 \pm 64$  nm and  $6 \pm 0.8$  nm average lengths and heights, respectively) similar to those formed by the unmodified Httex1 protein (Figure II.14-C). At 48 hours, AFM analyses at 48 hours confirmed that the Httex1-43Q pT3/AcK6 protein formed fibrillar aggregates comparable to those formed by unmodified and Httex1-43Q AcK6 with average height of  $6 \pm 0.5$  nm and  $6.1 \pm 0.4$  nm and average length of  $208 \pm 115$  nm  $150 \pm 87$  nm for Httex1-43Q pT3/AcK6 and Httex1-43Q AcK6 respectively (Figure II.14-C). In contrast, Httex1-43Q pT3 showed only small aggregates (average lengths and heights of  $71 \pm 30$  nm and  $4.6 \pm 0.5$  nm, respectively) (Figure III.1). The pT3 length and height statistics correspond to the same AFM analysis in Figure III.1. The comparison of the cross-sectional dimensions of each type of aggregate (Figure II.14-C) confirmed this observation. Similar observations were made at higher protein concentrations (30-45  $\mu$ M, Figure II.15).



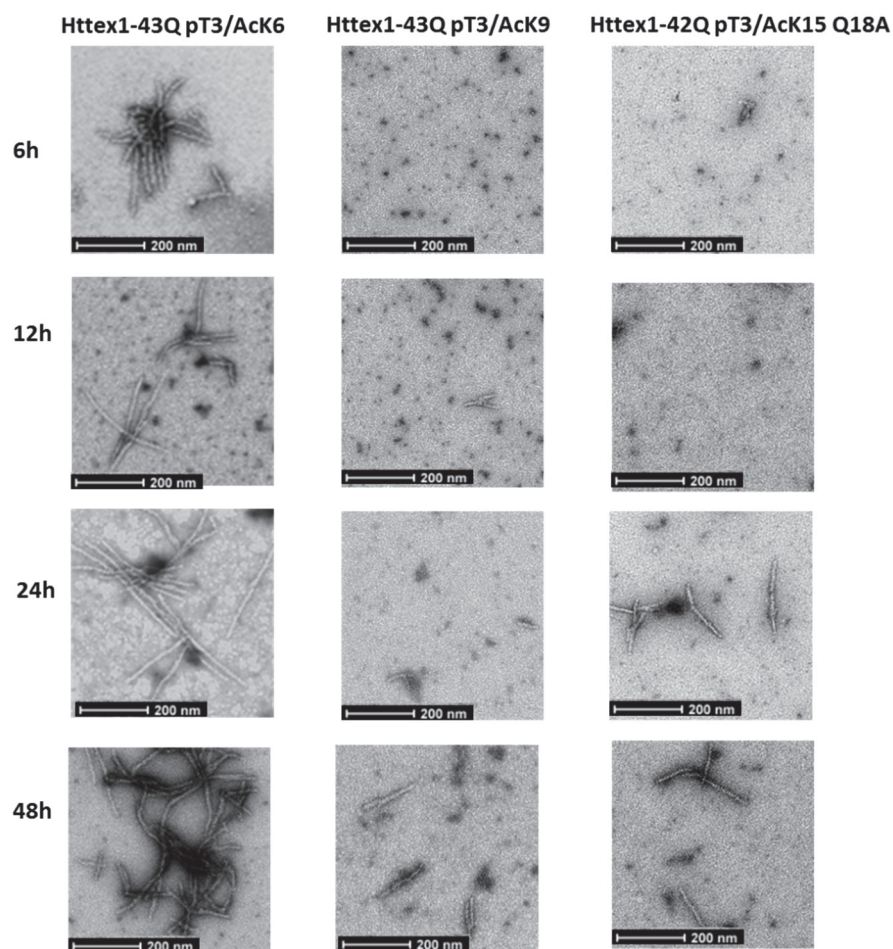


Figure II-13. TEM analysis of mutant Httex1 (pT3/AcK6-43Q, pT3/AcK9-43Q and pT3/AcK15-42Q Q18A)

Aggregation monitored overtime. Scale bars are 200 nm.

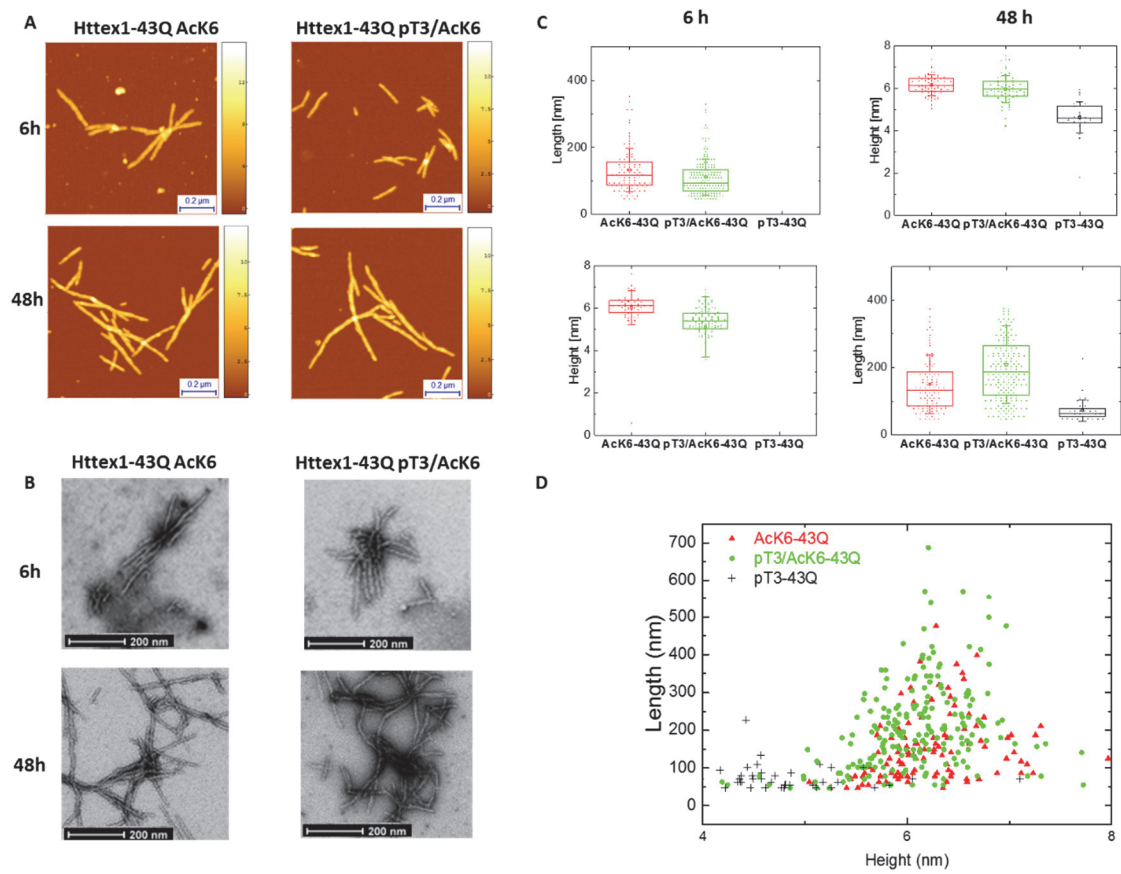


Figure II-14. Aggregation characterization of httex1-43Q AcK6 and pT3/AcK6 compared to Httex1-43Q pT3 by AFM

(A) and by TEM (B). The scale bars are 200 nm. (C) Height and length quantification of the aggregation by AFM. (D) Scatter plot – Height vs. Length at 2 days.



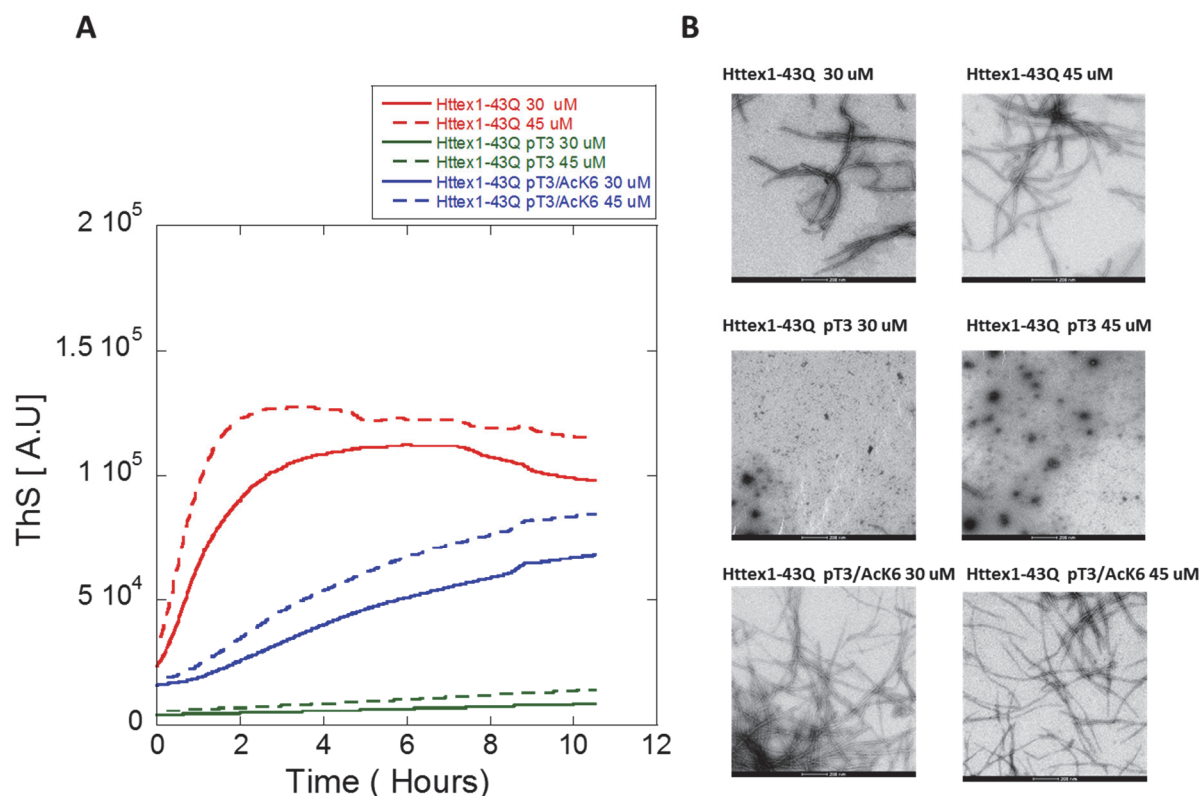


Figure II-15. *In vitro* aggregation for Httex1-43Q pT3 and pT3/AcK6

**(A)** *In vitro* aggregation kinetics for Httex1-43Q pT3 and pT3/AcK6 compared to unmodified Httex1-43Q monitored by Thioflavin S binding assay at 30  $\mu$ M and 45  $\mu$ M. **(B)** EM analysis of the sample after 10 hours of incubation at 37°C (scale bars are 200 nm).

To determine if the effect of acetylation at K6 on the aggregation inhibitory effects of phosphorylation at T3, we investigated by NMR the role of K6 in stabilizing/destabilizing the N-terminal helical conformation induced by pT3. We compared the behavior of the N-terminally protected phosphorylated and non-phosphorylated AcHtt2-17AcK6 peptides, where K6 was neutralized with acetylation, to that of AcHtt2-17. As it has become clear to us that native Htt is N-terminally acetylated, all the peptides used to investigate the interplay between T3 phosphorylation and K6 acetylation were N-terminally acetylated. As shown in Figure II.10-A, N-terminal acetylation does not significantly alter the conformational properties of Nt17. Both AcHtt2-17pT3 and AcHtt2-17pT3/AcK6 present the resonance of pT3 down-field shifted as compared to AcHtt2-17 and AcHtt2-17AcK6 (Figure II.16). However, the NOESY pattern of AcHtt2-17pT3 and AcHtt2-17pT3/AcK6 are similar, indicating that acetylation at K6 does not significantly alter the Nt17 helical conformation (Figure II.16). Our NMR results are confirmed by the CD analysis of the same peptides, which showed that pT3 and pT3/AcK6 Httex1 exhibit similar helical structure and contents (Figure II.17). These findings are consistent

with emerging evidence that the role of the Nt17 in regulating Httex1 aggregation is determined by factors that influence not only the conformation of this peptide but also its interactions with itself and the polyQ domain [198] [177] [212]. The existing data do not support a direct and simple relationship between Nt17 helicity and Httex1 aggregation, suggesting that Httex1 aggregation can proceed through distinct amyloidogenic conformations. Therefore, more studies are needed to dissect the different mechanisms by which PTMs or cross-talk between PTMs influence the intra- and intermolecular interactions of Httex1, the amyloidogenic conformation of the polyQ domain and Httex1 aggregation.

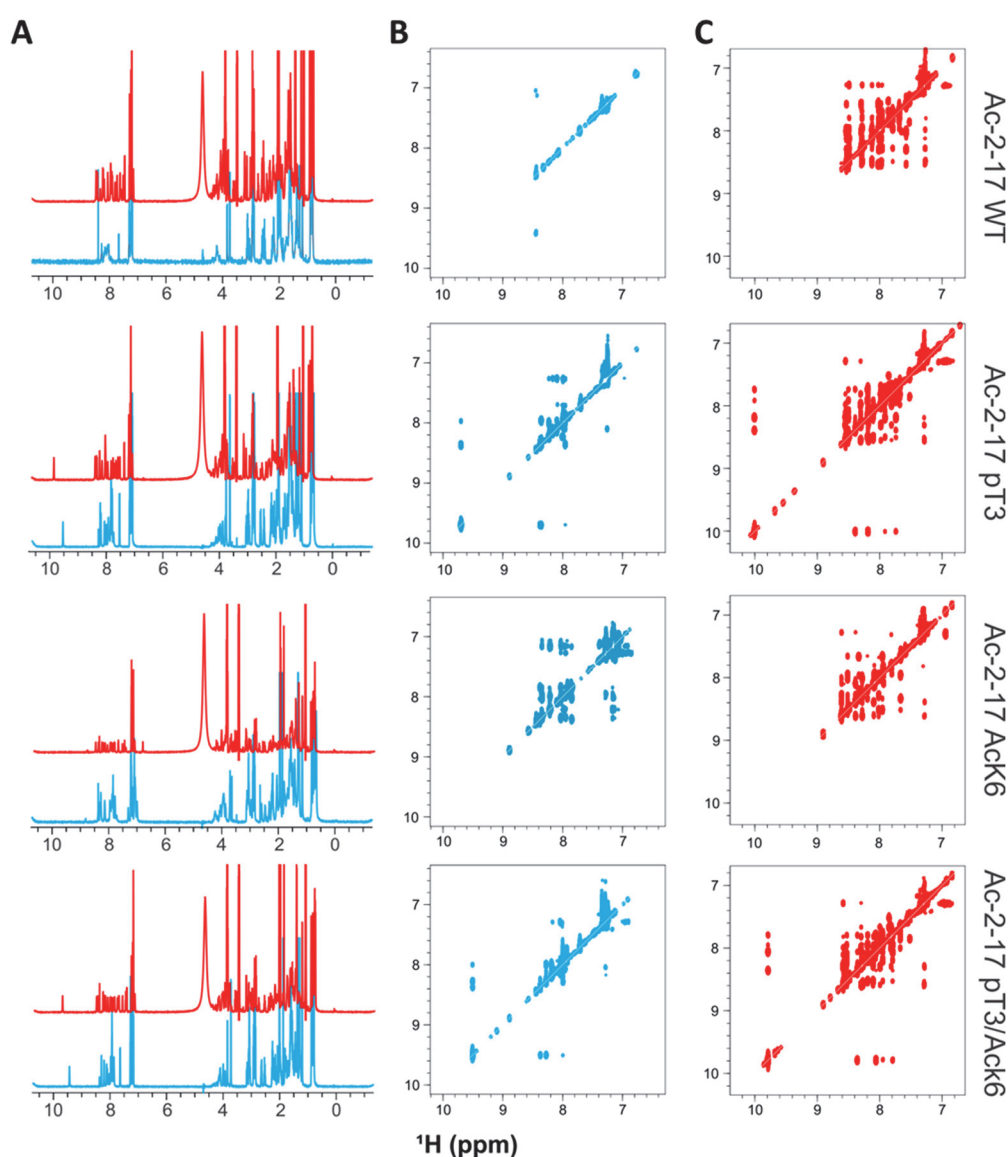


Figure II-16. NMR analysis of the effects of Acetylation on Htt peptides.

(A) 1D WATERGATE spectra of chemically modified Htt peptides: for each peptide experiments were acquired in 20mM phosphate buffer (Cyan) and with addition on 33% TFE (Red). (B) and (C) are 2D Homonuclear NOESY spectra respectively in phosphate buffer and TFE. As Methionine aminopeptidase cleavage of M1 and subsequent acetylation of A2 were found to be the most abundant

protein modifications in Htt, it has become clear to us that native Htt is N-terminally acetylated [316] [307], thus all the peptides used to investigate the cross-talk between pT3 and AcK6 were N-terminally acetylated.

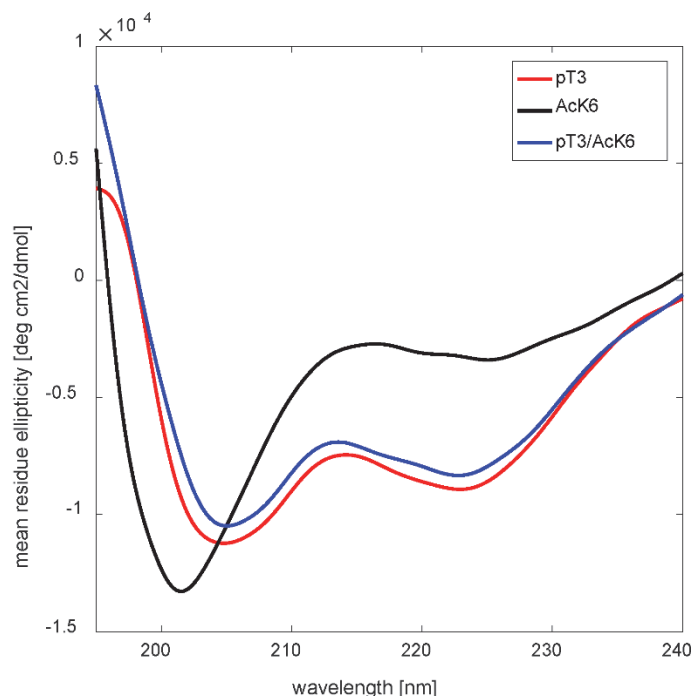


Figure II-17. Circular dichroism analysis of pT3, AcK6 and pT3/AcK6 Ac-Htt2-17 peptides.

### II.3.6 Conclusion

We have described herein the first semisynthesis of mutant Httex1 (43Q). Our improved method allows the production of milligram quantities of mutant Httex1 and enables the homogeneous Httex1 preparations with site-specific modifications at single or multiple residues. This enabled us for the first time, to perform detailed studies comparing the effects of phosphorylation at T3 and acetylation at K6, K9 or K15 and assessing the cross-talk between the two modifications (pT3/AcK6, pT3/AcK9 and pT3/AcK15) on the Httex1 aggregation. Our results demonstrated that acetylation of single lysine residues within the N-terminal 17 amino acids of Httex1 did not significantly modify the aggregation kinetics or structural properties of wild-type or mutant Httex1. In contrast, phosphorylation at T3 resulted in dramatic inhibition of mutant Httex1 aggregation, whereas the phosphomimetic T3D mutation resulted in only a partial inhibition of mutant Httex1 aggregation, demonstrating that this mutation does not fully reproduce the biophysical effects of authentic phosphorylation. Finally, we showed that K6, but not K9 or K15 acetylation reverses the inhibitory effect of T3 phosphorylation on Httex1 aggregation. Our results suggest that phosphorylation/dephosphorylation of T3 and/or the cross-talk between T3 phosphorylation and acetylation

represent PTM-dependent molecular switches for regulating the structure of Nt17 and possibly the aggregation of Htt and N-terminal Htt fragments *in vivo*.

## II.4 Experimental section

### II.4.1 Materials and Instrumentation

The peptides used in this work were either synthesized by Integrated Research Biotech Model (IRBM) through a collaboration with the CHDI Foundation or were purchased from CSBio Co. Glacial acetic acid (AcOH), Trifluoroacetic acid (TFA), guanidine hydrochloride (GuHCl), tris(2-carboxyethyl)-phosphine hydrochloride (TCEP), methoxyamine hydrochloride (MeONH<sub>4</sub>Cl), 4-mercaptophenylacetic acid (MPAA), 2-methyl-2-propanethiol (*t*-BuSH), sodium borohydride (NaBH<sub>4</sub>), nickel acetate (NiAc<sub>2</sub>), L-proline, L-methionine, D-trehalose, N,N-diisopropylethylamine (DIPEA), 1-Hydroxybenzotriazole hydrate (HOBt), triisopropylsilane (TIPS), ammonium iodide, 1,2-ethanedithiol (EDT), dimethylsulfide, methylene chloride (DCM), N-methylpyrrolidone (NMP) and dimethylformamide (DMF) were purchased from Sigma-Aldrich. Piperidine and diethyl ether were purchased from Acros. 2-2'-azobis[2-(2-imidazolin-2-yl)propane] dihydrochloride (VA-044) was purchased from Wako. HPLC-grade acetonitrile was purchased from Macherey-Nagel. 9-Fluorenylmethoxycarbonyl (Fmoc)-amino acids, *t*-butyloxycarbonyl(Boc)-amino acids, and 2-(1H-benzotriazole-1-yl)-1,1,3,3-tetramethyluronium hexafluorophosphate (HBTU) were purchased from Novabiochem or Anaspec. Rink amide MBHA resin was purchased from Eurogentec and TentaGel R Trt-Cl resin from Rapp Polymerr. ER2566 *E. coli* (E6901S) competent cells were purchased from New England Biolabs. Phenylmethanesulfonyl fluoride (PMSF) was purchased from Axonlab. Urea, dimethyl sulfoxide (DMSO), and isopropyl β-D-1-thiogalactopyranoside (IPTG) were purchased from Applichem. Primary mouse anti-Huntingtin monoclonal antibody was purchased from Millipore (MAB5492). Secondary goat anti-mouse antibody labeled with Alexa680 was purchased from Invitrogen (A-21057). PageRuler Prestained Protein Ladder (26617) from Thermo Scientific was used for SDS-PAGE. Microcon centrifugal filters with a MWCO of 100 kDa were obtained from Millipore (MRCF0R100). Formvar carbon film on 200-mesh copper grids (FCF200-Cu) and uranyl formate (16984-59-1) from Electron Microscopy Sciences were used for sample preparation for negative-stain transmission electron microscopy (TEM). Liquid chromatography electrospray ionization mass spectrometry (LC-ESI-MS) was performed using a C3 column (Agilent Poroshell 300SB-C3, 1 x 75 mm, 5 μm) with a gradient of 5% to 95% acetonitrile (0.1% v/v formic acid) at 0.3 mL/min over 6 minutes with UV detection at 214 nm and MS detection on a Thermo LTQ. Mass spectra were deconvoluted using the MagTran v. 1.03b software (Amgen). Matrix-assisted laser desorption ionization time-of-flight mass spectrometry (MALDI-TOF-MS) was performed on an AB Sciex 4700 instrument using a sinapinic acid matrix.

Ultra performance liquid chromatography (UPLC) analysis was done on a Waters UPLC system (Waters Acquity H-Class) using a C8 column (Waters Acquity UPLC BEH300, 1.7  $\mu$ m, 300Å, 2.1x150 mm) with UV detection at 214 nm using a 2.75 minute gradient of 10% to 90% acetonitrile (0.1% v/v trifluoroacetic acid) at 0.6 mL/min. Preparative high performance liquid chromatography (HPLC) was conducted on a Waters HPLC system (Waters 2535) using a C4 (Phenomenex Jupiter C4, 10  $\mu$ m, 300Å, 21.2 x 250 mm) or C18 (Waters XBridge C18, 10  $\mu$ m, 300Å, 21.2 x 250 mm) column with UV detection (Waters 2489) at 214 nm and manual fraction collection.

#### II.4.2 Solid Phase Peptide Synthesis

The T3D peptide N-acyl-benzimidazolinone (Nbz) was prepared using manual SPPS based upon the method developed by Blanco-Canosa et al.[354] 3-Fmoc-3,4-diaminobenzoic acid (Fmoc-Dbz-OH) was prepared by treating 3,4-diaminobenzoic acid (500 mg, 3.3 mmol) with Fmoc-OSu (1.1 g, 3.3 mmol) in 10 mL of 1:1 acetonitrile:0.1 M NaHCO<sub>3</sub>, pH 7.9 at RT with stirring for 16 h. The mixture was then acidified to pH ~1 and filtered through a sintered glass funnel. The filtrate was washed with diethyl ether, hexanes, and MeOH (3 x 10 mL each) then transferred to a glass flask and dried under reduced pressure. Rink amide MBHA resin (445 mg 0.2 mmol, 0.45 mmol/g) was washed with DMF (3x 5 mL) to swell. The resin was suspended in a solution of piperidine (20% in DMF, 5 mL), and the resulting suspension was agitated for 10 min. The resin was drained and washed with DMF (5 x 5 mL), and drained. In a separate flask, a solution of Fmoc-Dbz-OH in DMF (5 mL) was treated with HATU (380 mg, 1.0 mmol) and DIPEA (260 mg, 350  $\mu$ l, 2.0 mmol). After 15 minutes, the resin was suspended in the resulting solution; and the suspension was agitated for 2 h, then drained. To a second solution of Fmoc-Dbz-OH in DMF (5 mL) was added HATU (380 mg, 1.0 mmol) and DIPEA (260 mg, 350  $\mu$ l, 2.0 mmol). After 15 minutes, the resin was suspended in this solution and agitated for an additional 2 h. The resin was washed with DMF (5 x 5 mL) and DCM (5 x 5 mL) and drained. To a solution of allyl chloroformate (1.1 mL, 1.2 mg, 10 mmol) in DCM (5 mL) was added a DIPEA (70  $\mu$ l, 52 mg, 0.4 mmol). The resin was suspended in the resulting solution and agitated for 24 h, then drained and washed with DCM (5 x 5 mL) and DMF (5 x 5 mL). The resin was deprotected by treatment with a solution of piperidine (20% in DMF) as above. The first amino acid (K9) was activated with HATU (380 mg, 1.0 mmol) and DIPEA (260 mg, 350  $\mu$ l, 2.0 mmol) and incorporated by double 1-hour couplings. The remaining amino acids were installed by activation with HBTU/HoBt (1:1, 0.5 M in DMF, 3.0 mL) and DIPEA (1 M in DMF, 3.0 mL) with Fmoc deprotection with 20% piperidine between each residue. The resin was then washed with DCM (5 x 5 mL), drained, suspended in a solution of Pd(PPh<sub>3</sub>)<sub>4</sub> (40 mg, 0.04 mmol) and PhSiH<sub>3</sub> (0.5 mL, 430 mg, 4.0 mmol) in DCM (3.0 mL) and agitated for 30 minutes. The resin was drained, and the treatment was repeated. The resin was washed with DCM (5 x 5 mL) and treated with a solution of p-nitrophenylchloroformate (202 mg, 1.0 mmol) in DCM (3 mL) for 15

minutes with agitation. The resin was washed with DCM (3 x 5 mL) and DMF (3 x 5mL) then suspended in a solution of DIPEA (0.5 mL in DMF) and agitated for 30 minutes. The resin was then washed with DMF (3 x 5 mL) and DCM (3 x 5mL) and the chloroformate and base treatments were repeated. The peptide was then cleaved from the solid support and deprotected by treatment with 81.5/5/3/5/2.5/2/1.5 TFA/water/phenol/thioanisole/ethanedithiol/Me<sub>2</sub>S/NH<sub>4</sub>I (5 mL) for 4 h, precipitated in -20°C diethyl ether (40 mL) and lyophilized. Preparative C18-RP-HPLC using a linear gradient from 10-70% MeCN in H<sub>2</sub>O + 0.1 % TFA over 50 minutes and lyophilization of pure fractions provided Ac2-9 T3D Nbz peptide as a white solid (15 mg, 0.013 mmol, 6%).

### II.4.3 Cloning and expression of His<sub>6</sub>-Ssp-Htt10-90(A10C)-23Q/43Q and His<sub>6</sub>-Ssp-Htt18-90(Q18C)-22Q/42Q

The cDNAs corresponding to His<sub>6</sub>-Ssp-Htt10-90(A10C)-23Q/43Q and His<sub>6</sub>-Ssp-Htt18-90(Q18C)-22Q/42Q were synthesized and subcloned into pTWIN1 (eBiolabs, #N6951S, AmpR) by GeneART using the NdeI/PstI restriction sites. Chemo-competent *E.coli* ER2566 were transformed with the recombinant plasmids and the expression was performed as previously described.[178]

### II.4.4 Purification of Htt-A10C-90 23Q/43Q and Htt-Q18C-90 22Q/42Q

To overcome our previous method limitations (Scheme II.1-A), we utilized a new intein-based strategy that was recently developed in our laboratory to enable the generation of native and tag-free WT and mutant Httex1 to produce the recombinant fragment (2) [2]. This was achieved by the expression of Htt-A10C-90 23Q/43Q as an N-terminal Ssp DnaB intein fusion protein. This protein then underwent rapid, pH-controlled splicing resulting in the generation of Htt-A10C-90 23Q/43Q that lacks any additional amino acids at the C-terminus of the Htt fragment [2]. Cells expressing the protein of interest were harvested by centrifugation (4°C, 4000 RCF, 15 min) and resuspended in 10 ml/L medium in 40 mM Tris-Acetate, 5 mM EDTA, 0.3 mM PMSF and 20 mM cysteine. In the case of Htt-Q18C-90 22Q/42Q, which displayed high splicing propensity during the expression, 4 M urea was added directly to the lysis buffer. The cells were subsequently lysed by ultrasonication on ice (amplitude: 70%, time: 10 min, pulse on 59 sec pulse off 59 sec). The cell extract was separated from the cell debris by centrifugation (4°C, 39000 RCF, 30 min), the pH was adjusted to 7.0, and the resulting solution was incubated at room temperature for 3h to induce intein splicing. Urea (to give 4 M) was added to solubilize prematurely spliced Httex1 fragments present in inclusion bodies. The solution was acidified to 1.5 % TFA and boiled for 3 minutes. The precipitated proteins and other debris were removed by centrifugation (4°C, 39000 RCF, 30 min). The supernatant was collected, diluted 5-fold in -20°C acetone and incubated overnight at -20°C to precipitate the desired Httex1 fragment; the resulting precipitate was

collected by sedimentation (4°C, 6000 RCF, 10 min). The protein pellet was dried under vacuum and disaggregated by dissolving in a minimal volume of neat TFA. After removal of TFA under a stream of N<sub>2</sub>, the resulting residue was dissolved in dissolved 40 ml of 10% MeCN in water and filtered (0.2 µm). Purification *via* preparative RP-C4-HPLC column using a linear gradient from 10-40% MeCN in H<sub>2</sub>O + 0.1% TFA yielded the desired protein (r.t. ~40 min). Fractions were analyzed for purity by LC-ESI-MS and C8-UPLC, pooled and lyophilized to yield the desired protein fragments as white lyophilizates.

## II.4.5 Semisynthesis of Httex1

### II.4.5.1 Native chemical ligation and desulfurization of Httex1

Htt-A10C-90 43Q (2) lyophilized powder (10 mg, 0.9 µmol) was dissolved in neat TFA (250 µL). After 30 min, the TFA was removed under a stream of dry N<sub>2</sub>. The resulting thin film was dissolved in 5.0 mL ligation buffer (8 M urea, 0.5 M L-Proline, 30 mM D-Trehalose, 100 mM TCEP) and the pH of the solution was adjusted to 4 with 10 M NaOH. Methoxyamine hydrochloride (43 mg, 50 mmol) was added and the resulting solution was incubated for 90 min at 37 °C. The solution was cooled to room temperature and 4-mercaptophenylacetic acid (MPAA, 84 mg, 50 mmol) was added. The pH was adjusted to 7.0 with 10 M NaOH. Ac-2-9Nbz peptide (1) (4.0 mg, 3.6 µmol) was added to the reaction mixture and the progress of the native chemical ligation was monitored by LC-ESI-MS and UPLC. The solution was diluted to 20 mL with 20:10:70 AcOH:MeCN:H<sub>2</sub>O and filtered (0.2 µm). Purification *via* preparative RP-C4-HPLC using a linear gradient from 25-55% MeCN in H<sub>2</sub>O + 0.1% TFA yielded the desired A10C protein product (3) (r.t. ~35 min). The fractions were analyzed by LC-ESI-MS and C8-UPLC, pooled and lyophilized to yield the desired A10C protein product as a white lyophilizate (6.0 mg, 0.48 µmol, 53%); the lyophilizate was used directly in desulfurization.

Httex1-43Q A10C (6.0 mg, 0.48 µmol) was dissolved in neat TFA (250 µL). After 30 min, the TFA was evaporated under a stream of dry N<sub>2</sub>. The resulting thin film was dissolved in desulfurization buffer (2.0 mL; Desulfurization buffer: 100 mM TCEP, 40 mM L-methionine, 20 vol% acetic acid in H<sub>2</sub>O). Freshly prepared nickel boride suspension (1.0 mL) [348] was added to the resulting solution, and the resulting suspension was agitated at 37°C. The progress of the reaction was monitored by LC-ESI-MS (insoluble nickel was removed *via* centrifugation prior to analysis). After 2 h, a loss of 32 Da was observed. Insoluble nickel was removed from the reaction mixture *via* sedimentation (4°C, 4000 RCF, 10 min). The supernatant was diluted to 20 mL and filtered (0.2 µm). Purification *via* preparative RP-C4-HPLC using a linear gradient from 25-55% MeCN in H<sub>2</sub>O + 0.1% TFA yielded the desired protein product (r.t. ~34 min). The fractions were analyzed by LC-ESI-MS and C8-UPLC, pooled and lyophilized to yield the desired protein product as a white lyophilizate (4.4 mg, 0.35 µmol, 36%).

### II.4.5.2 Semisynthesis of site specifically modified WT and mutant Httex1

Post-translationally modified mutant httex1 43Q was prepared as described above except that the desired modified N-terminal peptide-Nbz was used for each ligation. Wild-type httex1 23Q proteins were also prepared as described above except that the desired N-terminal peptide-Nbz was ligated to the Htt-A10C-90 23Q protein fragment. For the Ack15 mutant Httex1 42Q, the same protocol was used except that the Htt-Q18C-90 42Q protein fragment was ligated to the Ac-2-17Nbz Ack15 peptide. Similarly, for Ack15 wild-type Httex1 22Q, the same protocol was used except that the Htt-Q18C-90 22Q protein fragment was ligated to the Ac-2-17Nbz Ack15 peptide. The protein products were characterized by MALDI-TOF, RP-UPLC and SDS-PAGE.

## II.4.6 Aggregation Analysis

### II.4.6.1 Concentration determination

The lyophilized protein was treated with neat TFA (1  $\mu$ L of TFA/50  $\mu$ g protein) for 30 minutes. The TFA was removed under a stream of dry  $N_2$ . The resulting thin film was dissolved in 1 X PBS (137 mM NaCl, 2.7 mM KCl, 10 mM  $Na_2HPO_4$ , 2 mM  $KH_2PO_4$ ) to give an approximate concentration of 20  $\mu$ M and the pH was adjusted to 7.4 by the addition of a small volume (1-3  $\mu$ L) of 1 M NaOH. Any remaining preformed aggregates were removed by filtration through 100kD molecular weight cutoff filters. The protein concentration was then determined using a UPLC calibration curve based upon amino acid analysis (detection at  $\lambda_{214}$ ) 60  $\mu$ L of the sample was sent for amino acid analysis (AAA) for concentration determination.

### II.4.6.2 Sedimentation assay

The protein was diluted to a concentration of 3  $\mu$ M for Expanded Httex1 (43Q) and 5  $\mu$ M for unexpanded Httex1 (23Q) with 1 X PBS and its concentration was confirmed by UPLC analysis. The aggregation experiment was initiated by incubation of the sample at 37°C. To monitor the soluble protein fraction, the aggregation experiment solution was returned to 25°C and mixed gently and an aliquot (35  $\mu$ L) was removed at each indicated time point and aggregates were removed by centrifugation (4°C, 20000 RCF, 20 minutes). The supernatant was analyzed by UPLC. The change in the area of the peak area was used to calculate the fraction of soluble protein compared to  $t=0$ . To estimate the rate constant of sedimentation and thus aggregation, we used the function where A is the initial concentration of soluble protein, c is the concentration of soluble protein at infinite time and b is the rate constant. We constrained for physical reasons the A and C values in a range varying between 0 and 1 plus/minus the standard error we commit on the measure. All the fits had an adjusted R-square between 0.91-0.99 for all curves (except for the Httex1-43Q pT3/Ack6 having a value of 0.85).



### II.4.6.3 Circular dichroism spectroscopy

For CD analysis of the aggregation process, aliquots (100  $\mu$ L) were removed from the aggregation experiments samples at the indicated time points and analyzed using a Jasco J-815 CD spectrometer and a 1.0 mm quartz cuvette. Ellipticity was measured from 195–250 nm at 25°C; data points were acquired continuously every 0.2 nm at a speed of 10 nm/min with a digital integration time of 2s and a bandwidth of 1.0 nm. Six spectra of each sample were obtained from each sample and averaged. The spectra were smoothed using a binomial filter with a convolution width of 99 data points and the resulting spectra were plotted as the mean residue molar ellipticity ( $\theta_{MRE}$ ).

### II.4.6.4 Transmission electron microscopy

For TEM analysis, 3  $\mu$ L of aggregation solution was spotted onto a Formvar/carbon-coated 200-mesh glow-discharged copper grid for 1 min. The grid was then washed twice with water, once with 0.7% (w/v) uranyl formate and stained for 30 seconds with 0.7% w/v uranyl formate. Imaging was performed on a Tecnai Spirit BioTWIN electron microscope equipped with a LaB6 gun and a 4K x 4K FEI Eagle CCD camera (FEI) and operated at 80kV.

### II.4.6.5 Atomic force microscopy (AFM)

Sample preparation, imaging and statistical analysis: We performed conventional AFM measurements in air of the sample deposited on positively functionalized mica. To functionalize the surface, after cleaving, the bare mica substrate was incubated with a 10  $\mu$ L drop of 0.05% (v/v) APTES ((3-aminopropyl)triethoxysilane, Fluka) in Milli-Q water for 1 minute at room temperature, rinsed with Milli-Q water and then dried by the passage of a gentle flow of gaseous nitrogen. The preparation of the mica AFM samples was performed at room temperature by depositing a 10  $\mu$ L aliquot of the fully concentrated solution onto the mica surface and allowing it to remain for 10 minutes. The sample was then rinsed with ultrapure water and dried under a gentle flow of nitrogen.

High-resolution images (1024x1024 pixels) were collected using an NX10 Atomic Force Microscope (Park Systems, South Korea) under ambient conditions and in amplitude modulation non-contact (NC-AM) mode. We imaged square areas of 2x2  $\mu$ m<sup>2</sup> and 4x4  $\mu$ m<sup>2</sup>. We performed all the measurements using ultra-sharp cantilevers (SSS-NCHR, Park Systems, South Korea) with resonance frequency of 330 kHz and a typical apical radius of 2 nm. The raw images were flattened using the built-in software (XEI, Park System, South Korea). To maintain consistency in the subsequent statistical analysis, all images were processed using the same parameters. The images were first flattened by a plane and then line-by-line in 1st regression order. This second step was repeated until a flat baseline was obtained in line profile of the image was reached. During

the process of flattening of the images, the aggregates were masked from the calculation to avoid modification and underestimation of their heights.

Statistical analysis of the cross-sectional dimensions of the fibrillar structures was performed using means of a home-built program (DNA-trace). In particular, the software enabled us to trace individual fibrils and to measure their length and their average heights. The-box-charts distributions and the scatter plots were created and performed using ORIGIN PRO.

#### **II.4.6.6 Thioflavin S (ThS) binding assay**

Httex1-43Q unmodified or with pT3 was prepared as showed in previous sections at different concentration (5, 10, 15, 20 and 30  $\mu$ M) in PBS buffer and supplemented with 10  $\mu$ M of ThS (T1892 SIGMA). 100  $\mu$ l aliquot was added in triplicate to 96-well microplate with clear bottom. The ThS fluorescence was then measured using an excitation filter wavelength of 440 nm and an emission filter wavelength of 480 in cycles of 10 min over-time, without shaking at 37°C using Fluostar Omega® plate reader.

#### **II.4.7 Nt17 peptide analysis**

##### **II.4.7.1 pH dependence studies**

For pH dependence studies, each peptide was weighed in a separate Eppendorf tube for each condition and dissolved in buffer at the desired pH (pH 3 and 4, 10 mM Sodium acetate, 75 mM NaCl; pH 5 and 6, 10 mM MES; pH 7-9, Tris-HCl, 75 mM NaCl; and 10 mM Glycine-NaOH, 75 mM NaCl pH 10). The secondary structure of each sample was then measured by CD. To determine the helical content at each pH we used a well-established equation for the prediction [355, 356]: where  $\theta_{222}$  represents the CD value at 222 nm and  $\theta_{208}$  (T is the temperature, and  $N_r$  is the number of residues).

##### **II.4.7.2 Nuclear Magnetic Resonance (NMR) studies**

Samples concentrated 0.250 mM were prepared by weighting the respective peptide and then diluting it in an aqueous solution buffered 20 mM phosphate at pH 7.0 pure or diluted with 33% in volume of deuterated TFE. All NMR spectra were recorded on a Bruker Avance III 600 MHz proton frequency spectrometer equipped with cryoprobe. One-dimensional spectra and the homonuclear two-dimensional total correlated spectroscopy (TOCSY) (mixing time of 80 ms) and nuclear Overhauser effect spectroscopy (NOESY) spectra (mixing time of 150-200-300 ms) were acquired at 283.2 and 298.2 K, using the WATERGATE technique for water suppression. Spectral assignment was readily obtained by comparing TOCSY and NOESY patterns.

## **II.5 Acknowledgements**

This work was supported by the CHDI foundation (A\_7627) and the Swiss National Science Foundation (31003A-146680). We thank Dr. Mahmood Haj-Yahya, Dr. John Warner, Dr. Elizabeth Doherty, Dr. Celia Dominguez and Dr. Andrea Caricasole for helpful discussions on the manuscript, and IRBM for generating the Nt17 peptides used in this study. We are grateful to Dr G. Kelly and Dr T. Frenkiel at the MRC Biomedical NMR Centre (The Francis Crick Institute) for providing access to the NMR facilities and help in acquiring spectra.

### III. Chapter III: Site-specific phosphorylation of Huntingtin exon 1 recombinant proteins enabled by the discovery of novel kinases

This research was originally published in Chembiochem. <https://doi.org/10.1002/cbic.202000508>

Anass Chiki <sup>[a]</sup>, Jonathan Ricci <sup>[a]</sup>, Ramanath Hegde <sup>[a]</sup>, Luciano A. Abriata <sup>[b]</sup>, Andreas Reif <sup>[a]</sup>,  
Driss Boudeffa <sup>[a]</sup>, and Hilal A. Lashuel <sup>\*[a]</sup>. 2020, Online ahead of print.

[a] Laboratory of Molecular and Chemical Biology of Neurodegeneration, School of Life Sciences, Brain Mind Institute, Ecole Polytechnique Fédérale de Lausanne (EPFL), CH-1015 Lausanne, Switzerland

[b] Protein Production and Structure Core Facility and Laboratory for Biomolecular Modeling, Ecole Polytechnique Fédérale de Lausanne (EPFL) and Swiss Institute of Bioinformatics (SIB), CH-1015 Lausanne, Switzerland

\*To whom correspondence should be addressed: Hilal A. Lashuel, Laboratory of Molecular and Chemical Biology of Neurodegeneration, Brain Mind Institute, Station 19, Ecole Polytechnique Fédérale de Lausanne, CH 1015 Lausanne, Switzerland. Tel: +4121 6939691; Fax: +4121 6931780; Email: [hilal.lashuel@epfl.ch](mailto:hilal.lashuel@epfl.ch)

**Author contributions:** A. Chiki and H.A. Lashuel designed the experiments and wrote the paper. H.A. Lashuel coordinated and supervised the study. A. Chiki and J. Ricci conducted and analyzed the experiments. R. Hegde performed the cellular validations. L.A. Abriata performed and wrote the NMR part. A. Reif helped with the optimisation of the expression in minimal media. D. Boudeffa performed experiments repeats. A. Lashuel acquired the funding for this work

## III.1 Abstract

Posttranslational modifications (PTMs) within the first 17 amino acids (Nt17) of exon1 of the Huntingtin protein (Httex1) play important roles in modulating its cellular properties and functions in health and disease. In particular, phosphorylation of threonine and serine residues (T3, S13, and/or S16) has been shown to inhibit Htt aggregation *in vitro* and inclusion formation in cellular and animal models of Huntington's disease (HD). In this manuscript, we describe a new and simple methodology for producing milligram quantities of highly pure wild type or mutant Httex1 proteins that are site-specifically phosphorylated at T3 or at both S13 and S16. This advance was enabled by 1) the discovery and validation of novel kinases that efficiently phosphorylate Httex1 at S13 and S16 (TBK1), at T3 (GCK) or T3 and S13 (TNIK and HGK); and, 2) the development of an efficient methodology for producing recombinant native Httex1 proteins using a SUMO-fusion expression and purification strategy. As proof of concept, we demonstrate how this method can be applied to produce Httex1 proteins that are both site-specifically phosphorylated and fluorescently labeled or isotopically labeled. Together, these advances should increase access to these valuable tools and expand the range of methods and experimental approaches that can be used to elucidate the mechanisms by which phosphorylation influences Httex1 structure, aggregation, interactome and function(s) in health and disease.

## III.2 Introduction

Huntington's disease (HD) is a devastating neurodegenerative disease for which there are currently no effective treatments or disease-modifying therapies. HD is characterized by severe motor symptoms such as chorea, bradykinesia, loss of motor control, rigidity [5, 29, 357], and difficulties with speech and swallowing [358]. As the disease progresses, HD patients experience cognitive impairments, personality change, and depression [359-361]. HD is a monogenic disease that is caused by a CAG expansion in the first exon (exon 1) of the *HTT* gene [6, 362], which is translated into a polyglutamine (polyQ) repeat in the huntingtin protein HTT (Figure III.1-A) [363]. Individuals with polyQ repeat lengths that extend beyond the pathogenic threshold of  $\geq 36$  glutamine residues go on to develop HD. The higher the number of polyQ repeats, the more severe the symptoms are, and the earlier is the age of disease onset [364]. Although the exact mechanisms underpinning neurodegeneration in HD remain unclear, converging evidence suggests that polyQ expansions increase the propensity of HTT proteins to aggregate and form pathological inclusions in a polyQ-dependent manner [365]; the longer the polyQ repeats, the higher is the propensity of HTT to aggregate and form inclusions [125, 366]. The formation of HTT aggregates and inclusions has been linked to cellular dysfunction and degeneration *via* different cellular mechanisms [155, 367, 368].

Increasing evidence suggests that nuclear HTT inclusions in *postmortem* tissues of HD patients [21] are formed as a result of the misfolding and aggregation of N-terminal HTT fragments of varying lengths, rather than the full-length HTT protein [369]. One of the most studied fragments corresponds to exon 1 of HTT (Figure III.1-A) (Httex1), which contains the polyQ domain and is generated by aberrant splicing [148] and possibly proteolytic processing of the protein [154]. Overexpression of mutant Httex1 containing polyQ repeats ranging from 80 to 175 glutamine residues is sufficient to induce a robust HD-like phenotype and pathology in various animal models (mice, *Drosophila*) [146, 155, 173], as well as in cell culture models of HD [155, 172]. *In vitro*, mutant Httex1 exhibits polyQ-dependent aggregation and forms amyloid-like fibrils in a concentration-dependent manner [170, 171].

Posttranslational modifications (PTMs) in the first 17 N-terminal amino acids (Nt17) of Httex1 can dramatically affect HTT aggregation, subcellular targeting, clearance, and toxicity [125, 284, 307]. Phosphorylation, acetylation [282, 307], ubiquitination and SUMOylation [284] have been shown to occur in the Nt17 domain, with indications that some of these modifications coexist on the same molecule [282]. Given the reversible nature of these modifications, we hypothesized that they could act as a molecular switch for regulating many aspects of HTT, including its structure, interactome, and cellular properties. Therefore, a better understanding of the mechanisms by which these PTMs influence HTT structure, aggregation, and cellular properties may offer new avenues for the development of more effective disease-modifying strategies. Indeed, several lines of evidence suggest that Nt17 PTMs could reverse the deleterious effects caused by polyQ expansions. For example, mutating both residues S13 and S16 in the Nt17 region to aspartate to mimic phosphorylation was shown to inhibit Httex1 aggregation, sufficiently modify the aggregation properties of full-length HTT and protect against mutant HTT-induced toxicity in a transgenic model of HD [209]. Additionally, mutant HTT was shown to be hyperphosphorylated at S13 and S16 in *STHdh* cells and HD mice [312, 314]. Furthermore, restoring Nt17 phosphorylation induces K9 acetylation and promotes HTT clearance by the proteasome and lysosome [282]. Finally, we recently showed that the levels of T3 phosphorylation (pT3) inversely correlated with polyQ repeat length in both preclinical models of HD and samples from HD patients [307, 308].

Until recently, studies on the effect of Nt17 PTMs have relied on the use of mutations to mimic PTMs. These include the substitution of serine and threonine residues by the acidic residues aspartic acid or glutamic acid to mimic phosphorylation [209, 307] or replacing lysine with glutamine to mimic lysine acetylation [211]. These approaches have several limitations that have precluded a more accurate understanding of the role of PTMs in regulating HTT biology and its role in HD, including the fact that PTM mimetics do not fully capture the size, charge state, or dynamic nature of a *bona fide* PTMs. For example, phosphomimetics allow only

partial mimicking of phosphorylation and do not reproduce the dynamic nature of this modification or its effects on the structural properties of Nt17<sup>25</sup>. It is, therefore, not surprising to observe conflicting findings concerning the effects of phosphomimetic on HTT aggregation when using different animal models [209, 307, 309].

To address these limitations, we recently developed a semisynthetic methodology that enables the site-specific introduction of single or multiple PTMs in WT and mutant. Using this approach, we gained new insight into how Httex1 aggregation and conformation are affected by Nt17 phosphorylation, acetylation, or the cross-talk between these two types of PTMs [223, 308, 329, 370, 371]. Moreover, the ability to generate site-specifically modified Httex1 proteins enabled us to develop very sensitive assays to detect and quantify phosphorylated Httex1 in complex samples for biomarker discovery [308, 372]. However, the current semisynthetic methods for the production of phosphorylated Httex1 proteins have some limitations: 1) they are time-consuming and require advanced technical capabilities in protein chemical synthesis; 2) introducing PTMs beyond residue 9 requires the introduction of a non-native Gln-18 to Ala mutation to enable native chemical ligation; and 3) they are not suitable for the production of both modified and isotopically labeled Httex1 proteins for structural studies using NMR and other methods.

To overcome these challenges, it is crucial to first identify the enzymes responsible for Nt17 phosphorylation and then develop efficient *in vitro* phosphorylation conditions that allow site-specific phosphorylation at the desired residues. Towards this goal, we performed kinase screening using a library of 298 kinases and identified several kinases that phosphorylate HTT efficiently and specifically at T3 or both S13 and S16. Next, we took advantage of the specificity and efficiency of these kinases to develop efficient methods that allowed the production of milligram quantities of homogeneously phosphorylated recombinant Httex1 at T3 or both S13 and S16. This was enabled by the recently developed SUMO-based Httex1 expression and purification strategy [238], enabling the generation of highly pure milligram quantities of Httex1 proteins. To demonstrate the versatility of these methods, we present examples that illustrate how they could be used to produce fluorescently and isotopically labeled phosphorylated untagged WT (23Q) and mutant (43Q) Httex1 proteins. Furthermore, using NMR, we provide some preliminary results on the cross-talk between S13 and S16 and how phosphorylation could influence the structural properties of Httex1. Together, these advances should pave the way for future studies to elucidate the effects of phosphorylation on the interactome, structural, and cellular properties of Httex1 that were previously not possible.

### III.3 Results and Discussion

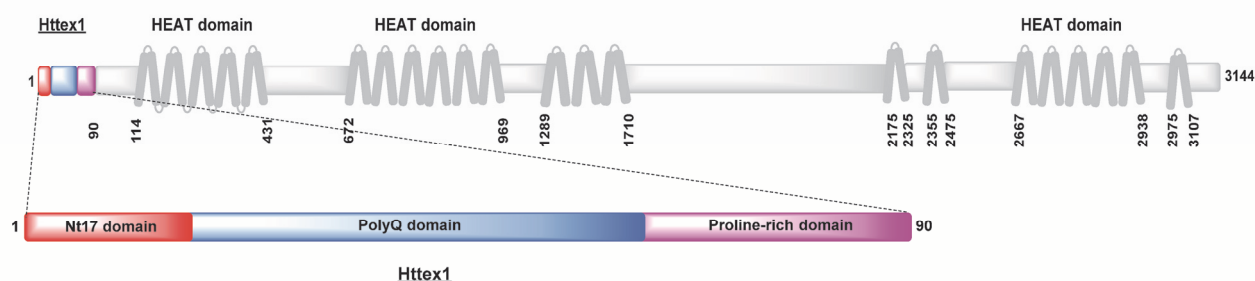
#### III.3.1 Identification and validation of kinases that phosphorylated Nt17 at T3, S13, and S16

To enable the site-specific enzymatic phosphorylation of Httex1 at T3, S13 or S16, we first needed to identify enzymes that phosphorylate HTT at these sites. Towards this goal, we performed a screening using the *In vitro* Kinase and Phosphopeptide Testing (IKPT) services from Kinexus [373], where Httex1-23Q and the Nt17 peptide were used as substrates to test a panel of 298 purified serine-threonine kinases. This led to the identification of several enzymes that phosphorylate Nt17 and Httex1 at both S13 and S16 (TBK1) or at T3 (GCK, TNIK, and HGK), respectively. We recently described the validation of TBK1 and demonstrated that it phosphorylates S13 and S16 efficiently and specifically *in vitro* and S13 in cells and *in vivo* [374]. Herein, we present for the first time the discovery and validation of the kinases that phosphorylate T3.

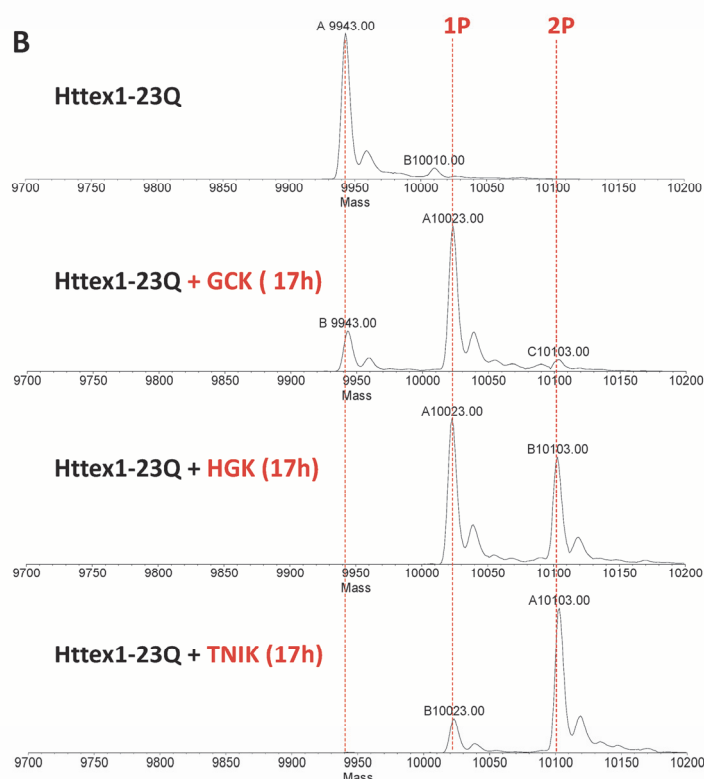
The top kinase hits that phosphorylated T3 in the context of Httex1 included MAP4K2 (GCK), MAP4K4 (HGK), and TNIK (Figure III.1-B and 1-C). These kinases are part of the STE20 kinase family and are involved in cellular signal transduction, including apoptosis, the cell cycle, and cell growth [375]. To determine the efficiency and specificity of these kinases, we performed *in vitro* phosphorylation reactions in which these kinases were co-incubated with Httex1-23Q (Figure III.1-B and 1-C) and monitored the extent of phosphorylation and number of phosphorylation sites by Electrospray Ionisation Mass Spectrometry (ESI/MS) and western blot (WB) using our well-tested and validated phospho-antibodies [329, 339, 372] specific for pT3, pS13, or pS16. As shown in Figure III.1-B, GCK phosphorylated Httex1-23Q mainly at one site, as indicated by the +80 Da mass shift observed by ESI/MS (Figure III.1-B). In contrast, HGK and TNIK phosphorylated Httex1-23Q at multiple sites, as illustrated by the appearance of two new peaks in the ESI/MS spectra that correspond to the phosphorylation of one or two sites (Figure III.1-B). Western blot analysis using pT3-, pS13- and pS16-specific antibodies enabled us to determine which sites were phosphorylated. As shown in Figure III.1-C, GCK phosphorylates mainly at T3, as indicated by a strong positive WB signal with the pT3 antibody (Figure III.1-C), and the absence of any bands in the WB developed using pS13 and pS16 antibodies. On the other hand, both T3 and S13 phosphorylation were detected with their respective antibodies when Httex1-23Q was co-incubated with HGK or TNIK (Figure III.1-C), which was consistent with the ESI/MS results showing phosphorylation at multiple sites in Nt17. Interestingly, the coexpression of each of these kinases with Httex1-16Q-eGFP in HEK 293 cells did not result in significant phosphorylation (Figure III.2). Nevertheless, these findings did not exclude the potential of using the newly discovered kinases as tools to prepare phosphorylated Httex1 *in vitro*. The efficiency and specificity of GCK in phosphorylating T3 *in vitro* suggest that it could be used as a valuable tool for the preparation of Httex1 proteins that are site-specifically and homogeneously phosphorylated at T3 (pT3).



A



B



C

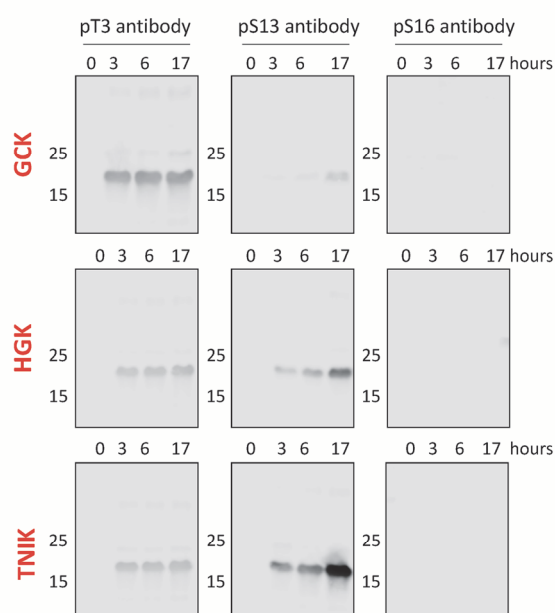


Figure III-1. *In vitro* T3 kinases validation.

(A) Schematic representation of HTT full length and Httex1. (B) ESI/MS analysis of Httex1-23Q before and after the phosphorylation reaction with GCK, HGK, or TNIK. (C) Western blot analysis of Httex1-23Q phosphorylation by GCK, HGK, and TNIK monitored over-time by homemade antibodies specific to pT3, pS13, or pS16.

Having shown that both GCK and TBK1 phosphorylate wild-type Httex1 with 23Q, we next sought to determine if they could phosphorylate mutant Httex1 (Httex1-43Q) with the same efficiency and specificity. Due to its high aggregation propensity, Httex1-43Q was tested at a lower concentration (20  $\mu$ M). As shown in Figure III.3, MALDI analysis indicated that GCK partially phosphorylated (~30%) mutant Httex1 at T3 (Figure III.3-A); even after a prolonged incubation time (16 hours), the extent of phosphorylation did not significantly

increase (Figure III.3-A). However, TBK1 rapidly phosphorylated Httex1-43Q at both S13 and S16 (Figure III.3-B). After 4 hours, most of the protein exhibited phosphorylation at two sites, and only a small portion of the protein was singly phosphorylated (Figure III.3-B). After 16 hours of incubation, the level of monophosphorylated Httex1-43Q decreased (Figure III.3-B). However, as shown in Figure III.3-C, we observed significant Httex1-43Q aggregation for both kinases, as indicated by the appearance of higher molecular weight species

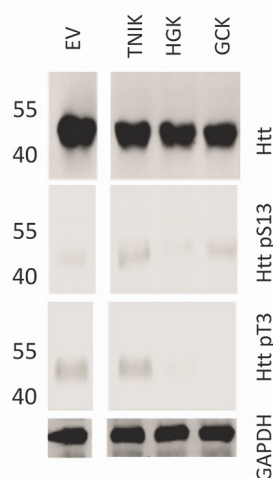


Figure III-2. Coexpression of Httex1-16Q-eGFP in HEK 293 cells with TNIK, HGK or GCK.

Representative Western-blot of Htt, Htt pT3 and Htt pS13 upon co-expression of Httex1-16Q-eGFP with the indicated kinases for 48 hours in HEK 293 cells.

In the WB (highlighted in red in Figure III.3-C). These species were shown to form after 2 hours of the phosphorylation reaction (Figure III.3-C). The formation of aggregates was caused by the conditions of the kinase reaction, which required a high protein concentration as well as incubation of the reaction mixture at 30°C. Thus, the high propensity of mutant HTT to aggregate *in vitro* precluded the generation of site-specific phosphorylated mHttex1 proteins through direct *in vitro* phosphorylation of the native Httex1 proteins by GCK and TBK1.

Table III-1. Expected and observed molecular weights for all the protein generated in this study.

Proteins	Expected molecular weight (Da)	Observed molecular weight (Da)
Httex1-23Q	9943	9943
Httex1-43Q	12505	12504; 12509; 12518 (MALDI); 12525 (MALDI)
Httex1-23Q pT3	10023	10023;10022
Httex1-43Q pT3	12585	12589;12594 (MALDI); 12604 (MALDI)
Httex1-23Q pS13/pS16	10103	10103;10102.53
Httex1-43Q pS13/pS16	12665	12665; 12672 (MALDI); 12681 (MALDI)
Httex1-23Q 13C/15N	10516	10503.7
Httex1-43Q 13C/15N	13218	13203.4
Httex1-23Q pT3 13C/15N	10596	10583.2
Httex1-43Q pT3 13C/15N	13298	13283.3
Httex1-23Q pS13/pS16 13C/15N	10676	10664.4
Httex1-43Q pS13/pS16 13C/15N	13378	13363.4
Httex1-23Q P90C	9949	9948.07
Httex1-43Q P90C	12511	12511.2
Httex1-23Q pT3 P90C	10029	10029.1
Httex1-43Q pT3 P90C	12591	12591.7
Httex1-23Q pS13/pS16 P90C	10109	10109
Httex1-43Q pS13/pS16 P90C	12671	12671.6
Httex1-23Q pT3 P90C ATTO	10661	10661.9
Httex1-43Q pT3 P90C ATTO	13223	13224.4
Httex1-23Q pS13/pS16 P90C ATTO	10741	10742
Httex1-43Q pS13/pS16 P90C ATTO	13303	13304.9

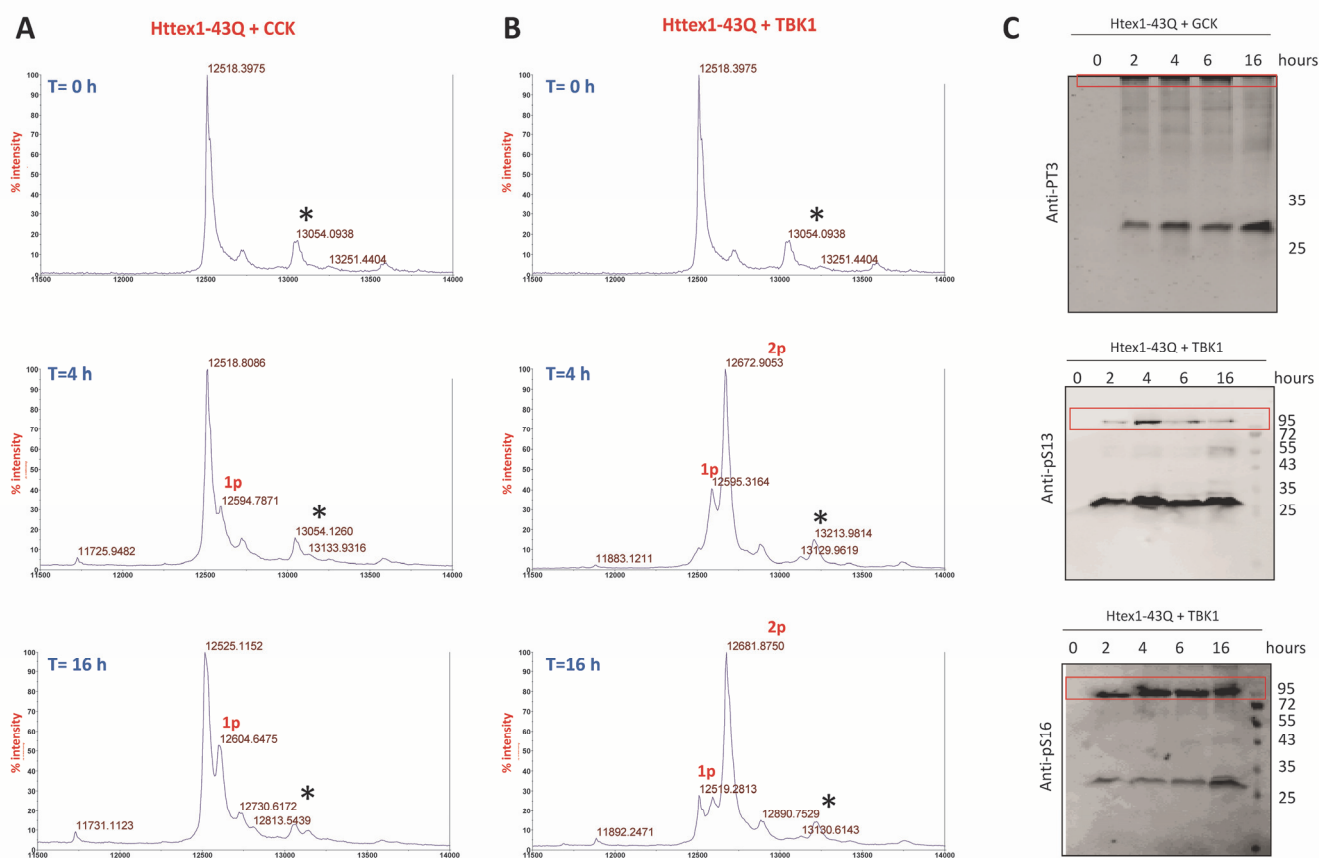


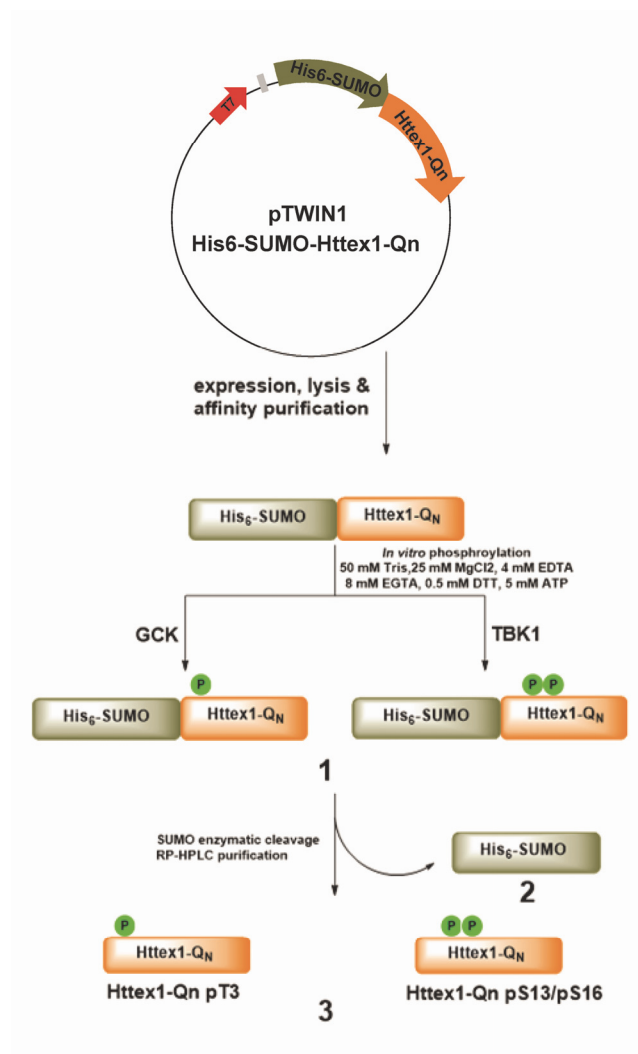
Figure III-3. *In vitro* phosphorylation of Httex1-43Q by GCK or TBK1.

Representative MALDI spectra of Httex1-43Q over-time phosphorylation by GCK (**A**) or by TBK1 (**B**) (T= 0 h is the same for both GCK and TBK1, sinapinic acid adducts are highlighted with a star). (**C**) Representative western blot of Httex1-43Q phosphorylation over time by GCK and TBK1 using pT3-, pS13-, or pS16-specific antibodies. Formed aggregates were observed during the phosphorylation reaction (highlighted by a red box).

### III.3.2 SUMO-based strategy for the generation of phosphorylated WT and mutant Httex1

To overcome the problems posed by the poor solubility of mutant Httex1, we took advantage of recent advances made by our group that enabled the efficient production of milligram quantities of highly pure WT and mutant Httex1 using the SUMO fusion strategy [238]. We showed that the fusion of SUMO to mutant Httex1 improves the expression of these proteins, increases their solubility, and facilitates their handling and purification. Therefore, we explored the possibility of performing the *in vitro* phosphorylation reaction directly on the mutant SUMO-Httex1 fusion protein (Scheme III.1) with the idea that the SUMO tag can later be cleaved from Httex1 by the enzyme ULP1 rapidly to yield site-specifically phosphorylated native Httex1 proteins (Scheme III.1). Therefore, we expressed Httex1 with 23 or 43 glutamine residues (Httex1-23Q or

Httex1-43Q, respectively) containing a His6-SUMO tag fused to the N-terminus (SUMO-Httex1-23Q and SUMO-Httex1-43Q), as previously described [238].



Scheme III-1. SUMO-based strategy for the generation of phosphorylated Httex1 proteins.

Schematic overview of the method used for the expression and purification of SUMO Httex1-Qn ( $n = 23$  or  $43$ ), which undergoes *in vitro* phosphorylation by TBK1 or GSK3 to generate SUMO-Httex1-Qn pT3 or SUMO-Httex1-Qn pS13/pS16 (**1**), then, the SUMO tag (**2**) was then cleaved by ULP1, and the desired phosphorylated Httex1-Qn (**3**) was purified by HPLC

After cell lysis, the fusion proteins were subjected to immobilized metal affinity chromatography (IMAC) (Figure III.4-A and III.4-B). Both SUMO-Httex1-23Q and SUMO-Httex1-43Q (SUMO-Httex1-Qn,  $n = 23/43$ ) were isolated by nickel affinity chromatography (Figure III.4-A and III.4-B, respectively), and the elution was analyzed by SDS-PAGE, as shown in Figure-III.4-A and III.4-B. Then, the fractions containing SUMO-Httex1-Qn were pooled and analyzed by ESI/MS and Ultra Performance Liquid Chromatography (UPLC) (Figure III.5-A and 3-B). Although SDS-PAGE showed the presence of some impurities in the sample, ESI/MS showed the

presence of mainly the SUMO-Httex1-Qn proteins (Figure III.5-A and III.5-B). This could be because these protein impurities that do not ionize well on ESI/MS. Such impurities are usually removed during RP-HPLC purification. The UPLC analysis showed a broad single peak corresponding to the fusion proteins, as was previously shown [238]. To investigate the efficiency of the *in vitro* phosphorylation of SUMO-Httex1-Qn, SUMO-Httex1-23Q and SUMO-Httex1-43Q were both incubated with TBK1 and GCK, and the reaction was monitored by ESI/MS. Both kinases phosphorylated the WT and mutant fusion proteins, as evidenced by the appearance of additional phospho groups (+80 Da) by ESI/MS (Figure III.6-A). After 6 hours, GCK induced complete phosphorylation of both the WT and mutant Httex1 at a single site (Figure III.6-A). In the case of TBK1, a mixture of 2 and 3 phosphorylation sites was observed (Figure III.6-A). Bearing in mind that TBK1 phosphorylates only two sites in Nt17 (S13 and S16) [374], we hypothesized that there are other potential TBK1 phosphorylation sites within the sequence of the SUMO tag.

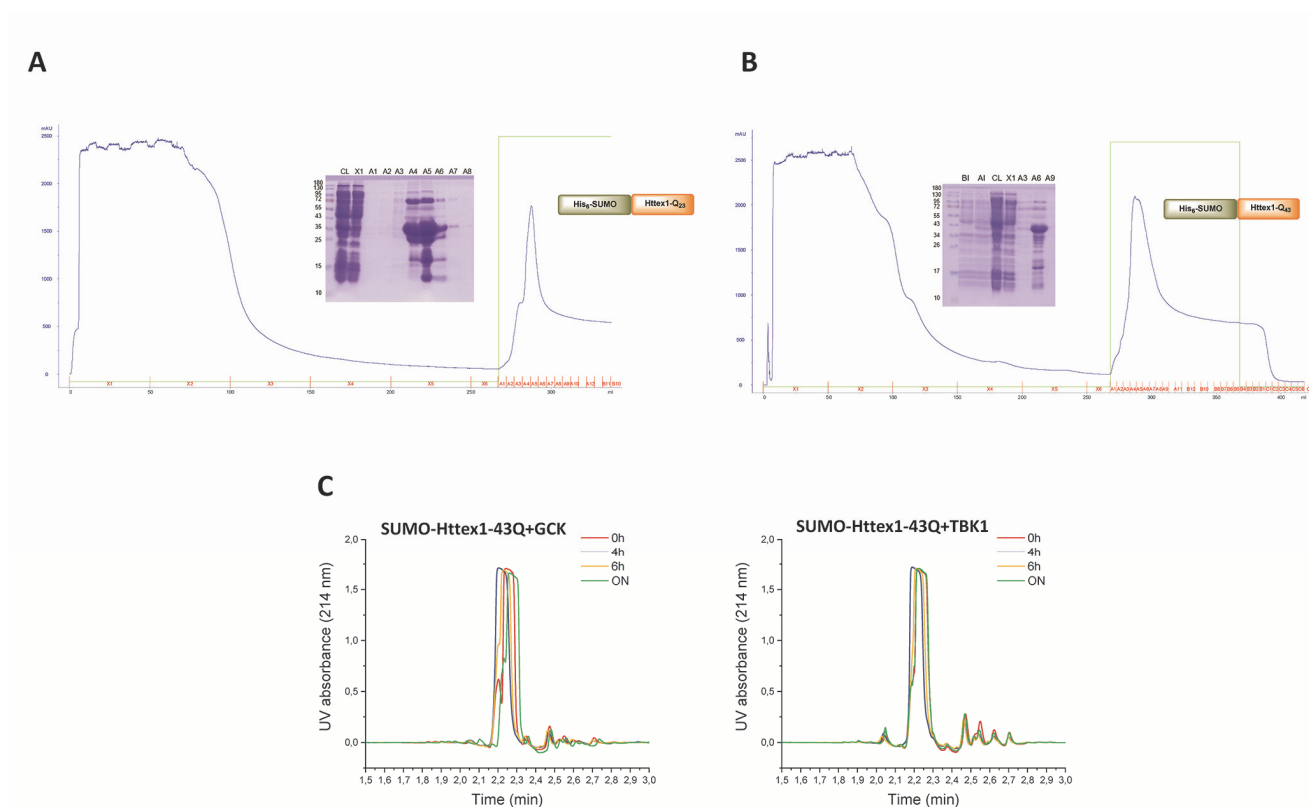


Figure III-4. SUMO-Httex1-Qn IMAC purification.

(A) Representative chromatogram of the IMAC purification of SUMO-Httex1-23Q, and (B) Representative chromatogram of the IMAC purification of SUMO-Httex1-43Q with the analysis of the fractions by SDS-PAGE. (C) UPLC spectra of the phosphorylation reaction of SUMO-Httex1-43Q by GCK or TBK1 over-time.

To reveal the actual state of phosphorylation, we performed a cleavage reaction of the SUMO tag by ULP1 on an analytical scale and analyzed the cleaved phosphorylated Httex1. Indeed, when analyzing the cleavage product from the reaction of SUMO-Httex1-23Q with GCK (6 hours of incubation), we observed that only 50%

of Httex1-23Q was phosphorylated (Figure III.6-B). On the other hand, the cleavage of SUMO-Httex1-23Q phosphorylated by TBK1 (6 hours of incubation) showed 100% phosphorylation at S13 and S16 only (Figure III.6-B), confirming our hypothesis that the third phosphorylation occurs on the SUMO protein. Consequently, we established that it is essential to perform analytical SUMO cleavage to monitor phosphorylation for all our future applications. Moreover, to achieve complete phosphorylation of the desired sites, the *in vitro* phosphorylation reactions were extended to 17 hours, especially for GCK kinase. To verify that the phosphorylation conditions and extended incubation time did not affect the stability of SUMO-Httex1-43Q, we followed the phosphorylation by GCK or TBK1 using UPLC (Figure III.4-C). For both kinases, the conditions did not affect the intensity of the SUMO-Httex1-43Q peak even after overnight incubation at 30°C (Figure III.4-C), suggesting the absence of aggregation under these conditions.

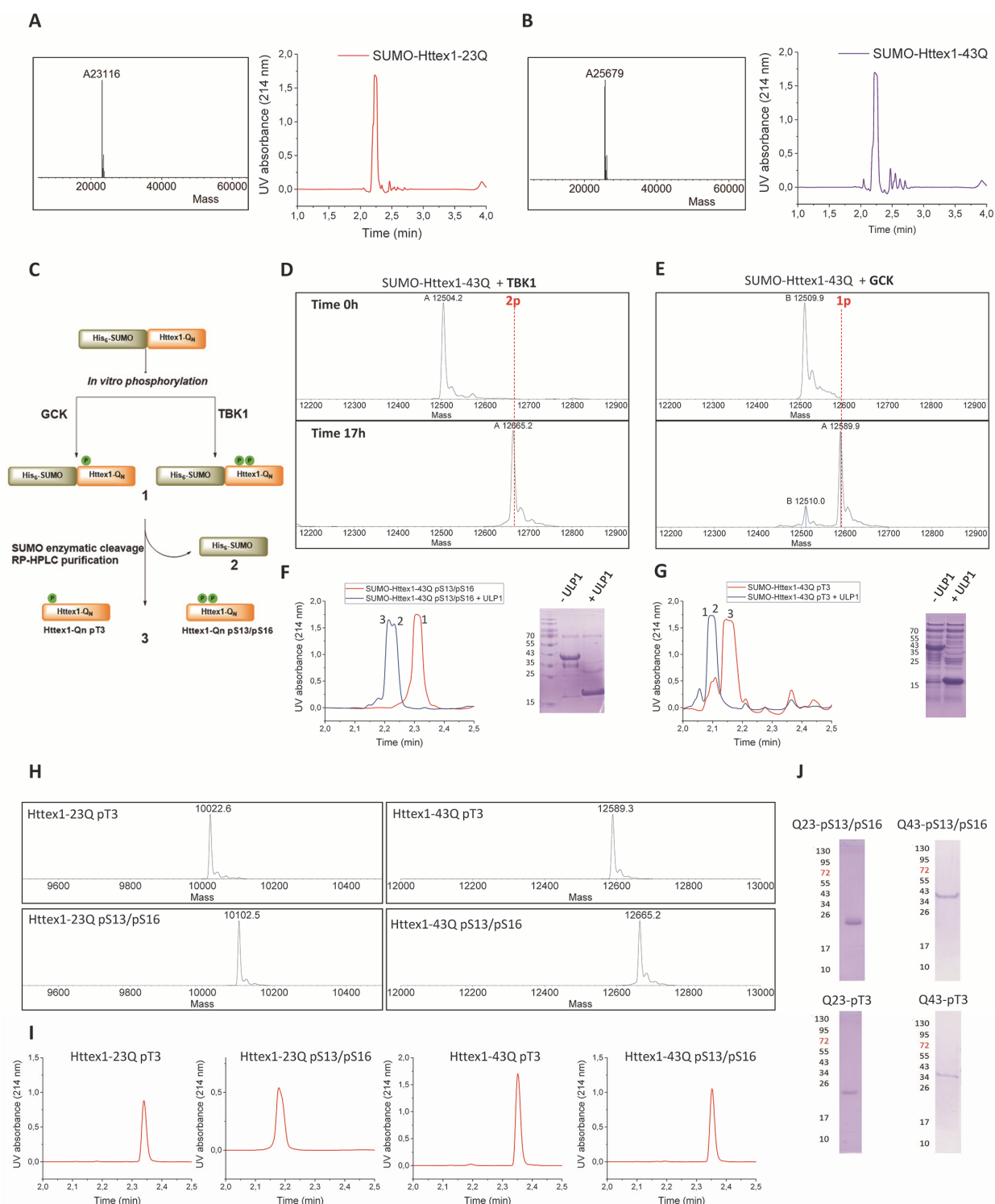


Figure III-5. SUMO-based strategy for the *in vitro* quantitative production of phosphorylated Httex1 23Q and 43Q using TBK1.

(A-B) Characterization of SUMO-Httex1-23Q (A) and SUMO-Httex1-43Q (B) by ESI/MS (left) and UPLC (right). (C) Schematic overview of the method used for phosphorylation of SUMO-Httex1-Q<sub>n</sub>. Monitoring of the phosphorylation reaction of SUMO-Httex1-43Q with TBK1 (D) and GCK (E) by ESI/MS after an analytical SUMO cleavage. Monitoring of the cleavage of the SUMO tag by ULP1 from phosphorylation reaction of SUMO-Httex1-43Q with TBK1 (F) or GCK (G). Purity characterization of Httex1-23Q pT3, Httex1-43Q pT3, Httex1-23Q pS13/pS16, and Httex1-43Q pS13/pS16 by (H) ESI/MS, (I) UPLC and (J) SDS-PAGE. (Expected molecular weights for the proteins are listed in Table III.1).



Having optimized and validated the phosphorylation of SUMO-Httex1-Qn, we performed a 10 mg preparative incubation, TBK1 phosphorylated SUMO-Httex1-23Q (Figure III.7-A) and SUMO-Httex1-43Q (Figure III.5-D) completely at both S13 and S16, as indicated by the addition of 2 phospho groups in the cleaved Httex1-Qn pS13/pS16 proteins (Figure III.7-A and Figure III.5-D). The specificity of the fusion proteins phosphorylation was confirmed by western blot analysis using specific pS13 and pS16 antibodies (Figure III.6-C). Once phosphorylation was confirmed, the SUMO tag was cleaved using ULP1, and the generation of the native phosphorylated Httex1-Qn proteins was monitored by UPLC and SDS-PAGE (Figure III.5-F and Figure III.7-C). After 15 min, cleavage of the SUMO tag was complete as indicated by the disappearance of the UPLC peak corresponding to SUMO-Httex1-Qn pS13/pS16 and the appearance of 2 new peaks for Httex1-Qn pS13/pS16 and the SUMO tag (Figure III.5-F and Figure III.7-C). This was further confirmed by SDS-PAGE, which showed the complete disappearance of SUMO-Httex1-Qn pS13/pS16 after the addition of ULP1 for 15 min (Figure III.5-F and Figure III.7-C). It should be noted that UPLC is a faster and more efficient tool to monitor this rapid cleavage reaction than SDS-PAGE. Next, the Httex1-Qn pS13/pS16 protein was separated from the SUMO tag and other impurities by reversed-phase HPLC (RP-HPLC) (Figure III.7-E and III.7-G). Httex1-Qn pS13/pS16 eluted first (~22 min) and was separable from the SUMO tag, which eluted later (~30 min) (Figure III.7-E and III.7-G). The fractions containing Httex1-Qn pS13/pS16 were pooled together, and the purities of Httex1-23Q pS13/pS16 and Httex1-43Q pS13/pS16 (final yields of 6.1 and 4 mg respectively) were analyzed by ESI/MS, UPLC, and SDS-PAGE (Figure III.5 H-J). Similarly, we used GCK to phosphorylate SUMO-Httex1-23Q and SUMO-Httex1-43Q at T3. Analysis of the overnight phosphorylation reaction by ESI/MS showed that the reaction was not complete (~80% completion for the WT and mutant Httex1), as indicated by the detection of a mixture of nonphosphorylated and singly phosphorylated species, by ESI/MS, Figure III.5-E and Figure III.7-B. However, due to the appearance of a tiny population of doubly phosphorylated species (Figure III.7-B), we decided not to push the phosphorylation reaction further with increased incubation time or the addition of more kinase in order to ensure single phosphorylation at T3. SUMO-Httex1-Qn phosphorylated by GCK was then incubated with ULP1 to remove the SUMO tag. After SUMO cleavage was confirmed by UPLC (Figure III.5-G and Figure III.7-D), the reaction mixture was subjected to RP-HPLC purification to separate Httex1-Qn pT3 from SUMO (Figure III.7-F and III.7-H). We were able to separate Httex1-pT3 23Q and Httex1-43Q pT3 from the nonphosphorylated and doubly phosphorylated species (highlighted in grey and green, respectively, in Figure III.7-F and III.7-H). Finally, the fractions containing Httex1-23Q pT3 and Httex1-43Q pT3 (final yields of 5 and 3.6 mg respectively) were pooled together and analyzed by ESI/MS, UPLC, and SDS-PAGE, as indicated in Figure III.5 H-J. This new protocol enabled us to enzymatically produce highly pure WT and mutant Httex1 phosphorylated at T3 or pS13/pS16 in milligram quantities for the first time. The complete characterization of the produced proteins (Httex1-23Q pT3, Httex1-23Q pS13/pS16,

Httex1-43Q pT3, and Httex1-43Q pS13/pS16) by ESI/MS, UPLC, and Coomassie SDS PAGE is shown in Figure III.5 H-J. With this optimized protocol in hand, we then moved to assess its utility to generate fluorescently and isotopically labeled and site-specifically phosphorylated Httex1 proteins for future use as valuable tools in structural studies (solution and solid-state NMR [376, 377]) and cellular studies to investigate the seeding and cell-to-cell transmission of HTT aggregates.

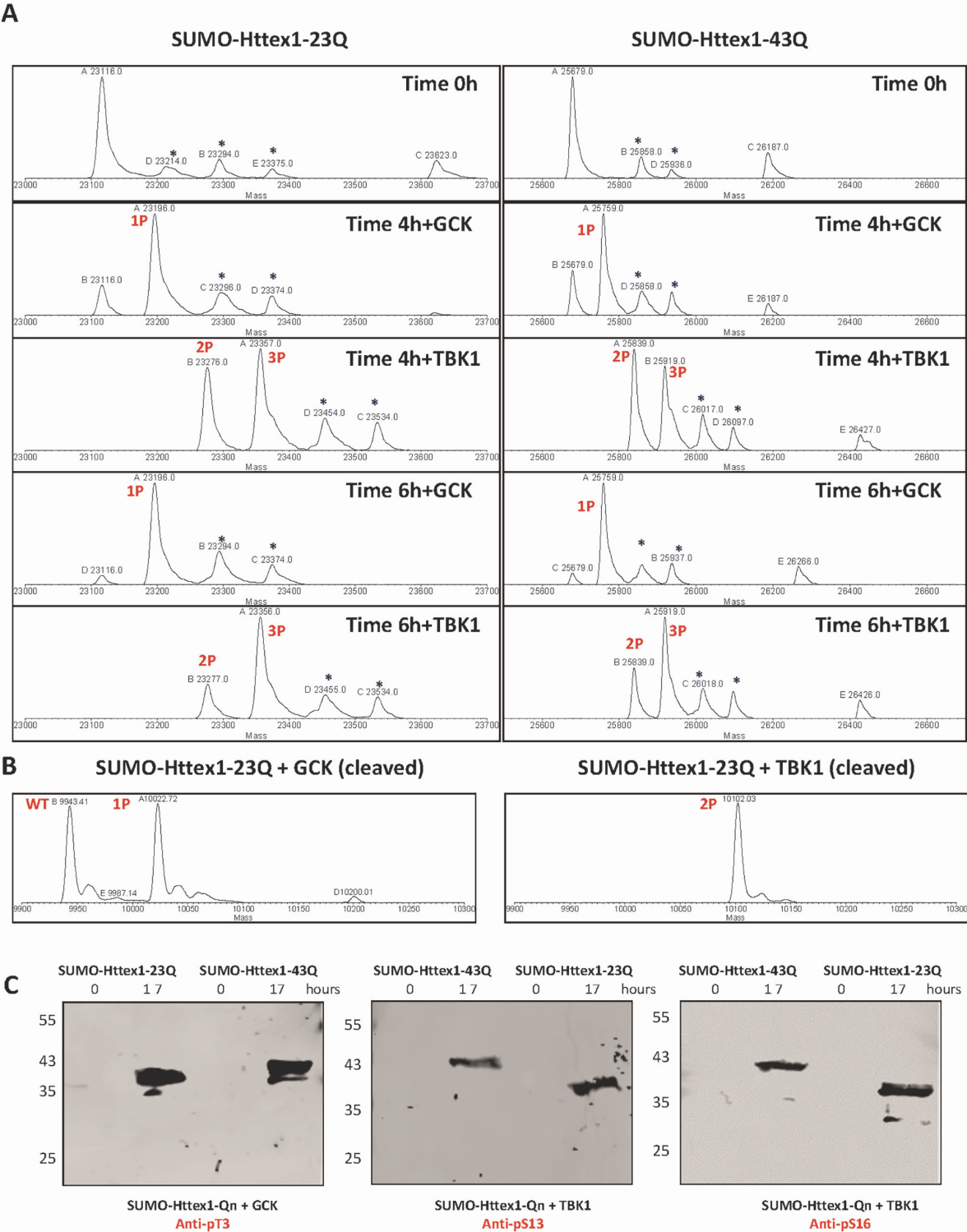


Figure III-6. SUMO-Httex1-Qn phosphorylation by GCK and TBK1.

(A) Phosphorylation of SUMO-Httex1-23Q and SUMO-Httex1-43Q by TBK1 or GCK over-time, followed by ESI/MS (stars are TFA adducts). (B) ESI/MS analysis of the phosphorylation reaction of SUMO-Httex1-23Q by GCK (left) and SUMO-Httex1-23Q by TBK1 (right) after SUMO tag cleavage by ULP1. (C) Representative western blot of SUMO-Httex1-23Q and SUMO-Httex1-43Q overnight phosphorylation by GCK and TBK1 using pT3-, pS13-, or pS16-specific antibodies.

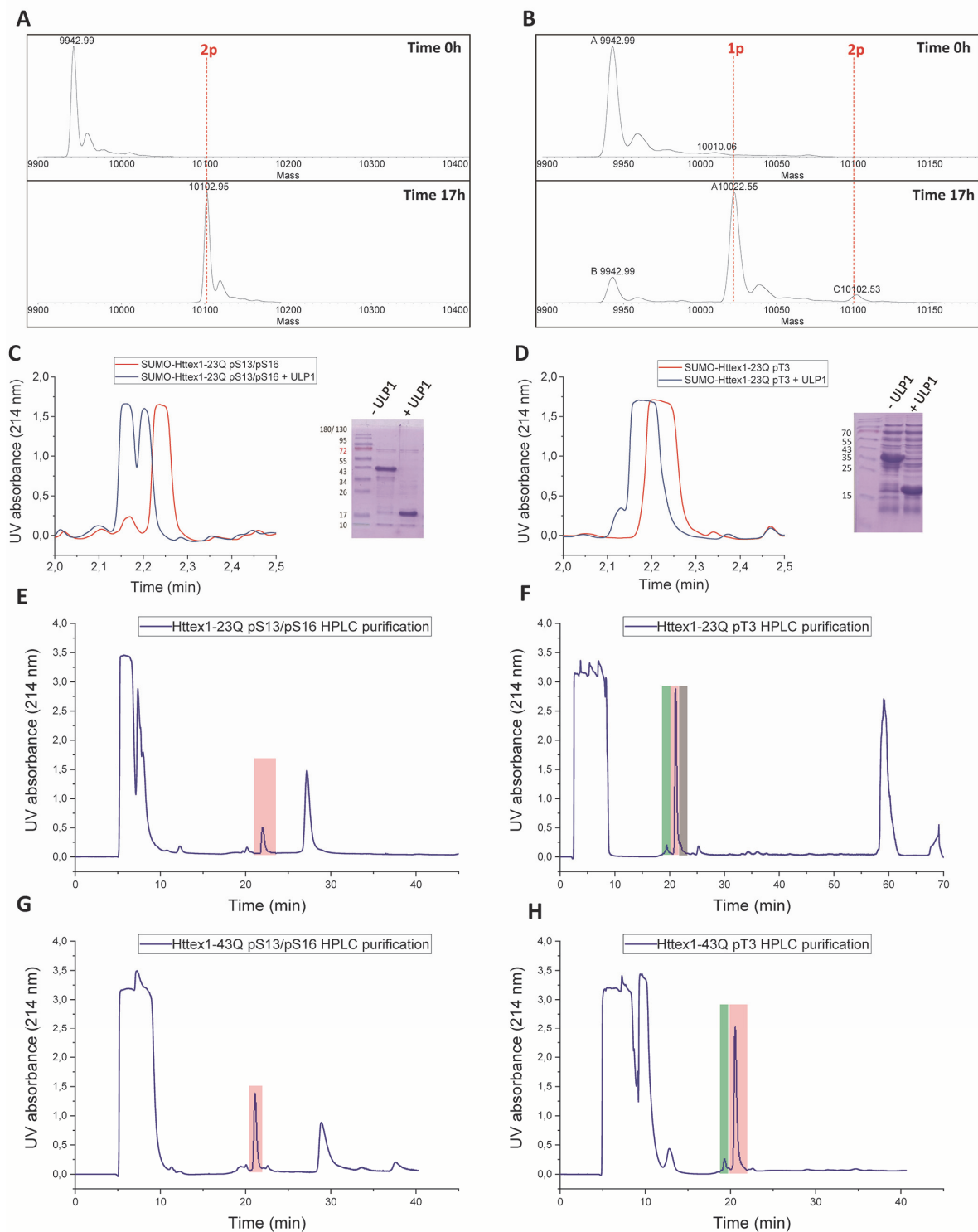


Figure III-7. Monitoring of the phosphorylation reaction of SUMO-Httex1-23Q

with TBK1 (**A**) and GCK (**B**) by ESI/MS after analytical SUMO tag cleavage by ULP1. Monitoring of the cleavage of the SUMO tag by ULP1 from SUMO-Httex1-23Q phosphorylation by TBK1 (**C**) or GCK (**D**). (**E-H**) RP-HPLC chromatogram for the purification of Httex1-23Q pS13/pS16 (**E**), Httex1-23Q pT3 (**F**), Httex1-43Q pS13/pS16 (**G**), Httex1-43Q pT3 (**H**). Red: proteins of interest, Green: Httex1 pT3 and pS13, Grey: Unphosphorylated.

### III.3.3 Generation of fluorescently labeled (ATTO-565 maleimide) phosphorylated WT and mutant Httex1

Fluorescently labeled HTT proteins are valuable tools to understand the HTT structure and aggregation mechanisms *in vitro* [315] and to monitor its subcellular localization [206], dynamics of aggregation [236] and clearance, cell-to-cell transmission [378] and cellular properties in HD cellular models. GFP family fusion proteins are commonly used in HD cellular studies to track the formation of cytoplasmic and nuclear HTT aggregates and inclusions [309, 323, 379-381]. However, these proteins are large compared to Httex1, which might significantly impact its structure and aggregation properties. Small molecule fluorescent probes present many advantages compared to fusion-labeled proteins; they are highly sensitive and stable and are likely to show less interference with the normal functions and interactome of the target protein. Amine-reactive probes can be used to label lysine residues; however, their labeling might result in the heterogeneous preparation of labeled proteins; additionally, lysines within the Nt17 domain play an essential role in the amphipathic helix, and by consequence, any small modification might perturb the Nt17 structure. Furthermore, until now, semisynthesis was required to introduce fluorescent molecules in Httex1 with PTMs [223]. To overcome these challenges, we introduced a single-site mutation of proline to cysteine (P90C) at the C-terminus of SUMO-Httex1-Qn to enable labeling with Atto-565-maleimide (Figure III.8-A). Maleimide fluorophores are highly specific for the thiol group of cysteine (P90C), and we showed previously that the reaction is rapid with the thiol of P90C [223].

Using the protocol described above, we produced phosphorylated Httex1-Qn P90C (Httex1-23Q pT3 P90C, Httex1-43Q pT3 P90C, Httex1-23Q pS13/pS16 P90C and Httex1-43Q pS13/pS16 P90C) (Figure III.9 and Figure III.10-A). Then, to perform the labeling, these proteins were disaggregated using neat TFA, as described by Reif et al. [238]. Next, the thin protein film was resuspended in 100 mM Tris pH 7.4, 6 M GdHCl, 50 mM trehalose, 0.5 M proline, and 1.1 equivalents TCEP [382], and the pH was adjusted to 7.4. The fluorescent dye Atto-565-maleimide (1.5 equivalents) was added to the protein, and the reaction was kept on ice for 30 min. The labeling reaction was monitored by ESI/MS, with the knowledge that the addition of ATTO-565 to a protein corresponds to the addition of 633 Da to the molecular mass. All 4 phosphorylated proteins were successfully fluorescently labeled as evidenced by the appearance of an additional 633 Da to their molecular weight, as demonstrated by ESI/MS (Figure III.10-B). After removal of the excess dye using a PD-10 column, the labeled phosphorylated proteins were purified by RP-HPLC, and the fractions containing the proteins were pooled and lyophilized. Figure III.8-B shows the final characterization of Httex1-23Q pT3 P90C, Httex1-43Q pT3 P90C, Httex1-23Q pS13/pS16 P90C and Httex1-43Q pS13/pS16 P90C by ESI/MS and UPLC.

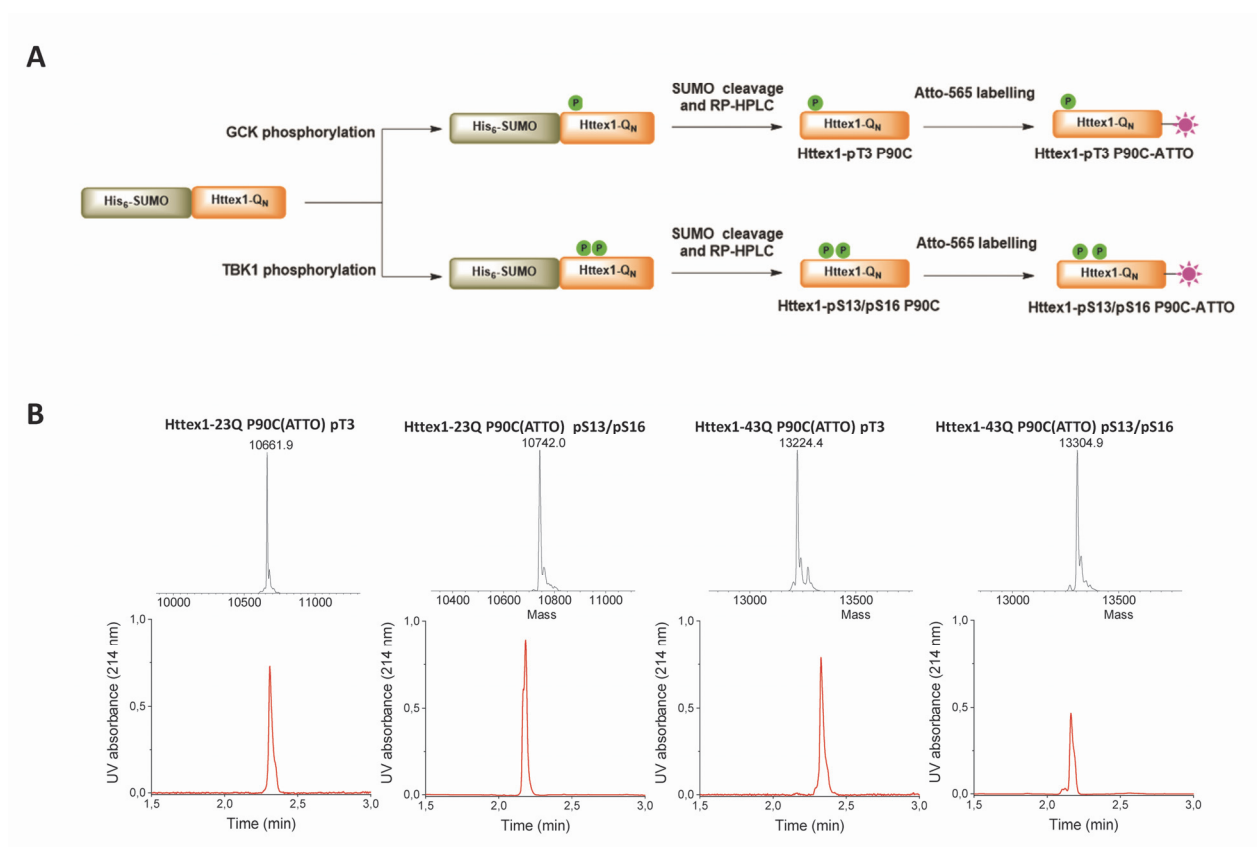


Figure III-8. Generation of phosphorylated and labelled Httex1 proteins.

Atto-565-maleimide labeling of phosphorylated Httex1. **(A)** Schematic representation of the strategy to prepare and label Atto-565 phosphorylated Httex1. **(B)** Final characterization by ESI/MS and UPLC of the indicated labeled phosphorylated Httex1 proteins. (Expected molecular weights for the proteins are listed in Table III.1).

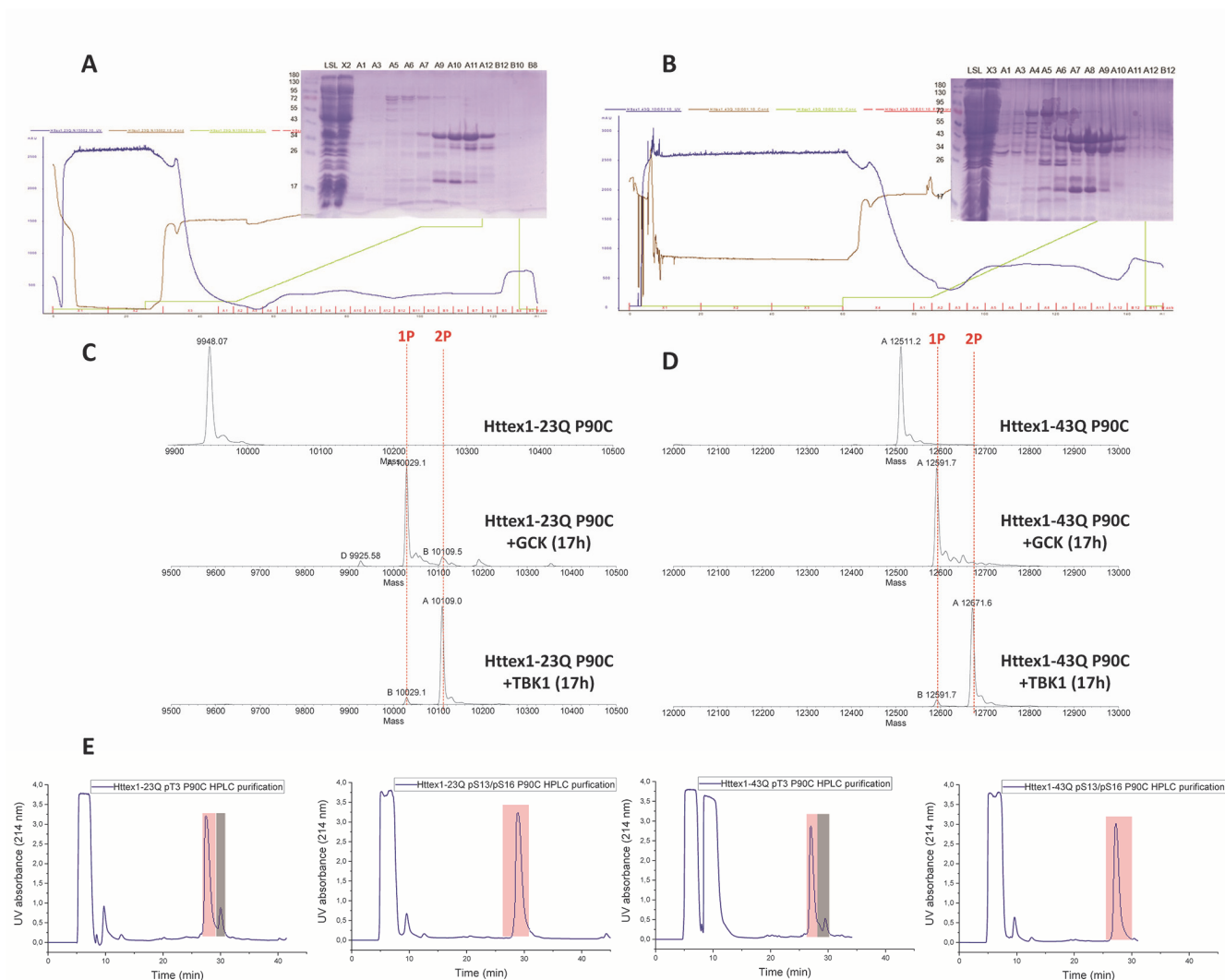


Figure III-9. Phosphorylation of SUMO-Httex1-Qn P90C.

(A) Representative chromatogram of the IMAC purification of SUMO-Httex1-23Q P90C, and (B) Representative chromatogram of the IMAC purification of SUMO-Httex1-43Q P90C with the analysis of the fractions by SDS-PAGE. (C) Monitoring of the phosphorylation reaction by GSK and TBK1 of SUMO-Httex1-23Q P90C by ESI/MS after analytical SUMO tag cleavage by ULP1 (D) Monitoring of the phosphorylation reaction by GSK and TBK1 of SUMO-Httex1-43Q P90C by ESI/MS after analytical SUMO tag cleavage by ULP1. (E) RP-HPLC purification chromatogram of Httex1-23Q pT3 P90C, Httex1-23Q pS13/pS16 P90C, Httex1-43Q pT3 P90C and Httex1-43Q pS13/pS16 P90C. Red: proteins of interest, Grey: Unphosphorylated

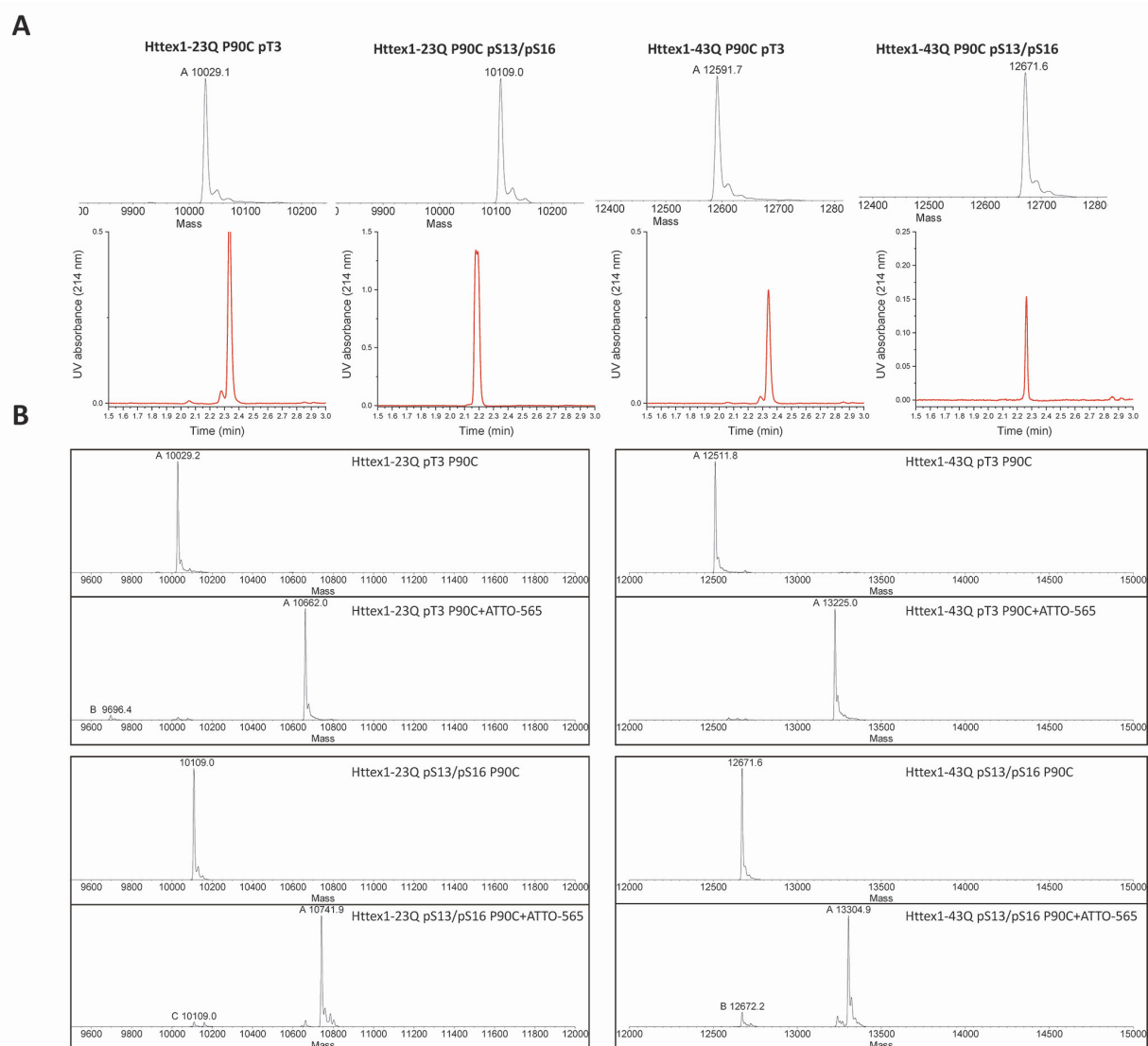


Figure III-10. *In vitro* ATT-565 labelling of phosphorylated proteins.

(A) Final characterization by ESI/MS (upper panel) and UPLC (lower panel) of Httpex1-23Q pT3 P90C, Httpex1-43Q pT3 P90C, Httpex1-23Q pS13/pS16 P90C or Httpex1-43Q pS13/pS16 P90C and the monitoring of their labelling by ATTO-565-maleimide by ESI/MS (B)



### III.3.4 Generation of phosphorylated $^{13}\text{C}$ - and $^{15}\text{N}$ -labeled Httex1 suitable for NMR applications

Solution NMR spectroscopy has provided valuable insights into the structure and dynamics of soluble N-terminal peptides and Httex1 constructs in several works [192, 193, 383, 384]. Additionally, NMR was shown using other protein systems to be highly sensitive to PTMs [385-388]. Previously, isotopic labeling of phosphorylated Httex1 was unaffordable by chemical synthesis, given the high costs of isotope-enriched amino acids. Having identified several kinases that phosphorylate Nt17 and developed an efficient strategy for the generation of recombinant Httex1 [238], we next sought to combine these advances to produce phosphorylated and isotopically labeled Httex1. When SUMO-Httex1-Qn was expressed in minimal media containing isotopically labeled ammonium chloride ( $^{15}\text{N}$ ) and glucose ( $^{13}\text{C}$ ), as previously reported [389], we observed an increase in cleavages in the sequence of the fusion protein (Figure III.11-A) leading to the generation of a fragment with a molecular weight of 7131 Da that corresponds to HTT 2-62, as indicated by ESI/MS in Figure III.11-B. This fragment was challenging to separate from Httex1 by HPLC (Figure III.11-C); the peaks of the 2 fragments did not resolve despite different gradient optimizations.

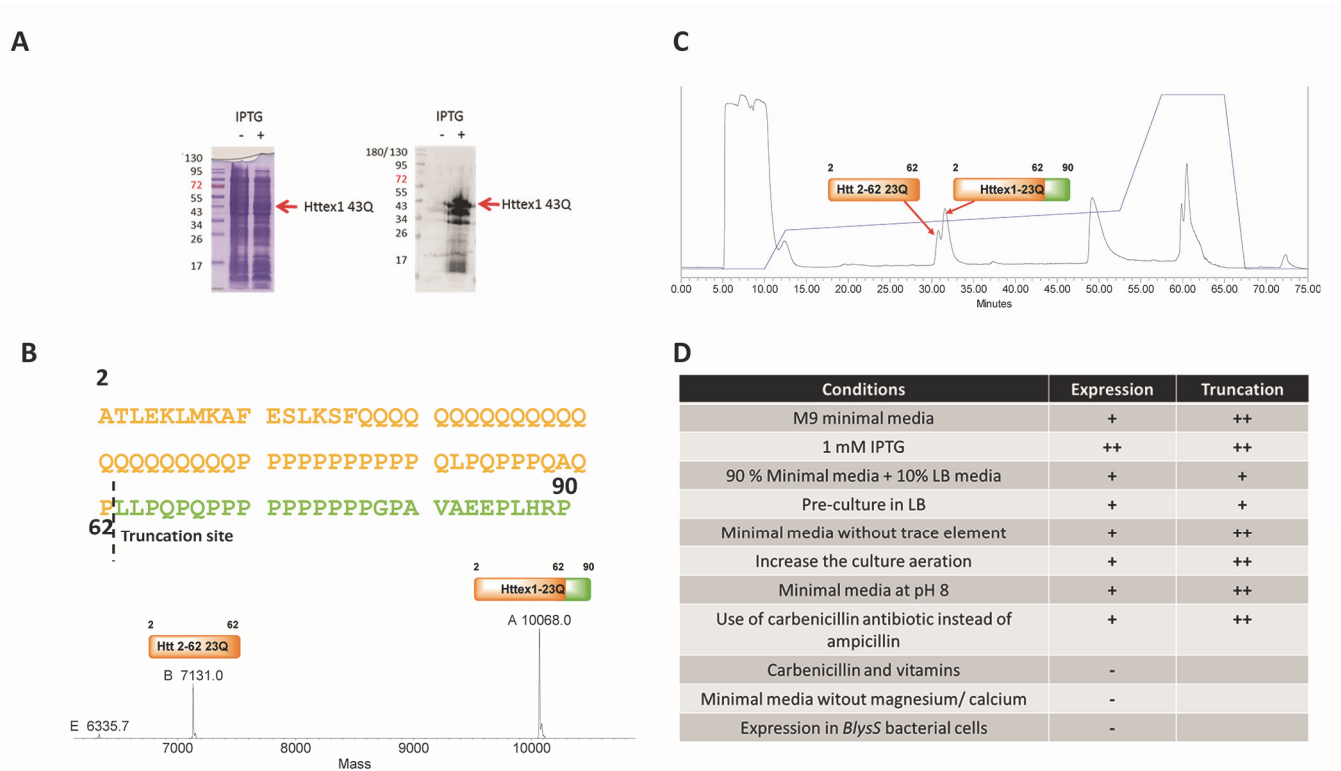


Figure III-11. Optimizing the expression of SUMO-Httex1-Qn in minimal media.

**(A)** SDS-PAGE and western blot analysis of the expression of SUMO-Httex1-43Q, highlighting the increased levels of truncation. **(B)** Analysis by ESI/MS of the elution fractions after HPLC of Httex1-23Q <sup>15</sup>N. The truncation position is highlighted within the sequence of Httex1-23Q (upper panel). **(C)** HPLC chromatogram showing the purification of Httex1-23Q <sup>15</sup>N after SUMO cleavage highlighting the HTT 2-62 truncation. **(D)** List of all the conditions that were tested to avoid truncation or lack of expression and obtained results (+ for high, ++ for very high, and – for absence).

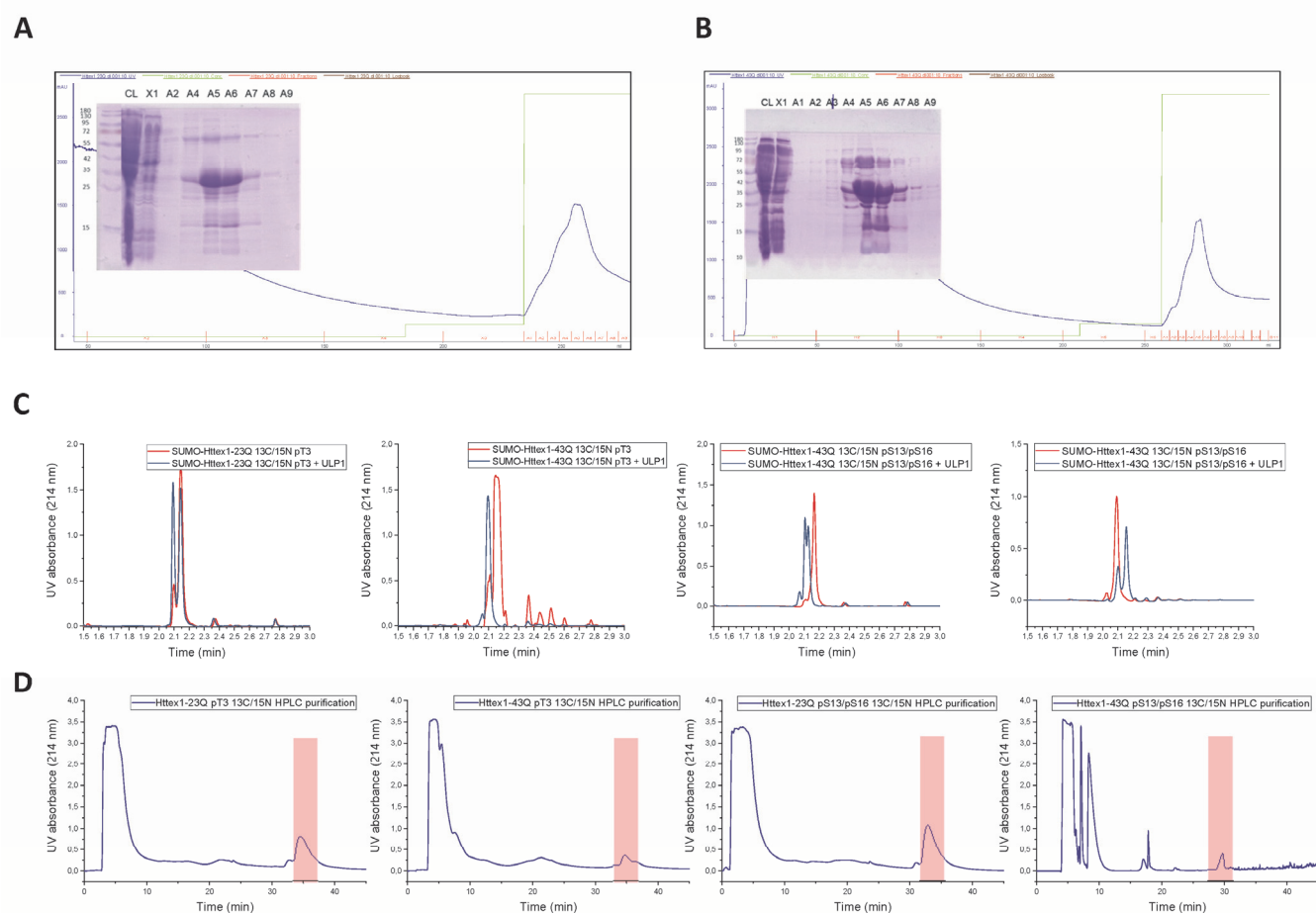


Figure III-12. Expression, phosphorylation and purification of Httex1-Qn by GCK and TBK1.

Representative chromatogram of the IMAC purification of SUMO-Httex1-23Q  $^{13}\text{C}/^{15}\text{N}$ , and **(B)** Representative chromatogram of the IMAC purification of SUMO-Httex1-43Q  $^{13}\text{C}/^{15}\text{N}$  with the analysis of the fractions by SDS-PAGE. **(C)** UPLC Analysis of the cleavage of the SUMO tag by ULP1 from the SUMO-Httex1-Qn  $^{13}\text{C}/^{15}\text{N}$  phosphorylated with GCK or TBK1. **(D)** HPLC purification of Httex1-23Q pT3  $^{13}\text{C}/^{15}\text{N}$ , Httex1-43Q pT3  $^{13}\text{C}/^{15}\text{N}$ , Httex1-23Q pS13/pS16  $^{13}\text{C}/^{15}\text{N}$  or Httex1-43Q pS13/pS16  $^{13}\text{C}/^{15}\text{N}$ . Red: proteins of interest.

Different conditions and media were tested (Figure III.11-D), but we observed significant truncations or a lack of protein expression under all conditions. The best alternative method we identified was to grow the bacterial cells in standard LB media, and when the optical density of the culture reached 0.3, the cells were centrifuged and transferred to the isotopically labeled minimal media followed by induction of the expression with IPTG overnight at 18°C was performed [390]. Using this protocol, we succeeded in expressing and purifying the doubly labeled WT or mutant SUMO-Httex1 through nickel affinity chromatography (Figure III.12-A and III.12-B), which was then subjected to *in vitro* phosphorylation by GCK or TBK1 (Figure III.13-A and III.13-B) followed by ESI/MS (Figure III.13-A and 6-B). We showed, as expected, that GCK phosphorylated SUMO-Httex1-23Q and Httex1-43Q at a single site (pT3) (Figure III.13-A) and TBK1 phosphorylated at 2 sites (pS13/pS16) (Figure III.13-B). The SUMO cleavage of the phosphorylated SUMO-Httex1-Qn  $^{13}\text{C}/^{15}\text{N}$  was monitored by UPLC (Figure III.12-C), and complete cleavage was indicated by the disappearance of the fusion protein peak and the appearance of 2 peaks corresponding to phosphorylated Httex1 and the SUMO tag (Figure III.12-C). Removal of the SUMO tag and purification of the labeled proteins by RP-HPLC was performed (Figure III.12-D). The purity of the proteins was verified by ESI/MS, UPLC, and SDS-PAGE (Figure III.13-C).

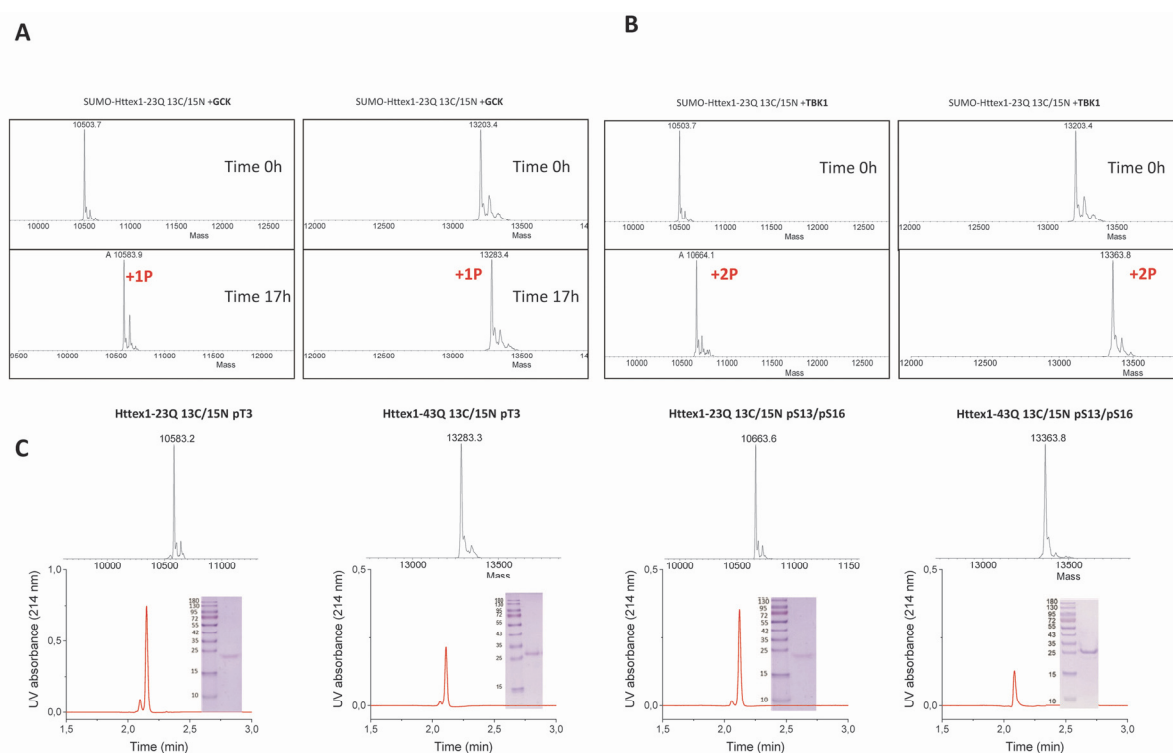


Figure III-13. Phosphorylation and characterization of  $^{13}\text{C}/^{15}\text{N}$  phosphorylated Httex1.

(A) Monitoring of the phosphorylation reaction of SUMO-Httex1-23Q  $^{13}\text{C}/^{15}\text{N}$  and SUMO-Httex1-43Q  $^{13}\text{C}/^{15}\text{N}$  by GCK. (B) Monitoring of the phosphorylation reaction of SUMO-Httex1-23Q  $^{13}\text{C}/^{15}\text{N}$  and SUMO-Httex1-43Q  $^{13}\text{C}/^{15}\text{N}$  by TBK1 after an analytical SUMO cleavage. (C) Final characterization by ESI/MS, UPLC, and SDS-PAGE of Httex1-23Q  $^{13}\text{C}/^{15}\text{N}$  pT3, Httex1-43Q  $^{13}\text{C}/^{15}\text{N}$  pT3, Httex1-23Q  $^{13}\text{C}/^{15}\text{N}$  pS13/pS16, and Httex1-43Q  $^{13}\text{C}/^{15}\text{N}$  pS13/pS16. (Expected molecular weights for the proteins are listed in Table III.1).

### III.3.5 Structural NMR studies of Httex1-23Q pT3 and Httex1-23Q pS13/pS16

With these proteins in hand, we then sought to gain insight into effect of Nt17 phosphorylation on the structural properties of Httex1. First, to test the quality and utility of our  $^{15}\text{N}/^{13}\text{C}$  labeled samples, we verified by  $^1\text{H}$  spectra that the samples contained no detectable amounts of unlabeled species, thus validating the success of the expression strategy presented above.  $^1\text{H}$ - $^{15}\text{N}$  HSQC NMR spectra were easily attainable for all the different proteins (unmodified, Httex1-23Q-pT3 and Httex1-23Q-pS13/pS16) (Figure III.14-A and 7-B). The signal spread, linewidths and stability over the course of one week for both phosphorylated forms were similar to those of the unmodified protein, indicating preserved disorder and equal or slower aggregation rates (Figure III.14-A and Figure III.14-B).

After assigning the backbone resonances of our unmodified Httex1 construct in the conditions of interest (pH 7, 25°C, Table III.2), we could use this information to interpret the differences between the HSQC spectra of unmodified and both phosphorylated forms. For Httex1-23Q  $^{13}\text{C}/^{15}\text{N}$  pS13/pS16 (Figure III.14-A), we observed strong downfield perturbations for S13 and S16 chemical shifts in the  $^1\text{H}$  dimension, as documented for phosphorylated serine [391, 392], along with smaller but sizeable perturbations of other residues within the Nt17 region including the first two glutamines of the polyQ tract (Q18 and Q19). However, we did not observe significant perturbations for the terminal glutamines (Q39 and Q40), nor for residues in the proline-rich or C-terminal regions. Similarly, for Httex1  $^{13}\text{C}/^{15}\text{N}$  pT3 (Figure III.14-B), we observed small but sizeable effects on the Nt17 residues, but not for the residues of the proline-rich and C-terminal regions. It is to be noted that no crosspeak for phosphorylated T3 was visible at pH 7 and 25°C. Moreover, T3 is also undetected in the unmodified protein under these conditions of neutral pH; however, we observed at pH 4.2 or lower a crosspeak at chemical shifts compatible with phosphorylated threonine while the crosspeaks for S13 and S16 remained close to their positions in the HSQC spectrum of the unmodified protein (Figure III.15-B).

Next, we obtained the backbone resonance assignments of the Httex1 construct doubly phosphorylated at S13 and S16, enabling a detailed residue-wise comparison of chemical shifts in contrast to the unmodified protein (Figure III.14-C and Table III.2). The phosphorylated serines exhibited large  $^1\text{H}$ ,  $^{15}\text{N}$  perturbations, as expected, and were the largest. Away from the serine residues throughout the sequence, the  $^1\text{H}$ ,  $^{15}\text{N}$  chemical shift perturbations slowly decay but peaking at residues 4, 7, 10, and 18. The location of these residues relative to S13 and S16 follows closely the spacing expected in a helical structure. Notably, in the unmodified protein, the  $^{13}\text{C}$  chemical shifts of CA and CB atoms indicated that this protein exhibited a large disorder but with a substantial helical propensity, especially at residues 17-19, consistent with previous reports [193, 384]. This helical propensity is retained in Httex1-23Q  $^{13}\text{C}/^{15}\text{N}$  pS13/pS16 according to the CA and CB chemical shifts (Figure III.14-C). To further explore the weak alpha-helical propensities, we titrated solutions of  $^{15}\text{N}$

labeled proteins with trifluoroethanol (TFE) [393], an agent well-known to expose helical structures. This experiment revealed large chemical shift dispersions on the unmodified and both phosphorylated forms, suggesting a similar latent helical propensity in all forms (Figure III.15-A).

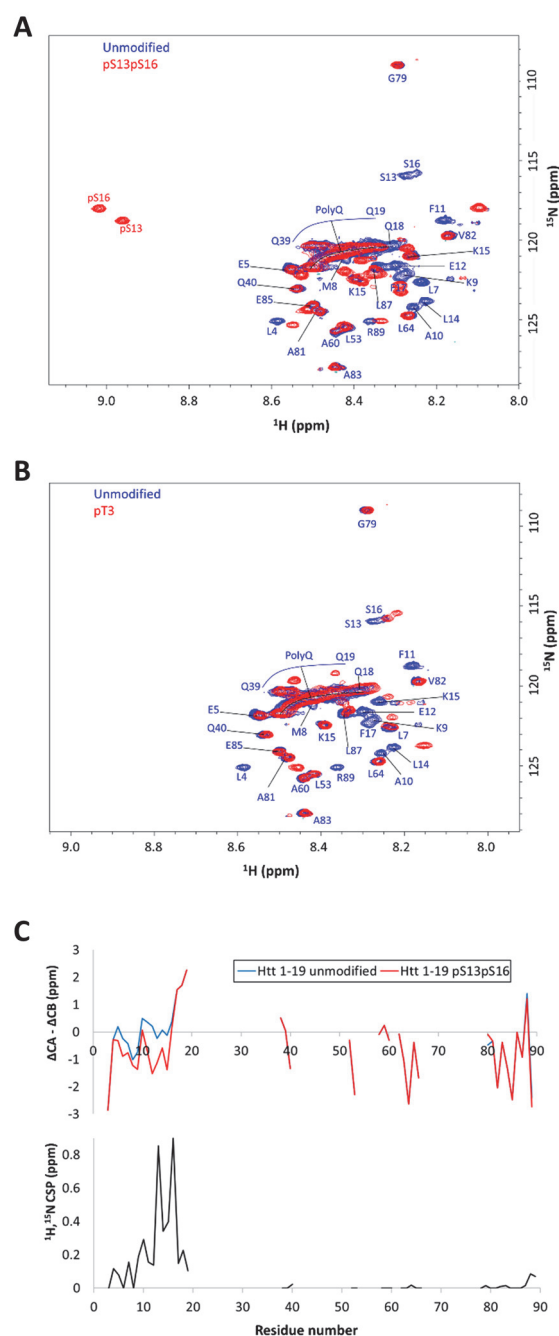


Figure III-14. NMR studies of Httex1-pT3 and pS13/pS16.

$^1\text{H}$ - $^{15}\text{N}$  HSQC NMR spectra of (A) Httex1-23Q pS13/pS16 and (B) Httex1-23Q pT3 in red, compared to the HSQC spectrum of unmodified Httex1-23Q in blue. All these spectra were acquired at pH 7 and 25°C, while for Httex1-23Q pT3 a further spectrum is shown at pH 4.2 in Figure III.15-B where the lower NH exchange rate improves resolution and intensity especially for the pT3 cross-peak which is undetectable at pH 7. The most important assignments of the unmodified and pS13pS16 forms are depicted. (C) The weighted chemical shift perturbations in  $^1\text{H}$  and  $^{15}\text{N}$  between the unmodified and pS13pS16 proteins (bottom) and a proxy for secondary structure propensities calculated as the difference of the residual CA and CB chemical shifts after subtraction of the random coil values (top). Notice that the slight beta propensity around residues 12 and 15 of Httex1-23Q pS13/pS16 could well arise as an artifact induced by the strong negative charges on Ser13 and Ser16 upon the subtraction of the random coil shift, without actually having any real structural implication (for pS13 and pS16 themselves we subtracted random coiled shifts of the phosphorylated amino acids, alleviating this problem).

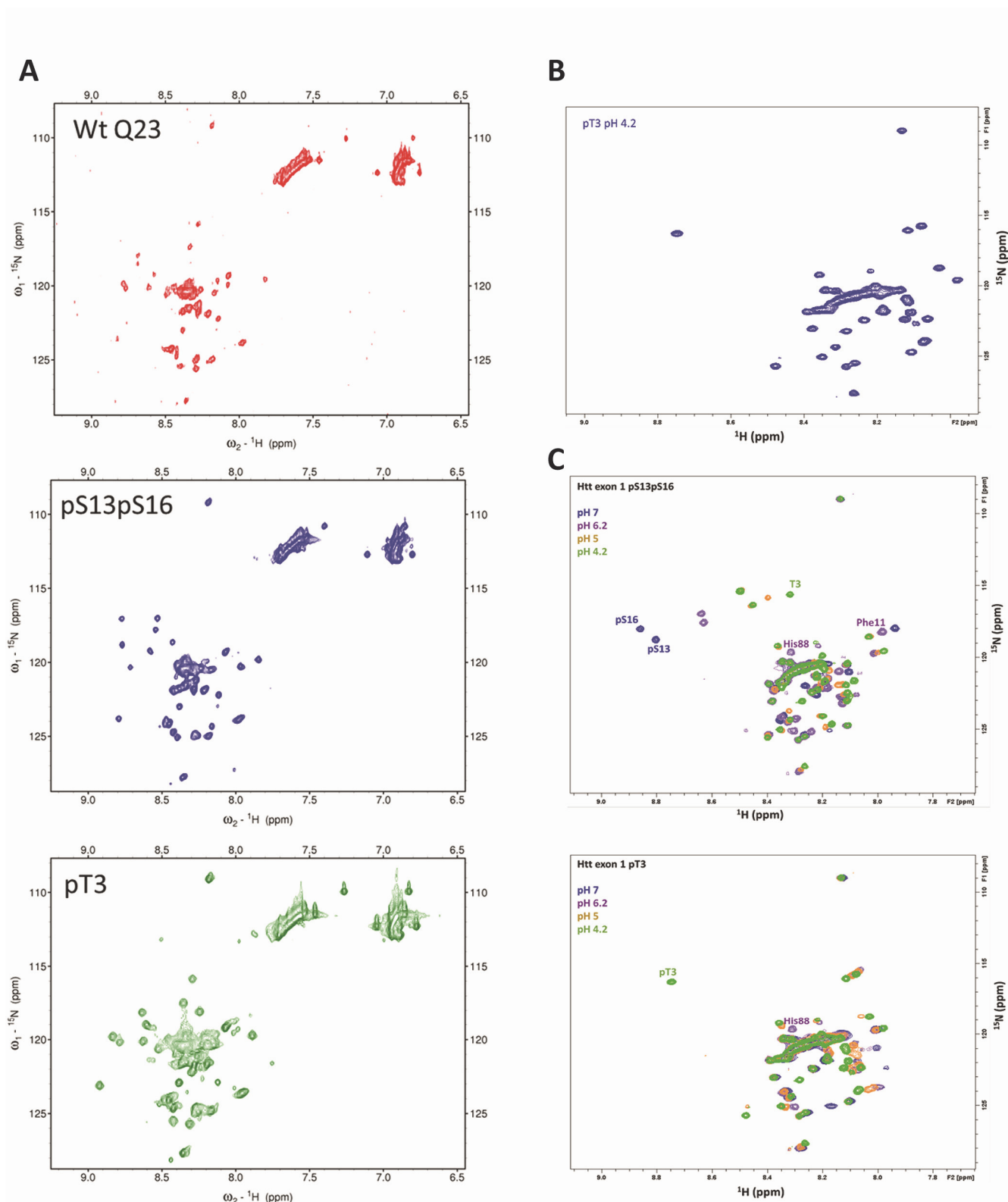


Figure III-15. NMR studies of Httex1-pT3 and pS13/pS16 in function of pH or TFE.

**(A)**  $^1\text{H}$ ,  $^{15}\text{N}$  HSQC spectra of unmodified, pS13pS16 and pT3 Httex1-23Q proteins in 20% trifluoroethanol, showing an increased chemical shift dispersion that likely reflects helical structuring occurring in all three species. **(B)**  $^1\text{H}$ ,  $^{15}\text{N}$  HSQC spectrum of Httex1-23Q pT3 acquired at pH 4.2 and 25°C, at which resolution and crosspeak intensity improve and the signal for pT3 becomes detectable. **(C)**  $^1\text{H}$ ,  $^{15}\text{N}$  HSQC spectra of Httex1-23Q pT3 and Httex1 pS13/pS16 proteins at pH 7, 6.2, 5 and 4.2, with the assignments of residues discussed in the text.



The pH of the buffer could also potentially affect the structure; therefore, we assessed the phosphorylated and unmodified proteins at different pHs. Increasing the pH above neutrality caused most of the signals to rapidly broaden beyond detection, starting at pH 7.5, in all the proteins (Figure III.15-C). On the other hand, when decreasing towards acidic pH, we found only slight shifts in the unmodified protein, suggesting virtually no substantial effects on the structure and dynamics of the proteins (Figure III.15-C). In the phosphorylated forms, the crosspeaks for pS13 and pS16 shifted considerably upfield as the pH decreased, most likely reflecting just protonation of the phosphate groups (Figure III.15-C). At the same time, crosspeaks of all the other residues were only slightly affected, indicating no substantial effects of the pH on the structure and dynamics of proteins. In all forms, a crosspeak likely corresponding to T3 appeared at pH 4.2 or lower, but this only reflects the slower H-N exchange at low pH without any significant effects on the other residues, nor does have any structural implications. In all cases, individual residues such as His88, Glu12, and sequence neighbors experienced shifts directly related to protonation as the pH decreased, but, again, these were likely just their protonation and not structural effects (Figure III.15-C).

### III.3.6 Real-time monitoring of TBK1 phosphorylation of Httex1 suggests that S13 phosphorylation occurs first and primes phosphorylation at S16.

The high sensitivity of NMR spectroscopy to phosphorylation and its technical simplicity, pose it as a valuable tool for real-time monitoring of Httex1 phosphorylation by kinases. Therefore, we sought to use it to assess potential cross-talk between phosphorylation at S13 and S16, as suggested by previous studies [282]. This experimental setup is much more straightforward than the use of antibody-based approaches such, has exquisite time resolution, and provides residue-level information on the structural consequences of phosphorylation, if any. We subjected the doubly labeled Httex1-23Q at a concentration of 200  $\mu$ M to phosphorylation by TBK1 in a compatible buffer with excess Mg-ATP (Figure III.16). The reaction was performed at 20°C in order to slow the enzymatic reaction and adequately monitor it in real time by HSQC spectra collected in under 3 minutes each, at high resolution without distortions. We observed the rapid decay of the crosspeaks corresponding to both serine residues (Figure III.16). In parallel, a new crosspeak appeared close to them, and another appeared in a downfield region consistent with a phosphorylated serine. Over-time, these two crosspeaks, tentatively assigned to an intermediate where only one serine is phosphorylated, faded out as those assigned to pS13 and pS16 in the pure pS13pS16 protein appeared and gained intensity (Figure III.16). A  $^1\text{H}$ ,  $^{13}\text{C}$  plane of a CBCA(CO)NH experiment collected 21 hours after initiation of the reaction revealed that the crosspeak for a phosphorylated serine in the intermediate shares  $^{13}\text{C}$  chemical shifts with Ser13 in the pS13pS16 protein (Figure III.17). We concluded that the intermediate corresponds to a species where Ser13 is phosphorylated but Ser16 is not. Interestingly, this was confirmed by the absence of a fourth cross-peak in

the region of phosphorylated serines that would have been attributed to an intermediate phosphorylated at S16 with S13 unmodified. These observations suggest that S13 phosphorylation primes phosphorylation at S16, similar to what has been suggested previously [282, 394]. Additionally, these findings were in accordance with our previous cellular and *in vivo* observation where we showed that TBK1 phosphorylated mainly S13 [374].

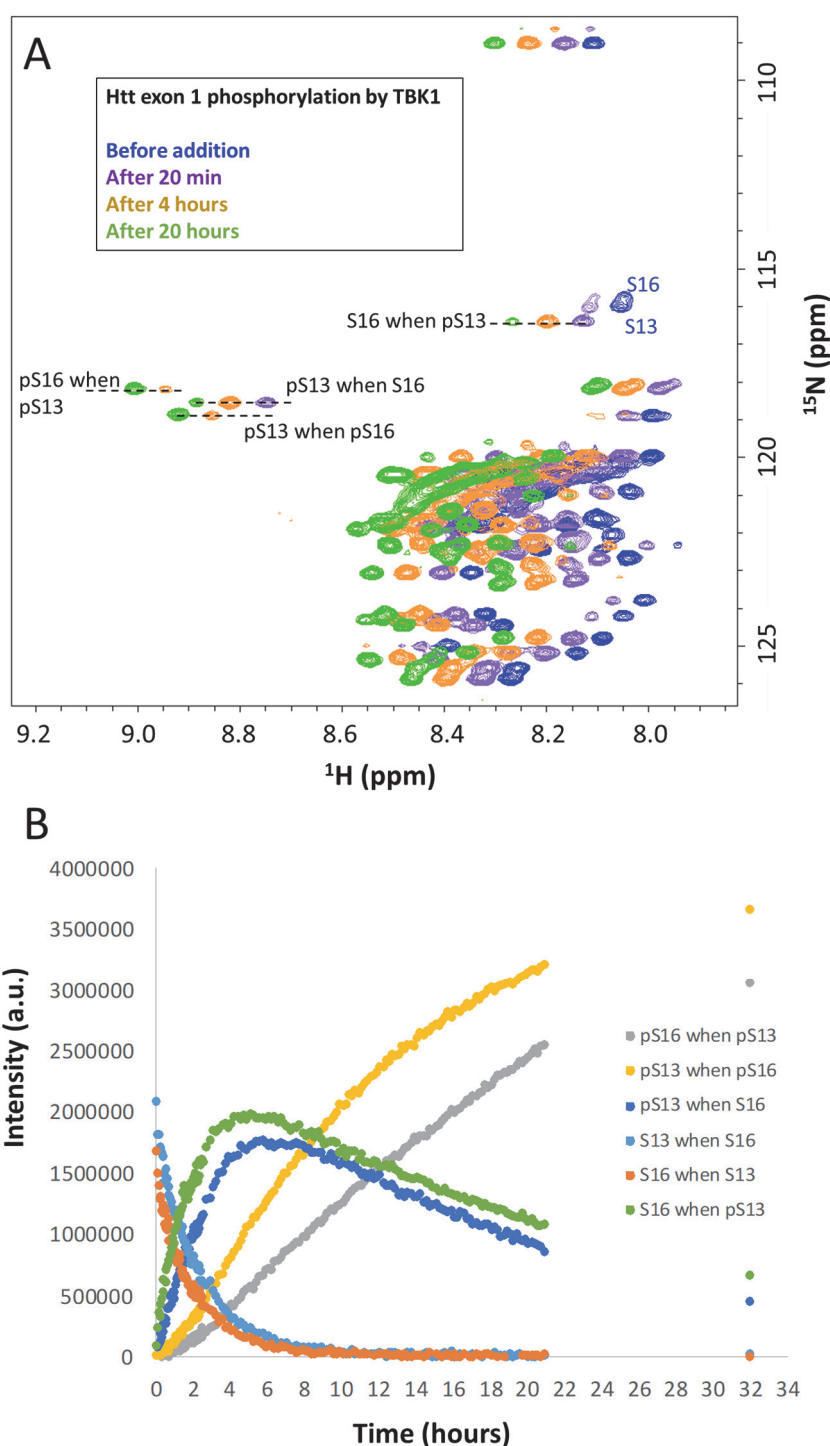


Figure III-16. Real-time monitoring of TBK1 phosphorylation of Httex1.

Phosphorylation of Httex1-23Q  $^{13}\text{C}/^{15}\text{N}$  followed by NMR. Monitoring of 500  $\mu\text{l}$  of a 200  $\mu\text{M}$  sample of doubly labeled Httex1-23Q as it is phosphorylated by TBK1 in buffer containing 15  $\mu\text{g}$  of TBK1 plus 5 mM Mg-ATP and a suitable buffer (30 mM HEPES, 5 mM  $\text{MgCl}_2$ , 5 mM EGTA, 1 mM DTT, pH 7.2) at 20°C. Each HSQC spectrum was acquired in 2 min and 50 seconds with a 0.5 recycle delay and 128  $^{15}\text{N}$  increments. Spectra were acquired serially over 21 hours with one final acquisition at 32 hours. **(A)** An example spectrum taken before TBK1 addition and after 20 min, 4 hours and 21 hours, offset to the left at increasing times for clarity; assignments of all observed S13 and S16 species are indicated. **(B)** The intensities of these cross-peaks over time, stressing the initial phosphorylation of S13 with subsequent phosphorylation at S16 leading to the final pS13/pS16 product.

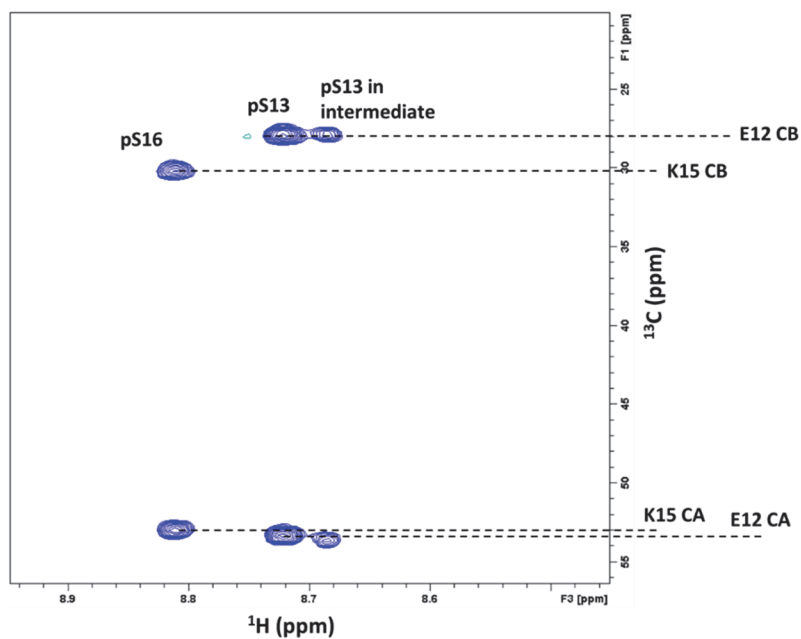


Figure III-17.  $^1\text{H}$ ,  $^{13}\text{C}$  plane of a CBCA(CO)NH spectrum collected after 21 hours of reaction between Httex1-23Q and TBK1.

The  $^{15}\text{N}$  frequency was not evolved, allowing an experimental acquisition time of 20 minutes to minimize changes occurring while the spectrum was acquired. The  $^{13}\text{C}$  chemical shifts of the residues preceding Ser13 and Ser16 are shown to support that the phosphorylation intermediate corresponds to Ser13, especially given the clear distinction between Glu12 and Lys15 CB shifts.

Table III-2. H, N,CA,CB assignments for human Httex1 unmodified and pS13pS16 in our working conditions, pH 7, 25 °C

Unmodified Htt exon 1						pS13pS16 Htt exon 1					
AA	No.	H	N	CA	CB	AA	No.	H	N	CA	CB
Thr	3			59.16	67.02	Thr	3			59.16	67.02
Leu	4	8.41	124.6	52.82	39.3	Leu	4	8.38	125.2	52.82	39.3
Glu	5	8.36	121.7	54.56	27.36	Glu	5	8.34	122.1	54.04	27.36
Lys	6			54.06	29.89	Lys	6	8.2	122.1	53.59	30.07
Leu	7	8.06	122.3	52.76	39.38	Leu	7	8.12	123.1	52.43	39.38
Met	8			52.63	29.85	Met	8	8.22	121.2	52.44	29.86
Lys	9	8.09	121.7	54.02	30.36	Lys	9	8.12	122.7	53.4	30.36
Ala	10	8.07	123.9	50.34	16.34	Ala	10	8.24	125.1	49.91	16.34
Phe	11	8.03	118.6	55.8	36.85	Phe	11	7.94	118	54.72	36.85
Glu	12	8.12	121.4	54.49	27.28	Glu	12	8.12	122.1	53.4	27.92
Ser	13	8.08	115.8	56.21	60.84	pSer	13	8.73	118.6	54.99	63.02
Leu	14	8.03	123.5	53.22	39.35	Leu	14	8.35	124.1	52.57	39.35
Lys	15	8.06	120.6	54.39	30.11	Lys	15	8.22	122.5	53.13	30.11
Ser	16	8.07	115.5	56.75	60.76	pSer	16	8.83	117.9	55.79	62.52
Phe	17	8.12	122.1	56.52	36.37	Phe	17	8.24	121.7	56.52	36.37
Gln	18	8.2	120	53.94	26.13	Gln	18	8.05	120.8	53.94	26.13
Gln	19	8.11	119.9	54.3	25.93	Gln	19	8.07	120.3	54.3	25.93
Gln	38			53.23	26.62	Gln	38			53.23	26.62
Gln	39	8.36	121.4	52.98	26.83	Gln	39	8.36	121.4	52.98	26.83
Gln	40	8.37	122.8	50.84	26.07	Gln	40	8.37	122.9	50.84	26.07
				60.16	29.18						
Gln	52	8.32	120.2	52.63	26.89	Gln	52			52.68	26.87
Leu	53	8.28	125.3	50.21	38.69	Leu	53	8.28	125.3	50.21	38.69
Pro	58			60.25	29.14	Pro	58			60.25	29.14
Gln	59	8.34	120.3	53.09	26.75	Gln	59	8.34	120.3	53.09	26.75
Ala	60	8.29	125.6	49.57	16.36	Ala	60	8.29	125.6	49.57	16.36
Pro	62			60.39	29.27	Pro	62			60.39	29.27
Leu	63	8.23	122.2	52.18	39.44	Leu	63	8.23	122.2	52.18	39.44
Leu	64	8.11	124.5	49.85	38.68	Leu	64	8.11	124.6	49.85	38.68
Pro	65			60.12	29.3	Pro	65			60.12	29.3
Gln	66	8.4	121.6	50.53	26.11	Gln	66	8.4	121.6	50.53	26.11
Pro	78			60.23	29.26	Pro	78			60.42	29.26
Gly	79	8.13	108.7	41.55		Gly	79	8.13	108.8	41.55	
Pro	80			60.01	29.28	Pro	80			60.39	29.28
Ala	81	8.31	124.2	49.54	16.37	Ala	81	8.31	124.2	49.54	16.37
Val	82	8.02	119.7	59.27	30.01	Val	82	8.02	119.7	59.27	30.01

Ala	83	8.29	127.8	49.47	16.34	Ala	83	8.28	127.9	49.47	16.34
Glu	84			53.36	27.7	Glu	84	8.34	123.9	53.36	27.7
Glu	85	8.34	123.9	51.49	26.96	Glu	85			51.49	26.96
Pro	86			60.37	29.18	Pro	86			60.37	29.18
Leu	87	8.19	121.6	52.47	39.58	Leu	87	8.18	121.5	52.47	39.58
His	88	8.15	120.2	53.06	27.86	His	88	8.22	119.9	52.41	27.39
Arg	89	8.13	124.9	50.91	27.3	Arg	89	8.2	124.9	50.91	27.64

## III.4 Conclusions

We have described here the first method for enzymatic generation of site-specifically phosphorylated WT and mutant Httex1 proteins. This was enabled by 1) the discovery and validation of novel kinases that efficiently phosphorylate Httex1 at S13 and S16 (TBK1 [374]), T3 (GCK) or T3 and S13 (TNIK and HGK); 2) developing conditions that allow performing *in vitro* phosphorylation reactions on mutant HTT under conditions where the protein is stable and remains soluble (SUMO-fusion proteins); and 3) developing efficient methods for the cleavage and purification of the final phosphorylated proteins. The use of the newly discovered kinases combined with the use of the SUMO fusion protein expression and purification method for producing recombinant Httex1 allowed the production of milligram quantities of site-specifically phosphorylated Httex1 proteins.

As a proof of concept, we used GCK- and TBK1-mediated phosphorylation protocols to produce unmodified or site-specific fluorescently labeled WT and mutant Httex1 phosphorylated at T3 or S13/S16. This approach could replace existing strategies based on the use of large fusion fluorescent proteins or the nonspecific introduction of fluorescent dyes onto lysine residues. In addition, we showed that our new method also addresses previous challenges associated with the generation of site-specifically phosphorylated and isotopically labeled mutant Httex1 proteins for structural studies by solution and solid-state NMR [376, 377]. Previous NMR studies have focused primarily only on investigating the structure of unmodified monomeric [383] and fibrillar [377] Httex1 proteins. Herein, we developed an optimized expression protocol for Httex1 in minimal media, which significantly reduces non-desired cleavages, thus enhancing the yield of recombinant isotopically labeled untagged, native or phosphorylated Httex1 suitable for NMR studies (Figure III.13). We showed that phosphorylation of the unmodified protein could be easily monitored by NMR spectroscopy with high structural and time resolution (Figure III.16). We also demonstrated that pT3 pS13/pS16 Httex1 remains largely disordered, with a gradient of helical propensity that starts around the first glutamine residues of the polyglutamine tract and gradually fades downstream, as in the unmodified protein. Our preliminary studies show that phosphorylation affects the chemical shifts of the target residues and their neighboring residues but mostly through electrostatic effects on the chemical shifts themselves and without any substantial effect on either the structure or dynamics. In particular, the last glutamine residues of the polyQ tract and all downstream residues through to the end of Httex1 appear to be insensitive to phosphorylation. We note that a recent, very detailed work on a minimal unmodified Nt-Q7 peptide by the Clore group [229] proposed a bifurcated assembly mechanism of aggregation, where the monomeric species (observable by NMR and initially representing > 98% of the sample) either self-associates to form a productive dimer that further oligomerizes or exchanges with a nonproductive dimer that does not oligomerize further. If the PTMs

alter the distribution of productive and non-productive dimers in this equilibrium, they could alter aggregation rates without producing strong effects on the bulk NMR features. Our modification protocols enable more detailed studies of this issue through NMR techniques sensitive to the minor populations. Furthermore, we establish for the first time that phosphorylation at S13 could prime phosphorylation at neighboring S16, thus underscoring the importance of further studies to investigate cross-talk between different Nt17 PTMs.

This new method described here eliminates the need to use phosphomimetic mutations at these residues and addresses many of the limitations of existing protein semisynthetic strategies for producing these proteins, including the requirement to introduce a nonnative residues at residue 18 (Q18A) [395]. Furthermore, unlike protein semisynthesis, this method is affordable, accessible, and enables the generation of milligram quantities of highly pure phosphorylated proteins. Finally, the high solubility of the SUMO-Httex1 fusion protein enables greater flexibility to handle and manipulate the protein, thus facilitating the introduction of PTMs and chemical functional groups or probes (e.g., a fluorescent dye, biotin) into mutant Httex1, which was not feasible in the absence or after removal of the SUMO tag.

We believe that these advances will open new opportunities and expand the experimental approaches aimed at elucidating the role of PTMs in regulating HTT structure, aggregation, pathology formation, and cell-to-cell propagation (Figure III.18). Moreover, the method described here can be extended to other PTMs, such as ubiquitination, SUMOylation, and acetylation, once the enzymes involved in regulating these modifications are identified. Finally, the ability to generate homogeneously modified proteins should facilitate the development of novel assays to quantify the levels of Nt17 modified forms of HTT in biological samples and assess their potential as biomarkers for early diagnosis or to monitor HD progression.



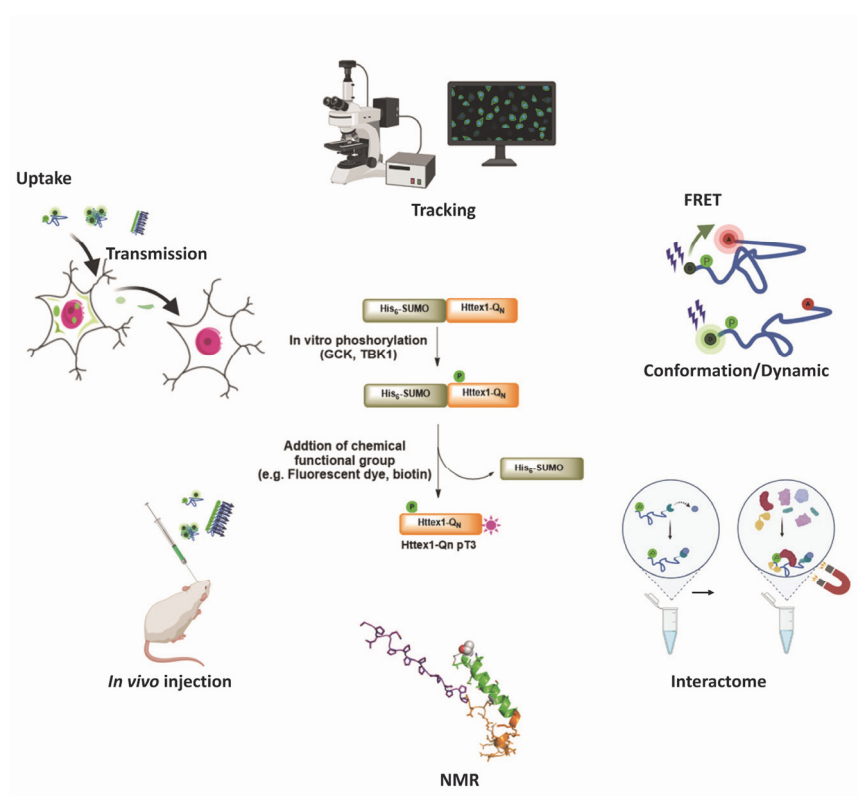


Figure III-18. Library of tools presented in this paper.

The tools presented in this paper offer new opportunities and enlarge the range of potential methods and experimental approaches that can be used to study the mechanisms by which the Nt17 phosphorylation influences the properties and functions of Httex1 in health and disease. (NMR depiction is adapted from [383]).

## III.5 Experimental Section

### III.5.1 Materials

The pTWIN1 vector, containing human Httex1 fused to His<sub>6</sub>-SUMO, was ordered from GeneArt Gene Synthesis (Regensburg-DE). *E. coli* B ER2566 was from New England Biolabs (Ipswich-USA). Ampicillin, DTT, isopropyl β-D-1-thiogalactopyranoside (IPTG), and PMSF were obtained from AppliChem. Imidazole, cOmplete Protease Inhibitor Cocktail, magnesium chloride (MgCl<sub>2</sub>), magnesium sulfate (MgSO<sub>4</sub>), and trifluoroacetic acid were purchased from Sigma-Aldrich Chemie GmbH, (Buchs-CH). EGTA solution was from Boston Bioproducts (Chestnut-USA). Mg-ATP was from Cayman chemical (Ann Arbor-USA). EDTA was from Fisher Scientific (Ecublens-CH), and Luria Broth (Miller's LB Broth) was from Chemie Brunschwig (Basel-CH). HPLC-grade acetonitrile was from Macherey-Nagel (Oensingen-CH). The spectrophotometer semimicro cuvette was from Reactolab (Servion-CH). The C4 HPLC column was from Phenomenex (Basel-CH). The HisPrep 16/10 column was from GE healthcare (Dietikon-CH). Purified recombinant TBK1 (0.62 mg/μl, cat. # NM\_013254) and GSK kinases (0.5 mg/μl, cat. # BC047865), from MRC PPU Reagents and service, Dundee-SCO, were stored at -80°C. The purity, the purification method, and the test activity result as well as the specific activity of TBK1

and GCK are provided by the vender in the flowing links: GCK (<https://mrcppureagents.dundee.ac.uk/view-protein-pdf/585524>) and TBK1 (<https://mrcppureagents.dundee.ac.uk/view-protein-pdf/585643>). Rabbit antibodies against pT3, pS13, and pS16 were homemade.

### III.5.2 Instruments

A Vibra-cell VCX130 ultrasonic liquid processor (Sonics), an Äkta 900 equipped with a fraction collector (GE Healthcare), and Waters UPLC and HPLC systems were used. For ESI-MS, a Finnigan LTQ (Thermo Fisher Scientific) was employed. A lyophilizer instrument (FreeZone 2.5 Plus) and a shaking incubator with a temperature regulator (Infors HT multitron Standard) were also used in the experiments.

### III.5.3 Kinase screening (IKPT service)

Kinase screening (IKPT service) was performed by Kinexus, Canada. Httex1-23Q at 1.4  $\mu$ M and WT Nt17 peptide (ATLEKLMKAFESLKSF) at 150  $\mu$ M was screened against a panel of 298 selected Ser/Thr kinases using a radiometric assay method with [ $\gamma$ - $^{33}$ P] ^ATP. The assay was initiated by the addition of [ $\gamma$ 33P] ATP and the reaction mixture incubated at ambient temperature for 30 minutes. After the incubation period, the assay was terminated by spotting 10  $\mu$ l of the reaction mixture onto a multiscreen phosphocellulose P81 plate. The multiscreen phosphocellulose P81 plate was washed 3 times for approximately 15 minutes each in a 1% phosphoric acid solution. The radioactivity on the P81 plate was counted in the presence of scintillation fluid in a Trilux scintillation counter.

### III.5.4 Expression of His6-SUMO-Httex1-Qn (n= 23 or 43)

The expression of His-SUMO-Httex1-Qn was performed as previously reported [238]. A pTWIN1 plasmid containing SUMO-Httex1-Qn with ampicillin (Amp) resistance was transformed into *E. coli* ER2566 using the heat shock method [396], and then the transformed bacteria were plated in an agar plate with ampicillin resistance. Next, a single colony was inoculated in a culture flask with 400 ml of LB+Amp (100  $\mu$ g/ml) medium and incubated with shaking (190 rpm) at 37°C overnight (preculture). Large expression of the protein (12 L) started the day after, at an optical density (OD<sub>600</sub>) of 0.15 was observed in multiple 5 L flasks (3 L of culture maximum per flask). When the OD<sub>600</sub> reached 0.5 to 0.6, the expression of HIS-SUMO-Httex1-Qn was induced with IPTG at a final concentration of 0.4 mM, and the culture was incubated at 18°C for 18 hours (overnight). The cells were harvested by centrifugation (3993  $\times$  g, 4°C, 10 min), and the cell pellet was kept on ice for further purification.

### III.5.5 Expression of His6-SUMO-Httex1-Qn (n= 23 or 43) in minimal isotopic media

The transformation of the plasmid and the preculture were performed, as mentioned above in LB+Amp media. Then, a large culture was grown first in LB+Amp media as similarly described to an OD<sub>600</sub> of 0.15. When the OD<sub>600</sub> reached 0.3, the cells were centrifuged (3993 × g, 4°C, 10 min) and resuspended in minimal media containing <sup>15</sup>N-labeled ammonium chloride and <sup>13</sup>C-labeled glucose for the production of <sup>13</sup>C/<sup>15</sup>N-labeled His-SUMO-Httex1-Qn. Then, the culture was induced at an OD less than 0.6 and incubated overnight at 18°C. The cells were harvested by centrifugation (3993 × g, 4°C, 10 min), and the cell pellet was kept on ice for immediate purification.

### III.5.6 Immobilized metal affinity chromatography (IMAC) purification

The bacterial pellet was resuspended in IMAC buffer A (50 mM Tris, 500 mM NaCl, 30 mM imidazole, pH 7.5, filtered through a 0.65 µm filter) supplemented with PMSF and complete protease inhibitors and then sonicated on ice for cell lysis (70% amplitude, total sonication time of 5 min, intervals of 30 seconds of sonication followed by a 30 seconds pause). The cell lysate was centrifuged (39191 × g, 4°C, 60 min), and the supernatant was filtered (0.45 µm, syringe filters) and loaded onto the Ni-NTA column on fast-performance liquid chromatography (FPLC) system at 4°C. The protein was then eluted with 100% IMAC buffer B (50 mM Tris, 500 mM NaCl, 500 mM imidazole, pH 7.5, filtered through a 0.65 µm filter). Coomassie SDS-PAGE was used to analyze the eluted fractions, and the fractions containing SUMO-Httex1-Qn were pooled together and kept on ice for subsequent phosphorylation.

### III.5.7 Quantitative *in vitro* phosphorylation of SUMO-Httex1-Qn by GCK and TBK1

SUMO-Httex1-Qn after IMAC purification was dialyzed against 4 L of TBS buffer overnight at 4°C, and its concentration was measured using a nanodrop UV spectrophotometer. The concentration was calculated by measuring the absorbance of the dialyzed or desalted protein solution at 280 nm, where the extinction coefficient was 1490 M<sup>-1</sup> cm<sup>-1</sup>. Ten milligrams of the fusion protein were removed, and the volume was adjusted to 18 mL. Then, 2 mL of 10X phosphorylation buffer (250 mM MgCl<sub>2</sub>, 80 mM EGTA, 40 mM EDTA, 10 mM DTT) was added. The pH of the mixture was adjusted to 7.4, and Mg-ATP was added at a final concentration of 5 mM. Finally, GCK or TBK1 was added at a ratio of 1:30 w/w to Httex1-Qn (666 µL in the case of GCK and 537 µL in the case of TBK1), and the enzymatic reaction was incubated at 30°C overnight (17 hours). To determine the completion of phosphorylation, 30 µL was removed and supplemented with 1 µL of ULP1 (1 mg/mL) to cleave the SUMO tag for analytical analysis. Ten microliters were injected for analysis by LC-ESI-MS (positive ionization mode). When the ESI/MS confirmed complete phosphorylation, the reaction solution was kept on ice for further processing.

### III.5.8 SUMO cleavage and HPLC purification

To cleave the SUMO tag from Httex1-Qn, 0.6 mL of ULP1 enzyme was added to the phosphorylation reaction mixture and incubated on ice for 15 min. Once UPLC confirmed SUMO cleavage, phosphorylated Httex1-Qn was purified by HPLC on a C4 column using a gradient of 25%-35% solvent B (HPLC-grade acetonitrile containing 0.1% v/v TFA) in solvent A (ultrapure water containing 0.1% v/v TFA). Collected fractions were analyzed for the presence of the desired protein by ESI/MS and pooled accordingly for lyophilization. The purity of the lyophilized protein was assessed by ESI/MS (ESI/MS spectra were deconvoluted with MagTran software), UPLC, and SDS-PAGE.

### III.5.9 Fluorescent labeling with Atto-565-maleimide

One milligram of phosphorylated Httex1-Qn P90C was disaggregated using neat TFA, as described by Reif et al. [238]. Then, the thin protein film was resuspended in 100 mM Tris, pH 7.4, 6 M GdHCl, 50 mM trehalose, 0.5 M proline, and 1.1 equivalents of TCEP [382], and the pH was adjusted to 7.4. Then, 1.5 equivalents of the fluorescent dye Atto-565-maleimide was added to the protein, and the reaction was kept on ice for 30 min. The reaction was monitored by ESI/MS, and upon completion, excess Atto-565-maleimide was removed using a PD10 column equilibrated with 20% acetonitrile in water. The protein was immediately injected onto a C4 300 Å 250 × 4.6 mm column. The protein was eluted using a gradient of 25 to 55% solvent B over 50 min. The collected fractions were analyzed by ESI/MS for the presence of the proteins of interest, and the corresponding fractions were pooled according to the different qualities. The final purity of the protein was determined by UPLC and ESI/MS.

### III.5.10 Nuclear magnetic resonance (NMR) spectroscopy

All NMR experiments were carried out in a Bruker Avance III 800 MHz spectrometer equipped with a CPTC cryoprobe. Spectra for protein analysis and resonance assignments were collected at 25°C on protein samples with approximately 100 µM concentrations, while spectra for monitoring phosphorylation kinetics were collected on 200 µM protein samples to achieve strong sensitivity in short acquisition times and at 20°C to slow the kinetics. Samples for phosphorylation kinetics were prepared in 30 mM HEPES, 5 mM MgCl<sub>2</sub>, 5 mM EGTA, 1 mM DTT, and 5 mM Mg-ATP with 10% D<sub>2</sub>O at pH 7.2 adjusted after the addition of ATP and prior to the addition of 15 µg of TBK1. All other samples were prepared in 10 mM Na<sub>2</sub>HPO<sub>4</sub> and 10% D<sub>2</sub>O buffer at pH 7. All spectra were acquired and processed using Bruker TopSpin 4.0 and analyzed with CARA and Sparky-NMRFAM.

HSQC spectra for monitoring the phosphorylation kinetics were acquired using a sensitivity-enhanced sequence with 2 scans, a short recycle delay of 0.5 seconds and 128  $^{15}\text{N}$  increments, (processed with 256 indirect points), a combination that in our hands resulted in high resolution, excellent intensity and no distortions in 2 min and 50 seconds of total acquisition time, which is relatively short compared to the phosphorylation rate in the set conditions. Resonance assignments for the unmodified and pS13pS16 proteins were obtained by analyzing a high-resolution HSQC experiment (sensitivity enhanced, 256 indirect points, 1 second recycle delay) and standard triple-resonance experiments: HNCO, HN(CA)CO, HNCA, HN(CO)CA, CBCA(CO)NH and HNCACB. All 3D experiments were acquired using standard pulse sequences, with 40 increments in  $^{15}\text{N}$ , 128 increments in the  $^{13}\text{C}$  dimensions, 1 second of recycle delay, and nonuniform sampling (NUS) at 50% for HNCACB or 25% for the other five spectra. Resonance assignments were aided by previously published assignments of Httex1[192, 193, 384].

The chemical shift perturbations in  $^1\text{H}$  and  $^{15}\text{N}$  between the unmodified and pS13pS16 proteins were computed as:

where  $\Delta\delta\text{H}$  is the difference in  $^1\text{H}$  chemical shifts and  $\Delta\delta\text{N}$  is the difference in  $^{15}\text{N}$  chemical shifts, and the factor 5 corresponds to the value widely used to weigh down the  $^{15}\text{N}$  shifts.

Secondary structure propensities from the  $^{13}\text{C}$  chemical shifts ( $\Delta\text{CA} - \Delta\text{CB}$ ) were obtained by subtracting the random coiled CA and CB chemical shifts of the amino acids from the experimentally observed CA and CB shifts and then subtracting the two differences. This indicator is insensitive to offsets or calibration problems in the  $^{13}\text{C}$  dimension; a positive value above +1 indicates alpha helical propensity, and a negative value under -1 indicates beta sheet propensity. For phosphorylated serine, the CA and CB chemical shifts reported by [391] were used as random coil references; for the other amino acids, we used the random coil shifts from [397].

### III.5.11 Coexpression of Httex1-16Q-eGFP and kinases in HEK 293 cells

HEK 293 cells were cultured in 95% air and 5%  $\text{CO}_2$  in Dulbecco's modified Eagle's medium (Gibco) supplemented with 10% fetal bovine serum (Gibco) and penicillin-streptomycin (Thermo Fisher). Plasmids GCK (MSP4K2) (cat. no. RC200472, OriGene), HGK (MAP4K4) (cat. no. RC215163, OriGene), and TNIK (Plasmid #45276 Addgene) were acquired. Transfections were carried out by Lipofectamine 2000 according to the manufacturer's protocol. Lysis was performed in RIPA lysis buffer (150 mM sodium chloride, Triton X-100, 0.5% sodium deoxycholate, 0.1% SDS (sodium dodecyl sulfate), 50 mM Tris, pH 8.0) supplemented with 1 $\times$  protease and phosphatase inhibitor 2, 3 mixture (Sigma). Cell lysates were then centrifuged at 15000 $\times$ g for

20 min, and the supernatant was collected as the soluble fraction. The protein concentration was measured using the BCA system, and approximately 20-60 µg of protein was processed for the WB assay. Antibodies used for western blotting were pT3-Huntingtin CHDI-90001528-2 from CHDI/Thermo Scientific, pS13 Huntingtin CHDI-90001039-1 from CHDI/Thermo Scientific, pS16-Huntingtin in-house generated, and GAPDH/14C10) 2118S from Cell Signaling.

### III.6 Acknowledgements

This work was supported by funding from CHDI (R01NS086452). We are grateful to Rajasekhar Kolla for critical review of the manuscript and Nour Chiki-Benmrad for technical assistant during her semester project. We thank the MRC PPU Reagents and Services facility (MRC I PPU, College of Life Sciences, University of Dundee, Scotland, [mrccpureagents.dundee.ac.uk](http://mrccpureagents.dundee.ac.uk)) for providing TBK1 and GCK kinases on a cost-recovery basis.

## IV. Chapter IV: Elucidating the role of cross-talk between N-terminal methionine oxidation and neighbouring post-translation modifications in regulating the conformation of Nt17 and Httex1 aggregation using an integrative experimental and molecular simulation approaches.

This chapter is part of a manuscript in preparation for invited submission in *Biomolecules (special issue : Computational Perspectives on Intrinsic Disorder-Based Functionality)* with the following authors:

Anass Chiki <sup>[a]‡</sup>, Zhidian Zhang <sup>[a][b]‡</sup>, Luciano A. Abriata <sup>[b]</sup>, Kolla Rajasekhar <sup>[a]</sup>, Lucien Krapp <sup>[b]</sup>,

Driss Boudeffa <sup>[a]</sup>, Matteo Dal Peraro <sup>[b]\*</sup>, and Hilal A. Lashuel <sup>[a]\*</sup>

‡ These authors contributed equally to this work

[a] Laboratory of Molecular and Chemical Biology of Neurodegeneration, School of Life Sciences, Brain Mind Institute, Ecole Polytechnique Fédérale de Lausanne (EPFL), CH-1015 Lausanne, Switzerland

[b] Laboratory for Biomolecular Modeling, Ecole Polytechnique Fédérale de Lausanne (EPFL), CH-1015 Lausanne, Switzerland

\*To whom correspondence should be addressed

**Authors contributions:** A. Chiki, Z. Zhang, L.A. Abriata, M. Dal pararo and H.A Lashuel designed the experiment and wrote the paper. M. Dal pararo and H.A. Lashuel coordinated and supervised the study. A. Chiki conducted and analyzed the vitro experimental part. Z. Zhang conducted and analyzed computational part. L.A. Abriata conducted and analyed the NMR part. K. Rajasekhar and D. Boudeffa performed experiments replications. L. Krapp help with the computation simulation. M. Dal pararo and H.A. Lashuel acquired the funding for this work.

## IV.1 Introduction

Huntington's disease (HD) is a fatal and autosomal neurodegenerative disease characterized by motor [5, 29] and cognitive declines [359], as well as psychiatric symptoms [66]. HD is caused by a mutation in the huntingtin gene (*HTT*), resulting in an expansion in the CAG repeat within its first exon [6, 362], which is then translated into extended polyglutamine (polyQ) repeat in the huntingtin protein (Htt) [363]. HD occurs when the length of the polyQ repeat is higher than the critical threshold of  $\geq 36$  [364]. At the neuropathological level, HD is characterized by neuronal degeneration in the striatum and the cortex [398, 399], and the formation and accumulation of nuclear inclusions are composed of mutant Htt aggregates and other proteins [21, 400]. Several studies have shown that these aggregates are composed of fibrillar and potentially oligomeric species derived from N-terminal fragments containing expanded polyQ repeats. One of the major N-terminal fragments found in these inclusions represents an N-terminal fragment that corresponds to exon1 of the Htt protein (Httex1) [147, 148]. Overexpression of mutant Httex1 alone with polyQ length ranging from 80 to 175, in different animal and cellular models, reproduces many aspects of HD pathology, including the formation of huntingtin inclusions [146, 155, 172, 173].

Although increasing evidence suggests that mutant Htt aggregation and toxicity play central roles in the pathogenesis of HD, the molecular events responsible for triggering mutant Htt aggregation, the nature of the toxic species, and the mechanisms by which they cause neurodegeneration remain unknown. Initial efforts focused on disentangling the relationship between Htt aggregation and toxicity and HD have focused on trying to identify modifiers of Htt aggregation based on targeting the polyQ repeat domain, which has been shown to be the primary sequence responsible for initiating Htt aggregation. However, recent studies suggest that post-translation modifications (PTMs) in close proximity or far from the polyQ domain have the potential to modify not only mutant Htt levels and functions but also its aggregation and toxicity [108, 282, 284, 286, 290, 305, 307, 321]. Interestingly, several of these PTMs occur within the first N-terminal 17 amino acids of Htt, which are directly flanked by the polyQ domain (Figure VI.1.1-A). These modifications include phosphorylation at multiple serine and threonine residues (T3, S13 and S16), and acetylation, ubiquitination, and SUMOylation at selected lysine residues (K6, K9, K15) (Figure VI.1.1-A). Mutating both S13 and S16 to aspartate to mimic the phosphorylation was shown to reverse the pathology of mutant Htt in an HD mouse model [209] and modulate Htt aggregation in different cellular models ) [146, 155, 172, 173]. Recently, we showed that phosphorylation at T3, S13 and/or S16 inhibited the aggregation of WT and mutant Httex1 *in vitro* [329, 382]. Furthermore, TBK1-mediated phosphorylation of mutant Httex1 at S13 and S16 lowers its levels and results in a significant reduction in Httex1 aggregation and inclusion formation in different cellular models and a *C. elegans* model of HD [401]. These findings, combined with our observation that the levels of pT3 are



decreased in pathological conditions [308], suggest that phosphorylation within the Nt17 domain protects against mutant Htt aggregation. Similarly, SUMOylation at multiple N-terminal lysine residues inhibits Httex1 aggregation *in vitro* [306]. Interestingly, although lysine acetylation at K6, K9 or K15 does not significantly alter the aggregation profile of Httex1 [382], acetylation at K6 was shown to significantly modify the aggregation inhibitory effects of phosphorylation at T3 [382]. Similarly, phosphorylation of S13 and S16 was shown to regulate Httex1 acetylation at K9 [282], and ubiquitination/SUMOylation at K6 and K9 [282, 321]. Finally, competing modifications, such as Ubiquitination and SUMOylation, were shown to exert different effects on Htt levels and degradation [284]. Together, these findings, combined with the fact that multiple reversible PTMs cluster within 10 amino acids in Nt17 suggest that many of these modifications act in concert rather than individually and that the Htt PTM code involves cross-talk between different PTMs, in particular, those that exist in close proximity to each other.

One PTM that remains unstudied and its effect on mutant Htt aggregation remains unknown is the oxidation of methionine 8 (oxM8). Methionine eight is highly conserved [323] and the levels of M8 oxidation were shown to be higher in R6/2 HD mouse model [325]. However, the absence of immunochemical methods to detect Methionine 8 oxidation have precluded studies aimed at understanding its relevance and potential roles in HD brain. Despite this, methionine oxidation is one of the most common modifications that occur under oxidative stress, which has been linked to the pathogenesis of HD [402] and other neurodegenerative diseases. Elevated levels of oxidative stress markers, as well as reactive oxygen species (ROS), were found in HD patient blood [403] and *postmortem* brains of HD patients [404]. Although there is no direct evidence establishing that methionine 8 is oxidized, several studies have suggested that this could occur under oxidative stress conditions and that M8 oxidation could act as a sensor of ROS to regulate HTT phosphorylation and localization [323, 324]. Given that this residue is located in the middle of Nt17 and is flanked by most of the Nt17 PTMs, it was suspected that M8 oxidation could influence the structure of Nt17 and HTT aggregation. Mitomi and colleagues [325] showed, using H<sub>2</sub>O<sub>2</sub> *in vitro*, that oxidation at M8 occurs only post-aggregation on non-soluble forms of mutant Httex1. Recent studies based on quantitative NMR showed that TiO<sub>2</sub> nanoparticles induced M8 oxidation and abolished the aggregation of a model peptide of Httex1 and reduces the binding of the model peptide to lipids micelles [326]. However, most of these studies were carried out either using Nt17 peptides, GST-tagged Httex1 protein [325], or a model peptide consisting of only the Nt17 linked to 7 or 10 polyQ which lack the proline-rich domain and most the C-terminal domain of Httex1 [326]. Additionally, H<sub>2</sub>O<sub>2</sub> was not removed from the solution during the experiments, which represent a harsh condition with extended incubation time and might affect other residues within the sequence such as histidine or phenylalanine [405] and by consequence the structure of Httex1.

Herein we propose an integrative approach combining both biophysical and computational studies in order to gain insight into the structural basis underlying the effects of Nt17 PTMs on the structure and aggregation of mutant Httex1. Given the location of M8 in the middle of all Nt17 PTMs and the reversible nature of this modification, we postulated that oxM8 could influence the effects of other Nt17 PTMs. To test this hypothesis, we investigated the potential cross-talk between M8 oxidation and selected Nt17 PTMs by assessing how the presence of different combinations of PTMs influences the structural properties of Nt17 and mutant Httex1 aggregation. For more comprehensive analysis and to gain insight into the structural consequences of M8 oxidation and its cross-talk with other Nt17 PTMs, we performed atomistic simulations focusing on how these different combinations of Nt17 PTMs influence Nt17 structure and helicity. To validate this approach, we performed preliminary NMR studies to assess the effect of M8 oxidation alone or combined with S13/S16 phosphorylation on the Httex1 structure. Our findings provide new insight into the PTM code of Nt17 and highlight the promise, potential and challenges associated with developing approaches that integrate atomistic molecular simulations and experimental data on post-translationally modified peptides and proteins.

## IV.2 Results

### IV.2.1 Production of oxidized mutant Httex1 proteins

Httex1 contains two Methionine residues within its Nt17 domain. The N-terminal Methionine is cleaved by aminopeptidase resulting in N-terminally acetylated alanine as the first residue [316]. This means that once expressed, Httex1 contains only a single methionine residue at position 8 (M8). Investigating the biological role of M8 oxidation is more challenging than other Nt17 PTMs such as phosphorylation, because there are no natural amino acids that mimic methionine oxidation and factors that are known to induce protein oxidation, such as oxidative stress, are not always chemoselective. Furthermore, it is not always possible to assess the extent of Methionine oxidation under cellular conditions, e.g., oxidative stress, that is known to induce M8 oxidation. Therefore, to investigate the effect of M8 oxidation on Httex1 aggregation, we sought to prepare mutant Httex1 proteins that are homogeneously oxidized at M8. Several protocols have been used to oxidize methionine residues in proteins *in vitro*, including treatment with hydrogen peroxide (H<sub>2</sub>O<sub>2</sub>), transition metal ions, 2,2-azobis(2-amidinopropane) dihydrochloride (AAPH), tert-butyl hydroperoxide (t-BHP), or UV exposure [406-409].

In the context of Httex1, previous studies have shown that treatment with H<sub>2</sub>O<sub>2</sub> allows for efficient oxidation of M8 within a GST-Httex1 fusion protein [325], the Nt17 [323] or Httex1 model peptide consisting of only

the Nt17 domain with ten additional glutamine restudies (Nt17Q10) [326]. Some of the limitations of these studies are 1) none of the used proteins represent the native sequence of Httex1; 2) the extent of M8 oxidation was not always assessed by mass spectrometry or other methods to determine if it was complete or the chemical homogeneity of the Httex1 peptides; and 3) the structural or aggregation properties of the protein and peptide models was assessed in the presence of the oxidizing agent,  $H_2O_2$ . It is known that such incubation of proteins under such harsh conditions for an extended time might affect other residues within the sequence such as histidine or phenylalanine [405], which could alter the sequence and biophysical properties of Httex1.

To overcome these limitations, we sought to develop a strategy for the production of native mutant Httex1 site-specifically oxidized at M8 (oxM8). We took advantage of recent advances from our lab that allows for the generation of mg quantities of highly pure mutant Httex1 fused to the SUMO protein [238], which enhances the solubility of mutant Httex1 (Figure VI.1-B). The desired PTMs (oxidation or phosphorylation) are introduced into Nt17 of the fusion protein followed by removal of the SUMO protein and purification of the modified mutant Httex1 by RP-HPLC [410].

Mutant Httex1, with 43 glutamine residues (mHttex1) fused to a SUMO tag protein at its terminal (SUMO-mHttex1) was expressed and purified as previously described (Figure VI.2-A) [238]. Next, the fusion protein was subjected to oxidation using 400 mM of hydrogen peroxide ( $H_2O_2$ ) in 50mM Tris, 500mM NaCl 500 mM Imidazole, pH 7.5. The oxidation reaction was monitored over time by ESI/MS (Figure VI.2-C). For each time point, an analytical cleavage of the SUMO tag using the ULP1 enzyme was performed, and the resulting cleaved product was analyzed by ESI/MS. As shown in Figure VI.2-C, the M8 residue was completely oxidized after 2 hours of incubation with  $H_2O_2$ . The oxidized SUMO-mHttex1 was then subjected to ULP1 cleavage. Upon verifying the complete removal of the SUMO tag was verified, m-Httex1-oxM8 was immediately purified by reverse phase HPLC (RP-HPLC) purification (Figure VI.2-E). The fractions containing the protein of interest were pooled together and lyophilized. The final purity of the mHttex1-oxM8 was verified by ESI/MS, UPLC, and SDS-PAGE (Figure VI.1-D).

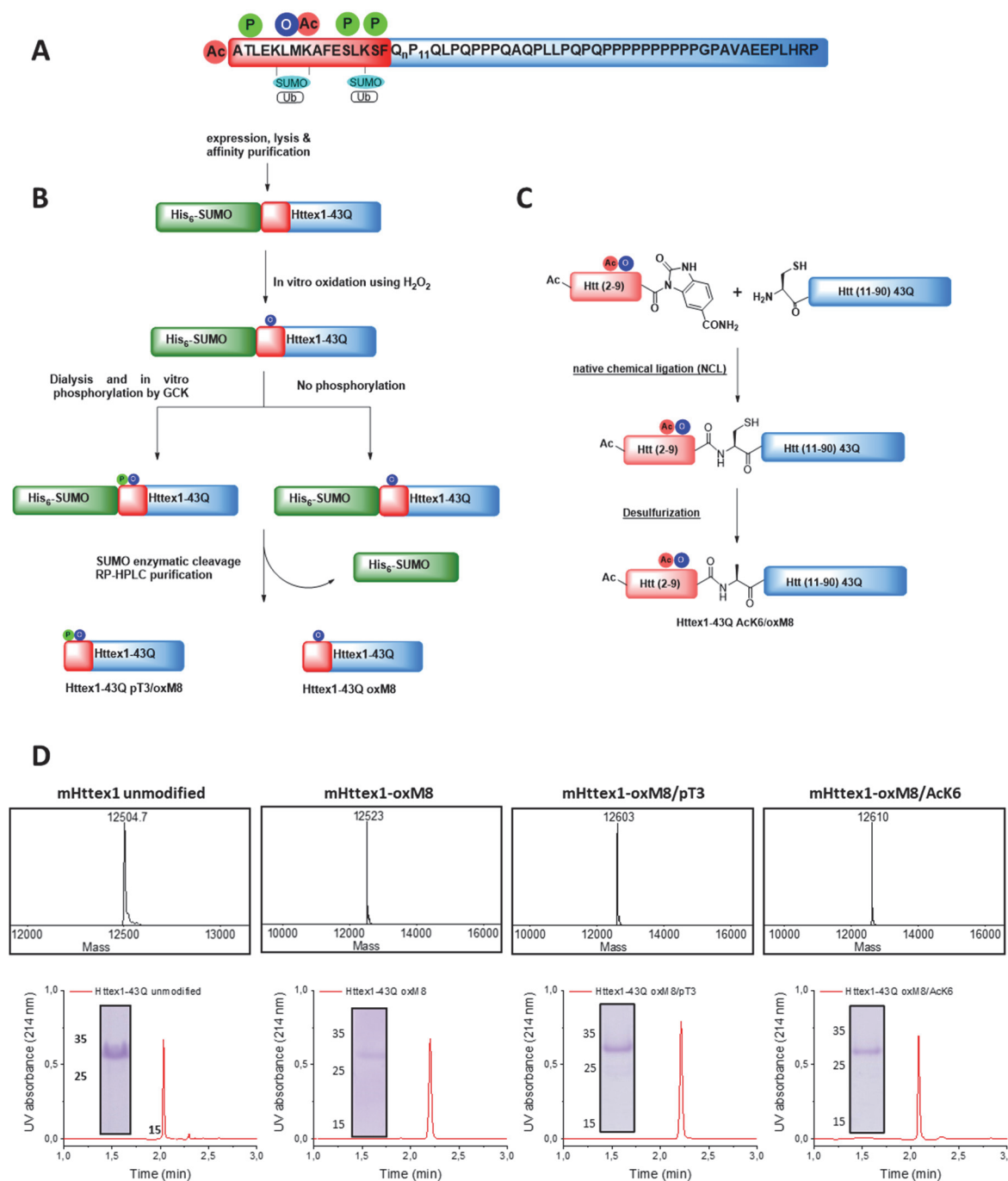


Figure IV-1. Chemical, semisynthesis and enzymatic methods for the generation of mHttex1 with single or multiple PTMs.

(A) Schematic presentation of Httex1 sequence highlighting the cluster of PTMs in the Nt17 domain. (B) Schematic presentation of the SUMO-based strategy used for the production of mHttex1-oxM8 and mHttex1 oxM8/pT3. The SUMO-mHttex1 was produced and purified by Nickel IMAC purification and subsequently oxidized or both oxidized and phosphorylated by GCK. Next, the SUMO tag was removed by ULP1, and the desired protein was purified by RP-HPLC. (C) Schematic representation for the semisynthetic strategy used for the generation of mHttex1-oxM8/AcK6 (adapted from [382]). (D) Characterization of mHttex1-oxM8, mHttex1-oxM8/pT3, mHttex1-oxM8/AcK6 and unmodified mHttex1 by ESI/MS, UPLC and SDS-PAGE

To investigate the effect of potential cross-talk between oxM8 and other Nt17 PTMs on mutant Httex1 aggregation, we generated mutant Httex1 proteins oxidized at M8 and phosphorylated at T3 (pT3) or acetylated at K6 (AcK6). To produce mHttex1 oxidized at M8 and phosphorylated at T3 (mHttex1-oxM8/pT3), we first generated SUMO-mHttex1-oxM8 as described above. After overnight dialysis, to remove the excess of H<sub>2</sub>O<sub>2</sub>, the fusion protein was co-incubated overnight with GCK kinase, a kinase that we recently reported to efficiently phosphorylate Httex1 specifically at T3 [410]. The extent of phosphorylation was monitored by ESI/MS. As shown in Figure VI.2-D, the SUMO-mHttex1-oxM8 showed an additional +80 Da, indicating the addition of a single phosphate group. The SUMO-mHttex1-oxM8/pT3 was then subjected to UPL1 cleavage to remove the SUMO tag completely, and mHttex1-oxM8/pT3 was purified by RP-HPLC (Figure VI.2-F). The purity of the protein was verified by ESI/MS, UPLC and SDS-PAGE (Figure VI.1.1-D).

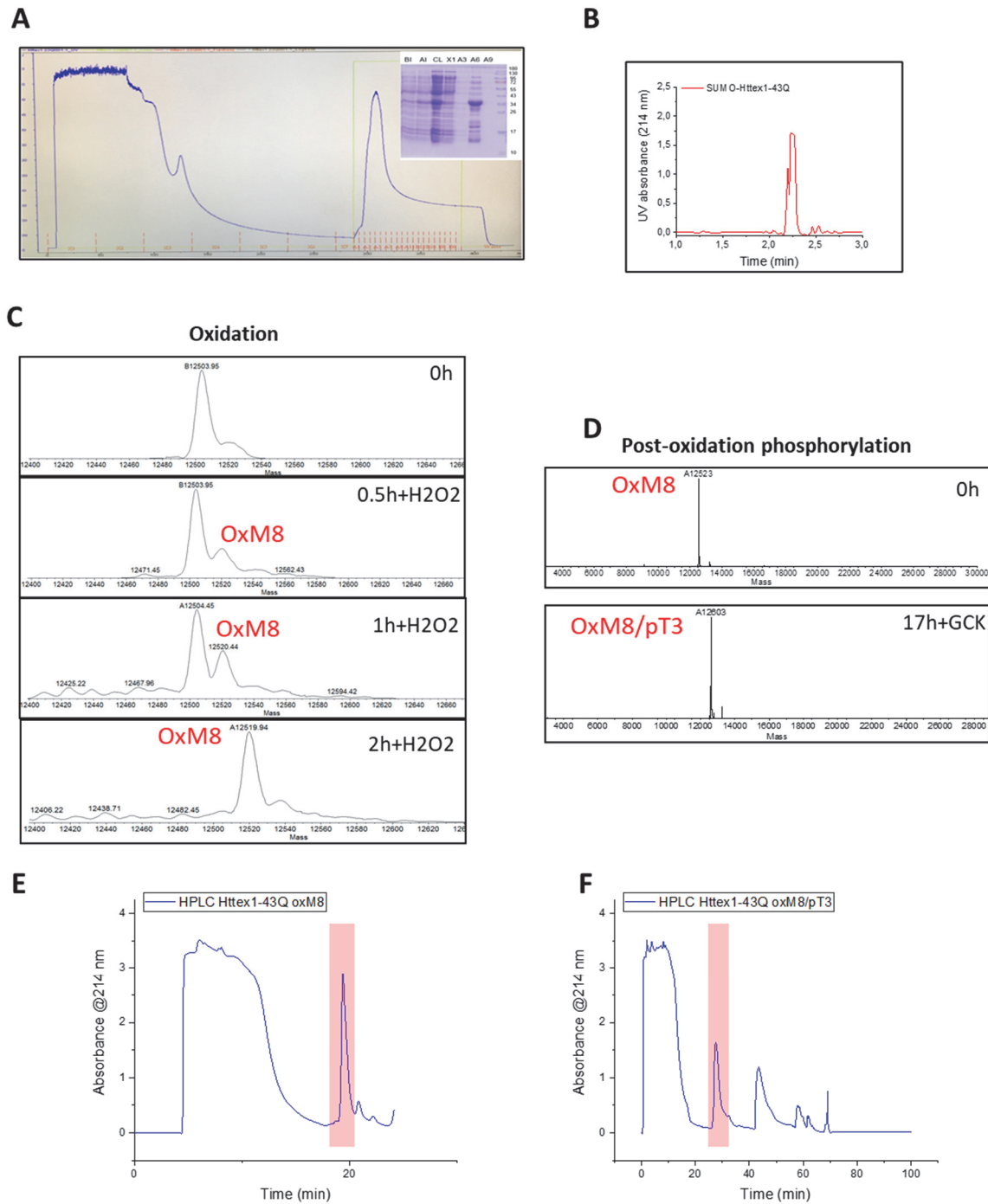


Figure IV-2. Purification, oxidation and phosphorylation of mHttex1

(A) Representative chromatogram of the IMAC purification of SUMO-mHttex1 and the analysis by SDS-PAGE of the purification fractions. (B) Analysis by UPLC of the fusion SUMO-mHttex1 after IMAC purifications. (C) Monitoring by ESI/MS of SUMO-mHttex1 oxidation by H<sub>2</sub>O<sub>2</sub> overtime after an analytical SUMO tag cleavage by ULP1. (D) Monitoring of SUMO-mHttex1 phosphorylation by GCK after an analytical SUMO tag cleavage by ULP1. (E-F) RP-HPLC chromatograms for the purification of mHttex1 oxM8 (E) and mHttex1 oxM8/pT3 (F). (protein of interest is highlighted in red).

To produce mutant Httex1 that is both oxidized at M8 and acetylated at lysine 6 (AcK6), we used our protein semisynthetic strategy (Figure VI.1.1-C) that we previously used to introduce single or multiple PTMs within Nt17 of mHttex1 [370]. mHttex1-AcK6/oxM8 was produced using native chemical ligation between Htt A10C-90 43Q and Ac-2-9-Nbz AcK6/oxM8 peptide (Characterization by ESI-MS and UPLC is shown in Figure VI.3-B), followed by desulfurization to convert the cysteine to the native Alanine 10 (Figure VI.3-C). The purity of mHttex1 AcK6/oxM8 was determined by SDS-PAGE, UPLC, and ESI/MS (Figure VI.1.1-D).

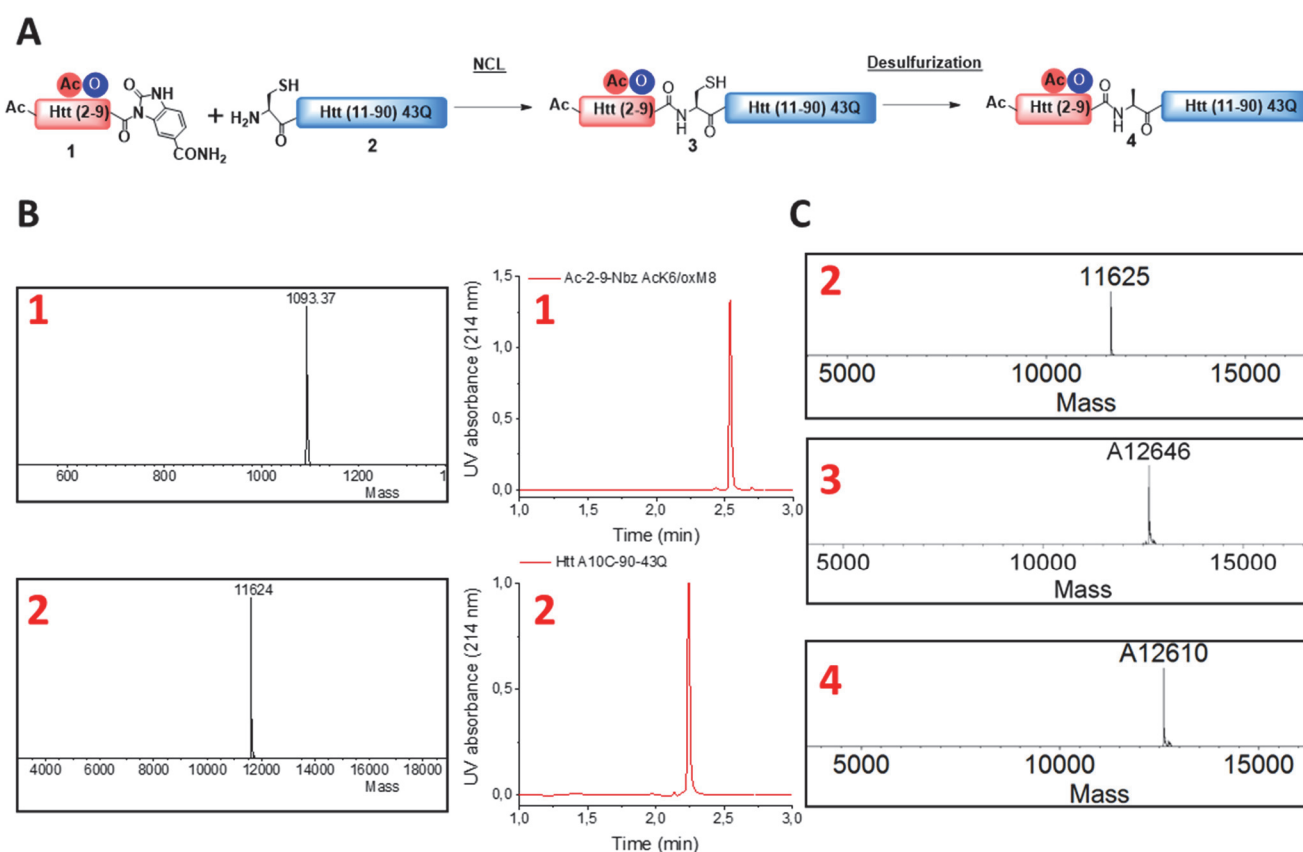


Figure IV-3. Semisynthesis of mHttex1-oxM8/AcK6

(A) Schematic representation for the semisynthetic strategy used for the generation of mHttex1-oxM8/AcK6 (4) (adapted from [382]). (B) Characterization by ESI/MS and UPLC of Htt Ac-2-9-Nbz oxM8/AcK6 (1) and Htt A10C-90 43Q (2), both are the starting material for the semisynthesis. The native chemical ligation of (1) and (2) was performed in (8 M urea, 0.5 M L-Proline, 30 mM D-Trehalose, 100 mM TCEP pH 7 and the ligation was monitored by ESI/MS (C). When the NCL was completed, the reaction solution containing mHttex1-oxM8/AcK6 A10C (3) was dialyzed and lyophilized and then desulfurized in 100 mM TCEP, 40 mM L-methionine, 20 vol% acetic acid in H<sub>2</sub>O pH 1, the desulfurization of Cys to Ala was monitored by ESI/MS.

### **IV.2.2 Oxidation at M8 delays the aggregation of mutant Httex1.**

To determine the effect of M8 oxidation on mutant Httex1, mHttex1-oxM8 and mHttex1 as control were subjected to a disaggregation protocol as previously reported [238] and any remaining preformed aggregates were removed by filtration through a 100 kDa filter before initiating the aggregation. The extent of aggregation was assessed by monitoring the kinetics of aggregation by quantifying the amount of soluble proteins at different time points using UPLC based sedimentation assay [178, 411, 412]. In addition, the effect of oxidation on the secondary structure and morphology of the fibrils was also assessed by circular dichroism (CD) and electron microscopy (EM). Figure VI.4-A shows the percentage of the remaining soluble protein over time. As expected unmodified mHttex1 exhibited almost a complete depletion of the soluble monomer (Figure VI.4-A) and full conversion into aggregates after 48 hours, which was confirmed by a shift from random to a beta-sheet structure by CD (Figure VI.4-B) and the presence of mature long fibrils as discerned by electron microscopy (EM) (Figure VI.4-C). In contrast, mHttex1-oxM8 showed a delay in the aggregation compared to the unmodified mHttex1 (Figure VI.4-A). The aggregation of mHttex1-oxM8 showed 70% and 29% remaining monomer after 12 and 24 hours, respectively, compared to 38% and 7% for the unmodified mHttex1 (Figure VI.4-A). However, after 48 hours, both proteins exhibited complete aggregation as discerned by the complete disappearance of soluble Httex1 (Figure VI.4-A) and the CD spectra of both proteins, which showed a signal that is consistent with predominantly  $\beta$ -sheet structures (Figure VI.4-B). The fibrils formed by mHttex1 oxM8 after 48 hours were similar to those formed by the unmodified mutant Httex1, suggesting that oxM8 influences the kinetics of aggregation, but not the final structure of the fibrils (Figure VI.4-C).



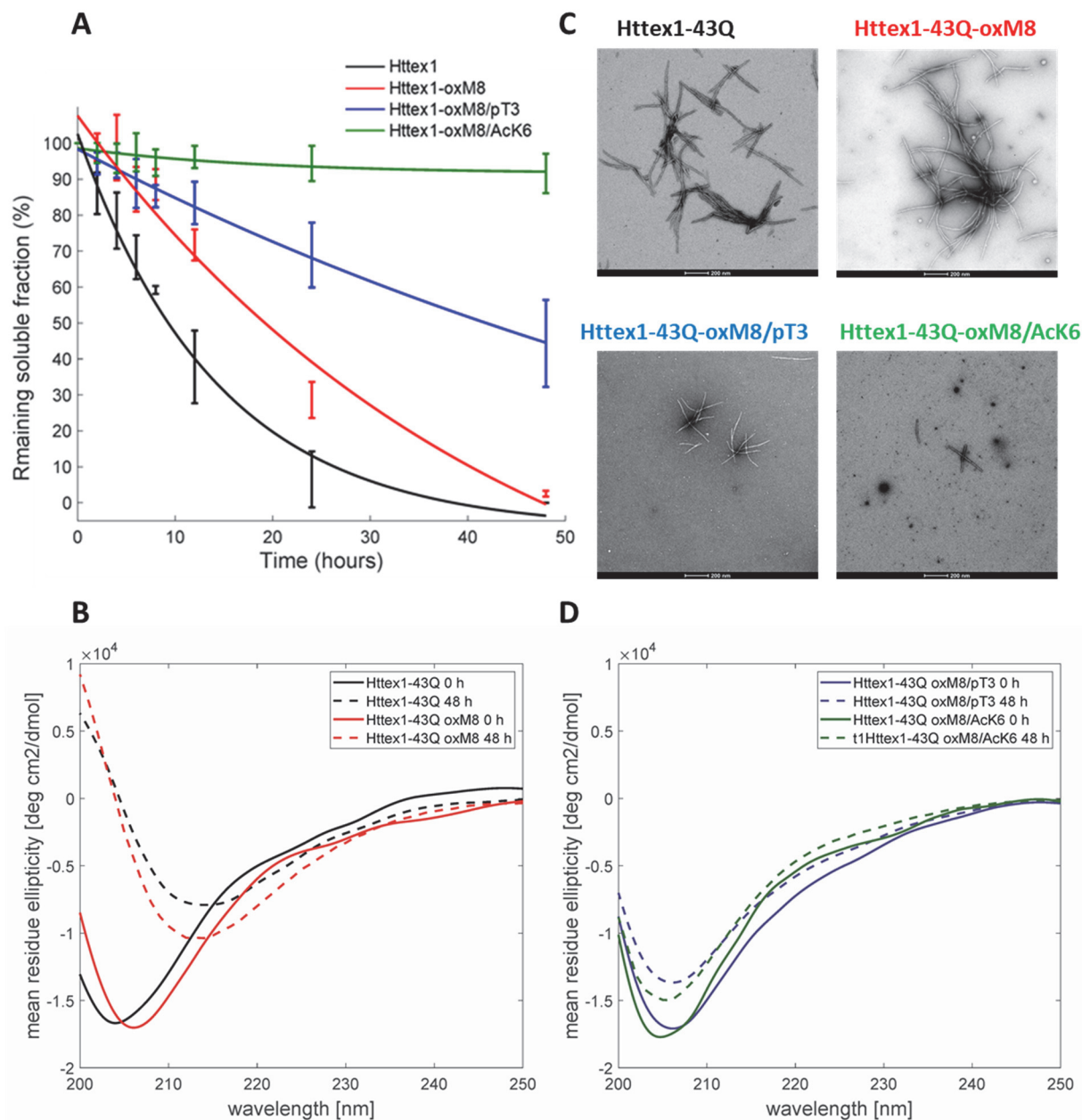


Figure IV-4. *De novo* aggregation of mutated mHttex1 with different PTMs

(A) Httex1 Aggregation studies (at 5  $\mu$ M) of mHttex1-oxM8, mHttex1-oxM8/pT3, mHttex1-oxM8/Ack6, and unmodified mHttex1 monitored by UPLC sedimentation assay to determine the proportion of remaining monomer. (B) Secondary structure analysis of unmodified mHttex1 and mHttex1-oxM8 by CD at time 0 h and time 48 h of aggregation. (C) Electron microscopy after 48 hours of aggregation (Scale bars are 200 nm). (D) Secondary structure analysis of mHttex1-oxM8 and mHttex1-oxM8 by CD at time 0 h and time 48 h post aggregation initiation.

Interestingly we consistently observed the presence of a population of oligomers for the oxidized Httex1 (Figure VI.4-C and VI.5). These populations of oligomers were observed in a higher amount after 4 hours of aggregation by EM, at which unmodified mHttex1 already showed fibrils formation (Figure VI.5). After 6 hours, mHttex1 oxM8 showed a mixture of oligomers and short fibrils (Figure VI.5), whereas only fibrils are observed in the case of the unmodified mHttex1. Altogether these results suggest that the delay in the aggregation of the oxidized mutant Httex1 could be associated with the formation and accumulation of oligomers (on- or off-pathway), which eventually convert into fibrils at later stages.

To investigate the effect of PTM cross-talk on aggregation within the Nt17 domain, we investigated and compared the aggregation kinetics and properties of Httex1-oxM8/pT3 and -oxM8/Ack6. Previously, we showed that phosphorylation at T3 significantly inhibits the aggregation of mutant Httex1 *in vitro* [370]. As shown in Figure VI.4, the oxidation of M8 does not seem to influence the inhibitory effect of phosphorylation at T3. Even after 48 hours of incubation at 48h, ~50 % of the protein remained soluble, whereas more than 98% of the unmodified proteins have been converted to fibrillar aggregates (Figure VI.4-A). The CD spectrum showed that the remaining protein retains a random coil signature suggesting that the remaining soluble protein represents monomers or disordered soluble oligomers (Figure VI.4-D). Analysis by EM showed the accumulation of oligomers and short fibrils similar to those we previously reported for mHttex1-pT3 [370]. On the other hand, oxidation of M8 in the context of the K6 acetylated mutant Httex1 dramatically altered the aggregation properties of the protein. Previously, we showed that acetylation of K6 or K9 does not significantly influence the aggregation of mutant Httex1. However, as shown in Figure VI.4-A, the presence of both acetylation at K6 and methionine oxidation at M8 (mHttex1- oxM8/Ack6) results in significant inhibition of mutant Httex1 aggregation. Only 8% of the mHttex1 oxM8/Ack6 aggregated after 48 hours (Figure VI.4-A) as determined by the sedimentation assay and confirmed by CD and EM, which show predominantly disordered conformation and the accumulation of only oligomers and small fibrils (Figure VI.4-C). These results suggest that the addition of M8 oxidation reversed the aggregation of Ack6 and illustrates how the combination of different Nt17 PTM could differentially influence the aggregation properties of the protein.

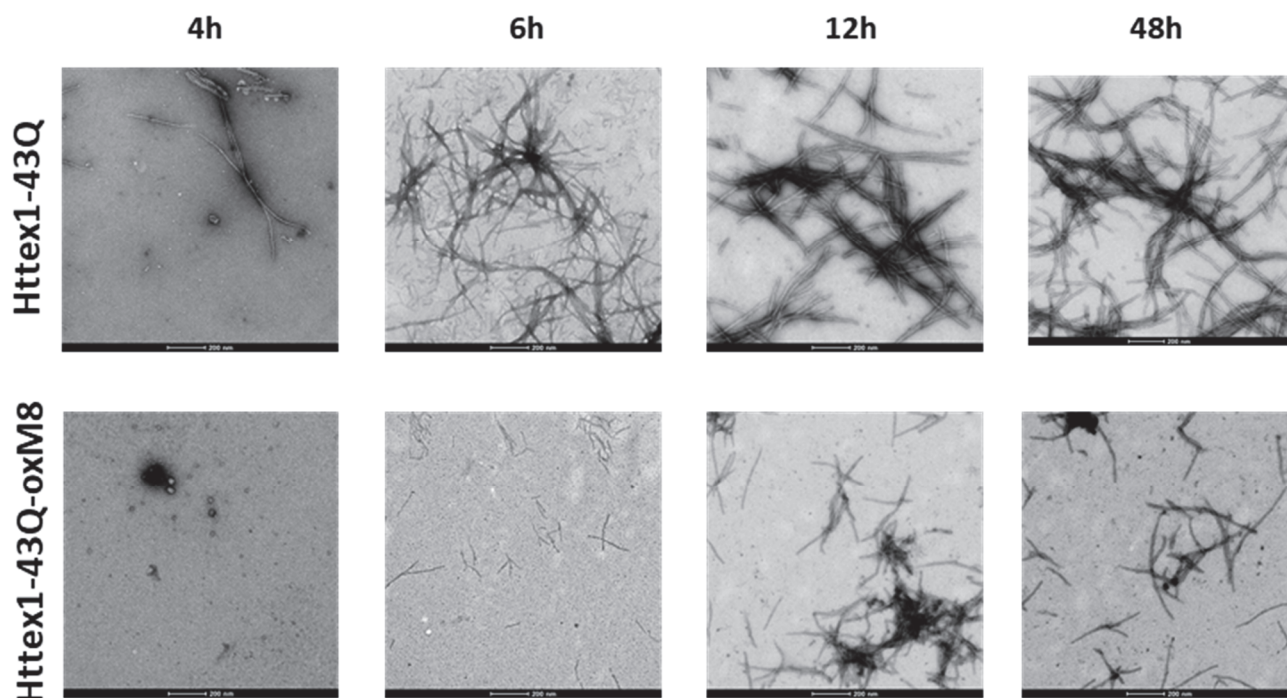


Figure IV-5. Over-time aggregation monitoring by electron microscopy of mHttex1 oxM8 compared to unmodified mHttex1 (at 10 uM).

### IV.2.3 Oxidation at M8 decreases the helicity of the Nt17 peptides

To gain insight into the mechanisms by which M8 oxidation and the combination of oxM8 and other PTMs influence the aggregation of mutant Httex1, we sought to investigate how these individual PTMs and their combination influence the structural properties of the Nt17 domain. The CD spectrum of the Nt17-WT peptide showed a minimum at 200-205 nm and shoulder around 222 nm (Figure VI.6, Table VI.1) with a calculated helical content of 11%. This is in accordance with previous observation suggesting that the Nt17 domain is predominantly disordered with a tendency to form transient  $\alpha$ -helical structures due to its amphipathic nature [329, 382, 413]. We confirmed that Nt17-Ack6 exhibited increased helical content (17%) compared to the Nt17-WT peptide (Figure VI.6) as previously reported [414]. Additionally, by CD we observed that Nt17-pT3 has higher propensity to adopt helical conformation compared to other Nt17 peptides, helical content of 32 % (Figure VI.6, Table VI.1). In contrast, when oxM8 was added to the three peptides, we observed a reduced CD signal at 222 nm for Nt17-oxM8, Nt17-oxM8/pT3 and Nt17-oxM8/Ack6 (Figure VI.6) indicating a decrease in the helical content which was confirmed by a fit to secondary structure content (See Table VI.1).

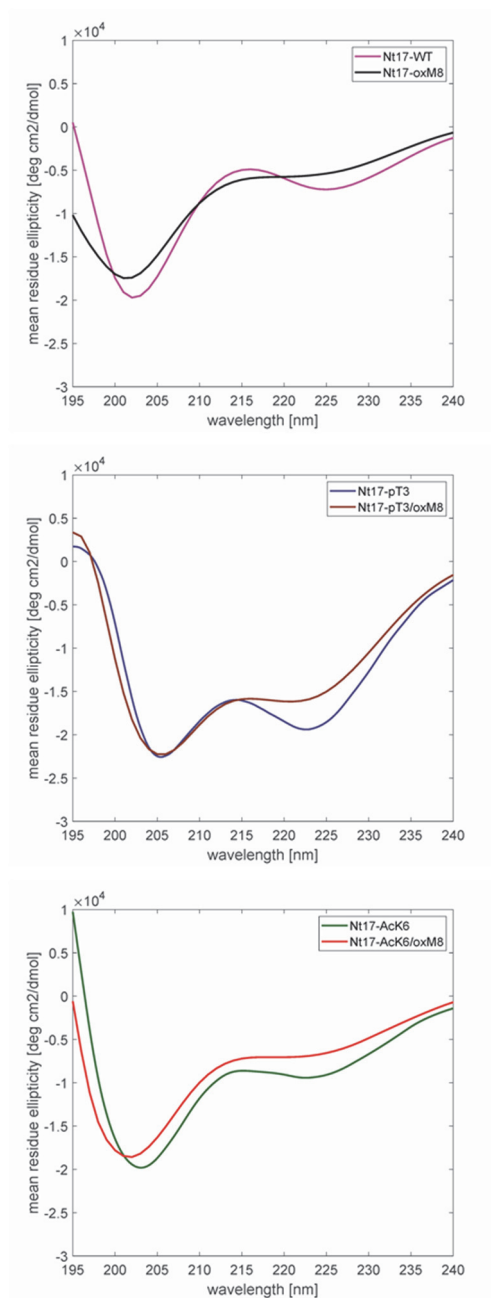


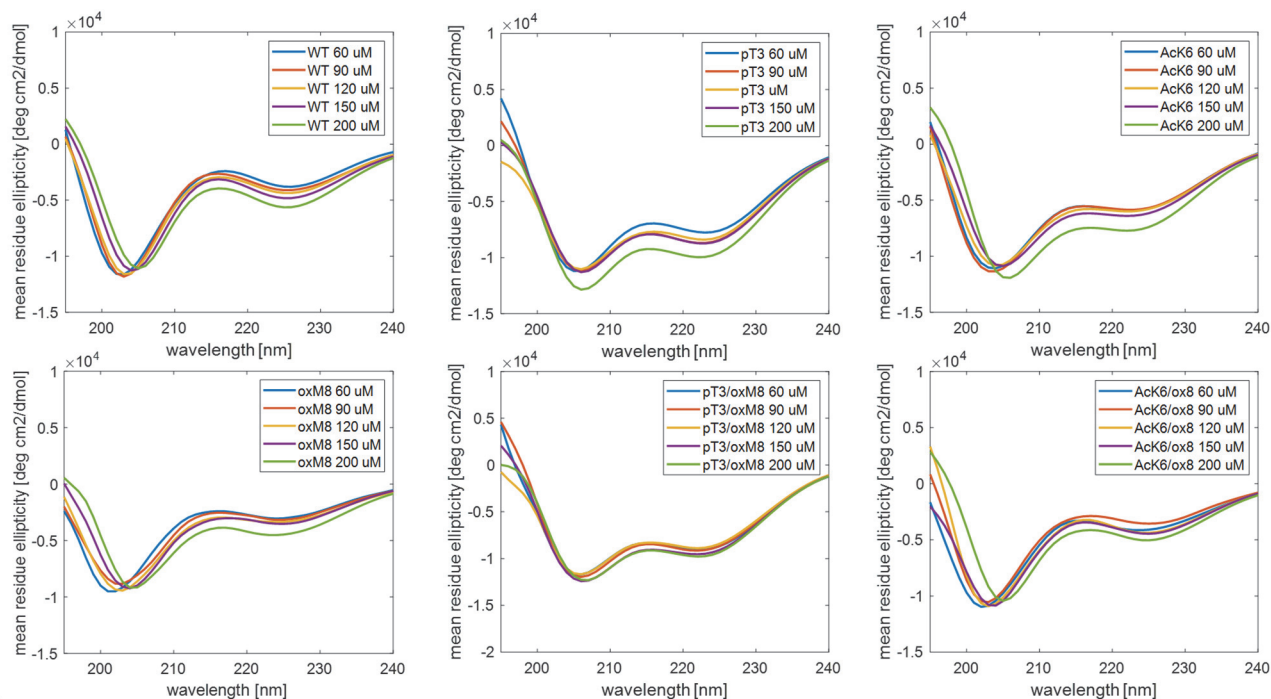
Figure IV-6. Far-UV CD spectra of Nt17-WT, and Nt17-oxM8, Nt17-AcK6, Nt17-AcK6/oxM8, Nt17-pT3 and Nt17-pT3/oxM8 at 60  $\mu$ M

Table IV-1. Helical content (%) calculated for the different peptides at 60  $\mu$ M.

Nt17 peptide	CD Helical content (%)
WT	11
oxM8	9
pT3	32
pT3/oxM8	30
AcK6	17
AcK6/oxM8	12

Furthermore, to investigate if the decrease in the helicity induced by oxM8 was consistent even at a high concentration of the peptides, we conducted CD analysis (Figure VI.7-A) at different Nt17 peptide concentrations (60, 90, 120, 150, and 200  $\mu$ M). As shown in Figure VI.7, All the peptides showed a small increase in the helical content with increasing concentrations (Figure VI.7-B). oxM8 slightly decreased the helical content of the WT and pT3 Nt17 peptides over the different concentrations, and the difference in helicity with or without oxidation was consistent at each concentration. However, the effect of M8 oxidation was more critical when it was added to AcK6 Nt17 peptide; it dramatically decreased its helical content over the whole range of tested concentrations (Figure VI.7-B). Altogether, this data suggests that the oxidation of M8 decreases the helicity of the Nt17 in the presence or absence of PTMs, and this can play a role in modulating the aggregation of mutant Httex1. However, more in-depth structural studies are needed to understand how M8 oxidation decreases the Nt17 helicity and link this effect to the aggregation properties of Httex1. However, given the number of PTMs and possible combinations of PTMs, this could be experimentally challenging, especially in the context of Httex1 or other longer N-terminal fragments.

**A**



**B**

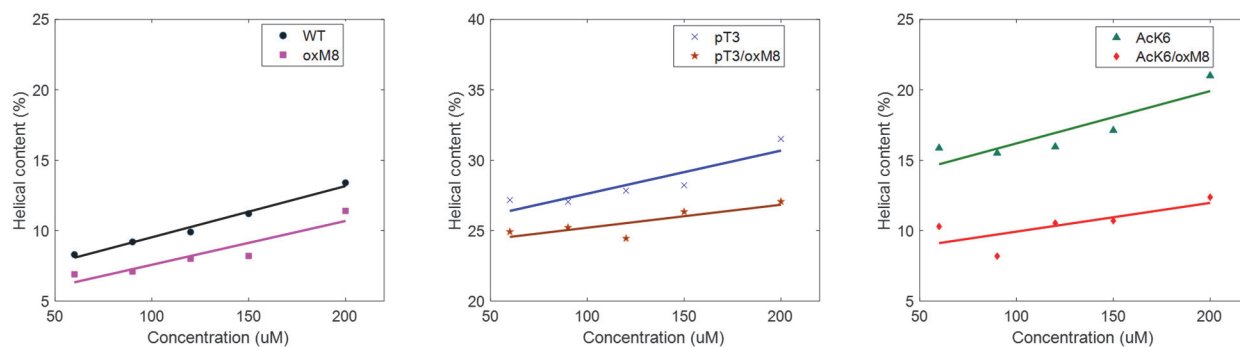


Figure IV-7. CD spectra and helical content for various Nt17 peptides

(A) Far-UV CD spectra of Nt17-WT, and Nt17-oxM8, Nt17-AcK6, Nt17-AcK6/oxM8, Nt17-pT3 and Nt17-pT3/oxM8 at 60, 90, 120, 150 and 200  $\mu$ M. (B) Helical content for the peptides in function of the different concentrations.

#### IV.2.4 Atomistic Molecular Dynamics (MD) reveals the consequences of M8 oxidation and its cross-talk with other PTMs on the Nt17 structure.

Computational studies were conducted using atomistic molecular dynamics (MD) to characterize in-depth the consequences of the PTMs code on the Nt17 structure. In these studies, we decided to include the first two glutamine residue as preliminary studies suggested that they could be involved in stabilizing the Nt17 conformations. Moreover, previous data from our laboratory have demonstrated that there is no difference in the overall structure between the Nt17 and the Nt19 (Nt17 + QQ) peptides (Data not shown). The Nt19 was simulated with single and multiple PTMs to analyze the cross-talk of M8 oxidation and phosphorylation at T3 or S13 as well as acetylation at K6. The simulations were run for a total of 13  $\mu$ s using the CHARMM36m [415] force field and a modified TIP3P water model [416].

Molecular dynamics showed that the addition of oxM8 to the unmodified Nt19 and Nt19-pT3, decreased their overall helicity by 20% and 21%, respectively (Figure VI.8-A), while a more drastic effect was observed for Nt19 AcK6, whose helicity decreased by 60% upon the addition of oxM8 (Figure VI.8-A). This data is in accordance with our *in vitro* CD data with also a more significant decrease in the helicity for Nt19 AcK6 upon the addition of oxM8 (29% decrease in the helicity, Figure VI.8-A).

To investigate the connection between the major conformations and the aggregation rate of mHttex1, we classified PTMs into 3 groups based on the *in vitro* and CD data (Figure VI.8-B). Group 1 comprised PTMs with higher helicity by CD and lower mHttex1 aggregation rates (Figure VI.8-B). Group 2 is composed of PTMs with lower helicity in CD data but as well as lower aggregation rate, while in Group 3, those with aggregation rates similar to unmodified mHttex1 (Figure VI.8-B). Based on MD data, PTMs in Group 1, resulted in stabilizing a helical structure of the first 8 N-terminal residues while the rest remained disordered (Figure VI.8-B). For Group 2, the abundance of N-terminal helix of pS13 was similar to the unmodified peptide, but a 94% decrease was observed for other types of helices in pS13 (Figure VI.8-B). For Group 3, the abundance of either short N terminal helix or other types of helices in oxM8 and AcK6 similar to that of the unmodified peptide (Figure VI.8-B). Based on these observations, combined with our experimental data, it appears that a higher abundance of a short N-terminal helix and lower abundance of other helical conformations in the MD simulations correlates with lower aggregation rates.

A

Nt19	WT vs. oxM8	pT3 vs. oxM8/pT3	AcK6 vs. oxM8/AcK6
MD % change in helicity	-20	-21	-60
CD % change in helicity	-18	-6	-29

B

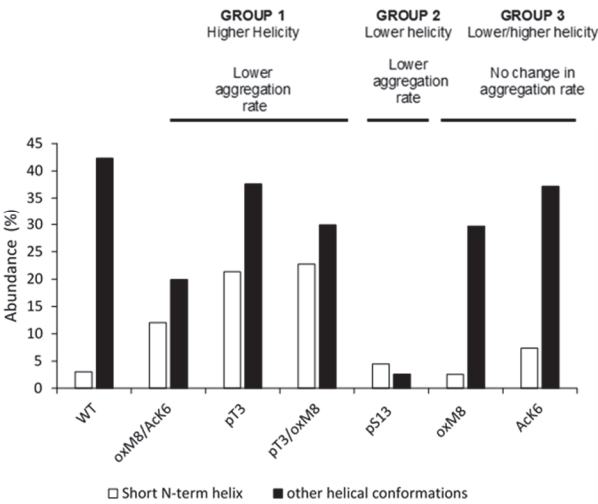


Figure IV-8. CD Vs MD helical content of the Nt17 peptides

(A) CD and MD both showed decrease in helicity when M8 was oxidized. (B) The abundance of N-term helix was high for PTMs that delayed aggregation

Furthermore, Methionine is very often positioned next to aromatic amino acids. Interestingly, the Sulfur group of e methionine and the ring in the aromatic residues interact *via* hydrophobic interactions. By consequence, oxidation at methionine can interrupt these interactions and induces structural changes [417]. Our MD data showed that the addition oxM8 to the different PTMs, increased the distance (data not shown) between the M8 sulfur group and the aromatic group in phenylalanine 11. This suggests that M8 oxidation disrupts the hydrophobic stabilization caused by the sulfur-ring bond.

#### IV.2.5 NMR structural studies using Httex1-oxM8

Our aggregation studies were carried out using full exon 1 (Httex1) with a Q43 expansion to enable monitoring aggregation within a tractable period of time, while on the contrary molecular dynamics simulations were



limited to the N-terminal peptide Nt19 (because bigger constructs wouldn't have been sampled as extensively). Therefore, to provide some minimal experimental support for the simulations, we acquired circular dichroism data on Nt19 peptides bearing single or multiple PTMs. To gain more insights into how M8 oxidation affects Httex1 structure and dynamics and assess more directly to what extent the simulation results approximate the true effects of the PTMs at the protein level, we performed Nuclear Magnetic Resonance (NMR) spectroscopy experiments on the Httex1-oxM8. We analyzed these results in comparison to NMR experiments performed on the unmodified protein.

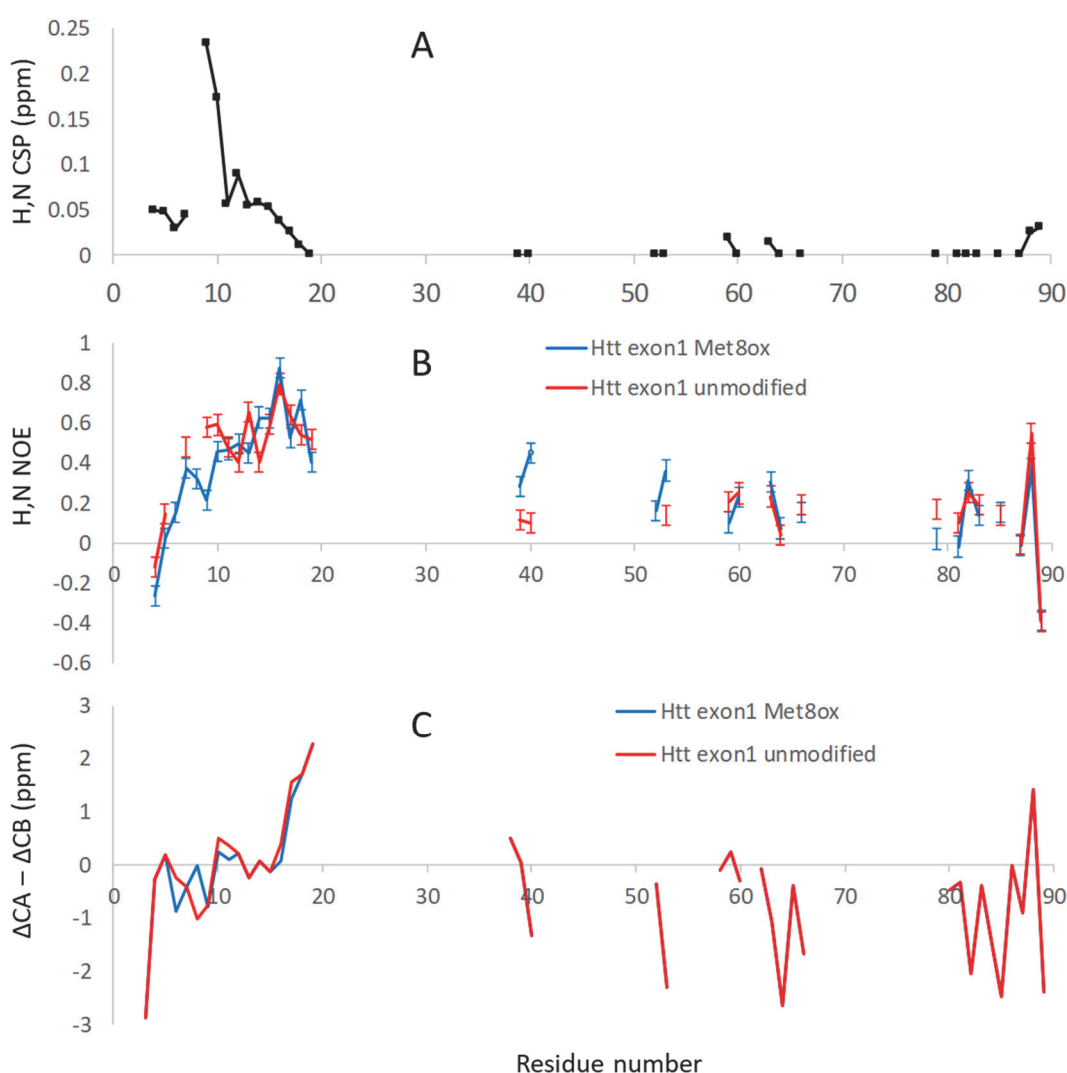


Figure IV-9. NMR characterization of Htt exon 1 with M8 oxidized, compared to unmodified Htt exon 1.

(A)  $^1\text{H},^{15}\text{N}$  chemical shift perturbation between modified and unmodified proteins. Gaps correspond to prolines and residues lacking  $^1\text{H},^{15}\text{N}$  assignments in at least one of the forms, such as M8 in the unmodified protein. (B)  $^1\text{H},^{15}\text{N}$  heteronuclear NOE profiles for both forms; gaps correspond to prolines, residues lacking  $^1\text{H},^{15}\text{N}$  assignments and heavily overlapped crosspeaks. (C) Secondary structure propensities as obtained from  $\Delta\text{CA} - \Delta\text{CB}$  profile, where  $\Delta$ s correspond to subtraction of amino acid-specific random coil chemical shifts from the measured shifts (standard methionine chemical shifts were subtracted for oxidized methionine).

Httex1-oxM8 displays an HSQC spectrum very similar to that of the unmodified protein (Figure IV-10 and IV.9-A), with a low signal dispersion natural of highly disordered proteins but with elevated heteronuclear  $^1\text{H}$ - $^{15}\text{N}$  NOE values that indicate residual structuring for residues 10-19 (Figure IV.9-B) and substantial alpha helical propensity for residues 17-19 as revealed by the CA and CB chemical shift deviations from random coil values ( $\Delta\text{CA}$ - $\Delta\text{CB}$ , Figure IV.9-C). These are essentially the same features well documented for the unmodified protein [192, 383, 384, 418]. After obtaining the backbone resonance assignment, we determined that the most shifted crosspeaks relative to the unmodified protein are those from residues of the N-terminal peptide, while crosspeaks from the polyQ, proline-rich and C-terminal regions remain unaffected. More precisely, Httex1-oxM8 exhibits small chemical shift perturbations only in the residues around M8 in the N-terminal peptide (Figure IV-9-A). Meanwhile,  $^1\text{H}$ - $^{15}\text{N}$  NOE and  $\Delta\text{CA}$ - $\Delta\text{CB}$  values experience no significant changes, except for a slightly higher NOE value for the methionine-oxidized protein at residues Q39 and Q40, though still rather low hence indicative of disorder in these residues, as in the unmodified protein. The  $\Delta\text{CA}$ - $\Delta\text{CB}$  data shows no strong secondary structure by Q39, and some very small beta propensity at Q40, for both forms, with virtually identical  $^{13}\text{C}$  chemical shifts. Interestingly,  $^1\text{H}$ ,  $^{15}\text{N}$  HSQC and  $^1\text{H}$ ,  $^{13}\text{C}$  HSQC spectra for both proteins show a gradient of chemical shifts that suggests the secondary structure propensity decreases gradually from  $\alpha$ -helical at Q18 to random coil at Q39, similar to the gradient reported from a series of spectra collected on Httex1 samples labelled at specific glutamine residues [193], and that we also reported for phosphorylated forms of Httex1 [418].

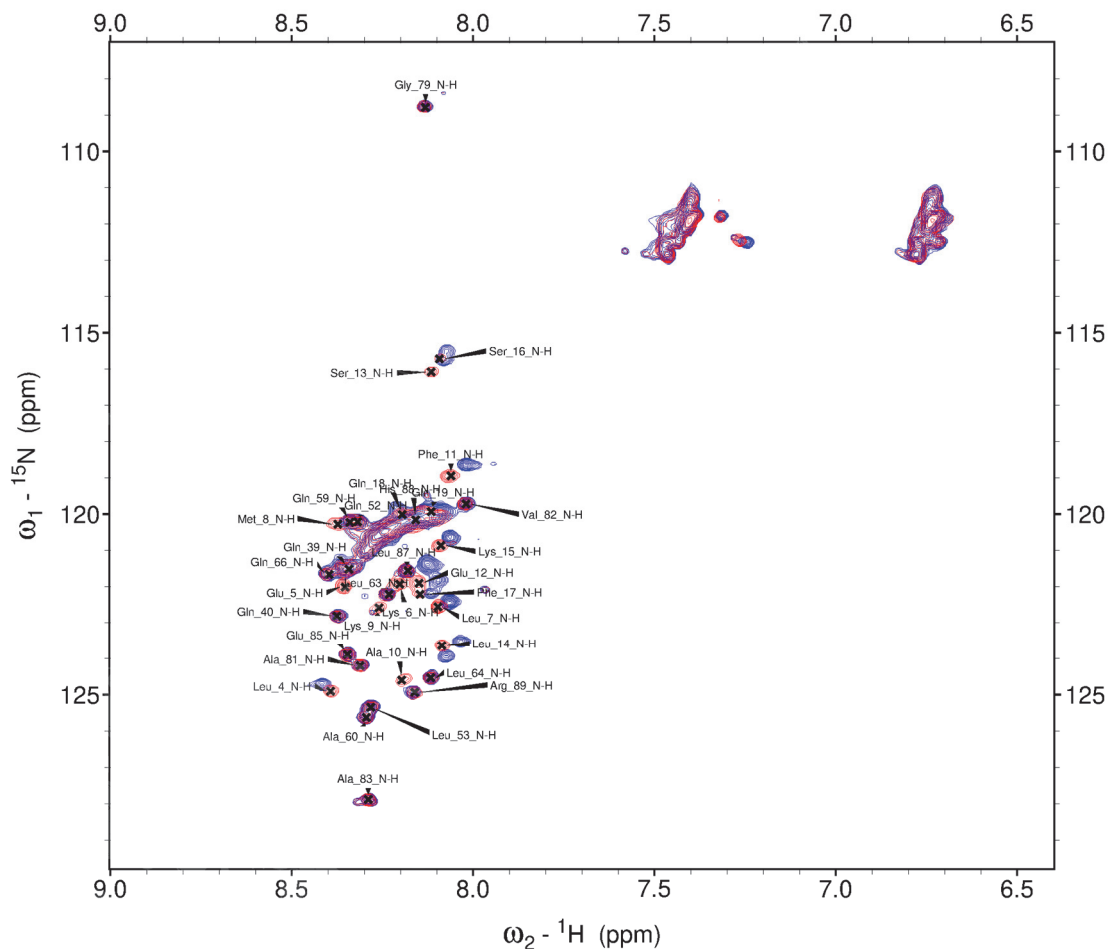


Figure IV-10. Overlay of  $^1\text{H}$ , $^{15}\text{N}$  HSQC spectra of wild type exon 1

Unmodified (blue) and with M8 oxidized (red) with the assignments of the form oxidized at M8 displayed. Spectra collected at 293 K on 200  $\mu\text{M}$  samples, at 800 MHz  $^1\text{H}$  frequency. Notice the affected crosspeaks map only to residues of the N-terminal peptide, while crosspeaks from the polyQ, proline-rich and C-terminal regions remain unaffected.

## IV.3 Discussion

Among all Htt PTMs, methionine oxidation remains the least well understood and studied. First, due to the lack of sensitive biochemical tools for its detection, second, the production and purification of oxidized mutant Httex1 have been challenging because of the high aggregation propensity of mutant Htt. Herein, we have described for the first time the production of mutant Httex1 oxidized at M8 using a strategy where methionine oxidation is introduced into the more soluble and stable SUMO-Httex1-43Q protein, which is then cleaved to generate the mHttex1-oxM8, which is then rapidly purified by RP-HPLC. This method enabled us to produce milligram quantities of mHttex1 oxM8 pure and without any residual H<sub>2</sub>O<sub>2</sub>, thus addressing one of the major limitations of previous studies. To investigate the cross-talk between M8 oxidation and Phosphorylation at T3 or S13/S16, we enzymatically introduced phosphorylation at T3 or S13 and S16 into mHttex1 oxM8 and generated homogeneously modified mutant Httex1 proteins bearing oxidized M8 with pT3 or pS13/pS16. In addition, we also used protein semisynthetic strategies, developed in our group [370], to generate mutant Httex1 proteins bearing oxidized M8 and acetylated K6 (mHttex1-Ack6/oxM8). We choose K6 because of its close proximity to M8 and the fact it is the only lysine residue in Nt17, which has been shown to influence the helicity of Nt17 and modify the effect of neighbouring PTMs on Nt17 structure and Httex1 aggregation [370]. These advances enabled us to investigate for the first time the role of cross-talk between these different PTMs in regulating Nt17 conformation and mutant Httex1 aggregation *in vitro*.

We demonstrated that oxidation at M8 delayed the aggregation of mHttex1 but did not alter the morphology of the structure of the Httex1 fibrils. We hypothesized that this delay is caused by methionine oxidation induced formation of oligomers at the early stages of the aggregation, which undergo slow conversion to fibrils. As shown in Figure VI.5 and highlighted in previous studies, oligomers are rarely observed during the fibrillization of the unmodified mutant Httex1 due to its high propensity to misfold and fibrillize. Interestingly, the effect of oxM8 was more striking when oxidation at M8 was combined with Ack6. Although acetylation at K6 was previously shown not to influence the aggregation of mutant Httex1, when this modification combined with oxidation at M8, we observed a strong inhibitory effect on mutant Httex1 aggregation and the accumulation of mainly oligomeric and short fibrillar structures. In contrast, the combination of methionine oxidation and phosphorylation at T3 did not modify the aggregation inhibitory effect induced by pT3.

Our findings are consistent with previous observations on the effect of methionine oxidation on the aggregation of other amyloid-forming proteins. For example, oxidation at Met-35 attenuates the aggregation amyloid- $\beta$ (1–40) [419, 420], A $\beta$ 1-42 and the highly amyloidogenic Arctic A $\beta$ 1-40 variant [421]. Oxidation of the

prion peptide PrP106-126 reduces as well its fibrillization [422]. Furthermore, Methionine oxidation was shown to inhibit the aggregation of alpha-synuclein protein and promote the formation of stable oligomers [423]. In the case of Httex1, the effect of M8 oxidation has only been studied in the context of model peptide, or fused to GST tag, or non-native Httex1 sequences lacking a significant part of the C-terminal domain of the protein fused to GST fusion protein. Using a model peptide of Nt17 plus ten glutamine residues, Nt17Q10, Ceccon et al. showed that oxidation at M8 abolished aggregation [326].

In order to understand the effect of methionine oxidation and its cross-talk with pT3 and AcK6, we performed CD and MD analysis of the different Nt17 WT, pT3, or AcK6 in the presence or absence of the M8 oxidation. We observed that in all the cases, methionine oxidation reduced the helical content Nt17, independent of co-occurring PTMs and peptide concentration. Consistent with our previous studies [329, 370], we observed that the effect of PTMs on the overall helicity of the Nt17 peptide did not correlate with their impact on the aggregation propensity of mutant Httex1 *in vitro*. However, it was noticed that all PTMs resulted in a slower aggregation rate have a higher abundance of short N-term helices at the first 8 N-term residues and lower abundance of other helical conformations.

## IV.4 Conclusion

Our findings on the effect of the cross-talk between the different Nt17 PTMs highlights the complexity of the protein PTM code and suggest that Htt normal function and aggregation is likely regulated by a complex interplay between different PTMs. One major challenge in addressing this complexity is the large number of possible PTM combinations even within short stretches of sequences in proteins, such as Nt17. This, combined with the challenges of introducing multiple PTMs into proteins, has led to either abandoning efforts to investigate this complexity or resorting to studying protein fragments. Our findings here show that while working with peptide fragments provides useful insights, extrapolations of findings from these fragments to predict their properties in the context of full-length proteins are not straight forward. Therefore, we believe there is an urgent need to develop a reliable computational approach that would enable rapid sampling and assessment of the effect of large number of PTMs and PTMs combinations. The work presented here represents our initial efforts on this direction and aims at exploring the extent to which this is possible using peptide systems in which the effect of PTMs can be experimentally and reproducibly predicted and measured.

## IV.5 Experimental section

### IV.5.1 Materials

pTWIN1 vector, containing human Httex1 fused to His6-SUMO, was ordered from GeneArt Gene Synthesis (Life Technologies). *E. coli* B ER2566 from NEB. Ampicillin, DTT, Isopropyl  $\beta$ -D-1-thiogalactopyranoside (IPTG), Hydrogen peroxide solution 30 % from Sigma and PMSF from AppliChem. Imidazole, complete Protease Inhibitor Cocktail, magnesium chloride (MgCl<sub>2</sub>), magnesium sulfate (MgSO<sub>4</sub>), and Trifluoroacetic acid from Sigma. EGTA solution from Boston Bioproducts. Mg-ATP from Cayman, EDTA from Fisher Scientific, Luria Broth (Miller's LB Broth) from Chemie Brunschwig. Acetonitrile HPLC-grade from Macherey Nagel. Spectrophotometer semi-micro cuvette from Reactolab. C4 HPLC column from Phenomenex. HisPrep 16/10 column from GE healthcare. GCK kinase (0.5  $\mu$ g/ $\mu$ l, cat. # BC047865) from MRC PPU Reagents. Uranyl formate (UO<sub>2</sub>(CHO<sub>2</sub>)<sub>2</sub>) and Formvar/carbon 200 mesh, Cu 50 grids from EMS. High Precision Cell made of Quartz SUPRASIL 1 mm light path from Hellma Analytics. Buffer Substance Dulbecco's (PBS w/o Ca and Mg) ancienne ref. 47302 (RT) SERVA from Witech. 100 kD Microcon fast flow filters from Merck Millipore.

### IV.5.2 Expression of His6-SUMO-Httex1-Qn (n= 23 or 43).

The expression and purification of His-SUMO-Httex1-43Q was performed as previously reported[238]. Httex1-43Q with a His-SUMO tag at its N-terminal were cloned in pTWIN1 plasmid with ampicillin (Amp) resistance. Then the plasmid was transformed in *E. coli* ER2566, and the resulting transformed bacterial cells were plated in an agar plate containing ampicillin resistance [396]. Next, 400ml LB+Amp (100 $\mu$ g/ml) medium was inoculated with a single colony and incubated at 37°C overnight in order to start the day after the 12L expression at an optical density (OD<sub>600</sub>) density of 0.15. When the OD<sub>600</sub> value was around 0.6, the culture was induced with 0.4 mM IPTG and incubated at 18°C overnight. The cells were harvested by centrifugation (3993 x g, 4 °C, 10 min) and resuspended in buffer A (50 mM Tris, 500 mM NaCl 30 mM Imidazole, pH 7,5, 0,65 $\mu$ m filtrated) with PMSF and protease inhibitors. The suspended bacterial pellet was subjected to sonication on ice (70% amplitude, total sonication time 5 min, intervals of 30 s sonication, 30 s pause), followed by centrifugation (39191 x g, 4 °C, 60 min). The supernatant was filtered (0.45  $\mu$ m, syringe filters) and passed through a Ni-NTA column. The protein then Eluted with 100% IMAC buffer B (50mM Tris, 500mM NaCl 15mM Imidazole, pH 7.5, 0.65 $\mu$ m filtrated). The purified fusion protein was kept ice for further reactions.

### IV.5.3 Production of Httex1-43Q oxM8 and Httex1-43Q oxM8/pT3

10 mg of the SUMO-Httex1-43Q (in 18 mL) fusion protein was treated with 1 mL of 30% H<sub>2</sub>O<sub>2</sub> to perform the oxidation directly on the SUMO fusion protein. After 2 hours of the reaction, 30 µL was supplemented with 1 µL of ULP1 (1 mg/mL), and the extent of the oxidation was verified by LC/MS. 1 oxidation corresponds to +16 Da to the molecular weight of Httex1-43Q. When the completion of the oxidation was confirmed, 400 µL of ULP1 enzyme was added to the reaction solution to cleave the SUMO tag, and the reaction was directly injected in RP-HPLC, C4 column using a gradient of 25-35 % solvent B (Acetonitrile + 0.1 TFA) in solvent A (H<sub>2</sub>O + 0.1 % TFA), over 40 min at 15 mL/min. The fractions were analyzed by LC/MS; the ones containing the protein were pooled and lyophilized. The quality of the protein was analyzed using LC/MS, UPLC, and SDS-PAGE.

For the generation of Httex1-43Q oxM8 and Httex1-43Q oxM8/pT3, the oxidation was performed as above, and when completed, the oxidized fusion protein was dialyzed against 4L of TBS buffer overnight at 4°C and then supplemented with 10X phosphorylation buffer to obtain a final buffer with the following composition and concentration: 50 mM Tris, 25 mM MgCl<sub>2</sub>, 8 mM EGTA, 4 mM EDTA, 1 mM DTT. 5 mM Mg-ATP was added to the solution, and the pH was adjusted, and finally, GCK was added at a ratio of 1:30 w/w (kinase protein) to the Httex1-43 oxM8 (666 µL), and the reaction was incubated at 30°C overnight. Next, the extent of the phosphorylation was verified by LC/MS, and when it was completed, 400 µL of ULP1 was added to the phosphorylation reaction solution to cleave the SUMO tag. Finally, Httex1-43Q-oxM8 was separated from the SUMO tag, and other impurities by HPLC and the fractions containing the protein were pooled and analyzed by LC/MS, UPLC, and SDS-PAGE.

### IV.5.4 Semi-synthesis of Httex1-43Q oxM8/Ack6

The semisynthesis of Httex1-43Q oxM8/Ack6 was performed as previously reported [382]. Briefly, 5 mg of Htt-A10C-90-43Q with free N-terminal cysteine was dissolved in neat TFA and the TFA was dried under nitrogen after 30 min. The dried Htt-A10C-90-43Q was redissolved in 5.0 mL ligation buffer (8 M urea, 0.5 M L-Proline, 30 mM D-Trehalose, 100 mM TCEP and 100 mM MPAA). The pH was adjusted to 7.0 with 10 M NaOH, and the peptide Ac-2-9Nbz Ack6/oxM8 peptide (2.5 mg) was added to the reaction mixture. The native chemical ligation was monitored by LC-ESI-MS until the complete consumption of A10C-90 43Q. Next, the ligation reaction was desalted with hitrap 26/10 desalting column, and fractions containing the Httex1-A10C-43Q oxM8/pT3 were pooled and lyophilized. In order to recover the native alanine, the protein mixture was disaggregated and dissolved in 100 mM TCEP, 40 mM L-methionine, 20 vol% acetic acid in H<sub>2</sub>O. Freshly prepared nickel boride suspension (1.0 mL) was added to the resulting solution, and the resulting suspension was

incubated at 37°C. After 2 h, a loss of 32 Da was observed. Insoluble nickel was removed from the reaction mixture *via* sedimentation (4°C, 4000 g, 10 min). The supernatant was subjected to RP-HPLC purification with a gradient of 25-55% buffer B (MeCN + 0.1% TFA) in buffer A (H<sub>2</sub>O + 0.1% TFA). The fractions containing Ac-Httex1-43Q oxM8/pT3 were analyzed by LC-MS and UPLC, pooled, and lyophilized. The final purity of the protein was checked by LC/MS, UPLC, and SDS-PAGE.

#### **IV.5.5 UPLC-Based sedimentation assay**

To perform aggregation studies, Httex1 was disaggregated as previously reported [238] using TFA, and after evaporating the TFA, the protein was filtered through a 100 kDa filter. The final volume was adjusted with PBS to have the desired concentration and incubated at 37°C. In order to determine the percentage of the remaining soluble monomer during the aggregation, 40 µL was taken at each indicated time point, and insoluble aggregates were removed by centrifugation (4°C, 20000 g, 30 minutes). The supernatant was injected into the UPLC. The peak area was measured for each time point and the changes in the area were used to calculate the fraction of soluble protein compared to t=0 being 100%. The exponential decay function was used to fit the data of different aggregation curves. All the mutant Httex1 aggregated protein curves had an adjusted R<sup>2</sup> ranging from 0.97-0.99 (except Httex1-43Q AcK6/oxM8 with R<sup>2</sup> = 0.78)

#### **IV.5.6 Electron microscopy**

For TEM analysis, 5 µl of aggregation solution was spotted onto a Formvar/carbon-coated 200-mesh glow-discharged copper grid for 1 min. The grid was then washed 3X with water and stained for 3X10 seconds with 0.7% w/v uranyl formate. Imaging was performed on a Tecnai Spirit BioTWIN electron microscope equipped with a LaB6 gun and a 4K x 4K FEI Eagle CCD camera (FEI) and operated at 80kV.

#### **IV.5.7 Circular dichroism**

100 uL of the mHttex1 proteins during the aggregation or 120 uL of the Nt17 peptides (at 60 uM in PBS) were removed from the mixture and analyzed using a Jasco J-815 CD spectrometer and a 1.0 mm quartz cuvette. Ellipticity was measured from 195–250 nm at 25°C. The spectra were smoothed using a binomial filter with a convolution width of 99 data points, and the resulting spectra were plotted as the mean residue molar ellipticity (θMRE). Then the helical content was calculated for each peptide based on three different formula (see below), and the final reported helical content for each peptide was the average resulting value:

Formula 1 [424] : , where θ<sub>222</sub> represents the CD value at 222 nm in mean residue molar ellipticity , = -3,000 and = -39,000



Formula 2 [425]: , where  $\theta_{222}$  represents the CD value at 222 nm in mean residue molar ellipticity, and  $T$  is the temperature, and  $N_r$  is the number of residues) .

Formula 3 [426] : , where  $\theta_{222}$  represents the CD value at 222 nm in mean residue molar ellipticity, and  $n$  = number of residues.

#### IV.5.8 Nuclear Magnetic Resonance spectroscopy

All NMR experiments were carried out in a Bruker Avance III 800 MHz spectrometer equipped with a CPTC cryoprobe. Spectra for were collected at 25°C on 200  $\mu$ M protein samples, in phosphate buffer at pH 7 with 10% D<sub>2</sub>O. All spectra were acquired and processed using Bruker TopSpin 4.0 and analyzed with CARA and Sparky-NMRFAM. <sup>1</sup>H,<sup>15</sup>N HSQC and heteronuclear NOE spectra were obtained with 256 points in the <sup>15</sup>N dimension, with 1 and 3 seconds of relaxation delay, respectively. Resonance assignments were obtained by analysing a high-resolution HSQC experiment (sensitivity enhanced, 256 indirect points, 1 second recycle delay) and standard triple-resonance experiments: HNCO, HN(CA)CO, HNCA, HN(CO)CA, CBCA(CO)NH and HNCACB. These 3D experiments were acquired using standard Bruker pulse sequences, with 40 increments in <sup>15</sup>N, 128 increments in the <sup>13</sup>C dimensions, 1 second of recycle delay, and nonuniform sampling (NUS) at 50% for HNCACB or 25% for the other five spectra. Spectral analysis was carried out with the program CARA, in a process aided by previously published assignments of Httex1 [418]. Chemical shift perturbations between the unmodified and Met8ox proteins were computed as:

where  $\Delta\delta H$  is the difference in <sup>1</sup>H chemical shifts and  $\Delta\delta N$  is the difference in <sup>15</sup>N chemical shifts, and the factor 5 corresponds to the value widely used to weigh down the <sup>15</sup>N shifts. Secondary structure propensities from the <sup>13</sup>C chemical shifts ( $\Delta CA - \Delta CB$ ) were obtained by subtracting the random coil CA and CB chemical shifts of the amino acids from the experimentally observed CA and CB shifts and then subtracting the two differences. This indicator is insensitive to offsets or calibration problems in the <sup>13</sup>C dimension; a positive value above +1 indicates alpha helical propensity, and a negative value under -1 indicates beta sheet propensity. For oxidized methionine we used the standard CA and CB chemical shifts of methionine as random coil references as we could not find reliable chemical shift data for oxidized methionine in random coil conformation.

### IV.5.9 Molecular Dynamics Simulations

The starting structure for molecular dynamics simulations was a fully extended form of HTT 1-19 peptide. The length of this extended conformation was 68 Å and the buffer distance between each side of the peptide and the periodic boundary was 10 Å, resulting in a water box with a width of 88 Å. HTT 1-19 peptide was solvated using explicit CHARMM36m modified TIP3P water model and 20 mM K<sup>+</sup> and Cl<sup>-</sup> ions. Simulation was conducted with GROMACS and CHARMM-GUI was used to generate inputs. CHARMM36m forcefield was used with modified residues TP2 and ALY for phosphorylated threonine and acetylated lysine residues. The phosphate group of phosphorylated threonine was in dianionic form. The oxidized methionine used in this simulation was an R diastereomer, and its parameters were obtained from previously published papers. System was minimized with steepest decent and equilibrated to 1 atm and 303.15 K with constraints on the backbone. The nonbonded interaction cut-off was 12 Å. The time step was 1 fs for equilibration and 2 fs for production. Nosé–Hoover temperature coupling method was used to maintain temperature, and isotropic Parrinello–Rahman method was used for pressure coupling. LINCS algorithm was used for H-bond. The production was run for 13 μs.

### IV.5.10 Data Analysis

To perform dPCA [427], the dihedral angles were calculated for Nt19 backbone, and a transformation from the space of dihedral angles ( $\varphi_n, \psi_n$ ) to metric coordinate space was done by taking trigonometric function ( $\sin \varphi_n, \cos \varphi_n$ ). Then, the transformed dihedral data of each post-translationally modified Nt19 was combined and a PCA analysis was done. A free energy map was generated with the first two components. The secondary structure was obtained with the DSSP [428] algorithm implemented in VMD [429].

We analyze and compare the effects of each post-translational modification of Nt1-19 on the dynamics using a statistical analysis of the distribution of pairwise distances between residues. For each MD of Nt1-19, we reduce the ensemble of conformations to a statistical description of the distances between all pairs of Cα in Nt1-19. For each pair of residues within Nt1-19, we compute the distribution of the Euclidean distances between the two Cα with a bin resolution of 0.5 Å. We therefore describe every MD with a corresponding distogram summarizing the dynamics of a structure. The differences in residue-residue dynamics between MD can be quantified using the Kullback-Leibler divergence from a reference distogram.

## V. Conclusion

### V.1 General conclusion

Httex1 has been detected in brain tissues from HD animal models [169] and HD patients [148], and it is thought to be generated by proteolysis and aberrant splicing [148, 154]. Consistent with this hypothesis, the overexpression of mutant Httex1 containing polyQ repeats ranging from 80 to 175 glutamine residues induced a robust HD-like phenotype in various animal models (mice, *Drosophila*) [34, 146, 155, 173] and cell culture models of HD [155, 172]. *In vitro*, mutant Httex1 exhibits a polyQ-dependent aggregation and forms amyloid-like fibrils in a concentration-dependent manner [170, 171, 310]. Most of these studies linking Httex1 to HD pathology have relied mainly on unmodified mutant Httex1. However, when Htt is isolated and analyzed by the mass spectroscopy, PTMs in the Nt17 domain were consistently detected and identified in cells, animal models, and human brain tissues. Surprisingly, only a few studies have investigated the role of the Nt17 PTMs on Httex1 aggregation and toxicity. Most of the PTMs in the Nt17 were shown to decrease Htt aggregation [307, 430] toxicity [282, 307, 309] and promote its clearance [282, 284, 401]. However, these studies have relied either on Httex1-like peptide models lacking most of the PRD domain or Httex1 fused to solubilizing protein tags such as GST, which can affect its structure and aggregation properties. Furthermore, in the absence of efficient enzymes for these PTMs, the researchers relied on PTMs mimetics, which do not fully capture the physical and chemical properties of the *bona fide* PTMs. To overcome these limitations, our laboratory has developed a semisynthetic strategy to produce WT Httex1-23Q pT3 [310]. However, it was challenging to extend this method to produce modified mutant Httex1 due to its high aggregation propensity.

Understanding the effect of each PTM and elucidating the structural and functional consequences of the potential cross-talk between multiple PTMs within the Nt17 region requires the development of methodologies that permit the efficient and site-specific introduction of single and multiple PTMs as well as the generation of homogenous preparations of mutant Httex1 proteins. To achieve these goals, in Chapter I, we developed for the first time the semisynthesis strategy to produce mutant Httex1 in high yields. This methodology enabled the production of homogenous and site-specifically modified mutant Httex1 at single or multiple sites. By consequence, we were able to elucidate the effect of single phosphorylation at T3 or acetylation K6, K9 or K15, as well as the cross-talk between the two modifications (pT3/AcK6, pT3/AcK9, pT3/AcK15), on mutant Httex1 aggregation. We demonstrated that single acetylation did not affect the aggregation kinetics or structural properties of wild-type or mutant Httex1. Nevertheless, phosphorylation at T3 inhibited the aggregation of mutant Httex1, unlike the phosphomimetic mutation at T3 (T3D) that was shown to only partially inhibit this aggregation, demonstrating that this mutation does not fully reproduce the biophysical effects of

phosphorylation. By NMR, we were able to show that residues 5 to 19 have a strong tendency to form a helix, in which these residues are in a nascent helix structure in an aqueous solution that can be stabilized by alcohols and, that the helical structure of Htt1-19 is strongly stabilized when T3 is phosphorylated. Finally, we showed that K6, but not K9 or K15 acetylation reversed the inhibitory effect of T3 phosphorylation on mHttex1 aggregation. However, both NMR and CD demonstrated that acetylation at K6 did not significantly alter the Nt17 helical conformation induced by pT3, thus, this data did not support a direct and straightforward relationship between Nt17 helicity and Httex1 aggregation. Interestingly, our TR-FRET analysis, in collaboration with IRBM, showed that pT3 modification reverses the conformational flexibility of mutant Httex1, suggesting that the molecular switch by which AcK6 affects the inhibition of pT3 depends on others interactions of the Nt17 with the other domains of Httex1. More in-depth structural studies, using high-resolution methods, are needed to dissect the different mechanisms by which the PTMs-dependent molecular switches regulate Htt structure and aggregation.

The availability of these tools opened the door for several new studies and collaborations, which were not possible before the work presented in this thesis. The semisynthesis strategy has been used heavily by our laboratory to introduce other PTMs (phosphorylation at S13/S16 [329], SUMOylation, ubiquitination) or fluorescent labels into WT and mutant Httex1 [223]. Moreover, highly solubilizing conditions were used during multiple chemical reactions to facilitate the manipulation of mutant Httex1 or highly aggregation-prone proteins. Interestingly, using these modified proteins, we developed, in collaboration with IRBM, an ultrasensitive immunoassay for the detection of pT3 in complex samples [308]. We demonstrated that pT3 levels are decreased in cellular model of HD as well as in HD Mice and Human HD Samples [308], and confirmed the deleterious nature of this modification. However, these tools can represent some limitations for researchers who are not familiar with such advanced methods. Indeed, our semisynthesis strategy is time-consuming and requires advanced technical capabilities in protein chemical synthesis. Additionally, for the introduction of PTMs beyond residue 9, a non-native Gln-18 to Ala mutation is required for native chemical ligation. Finally, this method was not suitable to produce modified and isotopically labeled Httex1 proteins for NMR structural studies.

By consequence, it is critical to discover the kinases responsible for the Nt17 phosphorylation to prepare site-specifically and enzymatically phosphorylated Httex1. Towards this goal, in chapter II, we identified two kinases (GCK and TBK1) that phosphorylate efficiently and precisely at T3 and both S13 and S16, respectively. Then, we combined this discovery with our recent advances in producing Httex1 with a solubilizing SUMO tag [238] to produce milligram quantities of homogenously phosphorylated recombinant Httex1 at T3 or both S13 and S16. Next, we used these methods to prepare, for the first time, isotopically labeled phosphorylated

---

Httex1 proteins. We showed that phosphorylated Httex1 could be monitored by NMR spectroscopy with high structural and time resolution. Our preliminary studies showed that phosphorylation affected the chemical shifts of the target and neighboring residues but without any remarkable effect on the structure compared to the WT Httex1. Furthermore, we explored NMR for monitoring in vitro phosphorylation of Httex1 by TBK1, which enabled us to monitor the reaction in real-time and with higher resolution. We have found that S13 phosphorylation primed the phosphorylation of S16, again highlighting the complex cross-talk between the Nt17 PTMs. To demonstrate the versatility, we produced phosphorylated and fluorescently labeled Httex1 protein, which can have a large spectrum of applications in vitro, cells, and in vivo (see the sections below).

Based on our work and others [282, 319, 323, 329, 370, 431], it is becoming more and more evident that cracking the PTMs cross-talk code within the Nt17 is a potential key for the development of new therapeutical strategies. To contribute to further understanding this code, we aimed to study the cross-talk of the overlooked M8 oxidation (oxM8) with other Nt17 PTMs. In chapter VI, we combined chemical ( $\text{H}_2\text{O}_2$ ), semisynthetic, and enzymatic (GCK) methods to produce mutant Httex1 proteins bearing oxidized M8 alone or in combination with other PTMS (pT3 or Ack6). We demonstrated that M8 oxidation delayed the aggregation of mHttex1. We suggested that this delay is caused by the formation of oligomers at the early stages of the aggregation. Interestingly, the effect of oxM8 was more striking when oxidation at M8 was combined with Ack6 where we observed a drastic inhibition of mHttex1 aggregation and the accumulation of mainly oligomeric and short fibrillar structures. Circular dichroism analysis of the Nt17 peptides with oxM8 alone or in combination with pT3 or Ack6, showed that oxM8 decreased the helical content of the Nt17 domain. These observations were validated by atomistic molecules dynamics studies analysis of these peptides, confirming that oxM8 reduced the helical content of the Nt17 independently of the presence of other PTMs within the same sequence. Interestingly, having all the pieces of the puzzle from our aggregation and structural studies in chapter II and chapter IV, we observed that all PTMs that causes the inhibition of Httex1 aggregation, have a higher abundance of short N-term helices at the first 8 N-term residues and lower abundance of other helical conformations.

## V.2 Future perspectives

For the future applications, it is crucial to pursue the efforts to discover the enzymes responsible for the Nt17 PTMs (e.g., kinases, acetyltransferases, SUMO ligases). The discovery of such enzymes will improve our protein synthesis methods to cover all the PTMs code within the Nt17 and enable new studies to address the knowledge gap between Htt PTMs and their role in Htt functions in health and disease.

*Understanding the early oligomerization events:*

We observed the presence of oligomers at the early stages of mHttex1 aggregation with PTMs (e.g., pT3, oxM8, oxM8/Ack6). Thus, a better understanding of how these modifications affect Httex1 structure at the monomeric level is needed. To achieve this goal, we aim to use recent advances in high-resolution structural studies. Thanks to the work in this thesis, we now have all the tools to produce Httex1 with single or multiple PTMs, chemical groups or probes (e.g., fluorescent dye, biotin, spin-label) that can be suitable for multiple applications such as relaxation-based NMR [228], electron paramagnetic resonance (EPR) spectroscopy combined with site-directed spin labeling [432], as well as single-molecule FRET [223]. These methods have been shown to be valuable in determining the structure of unmodified Httex1. However, before the work presented in this thesis, it was impossible to perform similar studies on Httex1 bearing PTMs or coupled with functional chemical groups. Next, to characterize and quantify the oligomerization events of modified Httex1, we intend to apply FCS fluorescence correlation spectroscopy (FCS), size-exclusion chromatography (SEC) combined with multi-angle light scattering (MALS). Finally, our laboratory will focus on isolating and enriching these post-translationally modified oligomers for further structural characterization and cellular applications.

*Protein tools for cellular applications:*

Nt17 phosphorylation showed inhibition of mutant *in vitro*; however, it is essential to study and confirm this effect in the context of cellular conditions and access the effect of phosphorylation, alone or in combination with other PTMs, on Htt inclusions formation, toxicity, clearance, and subcellular localization. Unnatural amino acids, such as photocaged [433] or non-hydrolyzable [434] phosphorylated amino acids, have been used to control in time and space the state of availability of the phospho-group or prevent its hydrolysis in the cellular environment. Furthermore, our laboratory has already used the semisynthesis strategy reported in this thesis to produce Httex1 with non-hydrolyzable phosphonate at S13 and S16 to prevent Httex1 dephosphorylation when introduced into the cellular environment and accurately access the effect of Httex1 phosphorylation on cellular mechanisms. To study Httex1 with single or multiple PTMs, it is essential to ensure their delivery to the cells. However, this can be challenging due to the amphipathic nature of the Nt17. Several methods have been used previously, such as electroporation, or the use of polymers and nanoparticles [435]. Interestingly, our group has used the TAT penetrating peptide fused to alpha-synuclein to facilitate its delivery to the cells. Thus, we can apply the same strategy in combination with our new tools to generate Httex1 with PTMs, and a TAT peptide that can be reversibly released when the protein is delivered to the cells. This strategy will enable efficient and reproducible delivery of the modified Httex1 to the cells.

*PTMs-dependent interactomes:*

In Chapter III, we reported a method to label Httex1 on cysteine residues efficiently. Similarly, biotin-maleimide can be added into post-translationally modified Httex1 proteins and perform pull-down experiments, by the mean of streptavidin coated beads, to discover the PTMs-dependent interactome by mass spectrometry. Additionally, photoactivatable unnatural amino acids, such as photo-methionine, could be added to the modified Httex1 during the semisynthesis. Photoactivation in the presence of cell lysate or brain tissues homogenates enables the methionine to bind to transient or weak interactors in a PTMs-dependent fashion.

In summary, the semisynthetic, enzymatic, and chemical strategies described here as well as the proteins generated using these methods, provide unique tools for the investigation of the role of the PTMs code in regulating Htt structure, function, toxicity, and interactions with other proteins both *in vivo* and *in vitro*. Furthermore, our results pave the way for the development of methods for the generation of post-translationally modified longer fragments of Htt. Such proteins represent valuable tools for the development and validation of methods and assays for the identification of HD biomarkers, Nt17 PTMs-based diagnostics and novel therapeutical pathways in HD.

## VI. Bibliography

1. Vale, T.C. and F. Cardoso, *Chorea: a journey through history*. Tremor and Other Hyperkinetic Movements, 2015. **5**.
2. Jummani, R.R. and M.S. Okun, *Sydenham chorea*. Archives of neurology, 2001. **58**(2): p. 311-313.
3. Eftychiadis, A. and T. Chen, *Saint Vitus and his dance*. Journal of Neurology, Neurosurgery & Psychiatry, 2001. **70**(1): p. 14-14.
4. Aubert, G., *Charcot revisited: The case of Bruegel's chorea*. Archives of neurology, 2005. **62**(1): p. 155-161.
5. Huntington, G., *On chorea*. 1872.
6. MacDonald, M.E., et al., *A novel gene containing a trinucleotide repeat that is expanded and unstable on Huntington's disease chromosomes*. Cell, 1993. **72**(6): p. 971-983.
7. Walker, F.O., *Huntington's disease*. Lancet, 2007. **369**(9557): p. 218-28.
8. Margolis, R.L. and C.A. Ross, *Diagnosis of Huntington disease*, 2003, Oxford University Press.
9. Evans, S.J., et al., *Prevalence of adult Huntington's disease in the UK based on diagnoses recorded in general practice records*. Journal of Neurology, Neurosurgery & Psychiatry, 2013. **84**(10): p. 1156-1160.
10. Albin, R.L. and D.A. Tagle, *Genetics and molecular biology of Huntington's disease*. Trends Neurosci, 1995. **18**(1): p. 11-4.
11. Zuccato, C., M. Valenza, and E. Cattaneo, *Molecular Mechanisms and Potential Therapeutical Targets in Huntington's Disease*. Physiological Reviews, 2010. **90**(3): p. 905-981.
12. Pringsheim, T., et al., *The incidence and prevalence of Huntington's disease: a systematic review and meta-analysis*. Movement Disorders, 2012. **27**(9): p. 1083-1091.
13. Andrew, S.E., et al., *The relationship between trinucleotide (CAG) repeat length and clinical features of Huntington's disease*. Nature genetics, 1993. **4**(4): p. 398-403.
14. Labbadia, J. and R.I. Morimoto, *Huntington's disease: underlying molecular mechanisms and emerging concepts*. Trends in biochemical sciences, 2013. **38**(8): p. 378-385.
15. Duyao, M., et al., *Trinucleotide repeat length instability and age of onset in Huntington's disease*. Nature genetics, 1993. **4**(4): p. 387-392.
16. !!! INVALID CITATION !!!
17. Brinkman, R.R., et al., *The likelihood of being affected with Huntington disease by a particular age, for a specific CAG size*. American Journal of Human Genetics, 1997. **60**(5): p. 1202-1210.
18. Nance, M., et al., *Analysis of a very large trinucleotide repeat in a patient with juvenile Huntington's disease*. Neurology, 1999. **52**(2): p. 392-392.
19. Craufurd, D., J.C. Thompson, and J.S. Snowden, *Behavioral changes in Huntington disease*. Cognitive and Behavioral Neurology, 2001. **14**(4): p. 219-226.
20. McColgan, P. and S.J. Tabrizi, *Huntington's disease: a clinical review*. European journal of neurology, 2018. **25**(1): p. 24-34.
21. DiFiglia, M., *Aggregation of Huntingtin in Neuronal Intranuclear Inclusions and Dystrophic Neurites in Brain*. Science, 1997. **277**(5334): p. 1990-1993.
22. Ross, C.A. and M.A. Poirier, *Opinion: What is the role of protein aggregation in neurodegeneration?* Nat Rev Mol Cell Biol, 2005. **6**(11): p. 891-8.
23. Shin, J.Y., et al., *Expression of mutant huntingtin in glial cells contributes to neuronal excitotoxicity*. J Cell Biol, 2005. **171**(6): p. 1001-12.
24. Aylward, E.H., et al., *Onset and rate of striatal atrophy in preclinical Huntington disease*. Neurology, 2004. **63**(1): p. 66-72.
25. Vonsattel, J.P., et al., *Neuropathological Classification of Huntingtons-Disease*. Journal of Neuropathology and Experimental Neurology, 1985. **44**(6): p. 559-577.
26. Vonsattel, J.P.G., *Huntington disease models and human neuropathology: similarities and differences*. Acta neuropathologica, 2008. **115**(1): p. 55-69.
27. de la Monte, S.M., J.P. Vonsattel, and E.P. Richardson, Jr., *Morphometric demonstration of atrophic changes in the cerebral cortex, white matter, and neostriatum in Huntington's disease*. J Neuropathol Exp Neurol, 1988. **47**(5): p. 516-25.



28. Kowall, N.W., R.J. Ferrante, and J.B. Martin, *Patterns of cell loss in Huntington's disease*. Trends in Neurosciences, 1987. **10**(1): p. 24-29.
29. Ross, C.A. and S.J. Tabrizi, *Huntington's disease: from molecular pathogenesis to clinical treatment*. The Lancet Neurology, 2011. **10**(1): p. 83-98.
30. Vonsattel, J.P. and M. DiFiglia, *Huntington disease*. J Neuropathol Exp Neurol, 1998. **57**(5): p. 369-84.
31. Rubinsztein, D.C. and J. Carmichael, *Huntington's disease: molecular basis of neurodegeneration*. Expert Rev Mol Med, 2003. **5**(20): p. 1-21.
32. Ruocco, H.H., et al., *Longitudinal analysis of regional grey matter loss in Huntington disease: effects of the length of the expanded CAG repeat*. Journal of Neurology, Neurosurgery & Psychiatry, 2008. **79**(2): p. 130-135.
33. Halliday, G., et al., *Regional specificity of brain atrophy in Huntington's disease*. Experimental neurology, 1998. **154**(2): p. 663-672.
34. Davies, S.W., et al., *Formation of neuronal intranuclear inclusions underlies the neurological dysfunction in mice transgenic for the HD mutation*. Cell, 1997. **90**(3): p. 537-548.
35. Gutekunst, C.A., et al., *Nuclear and neuropil aggregates in Huntington's disease: relationship to neuropathology*. J Neurosci, 1999. **19**(7): p. 2522-34.
36. Jansen, A.H., et al., *Frequency of nuclear mutant huntingtin inclusion formation in neurons and glia is cell-type-specific*. Glia, 2017. **65**(1): p. 50-61.
37. Trotter, Y., et al., *Cellular localization of the Huntington's disease protein and discrimination of the normal and mutated form*. Nat Genet, 1995. **10**(1): p. 104-10.
38. Gutekunst, C.A., et al., *The cellular and subcellular localization of huntingtin-associated protein 1 (HAP1): comparison with huntingtin in rat and human*. J Neurosci, 1998. **18**(19): p. 7674-86.
39. Aronin, N., et al., *Are there multiple pathways in the pathogenesis of Huntington's disease?* Philosophical Transactions of the Royal Society of London. Series B: Biological Sciences, 1999. **354**(1386): p. 995-1003.
40. Seredenina, T. and R. Luthi-Carter, *What have we learned from gene expression profiles in Huntington's disease?* Neurobiology of disease, 2012. **45**(1): p. 83-98.
41. Lunkes, A., et al., *Proteases acting on mutant Huntingtin generate cleaved products that differentially build up cytoplasmic and nuclear inclusions*. Molecular Cell, 2002. **10**(2): p. 259-269.
42. Becher, M.W., et al., *Intranuclear neuronal inclusions in Huntington's disease and dentatorubral and pallidolysian atrophy: correlation between the density of inclusions and IT15 CAG triplet repeat length*. Neurobiol Dis, 1998. **4**(6): p. 387-97.
43. Kuemmerle, S., et al., *Huntington aggregates may not predict neuronal death in Huntington's disease*. Ann Neurol, 1999. **46**(6): p. 842-9.
44. Slow, E.J., et al., *Absence of behavioral abnormalities and neurodegeneration in vivo despite widespread neuronal huntingtin inclusions*. Proc Natl Acad Sci U S A, 2005. **102**(32): p. 11402-7.
45. Nekooki-Machida, Y., et al., *Distinct conformations of in vitro and in vivo amyloids of huntingtin-exon1 show different cytotoxicity*. Proc Natl Acad Sci U S A, 2009. **106**(24): p. 9679-84.
46. Arrasate, M., et al., *Inclusion body formation reduces levels of mutant huntingtin and the risk of neuronal death*. Nature, 2004. **431**(7010): p. 805-10.
47. Saudou, F., et al., *Huntingtin acts in the nucleus to induce apoptosis but death does not correlate with the formation of intranuclear inclusions*. Cell, 1998. **95**(1): p. 55-66.
48. Bodner, R.A., et al., *Pharmacological promotion of inclusion formation: a therapeutic approach for Huntington's and Parkinson's diseases*. Proceedings of the National Academy of Sciences, 2006. **103**(11): p. 4246-4251.
49. Slow, E.J., et al., *Absence of behavioral abnormalities and neurodegeneration in vivo despite widespread neuronal huntingtin inclusions*. Proceedings of the National Academy of Sciences, 2005. **102**(32): p. 11402-11407.
50. Burton, A., *Inclusion bodies may be neuroprotective in Huntington's disease*. The Lancet Neurology, 2004. **3**(12): p. 699.
51. Guedes-Dias, P. and E.L. Holzbaur, *Huntingtin Fibrils Poke Membranes*. Cell, 2017. **171**(1): p. 32-33.
52. Bäuerlein, F.J., et al., *In situ architecture and cellular interactions of PolyQ inclusions*. Cell, 2017. **171**(1): p. 179-187. e10.
53. Rosas, H., et al., *Regional and progressive thinning of the cortical ribbon in Huntington's disease*. Neurology, 2002. **58**(5): p. 695-701.
54. Pearce, M.M.P., et al., *Prion-like transmission of neuronal huntingtin aggregates to phagocytic glia in the Drosophila brain*. Nature Communications, 2015. **6**.

55. Telenius, H., et al., *Somatic and gonadal mosaicism of the Huntington disease gene CAG repeat in brain and sperm*. Nature genetics, 1994. **6**(4): p. 409-414.
56. Hayden, M.R., *Huntington's chorea*. 2012: Springer Science & Business Media.
57. Oliva, D., et al., *Clinical and magnetic resonance features of the classic and akinetic-rigid variants of Huntington's disease*. Archives of neurology, 1993. **50**(1): p. 17-19.
58. Phillips, J.G., et al., *Bradykinesia and movement precision in Huntington's disease*. Neuropsychologia, 1996. **34**(12): p. 1241-1245.
59. Vuong, K., et al., *Gait, balance, and falls in Huntington disease*, in *Handbook of clinical neurology*. 2018, Elsevier. p. 251-260.
60. Rao, A.K., E.D. Louis, and K.S. Marder, *Clinical assessment of mobility and balance impairments in pre-symptomatic Huntington's disease*. Gait & posture, 2009. **30**(3): p. 391-393.
61. Arnulf, I., et al., *Rapid eye movement sleep disturbances in Huntington disease*. Archives of neurology, 2008. **65**(4): p. 482-488.
62. Yoon, G., et al., *Speech and language delay are early manifestations of juvenile-onset Huntington disease*. Neurology, 2006. **67**(7): p. 1265-1267.
63. De Tommaso, M., et al., *Dysphagia in Huntington's disease: correlation with clinical features*. European neurology, 2015. **74**(1-2): p. 49-53.
64. Aziz, N.A., et al., *Weight loss in Huntington disease increases with higher CAG repeat number*. Neurology, 2008. **71**(19): p. 1506-1513.
65. Heemskerk, A.-W. and R.A. Roos, *Aspiration pneumonia and death in Huntington's disease*. PLoS currents, 2012. **4**.
66. Paulsen, J.S., et al., *Neuropsychiatric aspects of Huntington's disease*. Journal of Neurology, Neurosurgery & Psychiatry, 2001. **71**(3): p. 310-314.
67. Baudic, S., et al., *Cognitive impairment related to apathy in early Huntington's disease*. Dementia and geriatric cognitive disorders, 2006. **21**(5-6): p. 316-321.
68. Butters, N., et al., *Memory disorders associated with Huntington's disease: Verbal recall, verbal recognition and procedural memory*. Neuropsychologia, 1985. **23**(6): p. 729-743.
69. Gomez-Tortosa, E., et al., *Visual processing disorders in patients with Huntington's disease and asymptomatic carriers*. Journal of neurology, 1996. **243**(3): p. 286-292.
70. Labuschagne, I., et al., *Visuospatial Processing Deficits Linked to Posterior Brain Regions in Premanifest and Early Stage Huntington's Disease*. Journal of the International Neuropsychological Society, 2016: p. 1-14.
71. Novak, M.J. and S.J. Tabrizi, *Huntington's disease: clinical presentation and treatment*, in *International review of neurobiology*. 2011, Elsevier. p. 297-323.
72. Kachian, Z.R., et al., *Suicidal ideation and behavior in Huntington's disease: Systematic review and recommendations*. J Affect Disord, 2019. **250**: p. 319-329.
73. Dale, M. and E. van Duijn, *Anxiety in Huntington's disease*. The Journal of neuropsychiatry and clinical neurosciences, 2015. **27**(4): p. 262-271.
74. Brandt, J., *Behavioral Changes in Huntington Disease*. Cogn Behav Neurol, 2018. **31**(1): p. 26-35.
75. Van Duijn, E., E. Kingma, and R. Van der Mast, *Psychopathology in verified Huntington's disease gene carriers*. The Journal of neuropsychiatry and clinical neurosciences, 2007. **19**(4): p. 441-448.
76. Group, H.S., *Tetrabenazine as antichorea therapy in Huntington disease: a randomized controlled trial*. Neurology, 2006. **66**(3): p. 366-372.
77. Dean, M. and V.W. Sung, *Review of deutetrabenazine: a novel treatment for chorea associated with Huntington's disease*. Drug design, development and therapy, 2018. **12**: p. 313.
78. Yero, T. and J.A. Rey, *Tetrabenazine (Xenazine), an FDA-approved treatment option for Huntington's disease-related chorea*. Pharmacy and Therapeutics, 2008. **33**(12): p. 690.
79. Moulton, C.D., C. Hopkins, and W.R. Bevan-Jones, *Systematic review of pharmacological treatments for depressive symptoms in Huntington's disease*. Movement Disorders, 2014. **29**(12): p. 1556-1561.
80. Unti, E., et al., *Antipsychotic drugs in Huntington's disease*. Expert Rev Neurother, 2017. **17**(3): p. 227-237.
81. Lambert, M.V., *Epilepsy, Tourette's syndrome and Huntington's disease: psychiatric aspects*. Medicine, 2004. **32**(8): p. 48-50.
82. Mestre, T. and K. Shannon, *Huntington disease care: From the past to the present, to the future*. Parkinsonism & related disorders, 2017. **44**: p. 114-118.
83. Dash, D. and T.A. Mestre, *Therapeutic update on Huntington's disease: symptomatic treatments and emerging disease-modifying therapies*. Neurotherapeutics, 2020: p. 1-15.

84. Shannon, K.M., *Recent Advances in the Treatment of Huntington's Disease: Targeting DNA and RNA*. CNS drugs, 2020. **34**(3): p. 219-228.
85. Tabrizi, S.J., et al., *Targeting Huntingtin Expression in Patients with Huntington's Disease*. N Engl J Med, 2019. **380**(24): p. 2307-2316.
86. Hilditch-Maguire, P., et al., *Huntingtin: an iron-regulated protein essential for normal nuclear and perinuclear organelles*. Human molecular genetics, 2000. **9**(19): p. 2789-2797.
87. Hoffner, G., P. Kahlem, and P. Djian, *Perinuclear localization of huntingtin as a consequence of its binding to microtubules through an interaction with  $\beta$ -tubulin: relevance to Huntington's disease*. Journal of cell science, 2002. **115**(5): p. 941-948.
88. DiFiglia, M., et al., *Huntingtin is a cytoplasmic protein associated with vesicles in human and rat brain neurons*. Neuron, 1995. **14**(5): p. 1075-1081.
89. Velier, J., et al., *Wild-type and mutant huntingtins function in vesicle trafficking in the secretory and endocytic pathways*. Exp Neurol, 1998. **152**(1): p. 34-40.
90. Li, J.-Y., M. Plomann, and P. Brundin, *Huntington's disease: a synaptopathy?* Trends in molecular medicine, 2003. **9**(10): p. 414-420.
91. Bessert, D.A., et al., *The identification of a functional nuclear localization signal in the Huntington disease protein*. Brain Res Mol Brain Res, 1995. **33**(1): p. 165-73.
92. Hackam, A.S., et al., *The influence of huntingtin protein size on nuclear localization and cellular toxicity*. J Cell Biol, 1998. **141**(5): p. 1097-105.
93. Xia, J., et al., *Huntingtin contains a highly conserved nuclear export signal*. Hum Mol Genet, 2003. **12**(12): p. 1393-403.
94. Takano, H. and J.F. Gusella, *The predominantly HEAT-like motif structure of huntingtin and its association and coincident nuclear entry with dorsal, an NF-kB/Rel/dorsal family transcription factor*. BMC Neuroscience, 2002. **3**.
95. Tartari, M., et al., *Phylogenetic comparison of huntingtin homologues reveals the appearance of a primitive polyQ in sea urchin*. Molecular Biology and Evolution, 2008. **25**(2): p. 330-338.
96. Saudou, F. and S. Humbert, *The Biology of Huntingtin*. Neuron, 2016. **89**(5): p. 910-26.
97. Andrade, M.A. and P. Bork, *HEAT repeats in the Huntington's disease protein*. Nat Genet, 1995. **11**(2): p. 115-6.
98. Imarisio, S., et al., *Huntington's disease: from pathology and genetics to potential therapies*. Biochem J, 2008. **412**(2): p. 191-209.
99. Palidwor, G.A., et al., *Detection of alpha-rod protein repeats using a neural network and application to huntingtin*. PLoS Comput Biol, 2009. **5**(3): p. e1000304.
100. Huang, B., et al., *Scalable production in human cells and biochemical characterization of full-length normal and mutant huntingtin*. PLoS One, 2015. **10**(3): p. e0121055.
101. Vijayvargia, R., et al., *Huntingtin's spherical solenoid structure enables polyglutamine tract-dependent modulation of its structure and function*. Elife, 2016. **5**: p. e11184.
102. Li, W., et al., *Expression and characterization of full-length human huntingtin, an elongated HEAT repeat protein*. J Biol Chem, 2006. **281**(23): p. 15916-22.
103. Guo, Q., et al., *The cryo-electron microscopy structure of huntingtin*. Nature, 2018. **555**(7694): p. 117-120.
104. Wong, Y.C. and E.L. Holzbaur, *The regulation of autophagosome dynamics by huntingtin and HAP1 is disrupted by expression of mutant huntingtin, leading to defective cargo degradation*. Journal of Neuroscience, 2014. **34**(4): p. 1293-1305.
105. Caviston, J.P., et al., *Huntingtin coordinates the dynein-mediated dynamic positioning of endosomes and lysosomes*. Molecular biology of the cell, 2011. **22**(4): p. 478-492.
106. Liot, G., et al., *Mutant Huntingtin alters retrograde transport of TrkB receptors in striatal dendrites*. Journal of Neuroscience, 2013. **33**(15): p. 6298-6309.
107. Zala, D., M.-V. Hinckelmann, and F. Saudou, *Huntingtin's function in axonal transport is conserved in Drosophila melanogaster*. PloS one, 2013. **8**(3): p. e60162.
108. Gauthier, L.R., et al., *Huntingtin controls neurotrophic support and survival of neurons by enhancing BDNF vesicular transport along microtubules*. Cell, 2004. **118**(1): p. 127-138.
109. Caviston, J.P., et al., *Huntingtin facilitates dynein/dynactin-mediated vesicle transport*. Proceedings of the National Academy of Sciences, 2007. **104**(24): p. 10045-10050.
110. Colin, E., et al., *Huntingtin phosphorylation acts as a molecular switch for anterograde/retrograde transport in neurons*. The EMBO journal, 2008. **27**(15): p. 2124-2134.

111. Engelender, S., et al., *Huntingtin-associated protein 1 (HAP1) interacts with the p150Glued subunit of dynactin*. Hum Mol Genet, 1997. **6**(13): p. 2205-12.
112. McGuire, J.R., et al., *Interaction of Huntingtin-associated Protein-1 with Kinesin Light Chain IMPLICATIONS IN INTRACELLULAR TRAFFICKING IN NEURONS*. Journal of Biological Chemistry, 2006. **281**(6): p. 3552-3559.
113. Gunawardena, S., et al., *Disruption of axonal transport by loss of huntingtin or expression of pathogenic polyQ proteins in Drosophila*. Neuron, 2003. **40**(1): p. 25-40.
114. Godin, J.D., et al., *Huntingtin is required for mitotic spindle orientation and mammalian neurogenesis*. Neuron, 2010. **67**(3): p. 392-406.
115. Elias, S., et al., *Huntingtin regulates mammary stem cell division and differentiation*. Stem cell reports, 2014. **2**(4): p. 491-506.
116. Duyao, M.P., et al., *Inactivation of the mouse Huntington's disease gene homolog Hdh*. Science, 1995. **269**(5222): p. 407-10.
117. White, J.K., et al., *Huntingtin is required for neurogenesis and is not impaired by the Huntington's disease CAG expansion*. Nat Genet, 1997. **17**(4): p. 404-10.
118. Nasir, J., et al., *Targeted disruption of the Huntington's disease gene results in embryonic lethality and behavioral and morphological changes in heterozygotes*. Cell, 1995. **81**(5): p. 811-23.
119. Zhang, Y., et al., *Depletion of wild-type huntingtin in mouse models of neurologic diseases*. Journal of neurochemistry, 2003. **87**(1): p. 101-106.
120. Leavitt, B.R., et al., *Wild-type huntingtin protects neurons from excitotoxicity*. J Neurochem, 2006. **96**(4): p. 1121-9.
121. Rigamonti, D., et al., *Huntingtin's neuroprotective activity occurs via inhibition of procaspase-9 processing*. J Biol Chem, 2001. **276**(18): p. 14545-8.
122. Zhang, Y., et al., *Huntingtin inhibits caspase-3 activation*. The EMBO journal, 2006. **25**(24): p. 5896-5906.
123. Huang, E.J. and L.F. Reichardt, *Neurotrophins: roles in neuronal development and function*. Annual review of neuroscience, 2001. **24**(1): p. 677-736.
124. Zigova, T., et al., *Intraventricular administration of BDNF increases the number of newly generated neurons in the adult olfactory bulb*. Molecular and Cellular Neuroscience, 1998. **11**(4): p. 234-245.
125. Steffan, J.S., et al., *The Huntington's disease protein interacts with p53 and CREB-binding protein and represses transcription*. Proceedings of the National Academy of Sciences, 2000. **97**(12): p. 6763-6768.
126. Steffan, J.S., et al., *The Huntington's disease protein interacts with p53 and CREB-binding protein and represses transcription*. Proc Natl Acad Sci U S A, 2000. **97**(12): p. 6763-8.
127. Bae, B.-I., et al., *p53 mediates cellular dysfunction and behavioral abnormalities in Huntington's disease*. Neuron, 2005. **47**(1): p. 29-41.
128. Dunah, A.W., et al., *Sp1 and TAFII130 transcriptional activity disrupted in early Huntington's disease*. Science, 2002. **296**(5576): p. 2238-43.
129. Futter, M., et al., *Wild-type but not mutant huntingtin modulates the transcriptional activity of liver X receptors*. Journal of medical genetics, 2009. **46**(7): p. 438-446.
130. Zuccato, C., et al., *Huntingtin interacts with REST/NRSF to modulate the transcription of NRSE-controlled neuronal genes*. Nat Genet, 2003. **35**(1): p. 76-83.
131. Seong, I.S., et al., *Huntingtin facilitates polycomb repressive complex 2*. Human Molecular Genetics, 2009. **19**(4): p. 573-583.
132. Kumar, A., M. Vaish, and R.R. Ratan, *Transcriptional dysregulation in Huntington's disease: a failure of adaptive transcriptional homeostasis*. Drug discovery today, 2014. **19**(7): p. 956-962.
133. Rui, Y.-N., et al., *Huntingtin functions as a scaffold for selective macroautophagy*. Nature cell biology, 2015. **17**(3): p. 262-275.
134. Ochaba, J., et al., *Potential function for the Huntingtin protein as a scaffold for selective autophagy*. Proceedings of the National Academy of Sciences, 2014. **111**(47): p. 16889-16894.
135. Strehlow, A.N., J.Z. Li, and R.M. Myers, *Wild-type huntingtin participates in protein trafficking between the Golgi and the extracellular space*. Human molecular genetics, 2007. **16**(4): p. 391-409.
136. Sahlender, D.A., et al., *Optineurin links myosin VI to the Golgi complex and is involved in Golgi organization and exocytosis*. The Journal of cell biology, 2005. **169**(2): p. 285-295.
137. Ratovitski, T., et al., *Huntingtin protein interactions altered by polyglutamine expansion as determined by quantitative proteomic analysis*. Cell Cycle, 2012. **11**(10): p. 2006-21.
138. Cornett, J., et al., *Polyglutamine expansion of huntingtin impairs its nuclear export*. Nature Genetics, 2005. **37**(2): p. 198-204.

139. Baquet, Z.C., J.A. Gorski, and K.R. Jones, *Early striatal dendrite deficits followed by neuron loss with advanced age in the absence of anterograde cortical brain-derived neurotrophic factor*. J Neurosci, 2004. **24**(17): p. 4250-8.
140. Cong, S.Y., et al., *Mutant huntingtin represses CBP, but not p300, by binding and protein degradation*. Mol Cell Neurosci, 2005. **30**(4): p. 560-71.
141. Nucifora, F.C., Jr., et al., *Interference by huntingtin and atrophin-1 with cbp-mediated transcription leading to cellular toxicity*. Science, 2001. **291**(5512): p. 2423-8.
142. Zuccato, C., et al., *Loss of huntingtin-mediated BDNF gene transcription in Huntington's disease*. Science, 2001. **293**(5529): p. 493-8.
143. Hodges, A., et al., *Regional and cellular gene expression changes in human Huntington's disease brain*. Hum Mol Genet, 2006. **15**(6): p. 965-77.
144. Martinez-Vicente, M., et al., *Cargo recognition failure is responsible for inefficient autophagy in Huntington's disease*. Nat Neurosci, 2010. **13**(5): p. 567-76.
145. Martin, D.D., et al., *Identification of a post-translationally myristoylated autophagy-inducing domain released by caspase cleavage of huntingtin*. Human molecular genetics, 2014. **23**(12): p. 3166-3179.
146. Mangiarini, L., et al., *Exon 1 of the HD gene with an expanded CAG repeat is sufficient to cause a progressive neurological phenotype in transgenic mice*. Cell, 1996. **87**(3): p. 493-506.
147. Landles, C., et al., *Proteolysis of mutant huntingtin produces an exon 1 fragment that accumulates as an aggregated protein in neuronal nuclei in Huntington disease*. Journal of Biological Chemistry, 2010. **285**(12): p. 8808-8823.
148. Sathasivam, K., et al., *Aberrant splicing of HTT generates the pathogenic exon 1 protein in Huntington disease*. Proc Natl Acad Sci U S A, 2013. **110**(6): p. 2366-70.
149. Goldberg, Y.P., et al., *Cleavage of huntingtin by apopain, a proapoptotic cysteine protease, is modulated by the polyglutamine tract*. Nature Genetics, 1996. **13**(4): p. 442-449.
150. Wellington, C.L., et al., *Caspase cleavage of gene products associated with triplet expansion disorders generates truncated fragments containing the polyglutamine tract*. J Biol Chem, 1998. **273**(15): p. 9158-67.
151. Qin, Z.H. and Z.L. Gu, *Huntingtin processing in pathogenesis of Huntington disease*. Acta Pharmacol Sin, 2004. **25**(10): p. 1243-9.
152. Goldberg, Y.P., et al., *Cleavage of huntingtin by apopain, a proapoptotic cysteine protease, is modulated by the polyglutamine tract*. Nat Genet, 1996. **13**(4): p. 442-9.
153. Martin, I., et al., *Ribosomal Protein s15 Phosphorylation Mediates LRRK2 Neurodegeneration in Parkinson's Disease*. Cell, 2014. **157**(2): p. 472-485.
154. El-Daher, M.T., et al., *Huntingtin proteolysis releases non-polyQ fragments that cause toxicity through dynamin 1 dysregulation*. Embo Journal, 2015. **34**(17): p. 2255-2271.
155. Martindale, D., et al., *Length of huntingtin and its polyglutamine tract influences localization and frequency of intracellular aggregates*. Nature Genetics, 1998. **18**(2): p. 150-154.
156. Schilling, G., et al., *Intranuclear inclusions and neuritic aggregates in transgenic mice expressing a mutant N-terminal fragment of huntingtin (vol 8, pg 397, 1999)*. Human Molecular Genetics, 1999. **8**(5): p. 943-943.
157. Slow, E.J., et al., *Selective striatal neuronal loss in a YAC128 mouse model of Huntington disease*. Hum Mol Genet, 2003. **12**(13): p. 1555-67.
158. Tebbenkamp, A.T., et al., *Transgenic mice expressing caspase-6-derived N-terminal fragments of mutant huntingtin develop neurologic abnormalities with predominant cytoplasmic inclusion pathology composed largely of a smaller proteolytic derivative*. Human molecular genetics, 2011. **20**(14): p. 2770-2782.
159. Waldron-Roby, E., et al., *Transgenic mouse model expressing the caspase 6 fragment of mutant huntingtin*. J Neurosci, 2012. **32**(1): p. 183-93.
160. Sugars, K.L. and D.C. Rubinsztein, *Transcriptional abnormalities in Huntington disease*. Trends Genet, 2003. **19**(5): p. 233-8.
161. Tian, J., et al., *Soluble N-terminal fragment of mutant Huntingtin protein impairs mitochondrial axonal transport in cultured hippocampal neurons*. Neuroscience bulletin, 2014. **30**(1): p. 74-80.
162. Graham, R.K., et al., *Cleavage at the caspase-6 site is required for neuronal dysfunction and degeneration due to mutant huntingtin*. Cell, 2006. **125**(6): p. 1179-1191.
163. Gafni, J. and L.M. Ellerby, *Calpain activation in Huntington's disease*. Journal of Neuroscience, 2002. **22**(12): p. 4842-4849.
164. Miller, J.P., et al., *Matrix metalloproteinases are modifiers of huntingtin proteolysis and toxicity in Huntington's disease*. Neuron, 2010. **67**(2): p. 199-212.

165. Ratovitski, T., et al., *N-terminal proteolysis of full-length mutant huntingtin in an inducible PC12 cell model of Huntington's disease*. Cell Cycle, 2007. **6**(23): p. 2970-81.
166. Ratovitski, T., et al., *Mutant huntingtin N-terminal fragments of specific size mediate aggregation and toxicity in neuronal cells*. J Biol Chem, 2009. **284**(16): p. 10855-67.
167. Farshim, P.P. and G.P. Bates, *Mouse models of Huntington's disease*, in *Huntington's Disease*. 2018, Springer. p. 97-120.
168. Crook, Z.R. and D. Housman, *Huntington's disease: can mice lead the way to treatment?* Neuron, 2011. **69**(3): p. 423-435.
169. Yang, H., et al., *Truncation of mutant huntingtin in knock-in mice demonstrates exon1 huntingtin is a key pathogenic form*. Nature communications, 2020. **11**(1): p. 1-15.
170. Scherzinger, E., et al., *Huntingtin-encoded polyglutamine expansions form amyloid-like protein aggregates in vitro and in vivo*. Cell, 1997. **90**(3): p. 549-558.
171. Hollenbach, B., et al., *Aggregation of truncated GST-HD exon 1 fusion proteins containing normal range and expanded glutamine repeats*. Philosophical Transactions of the Royal Society of London Series B-Biological Sciences, 1999. **354**(1386): p. 991-994.
172. Scherzinger, E., et al., *Self-assembly of polyglutamine-containing huntingtin fragments into amyloid-like fibrils: Implications for Huntington's disease pathology*. Proceedings of the National Academy of Sciences of the United States of America, 1999. **96**(8): p. 4604-4609.
173. Barbaro, B.A., et al., *Comparative study of naturally occurring huntingtin fragments in Drosophila points to exon 1 as the most pathogenic species in Huntington's disease*. Hum Mol Genet, 2015. **24**(4): p. 913-25.
174. Neueder, A., et al., *The pathogenic exon 1 HTT protein is produced by incomplete splicing in Huntington's disease patients*. Scientific Reports, 2017. **7**.
175. Kim, M.W., et al., *Secondary structure of Huntingtin amino-terminal region*. Structure, 2009. **17**(9): p. 1205-12.
176. Thakur, A.K., et al., *Polyglutamine disruption of the huntingtin exon 1 N terminus triggers a complex aggregation mechanism*. Nat Struct Mol Biol, 2009. **16**(4): p. 380-9.
177. Crick, S.L., et al., *Unmasking the roles of N- and C-terminal flanking sequences from exon 1 of huntingtin as modulators of polyglutamine aggregation*. Proc Natl Acad Sci U S A, 2013. **110**(50): p. 20075-80.
178. Vieweg, S., et al., *An Intein-based Strategy for the Production of Tag-free Huntingtin Exon 1 Proteins Enables New Insights into the Polyglutamine Dependence of Httex1 Aggregation and Fibril Formation*. J Biol Chem, 2016. **291**(23): p. 12074-86.
179. Butland, S.L., et al., *CAG-encoded polyglutamine length polymorphism in the human genome*. BMC Genomics, 2007. **8**: p. 126.
180. Gerber, H.-P., et al., *Transcriptional activation modulated by homopolymeric glutamine and proline stretches*. Science, 1994. **263**(5148): p. 808-811.
181. Johannessen, M., M.P. Delghandi, and U. Moens, *What turns CREB on?* Cell Signal, 2004. **16**(11): p. 1211-27.
182. Atanesyan, L., et al., *Polyglutamine tracts as modulators of transcriptional activation from yeast to mammals*. Biol Chem, 2012. **393**(1-2): p. 63-70.
183. Schaefer, M.H., E.E. Wanker, and M.A. Andrade-Navarro, *Evolution and function of CAG/polyglutamine repeats in protein-protein interaction networks*. Nucleic Acids Research, 2012. **40**(10): p. 4273-4287.
184. Ashkenazi, A., et al., *Polyglutamine tracts regulate autophagy*. Autophagy, 2017. **13**(9): p. 1613-1614.
185. Wetzel, R., *Physical chemistry of polyglutamine: intriguing tales of a monotonous sequence*. J Mol Biol, 2012. **421**(4-5): p. 466-90.
186. Altschuler, E.L., et al., *Random coil conformation for extended polyglutamine stretches in aqueous soluble monomeric peptides*. J Pept Res, 1997. **50**(1): p. 73-5.
187. Wang, X., et al., *Characterizing the conformational ensemble of monomeric polyglutamine*. Proteins, 2006. **63**(2): p. 297-311.
188. Bhattacharyya, A., et al., *Oligoproline effects on polyglutamine conformation and aggregation*. J Mol Biol, 2006. **355**(3): p. 524-35.
189. Nagai, Y., et al., *A toxic monomeric conformer of the polyglutamine protein*. Nat Struct Mol Biol, 2007. **14**(4): p. 332-40.
190. Masino, L., *Polyglutamine and neurodegeneration: structural aspects*. Protein Pept Lett, 2004. **11**(3): p. 239-48.
191. Kim, M., *Beta conformation of polyglutamine track revealed by a crystal structure of Huntingtin N-terminal region with insertion of three histidine residues*. Prion, 2013. **7**(3): p. 221-8.
192. Urbanek, A., et al., *Flanking Regions Determine the Structure of the Poly-Glutamine in Huntingtin through Mechanisms Common among Glutamine-Rich Human Proteins*. Structure, 2020.

193. Urbanek, A., et al., *A general strategy to access structural information at atomic resolution in polyglutamine homorepeats*. Angewandte Chemie International Edition, 2018. **57**(14): p. 3598-3601.
194. Rossetti, G., et al., *Conformations of the Huntingtin N-term in aqueous solution from atomistic simulations*. FEBS Lett, 2011. **585**(19): p. 3086-9.
195. Kelley, N.W., et al., *The Predicted Structure of the Headpiece of the Huntingtin Protein and Its Implications on Huntingtin Aggregation*. Journal of Molecular Biology, 2009. **388**(5): p. 919-927.
196. Jayaraman, M., et al., *Slow Amyloid Nucleation via alpha-Helix-Rich Oligomeric Intermediates in Short Polyglutamine-Containing Huntingtin Fragments*. Journal of Molecular Biology, 2012. **415**(5): p. 881-899.
197. Michalek, M., E.S. Salnikov, and B. Bechinger, *Structure and topology of the huntingtin 1-17 membrane anchor by a combined solution and solid-state NMR approach*. Biophys J, 2013. **105**(3): p. 699-710.
198. Williamson, T.E., et al., *Modulation of polyglutamine conformations and dimer formation by the N-terminus of huntingtin*. J Mol Biol, 2010. **396**(5): p. 1295-309.
199. Monsellier, E., et al., *Molecular Interaction between the Chaperone Hsc70 and the N-terminal Flank of Huntingtin Exon 1 Modulates Aggregation*. Journal of Biological Chemistry, 2015. **290**(5): p. 2560-2576.
200. He, W.-T., et al., *HSP90 recognizes the N-terminus of huntingtin involved in regulation of huntingtin aggregation by USP19*. Scientific Reports, 2017. **7**(1): p. 14797.
201. Atwal, R.S., et al., *Huntingtin has a membrane association signal that can modulate huntingtin aggregation, nuclear entry and toxicity*. Hum Mol Genet, 2007. **16**(21): p. 2600-15.
202. Michalek, M., E.S. Salnikov, and B. Bechinger, *Structure and Topology of the Huntingtin 1-17 Membrane Anchor by a Combined Solution and Solid-State NMR Approach*. Biophysical Journal, 2013. **105**(3): p. 699-710.
203. Michalek, M., et al., *Membrane interactions of the amphipathic amino terminus of huntingtin*. Biochemistry, 2013. **52**(5): p. 847-58.
204. Cote, S., et al., *Probing the Huntingtin 1-17 membrane anchor on a phospholipid bilayer by using all-atom simulations*. Biophys J, 2015. **108**(5): p. 1187-98.
205. Atwal, R.S. and R. Truant, *A stress sensitive ER membrane-association domain in Huntingtin protein defines a potential role for Huntingtin in the regulation of autophagy*. Autophagy, 2008. **4**(1): p. 91-3.
206. Rockabrand, E., et al., *The first 17 amino acids of Huntingtin modulate its sub-cellular localization, aggregation and effects on calcium homeostasis*. Hum Mol Genet, 2007. **16**(1): p. 61-77.
207. Westerlund, J.A. and K.H. Weisgraber, *Discrete carboxyl-terminal segments of apolipoprotein E mediate lipoprotein association and protein oligomerization*. J Biol Chem, 1993. **268**(21): p. 15745-50.
208. Gu, X.F., et al., *N17 Modifies Mutant Huntingtin Nuclear Pathogenesis and Severity of Disease in HD BAC Transgenic Mice*. Neuron, 2015. **85**(4): p. 726-741.
209. Gu, X., et al., *Serines 13 and 16 are critical determinants of full-length human mutant huntingtin induced disease pathogenesis in HD mice*. Neuron, 2009. **64**(6): p. 828-40.
210. Maiuri, T., et al., *The huntingtin N17 domain is a multifunctional CRM1 and Ran-dependent nuclear and cilia export signal*. Human Molecular Genetics, 2013. **22**(7): p. 1383-1394.
211. Chaibva, M., et al., *Acetylation within the First 17 Residues of Huntingtin Exon 1 Alters Aggregation and Lipid Binding*. Biophysical Journal, 2016. **111**(2): p. 349-362.
212. Tam, S., et al., *The chaperonin TRiC blocks a huntingtin sequence element that promotes the conformational switch to aggregation*. Nat Struct Mol Biol, 2009. **16**(12): p. 1279-85.
213. Zheng, Z., et al., *An N-terminal nuclear export signal regulates trafficking and aggregation of Huntingtin (Htt) protein exon 1*. J Biol Chem, 2013. **288**(9): p. 6063-71.
214. Lakhani, V.V., F. Ding, and N.V. Dokholyan, *Polyglutamine Induced Misfolding of Huntingtin Exon1 is Modulated by the Flanking Sequences*. Plos Computational Biology, 2010. **6**(4).
215. Darnell, G., et al., *Flanking polyproline sequences inhibit beta-sheet structure in polyglutamine segments by inducing PPII-like helix structure*. J Mol Biol, 2007. **374**(3): p. 688-704.
216. Darnell, G.D., et al., *Mechanism of cis-inhibition of polyQ fibrillation by polyP: PPII oligomers and the hydrophobic effect*. Biophys J, 2009. **97**(8): p. 2295-305.
217. Dehay, B. and A. Bertolotti, *Critical role of the proline-rich region in Huntingtin for aggregation and cytotoxicity in yeast*. Journal of Biological Chemistry, 2006. **281**(47): p. 35608-35615.
218. Chen, S.M., et al., *Amyloid-like features of polyglutamine aggregates and their assembly kinetics*. Biochemistry, 2002. **41**(23): p. 7391-7399.
219. Poirier, M.A., et al., *Huntingtin spheroids and protofibrils as precursors in polyglutamine fibrilization*. Journal of Biological Chemistry, 2002. **277**(43): p. 41032-41037.

220. Mishra, R., et al., *Inhibiting the nucleation of amyloid structure in a huntingtin fragment by targeting alpha-helix-rich oligomeric intermediates*. J Mol Biol, 2012. **415**(5): p. 900-17.
221. Sivanandam, V.N., et al., *The Aggregation-Enhancing Huntingtin N-Terminus Is Helical in Amyloid Fibrils*. Journal of the American Chemical Society, 2011. **133**(12): p. 4558-4566.
222. Pandey, N.K., et al., *The 17-residue-long N terminus in huntingtin controls step-wise aggregation in solution and on membranes via different mechanisms*. J Biol Chem, 2017.
223. Warner, J.B., et al., *Monomeric Huntingtin Exon 1 Has Similar Overall Structural Features for Wild-Type and Pathological Polyglutamine Lengths*. Journal of the American Chemical Society, 2017. **139**(41): p. 14456-14469.
224. Wagner, A.S., et al., *Self-assembly of Mutant Huntingtin Exon-1 Fragments into Large Complex Fibrillar Structures Involves Nucleated Branching*. J Mol Biol, 2018. **430**(12): p. 1725-1744.
225. Crick, S.L., et al., *Unmasking the roles of N-and C-terminal flanking sequences from exon 1 of huntingtin as modulators of polyglutamine aggregation*. Proceedings of the National Academy of Sciences, 2013. **110**(50): p. 20075-20080.
226. Sahoo, B., et al., *Folding Landscape of Mutant Huntingtin Exon1: Diffusible Multimers, Oligomers and Fibrils, and No Detectable Monomer*. PLoS One, 2016. **11**(6): p. e0155747.
227. Ceccon, A., et al., *Abrogation of prenucleation, transient oligomerization of the Huntingtin exon 1 protein by human profilin I*. Proceedings of the National Academy of Sciences, 2020. **117**(11): p. 5844-5852.
228. Ceccon, A., V. Tugarinov, and G.M. Clore, *Kinetics of Fast Tetramerization of the Huntingtin Exon 1 Protein Probed by Concentration-Dependent On-Resonance R(1ρ) Measurements*. J Phys Chem Lett, 2020. **11**(14): p. 5643-5648.
229. Kotler, S.A., et al., *Probing initial transient oligomerization events facilitating Huntingtin fibril nucleation at atomic resolution by relaxation-based NMR*. Proceedings of the National Academy of Sciences, 2019. **116**(9): p. 3562-3571.
230. Walters, R.H. and R.M. Murphy, *Examining polyglutamine peptide length: a connection between collapsed conformations and increased aggregation*. J Mol Biol, 2009. **393**(4): p. 978-92.
231. Bhattacharyya, A.M., A.K. Thakur, and R. Wetzel, *Polyglutamine aggregation nucleation: Thermodynamics of a highly unfavorable protein folding reaction*. Proceedings of the National Academy of Sciences of the United States of America, 2005. **102**(43): p. 15400-15405.
232. Sahoo, B., et al., *Aggregation Behavior of Chemically Synthesized, Full-Length Huntingtin Exon1*. Biochemistry, 2014. **53**(24): p. 3897-3907.
233. Chen, S.M. and R. Wetzel, *Solubilization and disaggregation of polyglutamine peptides*. Protein Science, 2001. **10**(4): p. 887-891.
234. Mishra, R., et al., *Serine phosphorylation suppresses huntingtin amyloid accumulation by altering protein aggregation properties*. J Mol Biol, 2012. **424**(1-2): p. 1-14.
235. Muchowski, P.J., et al., *Noninvasive measurement of protein aggregation by mutant huntingtin fragments or alpha-synuclein in the lens*. J Biol Chem, 2008. **283**(10): p. 6330-6.
236. Duim, W.C., et al., *Super-resolution fluorescence of huntingtin reveals growth of globular species into short fibers and coexistence of distinct aggregates*. ACS chemical biology, 2014. **9**(12): p. 2767-2778.
237. Bugg, C.W., et al., *Structural features and domain organization of huntingtin fibrils*. J Biol Chem, 2012. **287**(38): p. 31739-46.
238. Reif, A., et al., *Generation of Native, Untagged Huntingtin Exon1 Monomer and Fibrils Using a SUMO Fusion Strategy*. J Vis Exp, 2018(136).
239. Walsh, C.T., S. Garneau-Tsodikova, and G.J. Gatto Jr, *Protein posttranslational modifications: the chemistry of proteome diversifications*. Angewandte Chemie International Edition, 2005. **44**(45): p. 7342-7372.
240. Santos, A.L. and A.B. Lindner, *Protein posttranslational modifications: roles in aging and age-related disease*. Oxidative Medicine and Cellular Longevity, 2017. **2017**.
241. Mittal, S. and D. Saluja, *Protein post-translational modifications: role in protein structure, function and stability, in Proteostasis and Chaperone Surveillance*. 2015, Springer. p. 25-37.
242. Johnson, L.N. and R.J. Lewis, *Structural basis for control by phosphorylation*. Chem Rev, 2001. **101**(8): p. 2209-42.
243. Duan, G. and D. Walther, *The roles of post-translational modifications in the context of protein interaction networks*. PLoS Comput Biol, 2015. **11**(2): p. e1004049.
244. Dantuma, N.P. and H. van Attikum, *Spatiotemporal regulation of posttranslational modifications in the DNA damage response*. The EMBO journal, 2016. **35**(1): p. 6-23.



245. Mann, M., et al., *Analysis of protein phosphorylation using mass spectrometry: deciphering the phosphoproteome*. Trends in biotechnology, 2002. **20**(6): p. 261-268.
246. Hunter, T., *Protein kinases and phosphatases: the yin and yang of protein phosphorylation and signaling*. Cell, 1995. **80**(2): p. 225-236.
247. Garcia-Garcia, T., et al., *Role of protein phosphorylation in the regulation of cell cycle and DNA-related processes in bacteria*. Frontiers in Microbiology, 2016. **7**: p. 184.
248. Mishra, K. and V.K. Parnaik, *Essential role of protein phosphorylation in nuclear transport*. Experimental cell research, 1995. **216**(1): p. 124-134.
249. Johnson, G.V., *Tau phosphorylation and proteolysis: insights and perspectives*. Journal of Alzheimer's Disease, 2006. **9**(s3): p. 243-250.
250. Ardito, F., et al., *The crucial role of protein phosphorylation in cell signaling and its use as targeted therapy*. International journal of molecular medicine, 2017. **40**(2): p. 271-280.
251. Nishi, H., K. Hashimoto, and A.R. Panchenko, *Phosphorylation in protein-protein binding: effect on stability and function*. Structure, 2011. **19**(12): p. 1807-1815.
252. Stork, B., et al., *Regulation of autophagy by protein phosphorylation*. Protein phosphorylation in human health. Edited by C. Huang. IntechOpen, 2012: p. 97-118.
253. Gjertsen, B.T. and S.O. Døskeland, *Protein phosphorylation in apoptosis*. Biochimica et Biophysica Acta (BBA)-Molecular Cell Research, 1995. **1269**(2): p. 187-199.
254. Karve, T.M. and A.K. Cheema, *Small changes huge impact: the role of protein posttranslational modifications in cellular homeostasis and disease*. Journal of amino acids, 2011. **2011**.
255. Li, P., J. Ge, and H. Li, *Lysine acetyltransferases and lysine deacetylases as targets for cardiovascular disease*. Nature Reviews Cardiology, 2019: p. 1-20.
256. Narita, T., B.T. Weinert, and C. Choudhary, *Functions and mechanisms of non-histone protein acetylation*. Nature Reviews Molecular Cell Biology, 2019. **20**(3): p. 156-174.
257. Spange, S., et al., *Acetylation of non-histone proteins modulates cellular signalling at multiple levels*. The international journal of biochemistry & cell biology, 2009. **41**(1): p. 185-198.
258. Verdone, L., M. Caserta, and E.D. Mauro, *Role of histone acetylation in the control of gene expression*. Biochemistry and Cell Biology, 2005. **83**(3): p. 344-353.
259. Zhao, S., et al., *Regulation of cellular metabolism by protein lysine acetylation*. Science, 2010. **327**(5968): p. 1000-1004.
260. Scott, I., et al., *Lysine post-translational modifications and the cytoskeleton*. Essays in biochemistry, 2012. **52**: p. 135-145.
261. McBrien, M.A., et al., *Histone acetylation regulates intracellular pH*. Molecular cell, 2013. **49**(2): p. 310-321.
262. Cheung, P., et al., *Synergistic coupling of histone H3 phosphorylation and acetylation in response to epidermal growth factor stimulation*. Molecular cell, 2000. **5**(6): p. 905-915.
263. Yang, X.-J. and E. Seto, *Lysine acetylation: codified crosstalk with other posttranslational modifications*. Molecular cell, 2008. **31**(4): p. 449-461.
264. Kovacs, J.J., et al., *HDAC6 regulates Hsp90 acetylation and chaperone-dependent activation of glucocorticoid receptor*. Molecular cell, 2005. **18**(5): p. 601-607.
265. Sadoul, K., et al., *Regulation of protein turnover by acetyltransferases and deacetylases*. Biochimie, 2008. **90**(2): p. 306-312.
266. Yang, X.J. and S. Grégoire, *Metabolism, cytoskeleton and cellular signalling in the grip of protein Nε-and O-acetylation*. EMBO reports, 2007. **8**(6): p. 556-562.
267. Boyes, J., et al., *Regulation of activity of the transcription factor GATA-1 by acetylation*. Nature, 1998. **396**(6711): p. 594-598.
268. Soutoglou, E., N. Katrakili, and I. Talianidis, *Acetylation regulates transcription factor activity at multiple levels*. Molecular cell, 2000. **5**(4): p. 745-751.
269. Scott, I., M. Neutzner, and A. Neutzner, *Enzymes of ubiquitination and deubiquitination*. Essays in biochemistry, 2012. **52**: p. 37-50.
270. Wilkinson, K.D., *Regulation of ubiquitin-dependent processes by deubiquitinating enzymes*. The FASEB Journal, 1997. **11**(14): p. 1245-1256.
271. Nandi, D., et al., *The ubiquitin-proteasome system*. Journal of biosciences, 2006. **31**(1): p. 137-155.
272. Chen, Z.J. and L.J. Sun, *Nonproteolytic functions of ubiquitin in cell signaling*. Molecular cell, 2009. **33**(3): p. 275-286.

273. Pickart, C.M. and M.J. Eddins, *Ubiquitin: structures, functions, mechanisms*. Biochimica et Biophysica Acta (BBA)-Molecular Cell Research, 2004. **1695**(1-3): p. 55-72.
274. Pentecost, M., et al., *Evidence for ubiquitin-regulated nuclear and subnuclear trafficking among Paramyxovirinae matrix proteins*. PLoS Pathog, 2015. **11**(3): p. e1004739.
275. Wilkinson, K.A. and J.M. Henley, *Mechanisms, regulation and consequences of protein SUMOylation*. Biochemical Journal, 2010. **428**(2): p. 133-145.
276. Albuquerque, C., et al., *A new approach to study site-specific protein sumoylation (925.3)*. The FASEB Journal, 2014. **28**(1 supplement): p. 925.3.
277. Ghioni, P., et al., *The protein stability and transcriptional activity of p63 $\alpha$  are regulated by SUMO-1 conjugation*. Cell cycle, 2005. **4**(1): p. 183-190.
278. Santiago, A., et al., *p53 SUMOylation promotes its nuclear export by facilitating its release from the nuclear export receptor CRM1*. Molecular biology of the cell, 2013. **24**(17): p. 2739-2752.
279. Lyst, M.J. and I. Stancheva, *A role for SUMO modification in transcriptional repression and activation*, 2007, Portland Press Ltd.
280. Cui, Z.J., Z.Q. Han, and Z.Y. Li, *Modulating protein activity and cellular function by methionine residue oxidation*. Amino acids, 2012. **43**(2): p. 505-517.
281. Hoshi, T. and S. Heinemann, *Regulation of cell function by methionine oxidation and reduction*. J Physiol, 2001. **531**(Pt 1): p. 1-11.
282. Thompson, L.M., et al., *IKK phosphorylates Huntingtin and targets it for degradation by the proteasome and lysosome*. J Cell Biol, 2009. **187**(7): p. 1083-99.
283. Cong, X., et al., *Mass spectrometric identification of novel lysine acetylation sites in huntingtin*. Mol Cell Proteomics, 2011. **10**(10): p. M111 009829.
284. Steffan, J.S., et al., *SUMO modification of Huntingtin and Huntington's disease pathology*. Science, 2004. **304**(5667): p. 100-104.
285. Watkin, E.E., et al., *Phosphorylation of mutant huntingtin at serine 116 modulates neuronal toxicity*. PLoS One, 2014. **9**(2): p. e88284.
286. Jeong, H., et al., *Acetylation targets mutant huntingtin to autophagosomes for degradation*. Cell, 2009. **137**(1): p. 60-72.
287. Schilling, B., et al., *Huntingtin phosphorylation sites mapped by mass spectrometry. Modulation of cleavage and toxicity*. J Biol Chem, 2006. **281**(33): p. 23686-97.
288. Ratovitski, T., et al., *Post-translational modifications (PTMs), identified on endogenous huntingtin, cluster within proteolytic domains between HEAT repeats*. Journal of proteome research, 2017. **16**(8): p. 2692-2708.
289. Harding, R.J., et al., *Design and characterization of mutant and wildtype huntingtin proteins produced from a toolkit of scalable eukaryotic expression systems*. Journal of Biological Chemistry, 2019. **294**(17): p. 6986-7001.
290. Warby, S.C., et al., *Huntingtin phosphorylation on serine 421 is significantly reduced in the striatum and by polyglutamine expansion in vivo*. Human molecular genetics, 2005. **14**(11): p. 1569-1577.
291. Humbert, S., et al., *The IGF-1/Akt pathway is neuroprotective in Huntington's disease and involves Huntingtin phosphorylation by Akt*. Developmental cell, 2002. **2**(6): p. 831-837.
292. Colin, E., et al., *Huntingtin phosphorylation acts as a molecular switch for anterograde/retrograde transport in neurons*. EMBO J, 2008. **27**(15): p. 2124-34.
293. Rangone, H., et al., *The serum- and glucocorticoid-induced kinase SGK inhibits mutant huntingtin-induced toxicity by phosphorylating serine 421 of huntingtin*. European Journal of Neuroscience, 2004. **19**(2): p. 273-279.
294. Pardo, R., et al., *Inhibition of calcineurin by FK506 protects against polyglutamine-huntingtin toxicity through an increase of huntingtin phosphorylation at S421*. J Neurosci, 2006. **26**(5): p. 1635-45.
295. Warby, S.C., et al., *Phosphorylation of huntingtin reduces the accumulation of its nuclear fragments*. Mol Cell Neurosci, 2009. **40**(2): p. 121-7.
296. Metzler, M., et al., *Phosphorylation of huntingtin at Ser421 in YAC128 neurons is associated with protection of YAC128 neurons from NMDA-mediated excitotoxicity and is modulated by PP1 and PP2A*. J Neurosci, 2010. **30**(43): p. 14318-29.
297. Luo, S.Q., et al., *Cdk5 phosphorylation of huntingtin reduces its cleavage by caspases: implications for mutant huntingtin toxicity*. Journal of Cell Biology, 2005. **169**(4): p. 647-656.
298. Zala, D., et al., *Phosphorylation of mutant huntingtin at S421 restores anterograde and retrograde transport in neurons*. Hum Mol Genet, 2008. **17**(24): p. 3837-46.

299. Anne, S.L., F. Saudou, and S. Humbert, *Phosphorylation of huntingtin by cyclin-dependent kinase 5 is induced by DNA damage and regulates wild-type and mutant huntingtin toxicity in neurons*. Journal of Neuroscience, 2007. **27**(27): p. 7318-7328.
300. Jiang, M., et al., *Nemo-like kinase reduces mutant huntingtin levels and mitigates Huntington's disease*. Human Molecular Genetics, 2020. **29**(8): p. 1340-1352.
301. Rouaux, C., et al., *Critical loss of CBP/p300 histone acetylase activity by caspase-6 during neurodegeneration*. EMBO J, 2003. **22**(24): p. 6537-49.
302. El-Husseini, A.E., et al., *Dual palmitoylation of PSD-95 mediates its vesiculotubular sorting, postsynaptic targeting, and ion channel clustering*. J Cell Biol, 2000. **148**(1): p. 159-72.
303. el-Husseini Ael, D. and D.S. Bredt, *Protein palmitoylation: a regulator of neuronal development and function*. Nat Rev Neurosci, 2002. **3**(10): p. 791-802.
304. Yanai, A., et al., *Palmitoylation of huntingtin by HIP14 is essential for its trafficking and function*. Nat Neurosci, 2006. **9**(6): p. 824-31.
305. Yanai, A., et al., *Palmitoylation of huntingtin by HIP14 is essential for its trafficking and function*. Nature neuroscience, 2006. **9**(6): p. 824-831.
306. Sedighi, F., A. Adegbiyoro, and J. Legleiter, *SUMOylation Prevents Huntingtin Fibrillization and Localization onto Lipid Membranes*. ACS Chemical Neuroscience, 2020. **11**(3): p. 328-343.
307. Aiken, C.T., et al., *Phosphorylation of threonine 3: implications for Huntingtin aggregation and neurotoxicity*. J Biol Chem, 2009. **284**(43): p. 29427-36.
308. Cariulo, C., et al., *Phosphorylation of huntingtin at residue T3 is decreased in Huntington's disease and modulates mutant huntingtin protein conformation*. Proc Natl Acad Sci U S A, 2017. **114**(50): p. E10809-E10818.
309. Branco-Santos, J., et al., *Protein phosphatase 1 regulates huntingtin exon 1 aggregation and toxicity*. Human Molecular Genetics, 2017. **26**(19): p. 3763-3775.
310. Ansaloni, A., et al., *One-pot semisynthesis of exon 1 of the Huntingtin protein: new tools for elucidating the role of posttranslational modifications in the pathogenesis of Huntington's disease*. Angew Chem Int Ed Engl, 2014. **53**(7): p. 1928-33.
311. Ochaba, J., et al., *IKK $\beta$  slows Huntington's disease progression in R6/1 mice*. Proceedings of the National Academy of Sciences, 2019. **116**(22): p. 10952-10961.
312. Atwal, R.S., et al., *Kinase inhibitors modulate huntingtin cell localization and toxicity*. Nature Chemical Biology, 2011. **7**(7): p. 453-460.
313. Bowie, L.E., et al., *N6-Furfuryladenine is protective in Huntington's disease models by signaling huntingtin phosphorylation*. Proc Natl Acad Sci U S A, 2018. **115**(30): p. E7081-E7090.
314. Di Pardo, A., et al., *Ganglioside GM1 induces phosphorylation of mutant huntingtin and restores normal motor behavior in Huntington disease mice*. Proceedings of the National Academy of Sciences of the United States of America, 2012. **109**(9): p. 3528-3533.
315. Caron, N.S., et al., *Polyglutamine domain flexibility mediates the proximity between flanking sequences in huntingtin*. Proceedings of the National Academy of Sciences of the United States of America, 2013. **110**(36): p. 14610-14615.
316. Arnesen, T., et al., *The Chaperone-Like Protein HYPK Acts Together with NatA in Cotranslational N-Terminal Acetylation and Prevention of Huntingtin Aggregation*. Molecular and Cellular Biology, 2010. **30**(8): p. 1898-1909.
317. Sap, K.A., et al., *Global Proteome and Ubiquitinome Changes in the Soluble and Insoluble Fractions of Q175 Huntington Mice Brains*. Molecular & Cellular Proteomics, 2019. **18**(9): p. 1705-1720.
318. Hakim-Eshed, V., et al., *Site-specific ubiquitination of pathogenic huntingtin attenuates its deleterious effects*. Proceedings of the National Academy of Sciences, 2020. **117**(31): p. 18661-18669.
319. O'Rourke, J.G., et al., *SUMO-2 and PIAS1 modulate insoluble mutant huntingtin protein accumulation*. Cell Rep, 2013. **4**(2): p. 362-75.
320. Subramaniam, S., et al., *Rhes, a striatal specific protein, mediates mutant-huntingtin cytotoxicity*. Science, 2009. **324**(5932): p. 1327-30.
321. O'Rourke, J.G., et al., *SUMO-2 and PIAS1 modulate insoluble mutant huntingtin protein accumulation*. Cell reports, 2013. **4**(2): p. 362-375.
322. Ochaba, J., et al., *PIAS1 Regulates Mutant Huntingtin Accumulation and Huntington's Disease-Associated Phenotypes In Vivo*. Neuron, 2016. **90**(3): p. 507-20.
323. DiGiovanni, L.F., et al., *Huntingtin N17 domain is a reactive oxygen species sensor regulating huntingtin phosphorylation and localization*. Hum Mol Genet, 2016.

- 
324. Son, S., et al., *High-mobility group box 1 links sensing of reactive oxygen species by huntingtin to its nuclear entry*. J Biol Chem, 2019. **294**(6): p. 1915-1923.
325. Mitomi, Y., et al., *Post-aggregation Oxidation of Mutant Huntingtin Controls the Interactions between Aggregates*. Journal of Biological Chemistry, 2012. **287**(41): p. 34764-34775.
326. Ceccon, A., V. Tugarinov, and G.M. Clore, *TiO<sub>2</sub> nanoparticles catalyze oxidation of huntingtin exon 1-derived peptides impeding aggregation: A quantitative NMR study of binding and kinetics*. Journal of the American Chemical Society, 2018. **141**(1): p. 94-97.
327. Jana, N.R., et al., *Co-chaperone CHIP associates with expanded polyglutamine protein and promotes their degradation by proteasomes*. Journal of Biological Chemistry, 2005. **280**(12): p. 11635-11640.
328. Kalchman, M.A., et al., *Huntingtin is ubiquitinated and interacts with a specific ubiquitin-conjugating enzyme*. Journal of Biological Chemistry, 1996. **271**(32): p. 19385-19394.
329. DeGuire, S.M., et al., *N-terminal Huntingtin (Htt) phosphorylation is a molecular switch regulating Htt aggregation, helical conformation, internalization, and nuclear targeting*. Journal of Biological Chemistry, 2018. **293**(48): p. 18540-18558.
330. Riguet, N., et al., *Disentangling the sequence, cellular and ultrastructural determinants of Huntingtin nuclear and cytoplasmic inclusion formation*. bioRxiv, 2020: p. 2020.07.29.226977.
331. Frey, B., et al., *Monitoring alpha-synuclein oligomerization and aggregation using bimolecular fluorescence complementation assays: what you see is not always what you get*. J Neurochem, 2020.
332. Rowan, F.C., et al., *Insights into Aurora-A kinase activation using unnatural amino acids incorporated by chemical modification*. ACS Chem Biol, 2013. **8**(10): p. 2184-91.
333. Dawson, P.E., et al., *Synthesis of proteins by native chemical ligation*. Science, 1994. **266**(5186): p. 776-9.
334. Muir, T.W., *Semisynthesis of proteins by expressed protein ligation*. Annu Rev Biochem, 2003. **72**: p. 249-89.
335. Hackenberger, C.P. and D. Schwarzer, *Chemoselective ligation and modification strategies for peptides and proteins*. Angew Chem Int Ed Engl, 2008. **47**(52): p. 10030-74.
336. Dawson, P.E., *Native Chemical Ligation Combined with Desulfurization and Deselenization: A General Strategy for Chemical Protein Synthesis*. Israel Journal of Chemistry, 2011. **51**(8-9): p. 862-867.
337. Arndt, J.R., M. Chaibva, and J. Legleiter, *The emerging role of the first 17 amino acids of huntingtin in Huntington's disease*. Biomol Concepts, 2015. **6**(1): p. 33-46.
338. Ehrnhoefer, D.E., L. Sutton, and M.R. Hayden, *Small changes, big impact: posttranslational modifications and function of huntingtin in Huntington disease*. Neuroscientist, 2011. **17**(5): p. 475-92.
339. Bustamante, M.B., et al., *Detection of huntingtin exon 1 phosphorylation by Phos-Tag SDS-PAGE: Predominant phosphorylation on threonine 3 and regulation by IKKbeta*. Biochem Biophys Res Commun, 2015. **463**(4): p. 1317-22.
340. Singer, D., et al., *Synthesis of pathological and nonpathological human exon 1 huntingtin*. J Pept Sci, 2010. **16**(7): p. 358-63.
341. Heiser, V., et al., *Inhibition of huntingtin fibrillogenesis by specific antibodies and small molecules: implications for Huntington's disease therapy*. Proc Natl Acad Sci U S A, 2000. **97**(12): p. 6739-44.
342. Samuel, D., et al., *Proline is a protein solubilizing solute*. Biochemistry and Molecular Biology International, 1997. **41**(2): p. 235-242.
343. Samuel, D., et al., *Proline inhibits aggregation during protein refolding*. Protein Sci, 2000. **9**(2): p. 344-52.
344. Yu, W.B., et al., *Trehalose inhibits fibrillation of A53T mutant alpha-synuclein and disaggregates existing fibrils*. Arch Biochem Biophys, 2012. **523**(2): p. 144-50.
345. Liu, R., et al., *Trehalose differentially inhibits aggregation and neurotoxicity of beta-amyloid 40 and 42*. Neurobiol Dis, 2005. **20**(1): p. 74-81.
346. Ignatova, Z. and L.M. Gierasch, *Inhibition of protein aggregation in vitro and in vivo by a natural osmoprotectant*. Proc Natl Acad Sci U S A, 2006. **103**(36): p. 13357-61.
347. Wan, Q. and S.J. Danishefsky, *Free-radical-based, specific desulfurization of cysteine: a powerful advance in the synthesis of polypeptides and glycopolypeptides*. Angew Chem Int Ed Engl, 2007. **46**(48): p. 9248-52.
348. Yan, L.Z. and P.E. Dawson, *Synthesis of peptides and proteins without cysteine residues by native chemical ligation combined with desulfurization*. Journal of the American Chemical Society, 2001. **123**(4): p. 526-533.
349. Khurana, R., et al., *A general model for amyloid fibril assembly based on morphological studies using atomic force microscopy*. Biophysical Journal, 2003. **85**(2): p. 1135-1144.
350. Kad, N.M., et al., *Hierarchical Assembly of  $\beta$ 2-Microglobulin Amyloid In Vitro Revealed by Atomic Force Microscopy*. Journal of Molecular Biology, 2003. **330**(4): p. 785-797.

351. Usov, I., J. Adamcik, and R. Mezzenga, *Polymorphism Complexity and Handedness Inversion in Serum Albumin Amyloid Fibrils*. *Acs Nano*, 2013. **7**(12): p. 10465-10474.
352. Ruggeri, F.S., et al., *Influence of the beta-sheet content on the mechanical properties of aggregates during amyloid fibrillization*. *Angew Chem Int Ed Engl*, 2015. **54**(8): p. 2462-6.
353. Buck, M., *Trifluoroethanol and colleagues: cosolvents come of age. Recent studies with peptides and proteins*. *Quarterly Reviews of Biophysics*, 1998. **31**(3): p. 297-355.
354. Blanco-Canosa, J.B. and P.E. Dawson, *An efficient Fmoc-SPPS approach for the generation of thioester peptide precursors for use in native chemical ligation*. *Angew Chem Int Ed Engl*, 2008. **47**(36): p. 6851-5.
355. Luo, P. and R.L. Baldwin, *Mechanism of helix induction by trifluoroethanol: a framework for extrapolating the helix-forming properties of peptides from trifluoroethanol/water mixtures back to water*. *Biochemistry*, 1997. **36**(27): p. 8413-21.
356. Fodale, V., et al., *Polyglutamine- and temperature-dependent conformational rigidity in mutant huntingtin revealed by immunoassays and circular dichroism spectroscopy*. *PLoS One*, 2014. **9**(12): p. e112262.
357. Rosenblatt, A., et al., *Predictors of neuropathological severity in 100 patients with Huntington's disease*. *Annals of Neurology: Official Journal of the American Neurological Association and the Child Neurology Society*, 2003. **54**(4): p. 488-493.
358. Kagel, M.C. and N.A. Leopold, *Dysphagi in Huntington's disease: A 16-year retrospective*. *Dysphagia*, 1992. **7**(2): p. 106-114.
359. Marder, K., et al., *Rate of functional decline in Huntington's disease*. *Neurology*, 2000. **54**(2): p. 452-452.
360. de Boo, G.M., et al., *Early cognitive and motor symptoms in identified carriers of the gene for Huntington disease*. *Archives of Neurology*, 1997. **54**(11): p. 1353-1357.
361. Slaughter, J.R., M.P. Martens, and K.A. Slaughter, *Depression and Huntington's disease: prevalence, clinical manifestations, etiology, and treatment*. *CNS spectrums*, 2001. **6**(4): p. 306-308,325-326.
362. Gusella, J.F., et al., *A polymorphic DNA marker genetically linked to Huntington's disease*. *Nature*, 1983. **306**(5940): p. 234-238.
363. Kremer, B., et al., *A worldwide study of the Huntington's disease mutation. The sensitivity and specificity of measuring CAG repeats*. *N Engl J Med*, 1994. **330**(20): p. 1401-6.
364. Snell, R.G., et al., *Relationship between Trinucleotide Repeat Expansion and Phenotypic Variation in Huntingtons-Disease*. *Nature Genetics*, 1993. **4**(4): p. 393-397.
365. Morley, J.F., et al., *The threshold for polyglutamine-expansion protein aggregation and cellular toxicity is dynamic and influenced by aging in Caenorhabditis elegans*. *Proceedings of the National Academy of Sciences*, 2002. **99**(16): p. 10417-10422.
366. Chen, S., F.A. Ferrone, and R. Wetzel, *Huntington's disease age-of-onset linked to polyglutamine aggregation nucleation*. *Proceedings of the National Academy of sciences*, 2002. **99**(18): p. 11884-11889.
367. Huang, C.C., et al., *Amyloid formation by mutant huntingtin: threshold, progressivity and recruitment of normal polyglutamine proteins*. *Somatic cell and molecular genetics*, 1998. **24**(4): p. 217-233.
368. Waelter, S., et al., *Accumulation of mutant huntingtin fragments in aggresome-like inclusion bodies as a result of insufficient protein degradation*. *Molecular biology of the cell*, 2001. **12**(5): p. 1393-1407.
369. Ratovitski, T., et al., *Mutant Huntingtin N-terminal Fragments of Specific Size Mediate Aggregation and Toxicity in Neuronal Cells*. *Journal of Biological Chemistry*, 2009. **284**(16): p. 10855-10867.
370. Chiki, A., et al., *Mutant Exon1 Huntingtin Aggregation is Regulated by T3 Phosphorylation-Induced Structural Changes and Crosstalk between T3 Phosphorylation and Acetylation at K6*. *Angew Chem Int Ed Engl*, 2017. **56**(19): p. 5202-5207.
371. Daldin, M., et al., *Polyglutamine expansion affects huntingtin conformation in multiple Huntington's disease models*. *Sci Rep*, 2017. **7**(1): p. 5070.
372. Cariulo, C., et al., *Ultrasensitive quantitative measurement of huntingtin phosphorylation at residue S13*. *Biochemical and biophysical research communications*, 2020. **521**(3): p. 549-554.
373. Binukumar, B., et al., *Profiling of p5, a 24 amino acid inhibitory peptide derived from the CDK5 activator, p35 CDKR1 against 70 protein kinases*. *Journal of Alzheimer's Disease*, 2016. **54**(2): p. 525-533.
374. Hegde, R.N., et al., *TBK1 regulates autophagic clearance of soluble mutant huntingtin and inhibits aggregation/toxicity in different models of Huntington's disease*. *bioRxiv*, 2019: p. 869586.
375. Dan, I., N.M. Watanabe, and A. Kusumi, *The Ste20 group kinases as regulators of MAP kinase cascades*. *Trends in cell biology*, 2001. **11**(5): p. 220-230.
376. Lin, H.K., et al., *Fibril polymorphism affects immobilized non-amyloid flanking domains of huntingtin exon1 rather than its polyglutamine core*. *Nat Commun*, 2017. **8**: p. 15462.

- 
377. Boatz, J.C., et al., *Protofilament Structure and Supramolecular Polymorphism of Aggregated Mutant Huntingtin Exon 1*. J Mol Biol, 2020.
  378. Herrera, F., et al., *Visualization of cell-to-cell transmission of mutant huntingtin oligomers*. PLoS currents, 2011. **3**.
  379. Wang, H., et al., *Effects of overexpression of huntingtin proteins on mitochondrial integrity*. Hum Mol Genet, 2009. **18**(4): p. 737-52.
  380. Cao, F., et al., *Nuclear aggregation of huntingtin is not prevented by deletion of chaperone Hsp104*. Biochimica et Biophysica Acta (BBA)-Molecular Basis of Disease, 2001. **1537**(2): p. 158-166.
  381. Herrera, F. and J. Branco-Santos, *Threonine 3 regulates Serine 13/16 phosphorylation in the huntingtin exon 1*. Matters Select, 2019. **5**(5): p. e201905000005.
  382. Chiki, A., et al., *Mutant Exon1 Huntingtin Aggregation is Regulated by T3 Phosphorylation-Induced Structural Changes and Crosstalk between T3 Phosphorylation and Acetylation at K6*. Angew Chem Int Ed Engl, 2017.
  383. Baias, M., et al., *Structure and Dynamics of the Huntingtin Exon-1 N-Terminus: A Solution NMR Perspective*. Journal of the American Chemical Society, 2017. **139**(3): p. 1168-1176.
  384. Newcombe, E.A., et al., *Tadpole-like Conformations of Huntingtin Exon 1 Are Characterized by Conformational Heterogeneity that Persists regardless of Polyglutamine Length*. J Mol Biol, 2018. **430**(10): p. 1442-1458.
  385. Binolfi, A., et al., *Intracellular repair of oxidation-damaged  $\alpha$ -synuclein fails to target C-terminal modification sites*. Nature communications, 2016. **7**(1): p. 1-10.
  386. Theillet, F.-X., et al., *Site-specific NMR mapping and time-resolved monitoring of serine and threonine phosphorylation in reconstituted kinase reactions and mammalian cell extracts*. Nature protocols, 2013. **8**(7): p. 1416.
  387. Smith, M.J., et al., *Real-time NMR monitoring of biological activities in complex physiological environments*. Current opinion in structural biology, 2015. **32**: p. 39-47.
  388. Theillet, F.o.-X., et al., *Site-specific mapping and time-resolved monitoring of lysine methylation by high-resolution NMR spectroscopy*. Journal of the American Chemical Society, 2012. **134**(18): p. 7616-7619.
  389. Eliezer, D., et al., *Conformational properties of  $\alpha$ -synuclein in its free and lipid-associated states*. Journal of molecular biology, 2001. **307**(4): p. 1061-1073.
  390. Marley, J., M. Lu, and C. Bracken, *A method for efficient isotopic labeling of recombinant proteins*. Journal of biomolecular NMR, 2001. **20**(1): p. 71-75.
  391. Hendus-Altenburger, R., et al., *Random coil chemical shifts for serine, threonine and tyrosine phosphorylation over a broad pH range*. Journal of biomolecular NMR, 2019. **73**(12): p. 713-725.
  392. Liokatis, S., et al., *Simultaneous detection of protein phosphorylation and acetylation by high-resolution NMR spectroscopy*. Journal of the American Chemical Society, 2010. **132**(42): p. 14704-14705.
  393. Williamson, T.E., et al., *Modulation of polyglutamine conformations and dimer formation by the N-terminus of huntingtin*. Journal of molecular biology, 2010. **396**(5): p. 1295-1309.
  394. Kosten, J., et al., *Efficient modification of alpha-synuclein serine 129 by protein kinase CK1 requires phosphorylation of tyrosine 125 as a priming event*. ACS chemical neuroscience, 2014. **5**(12): p. 1203-1208.
  395. Chiki, A., et al., *Mutant Exon1 Huntingtin Aggregation is Regulated by T3 Phosphorylation-Induced Structural Changes and Crosstalk between T3 Phosphorylation and Acetylation at K6*. Angewandte Chemie-International Edition, 2017. **56**(19): p. 5202-5207.
  396. Froger, A. and J.E. Hall, *Transformation of plasmid DNA into E. coli using the heat shock method*. J Vis Exp, 2007(6): p. 253.
  397. Wishart, D.S. and B.D. Sykes, *The 13 C chemical-shift index: a simple method for the identification of protein secondary structure using 13 C chemical-shift data*. Journal of biomolecular NMR, 1994. **4**(2): p. 171-180.
  398. Reiner, A., et al., *Differential loss of striatal projection neurons in Huntington disease*. Proceedings of the National Academy of Sciences, 1988. **85**(15): p. 5733-5737.
  399. Rosas, H., et al., *Evidence for more widespread cerebral pathology in early HD: an MRI-based morphometric analysis*. Neurology, 2003. **60**(10): p. 1615-1620.
  400. Hodgson, J.G., et al., *A YAC mouse model for Huntington's disease with full-length mutant huntingtin, cytoplasmic toxicity, and selective striatal neurodegeneration*. Neuron, 1999. **23**(1): p. 181-192.
  401. Hegde, R.N., et al., *TBK1 phosphorylates mutant Huntingtin and suppresses its aggregation and toxicity in Huntington's disease models*. EMBO J, 2020: p. e104671.
  402. Kumar, A. and R.R. Ratan, *Oxidative Stress and Huntington's Disease: The Good, The Bad, and The Ugly*. Journal of Huntington's Disease, 2016. **5**: p. 217-237.

403. Chen, C.-M., et al., *Increased oxidative damage and mitochondrial abnormalities in the peripheral blood of Huntington's disease patients*. Biochemical and biophysical research communications, 2007. **359**(2): p. 335-340.
404. Polidori, M.C., et al., *Oxidative damage to mitochondrial DNA in Huntington's disease parietal cortex*. Neuroscience letters, 1999. **272**(1): p. 53-56.
405. Li, S., C. Schöneich, and R.T. Borchardt, *Chemical instability of protein pharmaceuticals: mechanisms of oxidation and strategies for stabilization*. Biotechnology and Bioengineering, 1995. **48**(5): p. 490-500.
406. Ji, J.A., et al., *Methionine, tryptophan, and histidine oxidation in a model protein, PTH: mechanisms and stabilization*. Journal of pharmaceutical sciences, 2009. **98**(12): p. 4485-4500.
407. Keck, R.G., *The use of t-butyl hydroperoxide as a probe for methionine oxidation in proteins*. Analytical biochemistry, 1996. **236**(1): p. 56-62.
408. Wasylaschuk, W.R., et al., *Evaluation of hydroperoxides in common pharmaceutical excipients*. Journal of pharmaceutical sciences, 2007. **96**(1): p. 106-116.
409. Luo, Q., et al., *Chemical modifications in therapeutic protein aggregates generated under different stress conditions*. Journal of Biological Chemistry, 2011. **286**(28): p. 25134-25144.
410. Chiki, A., et al., *Site-specific phosphorylation of Huntingtin exon 1 recombinant proteins enabled by the discovery of novel kinases*. bioRxiv, 2020: p. 2020.07.23.217968.
411. O'Nuallain, B., et al., *Kinetics and Thermodynamics of Amyloid Assembly Using a High-Performance Liquid Chromatography–Based Sedimentation Assay*. 2006. **413**: p. 34-74.
412. Jayaraman, M., et al., *Assays for studying nucleated aggregation of polyglutamine proteins*. Methods, 2011. **53**(3): p. 246-54.
413. Długosz, M. and J. Trylska, *Secondary structures of native and pathogenic huntingtin N-terminal fragments*. The journal of physical chemistry B, 2011. **115**(40): p. 11597-11608.
414. Pastore, A., et al., *The role of post-translational modifications on the energy landscape of Huntingtin N-terminus*. Frontiers in molecular biosciences, 2019. **6**: p. 95.
415. Huang, J., et al., *CHARMM36m: an improved force field for folded and intrinsically disordered proteins*. Nat Methods, 2017. **14**(1): p. 71-73.
416. Jorgensen, W.L., et al., *Comparison of simple potential functions for simulating liquid water*. The Journal of chemical physics, 1983. **79**(2): p. 926-935.
417. Valley, C.C., et al., *The methionine-aromatic motif plays a unique role in stabilizing protein structure*. J Biol Chem, 2012. **287**(42): p. 34979-91.
418. Chiki, A., et al., *Site-specific phosphorylation of Huntingtin exon 1 recombinant proteins enabled by the discovery of novel kinases*. Chembiochem, 2020.
419. Gu, M. and J.H. Viles, *Methionine oxidation reduces lag-times for amyloid- $\beta$  (1–40) fiber formation but generates highly fragmented fibers*. Biochimica et Biophysica Acta (BBA)-Proteins and Proteomics, 2016. **1864**(9): p. 1260-1269.
420. Friedemann, M., et al., *Effect of methionine-35 oxidation on the aggregation of amyloid- $\beta$  peptide*. Biochemistry and biophysics reports, 2015. **3**: p. 94-99.
421. Johansson, A.-S., et al., *Attenuated amyloid- $\beta$  aggregation and neurotoxicity owing to methionine oxidation*. Neuroreport, 2007. **18**(6): p. 559-563.
422. Bergström, L.A., et al., *Oxidation of the prion peptide PrP106-126 reduces the fibrillation but not the neurotoxicity and induces a partial PrPC independent neurotoxicity*. Biochimica Et Biophysica Acta-proteins and Proteomics, 2007. **1774**(9): p. 1118-1127.
423. Zhou, W., et al., *Methionine oxidation stabilizes non-toxic oligomers of  $\alpha$ -synuclein through strengthening the auto-inhibitory intra-molecular long-range interactions*. Biochimica et Biophysica Acta (BBA)-Molecular Basis of Disease, 2010. **1802**(3): p. 322-330.
424. Wei, Y., A.A. Thyparambil, and R.A. Latour, *Protein helical structure determination using CD spectroscopy for solutions with strong background absorbance from 190 to 230 nm*. Biochimica et Biophysica Acta (BBA)-Proteins and Proteomics, 2014. **1844**(12): p. 2331-2337.
425. Luo, P. and R.L. Baldwin, *Mechanism of helix induction by trifluoroethanol: a framework for extrapolating the helix-forming properties of peptides from trifluoroethanol/water mixtures back to water*. Biochemistry, 1997. **36**(27): p. 8413-8421.
426. Scholtz, J.M., et al., *Parameters of helix–coil transition theory for alanine-based peptides of varying chain lengths in water*. Biopolymers: Original Research on Biomolecules, 1991. **31**(13): p. 1463-1470.

- 
427. Mu, Y., P.H. Nguyen, and G. Stock, *Energy landscape of a small peptide revealed by dihedral angle principal component analysis*. Proteins, 2005. **58**(1): p. 45-52.
428. Kabsch, W. and C. Sander, *Dictionary of protein secondary structure: pattern recognition of hydrogen-bonded and geometrical features*. Biopolymers, 1983. **22**(12): p. 2577-637.
429. Humphrey, W., A. Dalke, and K. Schulten, *VMD: visual molecular dynamics*. Journal of molecular graphics, 1996. **14**(1): p. 33-38.
430. Mishra, R., et al., *Serine Phosphorylation Suppresses Huntingtin Amyloid Accumulation by Altering Protein Aggregation Properties*. Journal of Molecular Biology, 2012. **424**(1-2): p. 1-14.
431. Yalinca, H., et al., *The Role of Post-translational Modifications on the Energy Landscape of Huntingtin N-Terminus*. Front Mol Biosci, 2019. **6**: p. 95.
432. Bravo-Arredondo, J.M., et al., *The folding equilibrium of huntingtin exon 1 monomer depends on its polyglutamine tract*. Journal of Biological Chemistry, 2018. **293**(51): p. 19613-19623.
433. Richards, N.G., *Shining a light on post-translational modification*. 2008.
434. Rogerson, D.T., et al., *Efficient genetic encoding of phosphoserine and its nonhydrolyzable analog*. Nature chemical biology, 2015. **11**(7): p. 496-503.
435. Fu, A., et al., *Promises and pitfalls of intracellular delivery of proteins*. Bioconjugate chemistry, 2014. **25**(9): p. 1602-1608.



## VII. Curriculum Vitae

### Anass Chiki

Avenue de Longemalle 14  
1020 Renens, VD  
+41 79 768 25 39  
[anass.chiki@gmail.com](mailto:anass.chiki@gmail.com)

33 years  
Married  
Swiss citizen

### EDUCATION

- **Master of Science MSc in Bioengineering with a Minor in Biomedical technologies**, EPFL, Lausanne August 2013  
*Master's project: Impact of phosphorylation on tau biophysical properties*
- **Bachelor in Life Science and Technology**, EPFL, Life science school, Lausanne July 2011  
*Bachelor's project: Design of disposable urea biosensor based on piezoresistive Model*
- **Special Mathematics Courses**, Ecole Polytechnique Fédérale de Lausanne (EPFL), Lausanne, Switzerland July 2007
- **Classe préparatoire aux grandes écoles (CPGE)**, Tangier, Morocco July 2006
- **Baccalaureate in Applied Sciences**, Lycée Moulay Idriss, Fez, Morocco (*with high honors*) July 2005

### PROFESSIONAL EXPERIENCE

- **Laboratory of Molecular and Chemical Biology of Neurodegeneration (EPFL)** Since 2015  
PhD candidate in Biotechnology and Bioengineering
- **Laboratory of Molecular and Chemical Biology of Neurodegeneration (EPFL)** 2013 -2015  
Research Assistant
- **Gamma Institute**, Lausanne. teacher of Mathematics 2012
- **Macdonald's Restaurant Geneva**, Polyvalent responsibilities & crew trainer 2008-2012
- **Centre Vaudois d'Aide à la Jeunesse (CVAJ)**, Lausanne. (Biology, Chemistry, Mathematics and English) 2006-2011

### HONORS/AWARDS

EPFL scholarship for master studies.

Best Oral Presentation BMI symposium

6th place during a national intellectual game in Morocco organised by the education minister, number of participant : 150

## SKILLS

### Life sciences

Molecular and genetic biology  
 Protein expression  
 Protein purification by chromatography: anion exchange, reverse phase, size exclusion and immobilized metal affinity  
*In vitro* enzymatic and aggregation assays  
 Electrophoresis and western blotting  
 Cell cultures: bacterial, insect and mammalian  
 Light, confocal and electron microscopy  
 Biophysical characterization: UV-spectrometry, Mass Spectrometry, ultra-high performance liquid chromatography, circular dichroism, dynamic light scattering  
 Protein Chemistry: Native Chemical Ligation, Solid-phase peptide synthesis, protein labeling

### Computer sciences

Matlab  
 C/C++  
 JAVA  
 GIT  
 Agile Development Methods  
 Jira  
 Wordpress  
 Jupyter  
 ImageJ  
 Segment software

### Soft skills

Problem solving  
 Public speaking  
 Leadership  
 Versatile  
 Passionate  
 Organized  
 Multicultural

## LANGUAGES

**Mother tongue:** French, Arabic

**Fluent:** English

## PERSONAL INTERESTS

Football  
 Traveling and cultural exchange  
 Reading  
 Civilization history  
 Cooking  
 Spend time with my beloved family.

## PUBLICATIONS

- Site-specific phosphorylation of Huntingtin exon 1 recombinant proteins enabled by the discovery of novel kinases.**  
**Chiki A**, Ricci J, Hegde RN, Abriata LA, Reif A, Boudeffa D, Lashuel HA.  
 Chembiochem. 2020 Aug 17. doi: 10.1002/cbic.202000508. Online ahead of print.
- TBK1 phosphorylates mutant Huntingtin and suppresses its aggregation and toxicity in Huntington's disease models.**  
 Hegde RN, **Chiki A**, Petricca L, Martufi P, Arbez N, Mouchiroud L, Auwerx J, Landles C, Bates GP, Singh-Bains MK, Dragunow M, Curtis MA, Faull RL, Ross CA, Caricasole A, Lashuel HA.  
 EMBO J. 2020 Aug 5:e104671. doi: 10.15252/embj.2020104671. Online ahead of print.
- Extent of N-terminus exposure of monomeric alpha-synuclein determines its aggregation propensity.**  
 Stephens AD, Zacharopoulou M, Moons R, Fusco G, Seetalo N, **Chiki A**, Woodhams PJ, Mela I, Lashuel HA, Phillips JJ, De Simone A, Sobott F, Schierle GSK.  
 Nat Commun. 2020 Jun 4;11(1):2820. doi: 10.1038/s41467-020-16564-3.
- Phosphorylation of the overlooked tyrosine 310 regulates the structure, aggregation, and microtubule- and lipid-binding properties of Tau.**  
 Ait-Bouziad N, **Chiki A**, Limorenko G, Xiao S, Eliezer D, Lashuel HA.  
 J Biol Chem. 2020 Jun 5;295(23):7905-7922. doi: 10.1074/jbc.RA119.012517. Epub 2020 Apr 27.
- Unraveling the complexity of amyloid polymorphism using gold nanoparticles and cryo-EM.**  
 Cendrowska U, Silva PJ, Ait-Bouziad N, Müller M, Guven ZP, Vieweg S, **Chiki A**, Radamaker L, Kumar ST, Fändrich M, Tavanti F, Menziani MC, Alexander-Katz A, Stellacci F, Lashuel HA.  
 Proc Natl Acad Sci U S A. 2020 Mar 24;117(12):6866-6874. doi: 10.1073/pnas.1916176117. Epub 2020 Mar 11.

6. **A simple, versatile and robust centrifugation-based filtration protocol for the isolation and quantification of  $\alpha$ -synuclein monomers, oligomers and fibrils: Towards improving experimental reproducibility in  $\alpha$ -synuclein research.**  
Kumar ST, Donzelli S, **Chiki A**, Syed MMK, Lashuel HA.  
J Neurochem. 2020 Apr;153(1):103-119. doi: 10.1111/jnc.14955. Epub 2020 Feb 25.
7. **Chronic corticosterone aggravates behavioral and neuronal symptomatology in a mouse model of alpha-synuclein pathology.**  
Burtscher J, Copin JC, Rodrigues J, Kumar ST, **Chiki A**, Guillot de Suduiraut I, Sandi C, Lashuel HA.  
Neurobiol Aging. 2019 Nov;83:11-20. doi: 10.1016/j.neurobiolaging.2019.08.007. Epub 2019 Aug 14.
8. **N-terminal Huntingtin (Htt) phosphorylation is a molecular switch regulating Htt aggregation, helical conformation, internalization, and nuclear targeting.**  
DeGuire SM, Ruggeri FS, Fares MB, **Chiki A**, Cendrowska U, Dietler G, Lashuel HA.  
J Biol Chem. 2018 Nov 30;293(48):18540-18558. doi: 10.1074/jbc.RA118.004621. Epub 2018 Sep 5.
9. **Generation of Native, Untagged Huntingtin Exon1 Monomer and Fibrils Using a SUMO Fusion Strategy.**  
Reif A, **Chiki A**, Ricci J, Lashuel HA.  
J Vis Exp. 2018 Jun 27;(136):57506. doi: 10.3791/57506.
10. **The making of a Lewy body: the role of  $\alpha$ -synuclein post-fibrillization modifications in regulating the formation and the maturation of pathological inclusions**  
AL Mahul-Mellier, MF Altay, J Burtscher, N Maharjan, NA Bouziad, **A Chiki**, S Vingill, R Wade-Martins, J Holton, C Strand, C Haikal, JY Li, R Hamelin, M Croisier, G Knott, G Mairet-Coello, L Weerens, A Michel, P Downey, M Citron, HA Lashuel  
Preprint at <https://doi.org/10.1101/500058>, 2018
11. **Exploring the role of post-translational modifications in regulating  $\alpha$ -synuclein interactions by studying the effects of phosphorylation on nanobody binding.**  
El Turk F, De Genst E, Williams T, Fauvet B, Hejjaoui M, Di Trani J, **Chiki A**, Mittermaier A, Vendruscolo M, Lashuel HA, Dobson CM.  
Protein Sci. 2018 Jul;27(7):1262-1274. doi: 10.1002/pro.3412.
12. **Phosphorylation of huntingtin at residue T3 is decreased in Huntington's disease and modulates mutant huntingtin protein conformation.**  
Cariulo C, Azzollini L, Verani M, Martufi P, Boggio R, **Chiki A**, Deguire SM, Cherubini M, Gines S, Marsh JL, Conforti P, Cattaneo E, Santimone I, Squitieri F, Lashuel HA, Petricca L, Caricasole A.  
Proc Natl Acad Sci U S A. 2017 Dec 12;114(50):E10809-E10818. doi: 10.1073/pnas.1705372114. Epub 2017 Nov 21.
13. **Mutant Exon1 Huntingtin Aggregation is Regulated by T3 Phosphorylation-Induced Structural Changes and Crosstalk between T3 Phosphorylation and Acetylation at K6.**  
**Chiki A**, DeGuire SM, Ruggeri FS, Sanfelice D, Ansaloni A, Wang ZM, Cendrowska U, Burai R, Vieweg S, Pastore A, Dietler G, Lashuel HA.  
Angew Chem Int Ed Engl. 2017 May 2;56(19):5202-5207. doi: 10.1002/anie.201611750. Epub 2017 Mar 23.
14. **Nanoscale studies link amyloid maturity with polyglutamine diseases onset.**  
Ruggeri FS, Vieweg S, Cendrowska U, Longo G, **Chiki A**, Lashuel HA, Dietler G.  
Sci Rep. 2016 Aug 8;6:31155. doi: 10.1038/srep31155.
15. **Elucidating the Role of Site-Specific Nitration of  $\alpha$ -Synuclein in the Pathogenesis of Parkinson's Disease via Protein Semisynthesis and Mutagenesis.**  
Burai R, Ait-Bouziad N, **Chiki A**, Lashuel HA.  
J Am Chem Soc. 2015 Apr 22;137(15):5041-52. doi: 10.1021/ja5131726. Epub 2015 Apr 8.